VILNIUS GEDIMINAS TECHNICAL UNIVERSITY
AND
STATE RESEARCH INSTITUTE CENTER
FOR PHYSICAL SCIENCES AND TECHNOLOGY

Maksimas ANBINDERIS

INVESTIGATION OF DETECTION PROPERTIES OF PLANAR MICROWAVE DIODES BASED ON A3B5 SEMICONDUCTOR COMPOUNDS IN MILLIMETER–WAVELENGTH RANGE

DOCTORAL DISSERTATION

TECHNOLOGICAL SCIENCES
ELECTRICAL AND ELECTRONIC ENGINEERING (T 001)

Vilnius, 2023

The doctoral dissertation was prepared at State Research Institute Center for Physical Sciences and Technology in 2016–2022.
(The dissertation is defended as an external work.)

Scientific Consultant

Prof. Dr Algirdas SUŽIEDĖLIS (State Research Institute Center for Physical Sciences and Technology, Electrical and Electronic Engineering – T 001).

The Dissertation Defense Council of Scientific Field of Electrical and Electronic Engineering of Vilnius Gediminas Technical University and State Research Institute Center for Physical Sciences and Technology:

Chairman

Prof. Dr Algirdas BAŠKYS (Vilnius Gediminas Technical University, Electrical and Electronic Engineering – T 001).

Members:

Dr Alvydas LISAUSKAS (Institute of High Pressure Physics Polish Academy of Sciences, Physics – N 002),
Dr Rimantas SIMNIŠKIS (State Research Institute Center for Physical Sciences and Technology, Electrical and Electronic Engineering – T 001),
Prof. Dr Voitech STANKEVIČ (Vilnius Gediminas Technical University, Electrical and Electronic Engineering – T 001),
Prof. Dr Habil. Sigitas TAMULEVIČIUS (Kaunas University of Technology, Physics – N 002).

The dissertation will be defended at the public meeting of the Dissertation Defense Council of Electrical and Electronic Engineering in the Senate Hall of Vilnius Gediminas Technical University at **10 a.m. on 10 February 2023**.

Address: Saulėtekio al. 11, LT-10223 Vilnius, Lithuania.
Tel.: +370 5 274 4956; fax +370 5 270 0112; e-mail: doktor@vilniustech.lt

A notification on the intended defense of the dissertation was sent on 9 January 2023. A copy of the doctoral dissertation is available for review at Vilnius Gediminas Technical University repository https://etalpykla.vilniustech.lt and the Library of Vilnius Gediminas Technical University (Saulėtekio al. 14, LT-10223 Vilnius, Lithuania) and at the Library of State Research Institute Center for Physical Sciences and Technology (Saulėtekio al. 3, LT-10257 Vilnius, Lithuania).

Vilnius Gediminas Technical University book No 2023-001-M

doi:10.20334/2023-001-M

maksimas.anbinderis@vilniustech.lt

VILNIAUS GEDIMINO TECHNIKOS UNIVERSITETAS
IR
VALSTYBINIS MOKSLINIŲ TYRIMŲ INSTITUTAS
FIZINIŲ IR TECHNOLOGIJOS MOKSLŲ CENTRAS

Maksimas ANBINDERIS

PLANARINIŲ MIKROBANGŲ DIODŲ A3B5 PUSLAIDININKINIŲ JUNGINIŲ PAGRINDU DETEKCINIŲ SAVYBIŲ TYRIMAI MILIMETRINIŲ BANGŲ RUOŽE

DAKTARO DISERTACIJA

TECHNOLOGIJOS MOKSLAI
ELEKTROS IR ELEKTRONIKOS INŽINERIJA (T 001)

Vilnius, 2023

Disertacija rengta 2016–2022 metais Valstybiniame mokslinių tyrimų institute Fizinių ir technologijos mokslų centre.
(Disertacija ginama eksternu.)

Mokslinis konsultantas

prof. dr. Algirdas SUŽIEDĖLIS (Valstybinis mokslinių tyrimų institutas Fizinių ir technologijos mokslų centras, elektros ir elektronikos inžinerija – T 001).

Vilniaus Gedimino technikos universiteto ir Valstybinio mokslinių tyrimų instituto Fizinių ir technologijos mokslų centro Elektros ir elektronikos inžinerijos mokslo krypties disertacijos gynimo taryba:

Pirmininkas

prof. dr. Algirdas BAŠKYS (Vilniaus Gedimino technikos universitetas, elektros ir elektronikos inžinerija – T 001).

Nariai:

dr. Alvydas LISAUSKAS (Lenkijos mokslų akademijos Aukšto slėgio fizikos institutas, fizika – N 002),
dr. Rimantas SIMNIŠKIS (Valstybinis mokslinių tyrimų institutas Fizinių ir technologijos mokslų centras, elektros ir elektronikos inžinerija – T 001),
prof. dr. Voitech STANKEVIČ (Vilniaus Gedimino technikos universitetas, elektros ir elektronikos inžinerija – T 001),
prof. habil. dr. Sigitas TAMULEVIČIUS (Kauno technologijos universitetas, fizika – N 002).

Disertacija bus ginama viešame Elektros ir elektronikos inžinerijos mokslo krypties disertacijos gynimo tarybos posėdyje **2023 m. vasario 10 d. 10 val.** Vilniaus Gedimino technikos universiteto senato posėdžių salėje.

Adresas: Saulėtekio al. 11, LT-10223 Vilnius, Lietuva.
Tel.: (8 5) 274 4956; faksas (8 5) 270 0112; el. paštas doktor@vilniustech.lt

Pranešimai apie numatomą ginti disertaciją išsiųsti 2023 m. sausio 9 d.

Disertaciją galima peržiūrėti Vilniaus Gedimino technikos universiteto talpykloje https://etalpykla.vilniustech.lt ir Vilniaus Gedimino technikos universiteto bibliotekoje (Saulėtekio al. 14, LT-10223 Vilnius, Lietuva) ir Valstybinio mokslinių tyrimų instituto Fizinių ir technologijos mokslų centro bibliotekoje (Saulėtekio al. 3, LT-10257 Vilnius, Lietuva).

Abstract

Successful development of microwave technologies requires electromagnetic detectors capable of sensing high-frequency signals at low levels of microwave power. Bulk-barrier planar microwave diodes operating based on the major carrier phenomena are promising in high-frequency electromagnetic radiation sensing applications.

The dissertation aimed to develop and investigate new original planar microwave diodes with a lower spread of their electrical parameters and capable of detecting an electromagnetic signal in the millimeter-wavelength range.

The first chapter reviews the physical properties of microwave diode-based detectors with quasi-linear and non-linear current-voltage characteristics and microwave diodes with a two-dimensional electron gas channel. Then, the application technologies for microwave detectors and methods for their investigation using appropriate probing systems are discussed. The second chapter covers the aspects of the development of planar semiconductor microwave diodes based on GaAs, AlGaAs, and AlGaAs/GaAs compounds. Next, the methodology for investigation methods of electrical parameters and detection properties of the microwave diodes is presented. The third chapter presents the results of experimental investigations of the electrical parameters and detection properties of planar dual microwave diodes based on a semi-insulating or low-resistivity GaAs substrate, including current-voltage characteristics, detected voltage on power characteristics and dependence of voltage sensitivity on frequency in the millimeter-wavelength range. The fourth chapter presents theoretical estimations and experimental investigations of the electrical and detection properties of bow-tie type microwave diodes with partial gate above a two-dimensional electron gas channel based on a selectively doped GaAs/AlGaAs heterostructure.

The dissertation presents new developed planar microwave diodes, advanced techniques for investigating their properties, and ways for enhancing their detection properties. Five scientific papers were published on the topic of the dissertation: three papers in scientific journals included in the list of *Clarivate Analytics Web of Science* database with an impact factor, and two papers in conference proceedings included in the *Clarivate Analytics Web of Science* and *Scopus* databases. A European patent based on the results of the dissertation has been granted, and twelve reports, including the results of the dissertation, were presented at national and international scientific conferences.

Reziumė

Norint sėkmingai vystyti mikrobangų technologijas reikalingi elektromagnetinės spinduliuotės detektoriai, galintys aptikti silpnus aukštadažnius signalus. Mikrobangų diodai su energetiniu barjeru puslaidininkio tūryje, kurių veikimas pagrįstas pagrindinių krūvininkų reiškiniu, yra perspektyvūs aukštųjų dažnių elektromagnetinės spinduliuotės detekcijos taikymų srityje.

Šios disertacijos tikslas buvo sukurti naujus originalius planarinius mikrobangų diodus puslaidininkinių heterodarinių pagrindu, kurie pasižymėtų mažesniu elektrinių parametrų išbarstymu ir galėtų detektuoti elektromagnetinę spinduliuotę milimetrinių bangų ruože.

Pirmajame skyriuje apžvelgiami mikrobangų detektorių su kvazitiesinėmis ir netiesinėmis voltamperinėmis charakteristikomis bei mikrobangų diodų su dvimačiu elektronų dujų kanalu fizikiniai parametrai. Taip pat aptariamos mikrobangų detektorių taikymo technologijos ir aptariami jų parametrų matavimų būdai naudojant zondavimo sistemas. Antrajame skyriuje aprašomi planarinių mikrobangų diodų GaAs, AlGaAs ir AlGaAs/GaAs pagrindu kūrimo etapai ir procesai bei pateikiamos jų elektrinių parametrų ir detekcijos savybių tyrimo metodologijos. Trečiajame skyriuje aprašomi planarinių mikrobangų diodų ant laidaus GaAs padėklo bei planarinių mikrobangų AlGaAs diodų ant pusiau izoliuojančio padėklo elektrinių parametrų ir detekcijos savybių eksperimentinių tyrimų rezultatai: voltamperinės charakteristikos, voltvatinės charakteristikos, voltvatinio jautrio dažninės priklausomybės milimetrinių bangų ruože. Ketvirtajame skyriuje aprašomi peteliškės formos mikrobangų diodų su daline sklende virš dvimačio elektronų dujų sluoksnio AlGaAs/GaAs selektyviai legiruotame heterodarinyje elektrinių parametrų ir detekcijos savybių eksperimentiniai tyrimai ir teorinis įvertinimas.

Disertacijoje aprašomi nauji sukurti mikrobangų diodai, pasiūlomos pažangios jų tyrimo metodikos ir būdai leidžiantys pagerinti diodų detekcijos savybes. Pagrindiniai disertacijos rezultatai buvo paskelbti 5 mokslo straipsniuose: 3 – mokslo žurnaluose, įtrauktuose į *Clarivate Analytics Web of Science* duomenų bazės sąrašą su citavimo rodikliu, 2 – tarptautinių konferencijų medžiagoje, įtrauktoje į *Clarivate Analytics Web of Science* ir *Scopus* duomenų bazes. Disertacijoje atliktų tyrimų rezultatai buvo paskelbti 12 mokslinių konferencijų Lietuvoje ir užsienyje. Gautas Europinis patentas remiantis disertacijoje pateiktais rezultatais.

Notations

Abbreviations

2D – two-dimensional;
2DEG – two-dimensional electron gas;
3D – three-dimensional;
ACPW – air coplanar waveguide;
AM – amplitude modulated;
ALC – automatic level control;
BtDNG – bow-tie diodes with a narrow gate;
BtDWG – bow-tie diodes with a wide gate;
CMOS – complementary metal-oxide-semiconductor;
CV – capacitance-voltage;
CW – continuous wave;
DC – direct current;
DI – deionized;
DUT – device under test;
EHF – extremely high frequency;
EMF – electromotive force;
FET – field-effect transistor;
FM – frequency modulated;
HBTS – heterojunction bipolar transistor;

HF – high-frequency;
HFSS – high-frequency structure simulator;
HS – high Schottky;
IC – integrated circuit;
IR – infrared;
IV – current-voltage;
LBS – low barrier Schottky;
LO – low Ohmic;
LPE – liquid phase epitaxy;
LS – low Schottky;
MBE – molecular beam epitaxy;
MIMC – microwave/millimeter-wave monolithic integrated circuit;
MIMO – multiple-input and multiple-output;
MMW – millimeter-wavelength;
MW – microwave;
NEP – noise equivalent power;
PD – planar dual;
PDB – planar doped-barrier;
RF – radio frequency;
SCHV – Schottky-voltage;
SEM – scanning electron microscopy;
SI – semi-insulating;
SWR – standing wave ratio;
TEM – transverse electromagnetic;
TEMF – thermoelectric force;
TLM – transfer length method;
TWT – travelling-wave tube;
UV – ultraviolet;
VP – voltage-power;
VPE – vapor phase epitaxy;
VSWR – voltage standing wave ratio.

Contents

Introduction

Problem Formulation

Microwave frequencies range from 300 MHz up to 300 GHz. The electronics industry divides this wide range into bands and classes by frequencies according to the application options. Last but not least is the so-called millimeter-wavelength region. It is also called the extremely high-frequency range, which corresponds to frequencies of 30 GHz to 300 GHz (Zhang, Rajavel, Deelman & Fray, 2020). Electromagnetic radiation in the millimeter-wavelength range attracts the attention of scientists and engineers due to its numerous possible applications in modern fields of technology, such as imaging (Oka, Togo, Kukutsu & Nagatsuma, 2008; Wang, Chang & Cui, 2019), bio-medicine (Dalmay et al., 2010; Pastorino, 2015) material science (Smith, Weatherall & Barber, 2012; Kancleris, Laurinavičius & Anbinderis, 2004) and arranging broadband wireless communication networks (Rappaport et al., 2013; Huo, Dong & Xu, 2017). The short wavelengths of microwave electromagnetic radiation allow the electronic devices to be very small and very promising with respect to their extensive applications.

Electromagnetic radiation detectors, which can sense high-frequency signals even at low levels, are required to implement microwave range. Semiconductor diode structures are most commonly used today for electromagnetic detection.

Field-effect transistors (Teppe et al., 2005), backward tunnel diodes (Takahashi, Sato, Hirose & Hara, 2009), and a wide variety of Schottky junction-based microwave diodes (Siegel, 2002; Shashkin et al., 2007) have found application for sensing and detecting millimeter-wave radiation. The most popular are zero-biased low-barrier Schottky diodes (Hesler & Crowe, 2007), which have reached their commercial maturity due to good repeatability and competent reliability as well as high voltage sensitivity, wide bandwidth, and operation at room temperature. However, fundamentally, the Schottky diode is a surface-based operating device that makes it sensitive to manufacturing conditions and vulnerable to the impact of the environment. Therefore, the complexity of these diodes encourages the scientific and engineering community to pursue new original concepts of microwave diodes having detection processes situated in the bulk of a device.

Various bulk-barrier diodes operating based on the major carrier phenomena in semiconductors have been proposed, such as hot carrier and heterojunction diodes. Improvements in concepts of both hot carrier (Harrison & Zucker, 1966) and heterojunction (Lechner et al., 1980) diodes led to planar asymmetrically shaped and bow-tie designs. Planar microwave diodes based on high carrier mobility heterojunctions of A_3B_5 compounds, such as GaAs and AlGaAs (Gradauskas et al., 2010), and modulation-doped two-dimensional electron gas structures (Seliuta et al., 2004) are promising in high-frequency electromagnetic radiation sensing applications. Variations of these microwave diodes were investigated in search of optimal composition and design for better detection properties (Sužiedėlis, Ašmontas, Kundrotas, Gradauskas, Čerškus, Nargelienė & Anbinderis, 2012; Sužiedėlis et al., 2016a; Minkevičius et al., 2011; Kašalynas, Venckevičius, Seliuta, Grigelionis & Valušis, 2011; Kašalynas, Venckevičius & Valušis, 2013). However, their main drawback is low voltage sensitivity and high electrical resistance.

Relevance of the Dissertation

Most potential microwave applications in key technology fields, such as communication, imaging, science, and medicine, require electromagnetic radiation detectors with certain specifications. Devices capable of registering and measuring the power of microwave radiation must be robust, cost-effective, and have fast response time operating at room temperature. It is crucial for achieving comparatively high sensitivity properties in a wide frequency range and low electrical resistivity. Moreover, the detection properties should have minimal dependency on temperature, pressure, humidity, and other environmental factors. The search for advanced concepts of high-frequency electromagnetic detection stimulates the creation of new designs of bulk-based semiconductor microwave diodes, such as planar asymmetrically shaped devices based on non-uniform carrier heating phenomena with two-dimensional electron gas layer or with a small contact area as well as gate-controlled diodes.

Last but not least is the necessity for effective and convenient characterization systems of the described detectors. Evaluation of electrical parameters and detection properties of planar semiconductor microwave diodes can be performed using probing techniques allowing to perform reliable and timesaving measurements on the wafer.

Research Object

The object of this research is new planar microwave diodes fabricated based on AlGaAs/GaAs, AlGaAs, and GaAs semiconductor compounds.

Aim of the Dissertation

The main aim of the dissertation is to develop and investigate new microwave diodes with a lower spread of their electrical parameters and capable of detecting an electromagnetic signal in the millimeter-wavelength range.

Tasks of the Dissertation

To solve the problem and achieve the aim of the dissertation, the following tasks must be accomplished:

1. To master the fabrication techniques of semiconductor devices and to create new planar microwave diodes based on semiconductor structures for electromagnetic signal detection applications in the millimeter-wavelength range.
2. To investigate current-voltage characteristics using the direct current probing measurement method and to determine electrical parameters of the created microwave diodes.
3. To investigate the detection properties of the created microwave diodes in the millimeter-wavelength range and determine their voltage sensitivity using high-frequency probing techniques and by mounting the diodes in a waveguide transmission line.

Research Methodology

The following research methods were applied in this work: Poisson simulation (energy bands and electron density diagrams of the semiconductor structures); photolithography, wet chemical etching, thermal evaporation and annealing techniques (fabrication of the microwave diodes); finite element method (simulation of electric field distribution in the microwave diodes); direct current probing technique (electrical parameters of the microwave diodes); high-frequency probing technique with coaxial-waveguide transmission line and detector mount with microstrip line and waveguide transmission line (detection properties of the microwave diodes); statistical and analytical evaluation methods (validation of experimental results).

Scientific Novelty of the Dissertation

This research achieved the following scientific novelty:

1. The new design planar dual microwave diodes and bow-tie diodes with a gate over a two-dimensional electron gas layer were developed based on GaAs, AlGaAs, and AlGaAs/GaAs compounds. Their electrical parameters were determined, and their detection properties were investigated in a wide frequency range from 26 to 330 GHz.
2. It is evidenced that a partial metal gate covering either the narrow or wide parts of the asymmetrically shaped semiconductor structure can be used for the increase of voltage sensitivity of the bow-tie diode.
3. Measurement technique using a high-frequency probe station is proposed allowing to efficiently investigate the dependence of detected voltage on power and frequency characteristics of the detected voltage of planar microwave diodes in the 26.5–40 GHz frequency range.

Practical Value of the Research Findings

The designed and investigated new original planar dual microwave diodes and heterostructured bow-tie diodes with a gate over a two-dimensional electron gas layer fabricated based on AlGaAs/GaAs, AlGaAs, and GaAs compounds can be used as detector diodes in a transmission line for low-power measurements. Electrical parameters and high-frequency properties of the microwave diodes can be investigated using suggested direct current and high-frequency probe station measurement setups. This measurement approach can both save time and exclude the possibility of diode damage.

The research results of bow-tie gated diodes with a two-dimensional electron gas channel based on AlGaAs/GaAs heterostructure presented in this dissertation were used to implement the European patent:

– State Patent Bureau of the Republic of Lithuania, “Sensor for Electromagnetic Radiation of Microwave and Terahertz Frequencies” (European Patent No. 3582269).

The research results presented in this dissertation were also used for the implementation of two scientific projects:

1. Research Council of Lithuania, National Program “Towards Future Technologies,” “New Broadband Sensors of Electromagnetic Radiation on the Base of Two-Dimensional Electron Gas Channel” (grant No. LAT-03/2016, “Nauji plačiajuosčiai elektromagnetinės spinduliuotės jutikliai su dvimatėmis elektronų protakomis”).
2. Research Council of Lithuania, International Cooperation Program “Lithuania–Ukraine,” “New Microwave Diodes for Detection of Directed Electromagnetic Radiation” (grant No. S-LU-20-7, “Nauji mikrobangų diodai kryptinei elektromagnetinei spinduliuotei aptikti”).

Defended Statements

1. Planar dual microwave diodes and bow-tie microwave diodes with a partial gate over a two-dimensional electron gas layer fabricated based on GaAs, AlGaAs, and AlGaAs/GaAs semiconductor compounds, are suitable for pulsed and continuous millimeter-wavelength signal detection in the picowatts to milliwatts signal power range.
2. Partial gating by means of covering a narrow or wide part of the asymmetrically shaped selectively doped semiconductor structure with a metal layer allows increasing voltage sensitivity of the bow-tie microwave diodes up to two orders of magnitude.
3. The measurement setup developed based on a high-frequency probe station allows effective investigation of voltage detected across planar microwave wafer-based diodes and its dependence on power and frequency in the 26.5–40 GHz frequency range under conditions of various temperatures and illumination.

Approval of the Research Findings

The main results of the dissertation were published in five scientific papers: three papers in scientific journals included in the *Clarivate Analytics Web of Science* database with an impact factor and two papers in conference proceedings included in the *Clarivate Analytics Web of Science* and *Scopus* databases.

The research results on the dissertation's topic were presented at twelve scientific conferences:

– International Conference for Students and Young Researchers "*Open Readings"* (2017 & 2019), Vilnius, Lithuania.
– Conference of Young Scientists "*The Future of Lithuania: Electronics and Electrical Engineering*" (2017 & 2019), Vilnius, Lithuania.
– *"42-nd & 43-rd Lithuanian National Physics Conference"* (2017 & 2019), Vilnius & Kaunas, Lithuania.
– Conference of Young Scientists *FizTech* (2017), Vilnius, Lithuania.
– International Conference *"Progress in Electromagnetics Symposium"* (2017), Singapore.
– International Conference *"Energy Materials and Nanotechnology Vienna Meeting"* (2018), Vienna, Austria.
– *"The 8th International Conference on Electronics, Communications and Networks"* (2018), Bangkok, Thailand.
– *"6th International Conference on Sensors and Electronic Instrumentation Advances"* (2020), Porto, Portugal.
– International Conference *"Ukrainian Microwave Week"* (2020), Kharkiv, Ukraine.

Structure of the Dissertation

The dissertation consists of an introduction, four chapters, general conclusions, an extensive list of references, a list of the author's publications on the dissertation's topic, and a summary in Lithuanian.

The volume of the dissertation is 175 pages, including 85 figures, 26 formulas, and 11 tables. The dissertation has 224 reference sources.

Acknowledgments

I am deeply grateful to:

Prof. Dr Algirdas Sužiedėlis for assurance and assistance at every stage of the research.

Prof. Dr Steponas Ašmontas, Prof. Dr Jonas Gradauskas, and my colleagues from the Laboratory of Electronic Processes for their insightful comments and suggestions.

Center for Physical Sciences and Technology for the opportunity to accomplish my research and prepare this dissertation.

The Braun Center for Submicron Research at the Weizmann Institute of Science for help and knowledge in the fabrication of the samples.

Vilnius Gediminas Technical University for the opportunity to defend this dissertation.

My grandfather, Dr Tomas Anbinderis, and my father, Pavel Anbinderis, for leading me into the world of science, and my family for their unwavering support and belief in me.

1

Electrical, High-Frequency Detection Properties and Applications of Microwave Detectors

This chapter covers the review of electrical and HF properties of MW diode-based detectors with quasi-linear and non-linear current-voltage characteristics and heterostructured MW diodes with 2DEG. Next, the discussion covers possible application technologies for MW diodes in the MMW range and methods for investigating their electrical and HF properties using probing systems. The research results presented in this chapter were published in the author's publications Sužiedėlis et al., 2017a, 2017b; Ašmontas et al., 2020; Anbinderis et al., 2020; Anbinderis et al., 2021.

1.1. Electrical and High-Frequency Properties of Microwave Diodes with Quasi-Linear and Non-Linear Current-Voltage Characteristics

MW sensors are elements capable of sensing and measuring the electromagnetic radiation of MW, including the MMW range. At these wavelengths, power is the basic measure of the signal's magnitude rather than voltage or current. Power has been adopted as the primary measurement quantity of any RF (including MW range) signal propagating in a transmission line (waveguide) since the propagation distance in conductors becomes much smaller at these frequencies, and signal reflections, standing waves, and impedance mismatch can all become very significant error sources ("Principles of Power Measurement: A Primer on RF & Microwave Power Measurement," 2011).

A properly designed and calibrated power sensor can minimize these effects and allow for accurate and repeatable amplitude measurements ("Principles of Power Measurement: A Primer on RF & Microwave Power Measurement," 2011). Power measurement devices convert the RF power to a measurable DC or low-frequency signal using different methods ("Fundamentals of RF and Microwave Power Measurements," 2000). The main principle of measuring this kind of RF radiation is usually based on using either a detector mount with a detecting diode, a thermistor detector mount or a thermocouple detector mount for power measurements in the transmission line.

A thermistor detector (a bolometer detector type) is among the first power sensors. These power meters are used as primary standard transmission power meters for RF measurements due to satisfactory accuracy, long-term stability, and power substitution capability ("Fundamentals of RF and Microwave Power Measurements," 1977; Lindsay, 2016; Roy, Kush, & Dixit, 2011; Collier & Skinner, 2007). Still, the dynamical range of a thermistor is very limited (sometimes only –20 dBm to +10 dBm), it is easily damaged and has a slow response time, with a continuous wave CW burnout of only around +20 dBm (Lindsay, 2016; Collier & Skinner, 2007). Due to these disadvantages, thermistor mounts are not the detection technology of choice in current practical applications.

For more than 50 years, thermocouple detectors have been used as the best method for RF power measurements due to a good impedance match between thermocouple element and a transmission line as well as higher sensitivity than thermistors ("Fundamentals of RF and Microwave Power Measurements," 2000; Lindsay, 2016). An important feature that lets this detector type handle complex modulated signals or signals of multiple tones is the square-law detection characteristic ("Fundamentals of RF and Microwave Power Measurements," 2000). In addition, they are more rugged than thermistors, making useable power measurements from –30 dBm or –35 dBm to +20 dBm and having a lower measurement uncertainty due to the better SWR (Lindsay, 2016). On the downside, they exhibit slower measurement speeds than other sensors and have rise times in the millisecond range, thus making them suitable for measuring only the average power of the signal (Lindsay, 2016; Collier & Skinner, 2007). Although the sensitivity is higher than that of the thermistor detector, it is still relatively low, limiting usefulness when the RF power level is less than several microwatts (“Principles of Power Measurement: A Primer on RF & Microwave Power Measurement,” 2011).

It is worth mentioning that both the thermistor and thermocouple power meters operate on a heat-based principle, i.e., they are thermal sensors and are generally used for sensing and measuring only the average RF power.

Diode detectors are another type of power sensor with a wider dynamical range and a faster response than detectors working on the heating principle (Lindsay, 2016; Collier & Skinner, 2007), making them the detection technology of choice for practical measurements today. Although, thermal sensors have greater accuracy and, e.g., are used for calibration measurements or for absolute reference to national standards.

Generally, so-called detector mounts are used in diode-based power sensors. A detector mount consists of an MW rectifying semiconductor diode, serving as the main sensing element, and of RLC elements used for filtering. Rectifying diodes have long been used for relative power measurements at MW frequencies (“Fundamentals of RF and Microwave Power Measurements,” 1977). The earliest devices were simple crystal detectors that used PbS and a cat whisker to form a crude diode junction (“Principles of Power Measurement: A Primer on RF & Microwave Power Measurement,” 2011). They were suitable mostly for envelope detection and were used as non-linear mixer components in super-heterodyne receivers (“Fundamentals of RF and Microwave Power Measurements,” 2000). Nowadays, it is a broadband device that is used to detect, monitor, and measure a modulated signal of the MW and MMW range and is capable of measuring pulse signals of short duration (Vostkov, Revin & Shashkin, 2020; Sužiedėlis et al., 2016a; Gradauskas et al., 2010).

The main detection principle of an MW diode is based on current rectification at high power levels and acting as a non-linear resistor at low-power levels, conducting more current in the forward direction than in the reverse one (“Principles of Power Measurement: A Primer on RF & Microwave Power Measurement,” 2011). Diodes in MW power sensors directly convert HF energy to DC by rectifying MW currents, which arise from their non-linear *IV* characteristic (Fig. 1.1) (“Fundamentals of RF and Microwave Power Measurements,” 1977). DC voltage is measured and scaled to produce a power readout by the power meter (“Principles of Power Measurement: A Primer on RF & Microwave Power Measurement,” 2011). It is worth noting that the rectifying nature of the DC voltage induced under the MW radiation tends to expect a decay of detection properties with frequency (Gradauskas et al., 2010).

However, the widely known Si *p-n* junction diode with a non-linear *IV* characteristic was not suitable for MW detection because it was a slow device with limited frequency bandwidth as it is a minority carrier device. High impedance was inherent at zero bias; thus, the detected voltage of the *p-n* junction was very low if the MW signal was not large enough to drive the junction to the point where significant current begins to flow (≈ 0.7 V) (“Fundamentals of RF and Microwave Power Measurements,” 1977). Although efforts have been made to bias the *p-n* junction diode to cause significant rectified current, a large amount of noise and thermal drift still did not make it attractive for MW power detection (“Fundamentals of RF and Microwave Power Measurements,” 2000). It should be noted that recent studies suggest modern Si CMOS devices capable of operating between 100 and 700 GHz (Seok et al., 2010).

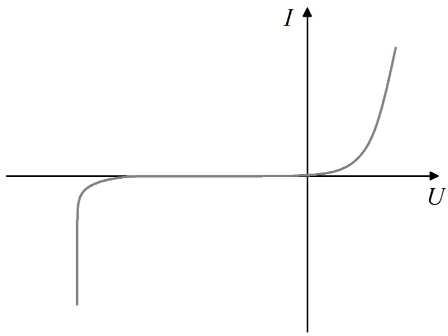

Fig. 1.1. *IV* characteristic of a detecting diode (“Fundamentals of RF and Microwave Power Measurements,” 2000)

Mathematically, the current I flowing through the detecting diode (Schottky type) can be described according to Equation 1.1 (“The Zero Bias Schottky Detector Diode,” 1994):

$$I = I_\mathrm{s}(\mathrm{e}^{\alpha U} - 1), \tag{1.1}$$

here, I_s is the saturation current (constant at a given temperature), and U is the voltage across the diode. Parameter $\alpha = q/nkT$, where k is Boltzmann’s constant, T is the absolute temperature of the diode, q is the elemental charge of the electron, and n is the non-ideality factor. Equation 1.1 can be written as in power series to better analyze the rectifying action (“Fundamentals of RF and Microwave Power Measurements,” 2000):

$$I = I_\mathrm{s}\left(\alpha U + \frac{(\alpha U)^2}{2!} + \frac{(\alpha U)^3}{3!} + \cdots + \frac{(\alpha U)^\mathrm{n}}{\mathrm{n}!}\right). \tag{1.2}$$

According to Equation 1.2, the current rectification in a diode is performed by the second and other even orders of the series. For small signals, only the second-order term is significant, so the diode is said to operate in the square-law region ("Fundamentals of RF and Microwave Power Measurements," 1977), i.e., when the MW input is not high enough to cause the diode to fully conduct in the forward direction, the diode behaves as a non-linear resistor and produces a DC output that is closely proportional to the squared MW input voltage ("Principles of Power Measurement: A Primer on RF & Microwave Power Measurement," 2011). In this region, the diode acts as a modulation-independent averaging detector. When the voltage is so high that the higher-order terms become significant, the diode response is no longer in the square-law region, and it then rectifies according to a quasi-square-law in the *IV* region, which is sometimes called the transition region ("Fundamentals of RF and Microwave Power Measurements," 2000). Above that range, the diode becomes a large signal rectifier and moves into the linear detection region when the average DC output voltage is proportional to the peak input voltage ("Fundamentals of RF and Microwave Power Measurements," 2000; Lindsay, 2016). In this region, the diode behaves like a peak detector (also called "envelope") and works in the forward direction ("Principles of Power Measurement: A Primer on RF & Microwave Power Measurement," 2011).

Typically, the square-law region is from the noise level up to ≈ –20 dBm input power, the transition region ranges from –20 to 0 dBm and the linear detection region is above 0 dBm ("Fundamentals of RF and Microwave Power Measurements," 2000; Lindsay, 2016; "Principles of Power Measurement: A Primer on RF & Microwave Power Measurement," 2011).

The simplified circuit of an unbiased diode device for detecting low-level MW signals is illustrated in Fig. 1.2.

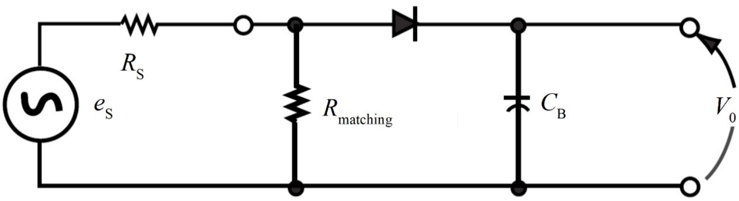

Fig. 1.2. Circuit diagram of the diode detector with a source and matching resistor ("Fundamentals of RF and Microwave Power Measurements," 2000)

The input MW signal is applied to a load-matching resistor, which is in series with a diode parallel to a capacitor (barrier). Typically, the diode's resistance for small RF signals is much larger than 50 Ω, and a separate matching resistor is used to set the power sensor's input termination impedance ("Fundamentals of RF and Microwave Power Measurements," 2000; "The Zero Bias Schottky Detector Diode," 1994). As the power rises, the diode controls the current/voltage across the capacitor, which is then read and processed into a voltage/power reading (Lindsay, 2016).

As mentioned above, detection occurs because the diode has a non-linear *IV* characteristic. As the voltage across the diode is rectified, then a DC output voltage results. Usually, a smoothing (not depicted in Fig. 1.2) capacitor is connected to the output of the diode to convert the pulsating DC to a steady DC voltage ("Principles of Power Measurement: A Primer on RF & Microwave Power Measurement," 2011).

The maximum power of the MW signal is transferred to the diode when the diode resistance matches the generator source resistance. The diode resistance at zero applied voltage can be found by differentiating Equation 1.1 ("Fundamentals of RF and Microwave Power Measurements," 1977):

$$R_0 = \frac{1}{\alpha I_s}. \tag{1.3}$$

The 0 stands for zero bias input voltage. Resistance R_0 strongly depends on temperature; thus, the diode voltage sensitivity and reflection coefficient are also strong functions of temperature ("Fundamentals of RF and Microwave Power Measurements," 1977). Thus, to minimize the temperature dependence, R_0 is much larger than the generator source resistance. On the other hand, when R_0 is too large, it results in a decrease in voltage sensitivity due to poor conversion of the MW signal into DC voltage ("Fundamentals of RF and Microwave Power Measurements," 1977). A compromise between good voltage sensitivity to small signals and good temperature performance results from making I_s of about 10 µA and R_0 between 1 to 2 kΩ ("Fundamentals of RF and Microwave Power Measurements," 2000). This compromise can be achieved in diodes that have a low-potential barrier across the metal-semiconductor junction – Schottky diodes.

As previously mentioned, the development of semiconductor diodes that operate in HF bands began with point-contact technology, which evolved from the PbS crystal and cat whisker diode types in early radio (Sze, 1981). The traditional point-contact diode formed a metal-semiconductor ("Fundamentals of RF and Microwave Power Measurements," 1977). The first point-contact diodes were extremely mechanically and electrically fragile, not repeatable (due to the very variable resistance and capacitance), and subject to change with time ("Fundamentals of RF and Microwave Power Measurements," 2000). LBS diodes succeeded in point-contact technology (Fig. 1.3). Precision semiconductor fabrication processes for Si made it possible to construct LBS diodes with metal-semiconductor junctions for MW frequencies that were very rugged because of the larger junction area and were consistent from diode to diode ("Fundamentals of RF and Microwave Power Measurements," 2000). LBS diodes became very popular in MW power sensing applications as they showed good MW performance and exhibited a low-potential barrier across their junction of

≈ 0.3 eV as well as low enough junction capacitance of ≈ 0.1 pF (junction capacitance and other parasitic reactances must be kept small to achieve frequency independent performance) ("Fundamentals of RF and Microwave Power Measurements," 2000). They were able to detect and measure power as low as –70 dBm (100 pW) at frequencies up to 18 GHz ("Fundamentals of RF and Microwave Power Measurements," 1977).

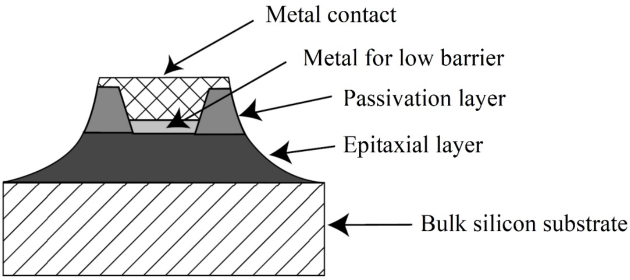

Fig. 1.3. Cross-sectional view of an LBS diode ("Fundamentals of RF and Microwave Power Measurements," 2000)

Detectors built based on the Schottky diode are used extensively in a wide range of MW and MMW applications (Siegel, 2002; Shashkin et al., 2007; Kearney, 1992; "Virginia Diodes Inc. Zero Bias Detector"), and their main advantage is high voltage sensitivity and repeatability (Hesler & Crowe, 2007; "Zero Bias Schottky Detector Diode," 1994; Sankaran & Kenneth, 2005). Still, in some cases, their application encounters undesirable shortcomings: because of the surface location of the Schottky (metal-semiconductor) junction, such diodes have poor long-term electrical stability and weak reliability characteristics at high-radiation levels (Harrison & Zucker, 1966; Sužiedėlis et al., 2016a; Shashkin et al., 2007; Kearney & Dale, 1990).

As the GaAs heterostructure semiconductor material technology advanced in the 1980s, such devices exhibited superior performance over Si at MW frequencies ("Fundamentals of RF and Microwave Power Measurements," 2000). GaAs is mainly used because of its high carrier mobility and fast response in the MW and MMW range. A PDB diode was introduced with advanced detection properties at higher frequencies (Malik et al., 1980). The sophisticated technology of the PDB diode fabrication relied on a material preparation process called MBE, suitable for growing very thin epitaxial layers ("Fundamentals of RF and Microwave Power Measurements," 2000) and the flexibility to alter the barrier height by adjusting doping concertation which made it the proper competitor to LBS diodes (Kearney, Condie & Dale, 1991; Dale, Neylon, Condie & Kearney, 1989a). It was shown (Dale, Neylon, Condie, Hobden & Kearney, 1990) that PDB diodes also have better $1/f$ noise properties than Schottky equivalents. Kearny (Dale, Neylon, Condie & Kearney, 1989b) was the first to suggest a GaAs PDB diode for MW and MMW detector application as an alternative to Schottky. The doping profile of the PDB device is n^+i-p^+-i-n^+, with intrinsic layers spaced between the n^+ and p^+ regions (Fig. 1.4) ("Fundamentals of RF and Microwave Power Measurements," 2000; Dale et al., 1989a; Malik et al., 1980).

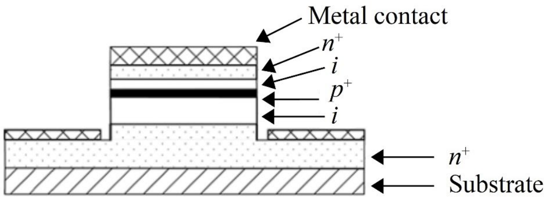

Fig. 1.4. Cross-sectional view of a PDB diode ("Fundamentals of RF and Microwave Power Measurements," 2000)

The *IV* characteristic of the PDB has a high degree of asymmetry, which is related to the alteration of the layer thickness and doping concertation (Dale et al., 1989a; Anand & Hillson, 1991), meaning that it can be "engineered" (Kearney, Kerr, Kelly, Condie & Dale, 1989; Couch & Kearney, 1989). The p^+ region is located between the two intrinsic layers i of unequal thickness.

This *IV* asymmetry is necessary for PDB devices to achieve direct rectification of the input MW signal at zero bias (Dale et al., 1989a). An important feature of the PDB diode is that the device can be designed having junction capacitance C_o, which is both extremely small (20 fF or less) and nearly independent of the bias voltage or metal contact pad area ("Fundamentals of RF and Microwave Power Measurements," 2000). Moreover, an increase in the dynamic range (Kelly, 1996) was achieved in comparison with the LBS Si Schottky diode due to the lower resistance of the junction, which lowers the RC time constant of the junction and increases the cut-off frequency of the diode ("Fundamentals of RF and Microwave Power Measurements," 2000; Kearney et al., 1989a).

In addition, a PDB diode is far less frequency-sensitive than a normal p-n junction diode because of the intrinsic layer at the junction as the equivalent capacitance of the p-n junction diode changes with voltage (MW power), but in the PDB diode, junction capacitance is determined by the intrinsic layer, which remains almost constant as a function of power ("Fundamentals of RF and Microwave Power Measurements," 2000).

The voltage sensitivity of PDB diodes reached up to 2700 V/W at 35 GHz frequency and 500 V/W at 94 GHz frequency (Kearney et al., 1991; Kearney, 1992). However, only concept devices were designed, and no major improvements in detection properties were reached (Vo & Hu, 2006; Vo et al., 2004; Hu, Van Tuyen & Rezazadeh, 2005), encountering inefficiency in practical application due to challenging doping tolerances.

An LBS metal-semiconductor junction and PDB diodes were introduced because of the low-barrier potential. Throughout the years, other types of diode-based sensors have been investigated and suggested for metrology applications. For example, backward diodes (a tunnel diode type) with high non-linearity for small signal detection in the MMW range (Burrus, 1963).

Due to the structure of a backward diode, the reverse current is higher than the forward current when a low voltage is applied. Jin et al. (2005) suggested a Si-based backward diode for zero-biased square-law low-frequency detection, and practical investigations were performed up to 1.8 GHz (Park et al., 2007). More successful investigations of backward diodes as MMW detectors suggested *n*-InAs/AlSb/*p*-GaAsSb heterostructure (Schulman & Chow, 2000; Schulman et al., 2001, 2002). The diodes were able to operate up to 110 GHz, although a vast decrease in voltage sensitivity was observed at frequencies higher than 10 GHz. Further improvements suggested a zero-biased backward diode for MMW detectors and mixers based on p^+-GaAsSb/*i*-InAlAs/*n*-InGaAs with voltage sensitivity up to 2100 V/W at 94 GHz (Takahashi, Sato, Nakasha & Hara, 2012) and operating up to 330 GHz (Patrashin et al., 2015a, 2015b), although high-level non-monotonic dependency of voltage sensitivity on frequency is still inherent as well as poor reliability.

As an alternative, MW diodes based on the major carrier phenomena were proposed (Shannon, 1979; Malik et al., 1980; Lechner, Kneidinger, Thim & Kuch, 1979, Lechner et al., 1980; Harrison & Zucker, 1966). Harrison (Harrison & Zucker, 1966) proposed a hot carrier point-contact MW detector with the operation based on the thermoelectric power of hot carriers (Požela & Repšas, 1968; Zucker, 1964; Harrison & Zucker, 1963) in semiconductors. Generally, these types of diodes are called thermoelectric. The operation of a thermoelectric diode is based on the occurrence of non-uniform free carrier heating in the electric field of the point contact (Sužiedėlis, Ašmontas, Kazlauskaitė & Gradauskas, 2009).

MW diode detectors operating based on the thermoelectric effect of hot carriers in bulk semiconductors are characterized by a wide operation frequency range, high burnout power, and high electrical stability over a long period of use (Ašmontas, Gradauskas, Sužiedėlis & Valušis, 2000). The mechanism involved is such that the detection sensitivity is independent of frequency, and the input impedance is independent of input power (Harrison & Zucker, 1966). The first *p*-type semiconductor diodes made with InSb and Ge operated in the X-band (Harrison & Zucker, 1966; Oshimoto & Kikuchi, 1973; Kikuchi & Oshimoto, 1981).

Various semiconductor materials and shapes, such as a small-area GaAs nn^+ junction (Sužiedėlis et al., 2016b) and small-area contacts of different metals with p-type Ge (Malik et al., 1980), small-area n-n^+ junctions in Si (Sze, 1981), were proposed in search of greater voltage sensitivity. However, the voltage sensitivity of Schottky diodes was still higher. The increase in voltage sensitivity by more than one order was achieved by the insertion of the AlGaAs/GaAs heterojunction in series with the n-n^+ junction of the point contact hot carrier diode (Sužiedėlis et al., 2009). The ternary $Al_xGa_{1-x}As$ compound was used as the additional input of the MW current rectification, and it was stated that the compound with $x = 0.3$ showed the highest voltage sensitivity values reaching 30 V/W in the X-band (Sužiedėlis et al., 2009; Ašmontas et al., 1999), although a decrease of the sensitivity was observed in the K_a-range (Sužiedėlis, Ašmontas, Kundrotas, Nargelienė & Gradauskas, 2012).

However, the construction of point-contact thermoelectric diodes, namely, the 3D structure of semiconductor crystal with a sharpened metallic whisker, limited the frequency range of operation and made it problematic to mount the diode in a rectangular waveguide, particularly in the HF range, and having both sensitive and fast detectors at the same time (Ašmontas et al., 2000). The construction of a thermoelectric diode is close to a typical point-contact diode (Fig. 1.5): a doped semiconductor in between small- and large-area Ohmic contacts. The electric power is inducted due to the non-homogeneous heating of free carriers when the MW field is applied to the semiconductor, i.e., the electron temperature difference determines the origin of thermoelectric voltage.

The construction of the asymmetrically necked planar bow-tie type diode was suggested as an analog to the point-contact thermoelectric diode (Ašmontas et al., 2000; Ašmontas & Sužiedėlis, 1994). The choice of planar construction allows one to reach impedance matching in a simpler way and to avoid both design and application limitations inherent in point-contact diodes (Gradauskas et al., 2010). Planar semiconductor technology allowed small surface-oriented MW diodes to be produced with both terminals lying on the same surface of the semiconductor wafer. The idea was based on a bigradient diode with an asymmetrically necked semiconductor structure with EMF appearing under the influence of a strong electric field (it was called a bigradient force) (Ašmontas, Požela & Repšas, 1971; Ašmontas, 1984). It was discovered by measuring *IV* characteristics in n-Ge (Ašmontas, Požela & Repšas, 1975) and n-Si (Ašmontas, 1975) semiconductors at temperatures of 300 K and 77 K. Although these bigradient diodes had high electrical resistance, so in planar thermoelectric diodes the more necked side was doped that resulted in lower electrical resistance and faster operation speed (Ašmontas et al., 2000). In this case, the detected voltage consists of both the bigradient and hot carrier thermoelectric forces (Ašmontas, Gradauskas, Kožič, Shtrikmann & Sužiedėlis, 2005; Ašmontas et al., 2009). Non-uniform heating in the planar thermoelectric diode was achieved, namely, using an asymmetrically necked thin semiconductor film containing the *n*-n^+-GaAs junction and the *n*-Si doped monocrystal structure (Ašmontas & Sužiedėlis, 1994; Ašmontas et al., 2005).

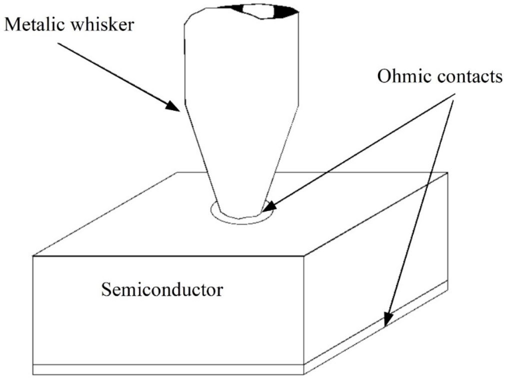

Fig. 1.5. Point-contact hot electron thermoelectric diode

Planar thermoelectric MW detecting diodes were able to operate from MW (Ašmontas & Sužiedėlis, 1994) up to the IR range (Sužiedėlis, Gradauskas, Ašmontas, Valušis & Roskos, 2003) including terahertz frequencies. They were able to withstand high-power electromagnetic radiation and had high operation speed determined by the carrier energy relaxation time of the picosecond order (Ašmontas, Gradauskas, Sužiedėlis, Širmulis & Urbelis, 2006); however, these diodes had low voltage sensitivity. Planar GaAs/AlGaAs heterojunction (Fig. 1.6) diodes outrivaled those diodes due to the ability to improve voltage sensitivity by choosing an appropriate AlAs mole fraction in the AlGaAs layer (Gradauskas et al., 2010) and due to the supplementary contribution of intervalley EMF of hot carriers (Sužiedėlis et al., 2014). Lechner (Lechner et al., 1979) was the first to investigate *n*-GaAs/*n*-AlGaAs heterojunctions grown on highly doped GaAs substrates using the LPE method for MW sensing applications. MW detector diodes made of these layers were chosen due to excellent lattice match and have operated successfully for the first time at frequencies up to 18 GHz. The open-circuit voltage sensitivity was comparable to that of commercially available Schottky barrier diodes. Semiconductor heterostructures revealed themselves as proper candidates for MW and IR detection (Ašmontas et al., 1997, 1999; Ašmontas, Gradauskas, Seliuta & Širmulis, 2001). It is worth mentioning that the non-linearity of the *IV* characteristic appears due to the heterostructure of two single-crystal materials with matched or slightly mismatched crystal lattices (Vostkov et al., 2020). Wideband HF applications required convenient construction of the detecting diodes; therefore, a planar design of heterojunction diodes was proposed (Sužiedėlis et al., 2003). Planar heterojunction diodes had better reliability than the Schottky diode as the active region is located in the bulk semiconductor structure of asymmetrically necked heterojunction diode (Sužiedėlis et al., 2016a).

A schematic view of the planar heterojunction diode detecting MW radiation is presented in Fig. 1.6. A polyimide film depicted in the figure acts as an upper transparent layer holding the semiconductor GaAs/AlGaAs mesa with metallic contacts beneath it.

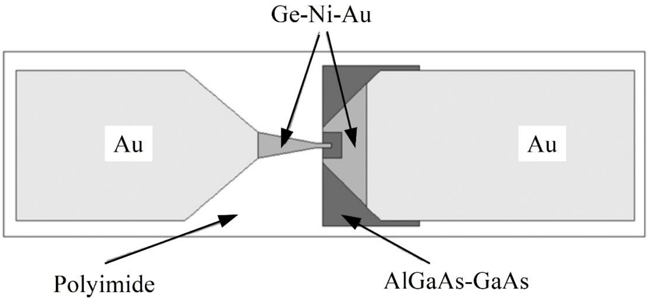

Fig. 1.6. Schematic top view of GaAs/AlGaAs planar heterojunction diode (Gradauskas et al., 2010)

AlGaAs/GaAs heterojunction planar MW diodes with detection properties based on free charge carrier heating were investigated for MW and IR applications (Ašmontas et al., 2010). The 5 μm^2 semiconductor heterostructure consisting of MBE-grown n-GaAs and n-$Al_{0.3}Ga_{0.7}As$ epitaxial layers of 300 nm thickness sandwiched between heavily doped n^+-GaAs and n^+-$Al_{0.3}Ga_{0.7}As$ contact layers was chosen to reduce the MW current's shunting through the substrate and increase the frequency range. The MBE technique allows growing structures with abrupt semiconductor junctions, which is essential to achieve a rectifying structure (Gradauskas et al., 2010), in contrast to the LPE method producing graded-gap Ohmic heterojunctions (Womac & Rediker, 1972). According to (Ašmontas et al., 2010), the non-linear *IV* characteristic is a superposition of characteristics of the Schottky metal-semiconductor junction and the AlGaAs/GaAs heterojunction. The metallic contact of the small upper area (Fig. 1.6) forms an LBS junction with the lightly doped n-AlGaAs layer, while during the MBE growth, another potential barrier located in the GaAs/AlGaAs heterojunction is formed (Gradauskas et al., 2010). Depending on the polarity of the applied voltage, the Schottky junction and heterojunction were biased in opposite directions, i.e., the forward bias voltage determines the backward Schottky diode, and the reverse bias voltage determines the backward heterojunction diode. These diodes were named "double-backward-diodes" since the structure acts as Schottky and heterojunction diodes connected in series in opposite directions, as depicted in Fig. 1.7.

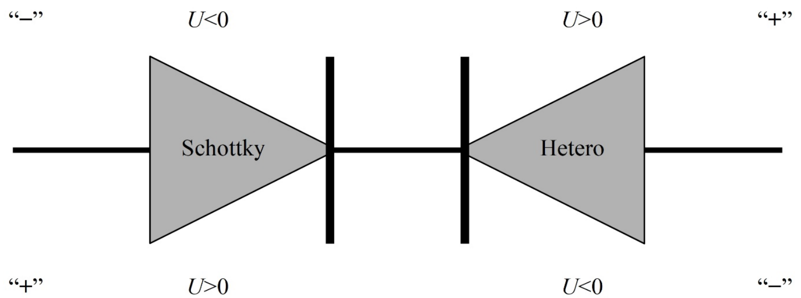

Fig. 1.7. Equivalent schematic view of a double-backward-diode. The polarity of applied voltage: upper "–" and "+" signs – backward Schottky diode; lower "+" and "–" signs – heterojunction diode biased in the backward direction (Gradauskas et al., 2010)

The voltage sensitivity reached 1000 V/W in the K_a-frequency range at room temperature, and the diodes were able to detect nanosecond pulses of CO_2 laser radiation (Ašmontas et al., 2010). At higher frequencies (W band), the voltage sensitivity was lower more than by one order, and at the D-band dropped down to 10 V/W. Further studies (Gradauskas et al., 2010) were performed on AlGaAs/GaAs heterojunction planar MW diodes with a doping density of n-$Al_{0.3}Ga_{0.7}As$ and n-GaAs layers equal to 10^{16} cm^{-3}. The asymmetry of the *IV* characteristic was evaluated as it is essentially important for the sensitivity properties. Higher asymmetry of the *IV* characteristics allows for expecting higher voltage sensitivity. The voltage sensitivity reached 2000 V/W in the K_a-frequency range at room temperature, and the dynamic range remained linear for power levels lower than 100 μW. However, the upper limit of the dynamic range decreased for diodes having higher voltage sensitivity, which questioned the reliability of these diodes at MW power higher than tens of milliwatts. The possibility to increase the voltage sensitivity at lower temperatures and the possibility of detection in the subMMW range was also reported, although radiation detection going from MW to IR range should not be expected.

Ašmontas and Sužiedėlis (Sužiedėlis et al., 2012b, 2013) proposed variations of the heterojunction planar MW diodes: GaAs/$Al_xGa_{1-x}As$ with different AlAs mole fraction ($x = 0.1, 0.2, 0.25, 0.3$) (Sužiedėlis et al., 2012b) and GaAs/AlGaAs heterojunction diodes with symmetrically doped narrow- and wide-gap semiconductors as well as heterojunction diode with different doping of semiconductor epitaxial layers n-GaAs and n-$Al_{0.2}Ga_{0.8}As$ (Sužiedėlis et al., 2013). The highest voltage sensitivity reached 200 V/W with $x = 0.2$ and more than 100 V/W with $x = 0.25$ in the W-band, while the voltage sensitivity of the GaAs/Al$_x$Ga$_{1-x}$As diodes with $x = 0.3$ and $x = 0.1$ was by at least one order lower. Thus, the optimal composition was determined. The current rectification and carrier heating phenomena were responsible for the emergence of the voltage response under MW radiation (Sužiedėlis et al., 2012b). Further studies (Sužiedėlis et al., 2016a) include large-area (3×10^{-9} m^2) and small-area ($(10 \div 100) \times 10^{-12}$ m^2) GaAs/Al$_x$Ga$_{1-x}$As heterojunction MW detection diodes with AlAs mole fraction 0.25. The non-ideality factor of the exponential *IV* characteristic was greater for the large-area heterojunction diode, as a larger area leads to a larger amount of imperfectness in the heterojunction. The height and width of the barrier were reported to be almost independent of the area of the heterojunction. Investigations revealed that these small-area heterojunction diodes are capable of detecting CW MW power in the K$_a$-frequency range with voltage sensitivity reaching up to 700 V/W and 10 V/W when measuring pulsed MW power with 50 Ω load parallel to the diode. The voltage sensitivity of the large-area heterojunction diodes was at least two orders lower, and a 50 Ω load was not necessary for pulsed measurements since the differential resistance of the diode was 150 Ω. The detected voltage was dependent linearly up to the milliwatt range, and the dynamic range was wider for the large-area heterojunction diodes. Temperature influence on the detection properties of the heterojunction diodes (Sužiedėlis et al., 2014) in the range of 150–300 K showed that the non-ideality factor of the *IV* characteristic increases with temperature decrease as well as the detected voltage. It was stated that at low-temperature, the dependence of detected voltage in GaAs/Al$_{0.25}$Ga$_{0.75}$As heterojunction is induced by rectification, while at higher frequencies, the intervalley EMF prevails.

To sum up, the most popular detectors in the MW and MMW range are those based on a zero-biased LBS diode, favorable in the small signal square-law and envelope detection (Hesler & Crowe, 2007; Hoefle et al., 2014). Definite advantages are inherent, such as high voltage sensitivity, low-noise characteristics, room temperature operation, large bandwidth, competent reliability, and good repeatability, making Schottky diodes the unquestioned leaders in the square detection race. The Schottky diodes have reached their commercial maturity allowing them to be purchased on the market ("Virginia Diodes Inc. Zero Bias Detector"). However, the complexity of the fundamental concept of a Schottky junction requires it to be formed on a semiconductor surface that makes the properties of the diode sensitive to manufacturing conditions and vulnerable to the impact of the environment. Other types of diodes are proposed as well, e.g., camel (Shannon, 1979), PDB (Malik et al., 1980), heterojunction (Lechner et al., 1980), hot carrier (Harrison & Zucker, 1966), all operating based on the major carrier phenomena in semiconductors. All these majority carrier devices, except for Schottky diodes, belong to the class of bulk-barrier diodes with the operation in the bulk of semiconductor material. More than fifty years ago, promising MW diodes were developed operating based on hot carrier phenomena in semiconductors under the action of a non-homogeneous electric field (Harrison & Zucker, 1963). Formerly, Harrison and Zucker (Harrison & Zucker, 1963) proposed an original MW diode. The development of Schottky diodes brought scientists and engineers to camel diodes when in 1979, Shannon proposed to replace the metal-semiconductor barrier with the n^{++}-p^{+}-n structure (Shannon, 1979). In 1980, Malik et al. proposed to insert layers of an intrinsic semiconductor between the oppositely doped layers, and the camel diode structure was transformed into the n^{+}-i-p^{+}-i-n^{+} PDB structure (Malik et al., 1980). Schottky junction-based and PDB diodes have found applications for pulsed MW power measurements. Further improvements in these point-contact diodes turned into the planar bow-tie asymmetrically necked design of the diodes where n^{+}-n Si homojunction was used (Ašmontas & Sužiedėlis, 1994). Planar diodes were successful in sensing electromagnetic radiation from the MW to the IR, including the terahertz frequency range (Ašmontas & Sužiedėlis, 1994; Sužiedėlis et al., 2003; Minkevičius et al., 2011). These planar diodes were successfully used for heterodyne (Minkevičius et al., 2011) and spectroscopic (Kašalynas et al., 2011) terahertz imaging, and detection (Seliuta et al., 2004) sensing (Palenskis et al., 2018). Another kind of MW diode having the active region situated in the bulk of a device is the heterojunction diode. In 1980, Lechner et al. reported a heterojunction diode that detected MW radiation on the GaAs/AlGaAs heterojunction barrier. In the sense of increasing their voltage responsivity, the point-contact (Ašmontas et al., 1971) and planar (Ašmontas, 1984) heterojunction diodes were revealed as counterparts of the hot carrier MW diodes that are worth attention. Later, a sensitive heterojunction diode was investigated in terms of the detection of electromagnetic radiation in a wide frequency range from MW to IR frequency (Gradaukas et al., 2010).

It should be noted that other studies of different types of MW-detecting diodes with non-linear characteristics include submicron area InAs/AlSb/AlGaSb heterojunction-based backward diode with interband tunnelling (Zhang et al., 2011), zero bias resonant tunnelling Schottky diodes based on AlAs/InGaAs/InAs (Chahal, Morris & Frazier 2005), low-barrier diodes based on InGaAs/AlGaAs/GaAs heterostructure (Vostkov et al., 2020), asymmetric spacer tunnel layer diodes (Zainul Ariffin et al., 2018), semimetal/semiconductor diode based on ErAs/InAlGaAs heterojunction (Young, Zimmerman, Brown & Gossard 2005), Fermi-level managed barrier diodes based on InP/InGaAs heterojunction (Ito & Ishibashi, 2017), heterostructured low-barrier diodes with a graded-gap AlGaInAs barrier (Nadar et al., 2017), GaAsSb-based backward tunnel diodes (Takahashi et al., 2009).

As for commercial applications, the MW diode-based sensors must be not only sensitive and fast but also reliable and inexpensive. Thus, the best possible design of MW detecting diode is still on the way.

1.2. Electrical Properties of Heterostructured Microwave Diodes with Two-Dimensional Electron Gas

As discussed in Section 1.1, the employment of carrier heating phenomena in MW and MMW sensing devices allowed certain advances. Asymmetrically shaped planar hot-carrier-based MW diodes could detect wideband electromagnetic radiation from MW to terahertz frequency range (Sužiedėlis et al., 2003). Wideband operation is set by pulse relaxation time; however, the voltage sensitivity of these diodes was relatively low. It was suggested (Seliuta et al., 2004) that a promising way to proceed successfully in diode-based electromagnetic sensors is to employ 2DEG systems as active constituents in MW diodes. The 2DEG is formed in modulation-doped structures as free electrons are spatially separated from ionized donors and enclosed within several nanometers in a narrow potential well near the interface (Seliuta et al., 2007a; Stormer, Dingle, Gossard, Wiegmann & Sturge, 1979; Hiyamizu, Saito, Nanbu & Ishikawa, 1983). The higher mobility of free electrons is inherent to the modulation-doped heterostructures; thus, an increase in voltage sensitivity should be expected.

Transistor-like structures, such as FET, with 2D semiconductor materials, are commercially successful and widely used for sensing and detection of subterahertz and terahertz radiation (Knap, Deng, Rumyantsev & Shur, 2002; Knap et al., 2002b, 2004; Watanabe, 2013; Teppe et al., 2005; Veksler, 2006; Rogalski & Sizov, 2011; Lisauskas et al., 2009; Boppel et al., 2012; Zagrajek et al., 2019). FET technology is predominantly Si-based. Other semiconductor compounds, such as GaAs, InAs, or graphene, offer the possibility of realizing 2D electron systems and higher electron mobility than in Si (Karcher, 2016). Dyakonov and Shur suggested using a high-mobility FET with a 2DEG channel as detectors, mixers, or multipliers (Dyakonov & Shur, 1996) up to submillimeter-wavelengths. Operation is based on quadratic detection by exciting waves of electron density, i.e., non-linear properties of 2D plasma waves in the gated channel (Shur & Ryzhii, 2004). The resulting DC voltage arising between the source and drain is proportional to the power of the incident radiation. It is essential to note that non-linear properties of plasma wave excitations in the transistor channel enable the detection of radiation with frequencies substantially higher than the transistor cut-off frequency since the plasma wave’s velocity is much larger than the drift velocity of 2D electrons in the transistor channel

(Dyakonov & Shur, 1996). A FET, biased by the gate-to-source voltage and subjected to electromagnetic radiation, can produce a constant drain-to-source voltage, which has a resonant dependence on the radiation frequency with a maximum at the plasma oscillation frequency ω_o (Knap et al., 2004; Dyakonov & Shur, 1996). It was shown that plasmon resonant (Knap et al., 2002a) and non-resonant (Knap et al., 2002b) detection is inherent to FET devices based on GaAs/AlGaAs. The width of the resonance curve is specified by the inverse of the electron momentum relaxation time, $1/\tau_i$. When $\omega_0\tau_i>>1$, the FET operates as a resonant detector. In a contrary case, when $\omega_0\tau_i<<1$, the plasma oscillations are overdamped, and the transistor response is a smooth function of the radiation frequency, representing a non-resonant broadband detection regime. The most promising application appears to be broadband terahertz detection at room temperature in a non-resonant regime for imaging and communication applications (Knap et al., 2013), although it was found that the resonant detectors are more sensitive than the broadband detectors. Resonant-tunnelling transistor with high mobility of electrons in a 2DEG channel was investigated for subMMW detection (Ryzhii, Khmyrova & Shur 2000). Higher performance was achieved due to the combination of strong non-linearity of the resonant-tunnelling current, negative differential conductivity, and excitation of plasma waves in the 2DEG layer (Ryzhii et al., 2000). FETs with a grated gate based on the modulation-doped GaAs/AlGaAs heterostructure demonstrated a striking voltage-tuned resonant detection in the subterahertz range (Peralta et al., 2002). The 2DEG was formed in a uniformly metalized double-quantum-well channel. Other applications of 2DEG for MMW and terahertz radiation sensing include ultrafast hot electron bolometric detectors (Yngvesson, 2000), bolometric mixers with a ballistic cooling mechanism (Lee, Pfeiffer & West 2002), quantum Hall photodetectors integrated with a log-periodic antenna (Kawaguchi, Hirakawa & Komiyama, 2002), and graphene nanowire diodes (Winters, Thorsell, Strupinski & Rorsman, 2015).

The new concept of a planar asymmetrically shaped MW detecting diode based on non-uniform heating of the 2DEG was suggested by (Seliuta et al., 2004; Juozapavičius et al., 2004). The MW diodes were based on a modulation-doped GaAs/$Al_{0.25}Ga_{0.75}As$ structure. The asymmetrical shape (Fig. 1.8) ensures two different gradients of the inhomogeneous electric field concentrated at the neck of the structure (Seliuta et al., 2004, 2007a).

The metalized leaf on the left concentrates the incident signal onto the mesa apex of the right leaf, which contains the 2DEG layer (Valušis et al., 2005). As discussed in Section 1.1, bigradient EMF together with n-n^+ TEMF occurs when a diode of such design is placed in a strong MW electric field. Incident radiation is coupled to the 2DEG layer, and the diode mesa itself acts as an antenna, which is possible because its shape resembles that of a bow-tie antenna (Seliuta et al., 2004). Non-uniform heating in an asymmetrical structure causes different fluxes of hot carriers; thus, the voltage signal appears over the ends of the diode. GaAs/AlGaAs compound was chosen to increase the voltage sensitivity, as carrier heating is proportional to carrier mobility. Additionally, when one part of the asymmetrically shaped diode neck is doped, i.e., modulation doping, it also allows for higher voltage sensitivity values and fast response operation, and lower resistance.

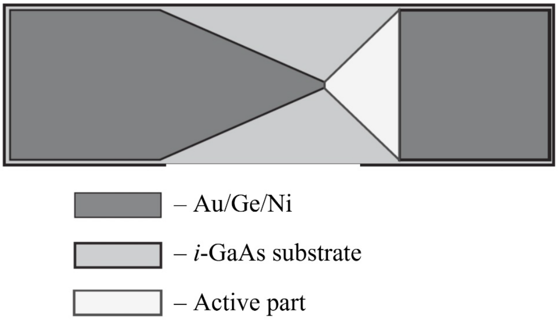

Fig. 1.8. Planar asymmetrically shaped bow-tie type diode with 2DEG layer (Seliuta et al., 2004)

It was reported (Juozapavičius et al., 2004) that at 10 GHz, the voltage sensitivity of the diodes at 77 K reached 20 V/W, although, at room temperature, it dropped to 0.1–1 V/W due to a decrease in electron mobility. In the K_a-frequency range, the voltage sensitivity dropped by one order (Juozapavičius et al., 2004) and remained nearly independent up to 0.8 THz (Seliuta et al., 2004) following the plateau. The detected voltage depended linearly on the MW power over two orders of magnitude, up to 10 mW at 77 K and 100 mW at room temperature; thus, it was proposed that these diodes are suitable for power measurements. Investigation at higher frequencies up to 2.25 THz (Seliuta et al., 2004) showed that voltage sensitivity dropped by more than two orders of magnitude due to antenna effects that cause weaker coupling of incident radiation. In addition, it was determined (Valušis et al., 2005) that the width of the neck of the diode can influence detection properties as well. Diodes having 12 μm neck width showed voltage sensitivity up to 0.3 V/W, while 3 μm width diodes showed 0.5 V/W at 100 GHz. Higher voltage sensitivity in diodes with narrower width of the neck was associated with a larger amplitude of the MW electric field.

The reduction of the neck was also investigated by (Seliuta et al., 2007a). Diodes with a narrower neck width caused stronger asymmetry of the *IV* characteristic due to the sharper and more narrow shape of the electric field distribution. The distribution and value of the electric field are defined by the current direction due to the accumulation of electron space charge in the vicinity of the neck (Seliuta et al., 2007b). It was reported that if the neck width of the diode was 5 μm or less, the non-locality could start to predominate since the change of the electric field along the structure becomes comparable with the electron ballistic length (Seliuta et al., 2007a). The nonlocal effect was associated with electron drift velocity overshoot as ballistic electrons cross the structure without scattering. The voltage sensitivity of the diodes with the 2 μm neck width was more than three times higher than that of those with the 12 μm neck width.

Next, two kinds of modulation-doped AlGaAs/GaAs heterostructures having different underlying structures were investigated (Kozič et al., 2005). Different quality of the 2DEG channel was obtained for AlGaAs/GaAs modulation-doped heterostructures on a semi-insulating GaAs substrate with and without a superlattice buffer structure. The buffer superlattice was composed of 30 periods of undoped GaAs/$Al_{0.25}Ga_{0.75}As$ layers having different underlying structures (Kozič et al., 2005). The VP characteristics of the planar diodes with buffered and non-buffered structures had opposite polarity. The detected voltage polarity of the buffered diode corresponded to the TEMF in the n-n^+ semiconductor junction. This matched the case of non-uniform carrier heating in the 2DEG channel having a lower carrier concentration than in the alloyed metallic region. The detected voltage polarity of the non-buffered diode corresponded to the sign of the asymmetry of the *IV* characteristic. This matched the case of non-uniform heating in the alloyed region having a lower carrier concentration than in the 2DEG channel. The dynamic range of the detected voltage was limited by 1 W at room temperature for the buffered structure and by 110 mW for the non-buffered structure. At liquid nitrogen temperature (77 K), the dynamic range was narrower by several orders in both cases. It was associated with hot electron transition to higher energetic valleys and more power-sensitive Gunn domains formation phenomena under the influence of a strong MW electric field at a lower temperature when an electron with higher mobility was more power-sensitive (Kozič et al., 2005; Hill & Robson, 1982). The highest voltage sensitivity was 200 V/W at 77 K temperature in the case of a non-buffered structure (Kozič et al., 2005).

The gate-influenced increase of voltage sensitivity in asymmetrically and symmetrically shaped 2DEG MW diodes fabricated based on selectively-doped AlGaAs/GaAs heterostructure with a δ-doped AlGaAs barrier was investigated in (Sužiedėlis et al., 2006, 2007a). The diode gate was created as an extension of its metallic contact for several micrometers above the 2DEG channel, causing a higher non-uniformity of the electric field in the vicinity of the neck of the sample (Seliuta et al., 2007a). The *IV* characteristics of the asymmetrically and symmetrically shaped MW diodes were linear at low applied voltages and turned to sublinearity with the voltage increase due to electron mobility decrease in a high electric field. The VP characteristic at room temperature, the asymmetrically shaped structure, and the symmetrical structure were linear in the power range of 1 to 10 mW. At liquid nitrogen temperature, the VP characteristic followed the linear law for both asymmetrically and symmetrically shaped structures at lower power and turned to sublinear with an increase in power. A weak frequency dependence on voltage sensitivity was observed in the X- and K_a-frequency ranges in the case of the symmetrical structure (0.35 V/W), while in the case of the asymmetrical structure, the decrease in voltage sensitivity was inherent at higher frequencies. It was associated with two competing detection mechanisms: the bigradient detection and the MW detection that arises due to charge inhomogeneity created by the gate introduced above the 2DEG layer near the contact of the diode (Sužiedėlis et al., 2007a; Seliuta et al., 2007a). It was suggested that the possibility of detecting electromagnetic radiation in the subMMW wavelength range should be expected in the case of symmetric gated selectively-doped structures. It was reported by (Seliuta et al., 2007a) that the voltage sensitivity (at 10 GHz) of the gated asymmetrical bow-tie MW diode based on $GaAs/Al_{0.3}Ga_{0.7}As$ modulation-doped structure reached 2.5 V/W at room temperature and 40 V/W at liquid nitrogen temperature.

Planar diodes based on AlGaAs/GaAs structures with a homogeneously doped barrier, pseudomorphic AlGaAs/InGaAs/GaAs structures with 10 periods of undoped GaAs/AlGaAs layers, and diodes based on AlGaAs/GaAs structures with δ-doped and homogeneously doped barrier were investigated in (Ašmontas et al., 2007, 2009). Linear detected voltage dependence on MW power up to 10 mW was observed for all investigated diodes at room and liquid nitrogen temperatures. The non-monotonic character of the VP characteristics observed at higher MW powers was associated with the origin of negative differential resistance in the *n*-GaAs layer due to the Gunn Effect (Ašmontas et al., 1998, 2009). The diode having a homogeneously doped barrier reached a voltage sensitivity of 0.3 V/W at room temperature and 20 V/W at liquid nitrogen temperature in the frequency range from 26 GHz to 120 GHz. The planar diode having a δ-doped barrier layer demonstrated a voltage sensitivity of 2 V/W at room temperature and up to 120 V/W at liquid nitrogen temperature. Voltage sensitivity of the pseudomorphic selectively-doped AlGaAs/InGaAs/GaAs structures containing a single $In_{0.15}Ga_{0.85}As$ layer was 0.6 V/W at room temperature, while at liquid nitrogen temperature, the value reached 38 V/W. As reported by (Ašmontas et al., 2007), the voltage sensitivity of the planar diode does not change from 10 GHz to 120 GHz, while at higher frequencies (>120 GHz), the sensitivity decreases due to the frequency dependence of the electron capture cross-section in GaAs and InAs.

As already discussed, the voltage sensitivity of asymmetrically necked structures is proportional to carrier mobility, as follows from the phenomenological theory (Ašmontas & Sužiedėlis, 1994). Higher values of voltage sensitivity of the diodes based on AlGaAs/GaAs structures with δ-doped barrier layer were explained by the reduced thickness of the doped layer, thus causing higher electron mobility (Ašmontas et al., 2009; Schubert, Pfeiffer, West & Izabelle, 1989). The pseudomorphic selectively doped AlGaAs/InGaAs/GaAs heterostructure was also chosen due to the higher electron mobility in the InGaAs quantum well channel as well as the higher 2DEG density (Ašmontas et al., 2009; Chan, Lightner, Patterson & Yu, 1990). The InGaAs layer should be thin enough, not exceeding the critical thickness; otherwise, the electrical and optical features of the modulation-doped structure undergo considerable changes due to the strains of the crystal lattice (Kozič et al., 2006, Misiewicz, 1996).

Planar MW diodes with a δ-doped barrier layer were compared to planar MW diodes with a smoothly doped AlGaAs barrier (Sužiedėlis et al., 2007b). Diodes with a δ-doped barrier demonstrated a better linearity of the VP characteristic in the 1–10 mW power range at both room and liquid nitrogen temperatures. Planar MW diodes with a smoothly doped barrier had higher voltage sensitivity values and more plane frequency dependence in the 26–120 GHz range. Lower voltage sensitivity values of the diode with a δ-doped barrier were associated with a stronger influence of the metal-semiconductor junction in separate layers. These junctions occur where alloyed metallic contacts intercourse with modulation-doped structure and can be treated as pairs of a Schottky-like junction connected in the opposite direction, thus causing shunting of the 2DEG layer.

Other studies (Valušis et al., 2002; Seliuta et al., 2007b; Minkevičius et al., 2011) reported sensitivity of 2–6 V/W and 13 V/W (Palenskis et al., 2018) below 1 THz for the Si lens-coupled bow-tie diode with an $In_{0.54}Ga_{0.46}As$ layer grown on an InP substrate with one InAs monolayer in between.

It should be noted that the aforementioned MW diodes are mainly fabricated of more or less complex epitaxial semiconductor structures, in most cases grown by means of the MBE technology. Moreover, in all cases, these diodes demonstrated well-pronounced asymmetry of the *IV* characteristics above 0.1 V. This notable feature was explained in (Seliuta et al., 2007a) by a different spatial accumulation of 2D electrons in the vicinity of the neck of the planar modulation-doped bow-tie type MD diode. As the voltage increases and the electric field becomes stronger, the electrons become hot and accumulate differently in the vicinity of the neck due to the geometrical shape of the structure. However, the voltage sensitivity of the discussed bow-tie diodes is lower than that of the FETs.

1.3. Application Technologies of Electromagnetic Radiation in Millimeter-Wave Range

The MMW region of the electromagnetic spectrum is considered to be the range of wavelengths from 10 mm to 1 mm (Oka et al., 2008). This means that MMW is longer than IR waves, e.g., but shorter than radio waves. The MMW and subterahertz radiation propagation characteristics (i.e., the ability to penetrate through a dielectric medium and atmosphere), wide bandwidth (i.e., stipulating high data transfer rates), and a small component size (i.e., MMW circuits can be configured on IC) make it attractive for a variety of modern applications, such as broadband high-speed wireless communication networks, radar technology, imaging systems, and bio-medicine. Moreover, in certain cases when devices must operate independent of environmental and atmospheric conditions, MMW propagation has definite supremacy if compared to IR or visible spectral ranges (Goldsmith, Hsieh, Huguenin, Kapitzky & Moore, 1993).

Operation of most devices for MMW applications, such as radars, ultra-wideband systems, impedance meters, resonator sensors, and noise-using devices, is based on the generator/transmitter and detector/receiver principle (Belen, Mahouti, Gūnes & Partal, 2018). Other devices, such as radiometers, detect the thermal radiation of objects over a distance (Polivka, 2007).

The short wavelength of the EHF range makes it advantageous in radar technology due to the ability to use micro/nanoscopic components, high resolution, and accuracy. An MMW system operating at 76–81 GHz, with a corresponding wavelength of 4 mm, can detect movements that are as small as a fraction of a millimeter (Iovescu & Rao, 2020).

MMW radars are used in imaging and tracking applications (Brooker, 2005). There are mainly several types of radar systems, including pulsed-type radars, Doppler-effect radars, and FM-CW radars (Polivka, 2007; Belen et al., 2018). The operation principle of any radar technology is based on the reflection of the transmitted electromagnetic signal from objects in its path. Analysis of the reflected signal allows for determining the range, velocity, motion, and angle or presence of the object (Belen et al., 2018; Iovescu & Rao, 2020).

Pulsed radars are mainly designed for long transmission distances. These types of radar are used in real-time targeting systems and feature a low-noise power ratio and high frame rate, and good interference immunity (Zhang et al., 2020). A short pulse is sent in emitting mode, and the echo signal returns to the radar in silent mode (Van et al., 2019). Pulsed radars have narrow bandwidth as it allows targeting distant objects when the beam is not fanning out (Polivka, 2007). However, due to the narrow bandwidth, the resolution of pulsed radars is only in the meter-centimeter range (Zhang et al., 2020); thus, pulsed radars are usually not the subject of choice for imaging systems.

Doppler-effect radars work in unmodulated CW signal mode and are capable of measuring the velocity of objects by processing the frequency shift in a transmitted and reflected signal (Polivka, 2007). It is well known that Doppler radars are widely used for commercial applications (Polivka, 2007; Belen et al., 2018), such as automotive speed measurements or intruder detection. Other applications include measurements of the expenditure of poured construction materials and the speed of objects in a dense environment (e.g. mining) (Polivka, 2007). It was reported (Belen et al., 2018; Van et al., 2019) that MW and MMW Doppler radars found their use in healthcare (systems for continuous sensing of human tissue and organ vital signs, arterial wall movement detection, cancer tumor detection, thorax movement detection as a breathing rate analyzer) and rescue (location of victims under collapsed buildings).

Texas instruments (Iovescu & Rao, 2020) developed MMW radars based on a CMOS working in the FM-CW mode. A radar operation is based on heterodyning since it sweeps the transmitted signal over a frequency band and multiplies the transmitted signal with the reflected signals (Zhang et al., 2020; Polivka, 2007). By knowing the beat frequency, the frequency band, and sweep period time, the distance and velocity can be obtained. Therefore, FM-CW radars combine the Doppler-radar's capability to measure the object's velocity with the added ability to measure the object's distance (unlike pulsed radars, FM-CW radars can measure the distance from zero) (Polivka, 2007; Brooker, Bishop & Scheding, 2001). High resolution is also inherent to FM-CW radars and is in the range of several millimeters due to a wide bandwidth (Zhang et al., 2020; Hafner, Dūrr, Waldschmidt & Thoma, 2020). Texas instruments FM-CW radars are employed in advanced driver assistance systems ("Texas Instruments: Automotive mmWave Sensors"), such as autonomous driving, building automation systems, and autonomous drones ("Texas Instruments: Industrial mmWave radar sensors"). Toyota Motor Corporation also reported (Tokoro, Kuroda, Kawakubo, Fujita & Fujinami, 2003) the development of MMW FM-CW radars for adaptive cruise control, automatic braking, lane intrusion, blind spot detection, and pre-crash systems. Other applications of FC-MW radar systems, e.g., are airplane radio altimeters (Polivka, 2007), liquid level sensors ("Vega: First radar level sensor for liquids with 80 GHz;" Gennarelli, Romeo, Scarfi & Soldovieri, 2013; Armbrecht et al., 2008), 3D holographic imaging for non-destructive testing of materials (Zhang et al., 2020; Oka et al., 2008).

MMW imaging can be described as a technique that combines the measurement of electromagnetic radiation arriving from objects and the reconstruction of 2D/3D real-time images by received signal processing. Receivers (cameras) detect the MMW signal (energy) on the imaging plane and record the relative intensity of each pixel (Polivka, 2007). Generally, there are two main operational principles of MMW imaging sensors: active imaging and passive imaging (Sato & Mizuno, 2010). In the case of active imaging, the MMW source is used to radiate the desired object, and the image of the object is reconstructed by processing the amplitude or phase of the reflected signal obtained using the receiver array. Passive imaging, employed in radiometers, is based on measuring the distribution of MMW radiation temperatures (Meng et al., 2018), i.e., thermal noise emitted from the object using high-sensitivity and low-noise receivers.

Imaging systems usually employ focal plane imaging systems in the 3–2 mm wavelength range (Goldsmith et al., 1993), giving images with a resolution of several millimeters. These systems are used for far-distance imaging (Oka et al., 2008). Other imaging techniques include mechanical scanning when detectors are swept in the XY direction, phased array imaging for electromagnetic radiation arriving from different directions, interferometric imaging, imaging with synthetic aperture, and helical scanning (Oka et al., 2008; Goldsmith et al., 1993; Meng et al., 2018; Ašmontas, Kiprijanovič, Levitas, Matuzas & Naidionova, 2015).

MMW imaging systems are used in radio astronomy (usually interferometric imaging systems) and atmospheric radiometry due to atmosphere opacity at certain frequencies, which are so-called atmospheric windows. Generally, water vapor and oxygen cause MMW attenuation due to atmospheric absorption, but moderately low attenuation is inherent for frequencies near 35, 94, 140, and 220 GHz due to resonances of atmospheric gases (Oka et al., 2008; Shen et al., 2007). On the other hand, vapor line absorption peaks at 22, 184, 324 GHz and oxygen absorption at 60, 118 GHz are used for high-atmosphere studies. A high-sensitivity cryogenically cooled focal plane array camera for the Arecibo Radio Telescope is used in radio astronomical spectroscopy at 85–115 GHz region (Goldsmith et al., 1993; Cortes-Medellin et al., 2015). Remote sensing of trace gases is used in studies of Earth's atmosphere (Goldsmith et al., 1993), and radiometers are used in radio telescopes for distant space object's surface temperature measurements (Polivka, 2007). Multi-frequency imaging MW space-borne radiometer for investigations of atmospheric and oceanic parameters, including precipitation, soil moisture, global ice and snow cover, sea surface temperature and wind speed, atmospheric cloud water, and water vapor was discussed by (Peichl, Dill, Greiner & Reutlingen, 2007).

Objects can be identified by MMW radiation. For example, experiments by (Watanabe et al., 2013) demonstrated MMW imaging using InP- and GaAs-based plasmonic transistors for hidden substances, such as water contents in tree leaves or tea leaves in Al-coated plastic packages. It was investigated (Goldsmith et al., 1993) that reflectance and transmission loss signal levels are different for different materials, as well as for the human body at 95 GHz. Some dielectric materials have a reflectivity of 2 to 4 times that of human skin, while clothing provides little absorption or extended reflectivity (Goldsmith et al., 1993). MMWs easily penetrate cloth and are strongly reflected by metallic materials, and metallic materials have low emissivity (Oka et al., 2008; Smith et al., 2012). Moreover, according to the blackbody radiation principle, natural autonomous electromagnetic emission, including MMW, is inherent for all objects with a physical temperature higher than absolute zero; thus, they can act as thermal sources (Oka et al., 2008; Meng et al., 2018; Peichl et al., 2007). Temperature resolution can be measured using radiometers with low-noise receivers (Polivka, 2007). Hence, a significant contrast can be imaged between the emissivity of the human body and the reflection of metallic objects (Smith et al., 2012). Many materials, such as solid dielectric materials or explosives, were investigated for the generation of electromagnetic radiation in the MW–MMW range (Novac, Senior, Farage, Smith & Xiao, 2018). Consequently, due to features of autonomous radiation and reflectance of incident radiation, as well as high resolution and penetration capability, non-invasive MMW near-focus imaging systems with multiple detectors or mixer arrays are used for security inspection and surveillance, concealed weapon or contraband detection (Oka et al., 2008; Zhang et al., 2020; Goldsmith et al., 1993; Polivka, 2007; Sato & Mizuno, 2010; Meng et al., 2018; Shen et al., 2007; Peichl et al., 2007; Smith et al., 2012; Cortes-Medellin et al., 2015). A method for identifying materials using dielectric properties through active MMW imaging is described by (Smith et al., 2012) based on MMW reflectometry that allows for identifying the composition of a detected object. The object is illuminated with multiple MMW frequencies, and complex reflection properties are determined, which are then compared to the database, thus letting to determine the likely composition of the materials. A passive helical scanning imaging system working at 94 GHz for this purpose is described by (Meng et al., 2018). Using smooth metal reflectors, the MMW radiation from the object is directed to the focusing antenna. The MMW frequency for imaging is determined by the matter of choice, as lower frequencies allow deeper penetration of the material, while higher frequencies are used for fine resolution (Oka et al., 2008). Other technologies include active and passive security gates, handheld passive scanners, and passive video-rate cameras (Oka et al., 2008). For example, the SynviewHead 300 system based on the FM-CW radar can be used for these purposes (Zhang et al., 2020). Smith Detection Group produces airport body scanner systems using the MMW technology to detect concealed contraband of any materials ("Smiths Detection: eqo People screening with automatic detection;" Accardo & Chaudhry, 2014). Using low-power MMW, the scanners provide an outline of the human body and reveal concealed objects. Fujitsu produces 94 GHz band passive MMW imaging sensors (Sato & Mizuno, 2010; Shen et al., 2007). These and other systems are widely deployed in many airports in the EU, USA, China, Japan, Australia, and the UK (Wang et al., 2019).

Large-area imaging systems for the detection of concealed objects under a cloth at a distance of 25 meters are discussed by (Jepsen, Cooke & Koch, 2011).

Active 2D/3D MMW imaging is used for the detection of hidden cracks in concrete constructions and surfaces or other internal defects (Oka et al., 2008; Zhang et al., 2020; Polivka, 2007). Since blackbody radiation is not present, in this case, an active imaging system based on the Gunn oscillator and phased array is used for MMW radiation at 75–110 GHz. The MMW pass through materials, such as wallpaper and lining paint, but are scattered on impact with fine cracks mapping their shape (Oka et al., 2008). It was reported that the same crack scan MMW imaging could also be used in the food industry to check the maturity of fruits and vegetables and for termite damage in wood (Oka et al., 2008; Pastorino, 2015) and computed tomography to reveal the internal structure of the material (Guerboukha, Nallappan & Skorobogatiy 2018).

Radiometers are also suitable for ionized gas or plasma spectroscopy (Polivka, 2007). Dual mode (active and passive) imaging system for plasma diagnostics of small-scale structures was described by (Shen et al., 2007) and developed by the Princeton Plasma Physics Laboratory. The operation is based on high-resolution localized measurements at 110, 140, and 170 GHz of the density of plasma fusion fluctuations and microturbulence from the reflection of MMW from plasma cut-off surfaces. The system uses a mixer array, which detects a small portion of the electron cyclotron resonance heating power. This allows for performing imaging diagnostics of 2D and 3D structures of an electron temperature and density (Shen et al., 2007).

An airborne radiometric imaging system with a polarimetric analyzer operating at 37 and 90 GHz was described (Collins, Ross Warren & Paul, 1996; Cenanovic, Koppel, Ringel & Schmidt, 2013) for a regional scale sea ice mapping by processing temperature differences of radiation at two orthogonal polarizations (vertical and horizontal, i.e., parallel and perpendicular to the incidence plane) in free space. Investigation of the MMW polarization produces tensor characterization of objects or media (Polivka, 2007). MMW vision plane landing systems based on focal plane array MMW passive imagining radiometric camera at 94 GHz are used for pilot assistance during take-off and landing in adverse weather conditions (Goldsmith et al., 1993; Polivka, 2007; Shen et al., 2007). This system, e.g., is used at Turner’s Falls Airport in Massachusetts, USA.

Imaging using the synthetic aperture ultra-wideband radar technique allows for high-quality images of metallic and organic objects in the MW–MMW range (Ašmontas et al., 2015).

Holographic imaging using the FM-CW radar was described by (Oka et al., 2008). Using the magnitude and phase data of the signal in MW–MMW, the image is reconstructed employing a 2D/3D Fourier transform algorithm.

Scanning near field microscopy technique for the investigation of material homogeneity using MMW was described by (Kancleris, Laurinavičius & Anbinderis, 2004). The method is based on dielectric constant homogeneity imaging using dielectric probes in the waveguide channel and measuring the phase and amplitude of the signal reflected from/transmitted through the material. The probes provided local excitation and reception, and a homogeneity map was produced by probing the material with MMW at different points (Kancleris et al., 2004).

Other applications of MMW imaging include harbor navigation/surveillance in fog, highway traffic monitoring in fog, helicopter and automotive collision avoidance in fog, and environmental remote sensing data associated with weather, pollution, soil moisture, oil spill detection, and monitoring of forest fires, defense applications, geoscience applications, art conservation, pharmaceutical industry for quality control of tablet coating, life detection in the wreckage (Oka et al., 2008; Van et al., 2019; Shen et al., 2007; Peichl et al., 2007; Jepsen et al., 2011; Guerboukha et al., 2018; Mittleman, 2017).

MMW radiation is non-ionizing (with a typical photon energy of 1 meV or less (Zhang et al., 2020)), and thus, it is harmless at moderate power levels. The MMW therapy applications are in the frequency range of 40 to 70 GHz. It is known as low-intensity millimeter electromagnetic therapy and was investigated for oncology treatment purposes using special medical generators. The possible applications include the treatment of benign and malign tumors, palliative treatment for pain relief and intoxication syndrome, gastric polyp treatment, breast, and other cancers, and post-surgery treatment for the reduction of applications and prevention of metastases (Teppone & Avakyan, 2010). Although, it should be noted that these are early-stage investigations.

Several subterahertz pulsed imaging systems have been reported (Woodward, Wallace, Arnone, Linfield & Pepper, 2003; Yu, Fan, Sun & Pickwell-Macpherson, 2012; Kašalynas et al., 2016) for the detection of epithelial cancers, such as basal cell carcinoma. Spectroscopy studies using time-domain analysis have shown structural changes between diseased and healthy tissue determined as an imaging contrast (Woodward et al., 2003; Yu et al., 2012).

It was also reported (Yu et al., 2012) that cancer often leads to the local increased blood supply, and some tumors cause increased water content in the affected tissues. It can be detected by subterahertz imaging since the water strongly absorbs HF radiation, causing a lower refractive index and absorption coefficient in cancer-affected areas. Moreover, higher absorption is inherent to breast cancer, which was concluded by investigations at 108 GHz using 3 mW power radiation and a high-sensitive Schottky diode (Yu et al., 2012), and magnetic nanoparticles can enhance breast cancer imaging (Pastorino, 2015). In the case of metastatic lymph node metastasis, the studies revealed that metastasis cause lower amplitude of the reflected single when illuminated by subterahertz radiation (Yu et al., 2012).

The MMW impedance spectroscopy analysis was used to study biological cell discrimination (Dalmay et al., 2010). Stem cells from the central nervous system use a biosensor chip, which consists of two microstrip resonators coupled through to a comb capacitor. The operation principle is based on the high sensitivity of the sensor to dielectric and conductive perturbations lying in the same range as the typical impedance of a single biological cell in the MMW region (Dalmay et al., 2010).

MMW imaging has also been reported (Pastorino, 2015) to be suitable for differential diagnoses of cerebral stroke and wireless capsule endoscopy.

The bandwidth shortage and channel congestion have escalated the move to the MMW range for telecommunication systems, allowing to augment saturated 0.7–2.6 GHz radio spectrum and new opportunities for providing higher data transfer rate (Al-Ogaili & Schubair, 2016; Rappaport et al., 2013).

MMWs are incorporated in the recently developed fifth-generation technology standard for broadband cellular networks and wireless links. It was reported (Huo et al., 2017; Al-Ogaili & Schubair, 2016) that the expected data rate for the fifth-generation peak downlink can reach 10 Gbit/s. The most significant features of MMW that increase the performance of fifth-generation wireless networks are the extensively increased bandwidth that directly leads to much higher bit rates, lower outage probability, lower latency due to highly directional links in ultra-dense networks, and lower infrastructure costs (Al-Ogaili & Schubair, 2016; Rappaport et al., 2013).

As previously mentioned, characteristics of the Earth’s atmosphere produce both problems and solutions for MMW applications. Atmospheric attenuation is sufficiently high at frequencies around 60 GHz (5 mm) due to the electromagnetic energy absorption peak caused by oxygen molecules. Thus, the short signal path length makes the 60 GHz band not suitable for use in long-range radio systems. Although this limitation comes in handy for the operation of secure short-range point-to-point communication links, as it allows for the restriction of the coverage distance as well as to achieve multiple frequency reuse without interference (“The Use of Radio Frequencies Above 20 GHz by Fixed Services”). There are several applications that exploit the advantage of the 60 GHz band. For example, short-hop point-to-point terrestrial links that provide the final connection to customers from an optical fiber or cable network (high-definition speech, video streaming, or ultrafast data transmissions) (“The Use of Radio Frequencies Above 20 GHz by Fixed Services”) and inter-satellite communication (cross-linking) due to the almost absence of oxygen at geostationary altitudes (“NASA 60 GHz Intersatellite Communication Link Definition Study”).

Devices that conform to the IEEE 802.11 wireless networking standard operate at frequencies 57 to 71 GHz (Huo et al., 2017). These frequencies allow for achieving a multigigabit-per-second data rate for short-range wireless communication systems (Zheng, Su, Pan, Qamar & Ho, 2018). Moreover, the employment of MMW for wireless networks allows for mesh-like connectivity with cooperation between base stations, thus having better coverage and lower propagation losses in large areas (Rappaport et al., 2013).

Researchers are working on a technology that will use the MMW communication system to wirelessly transmit an ultra-reliable and low-latency video signal to VR headsets (Elbamby, Perfecto, Bennis & Doppler, 2018). The high directionality of the 60 GHz indoor channels allows for eliminating the need for wires or fibers.

The trend of increasing demand for bandwidth stimulates researchers to develop next-generation wireless technology systems that are shifting to the subterahertz range and are widely investigated for numerous applications. Subsequent wireless communication technology generations will employ carrier frequencies above 100 GHz, reaching the prospective 100 Gbit/s peak data rate (Tohme et al., 2014; Nagatsuma et al., 2016) with the bandwidth of tens gigahertz and should replace the fifth-generation infrastructure when it becomes insufficient. Numerous investigations are being conducted with various systems showing data rates and propagation distances at different frequencies. One of the first examples was the demonstration of a television broadcast at 120 GHz in Japan during the 2008 Olympic Games (Mittleman et al., 2017). In general, MMW and subterahertz bands above 100 GHz can be divided into three groups: 100–150 GHz for long-distance (1–10 km), up to 350 GHz for medium-distance (100 m–1 km), and up to 500 GHz for indoor (10–100 m) communications (Nagatsuma, Ducournau & Renaud, 2016). Investigations (Ma, Shrestha, Moeller & Mittleman, 2018) at frequencies 100, 200, 300, and 400 GHz report achieving 1 Gbit/s data rate for indoor highly directional wireless links, both line-of-sight and non-line-of-sight measurements and higher data rates are anticipated. The receiver was based on the zero-bias Schottky diode, while the Virginia Diodes frequency multiplier chain and pulsed generator were used for the transmitter. Both the receiver and the transmitter use horn antennas for coupling the highly directional vertically polarized signal. 8.2 Gbit/s data rate transmission over meter ranges at 300 GHz was achieved (Tohme et al., 2014) using pseudomorphic high electron mobility GaAs transistors and a frequency-multiplied source. The 120 GHz communication system (Nagatsuma et al., 2016) demonstrated up to 20 Gbit/s data rate transmission for distances no more than 5 km and 18 GHz bandwidth. Other investigations (Nagatsuma et al., 2016) report the data rate of 50 Gbit/s at 300 GHz using real-time amplitude signaling, 60 Gbit/s at 200 GHz, 46 Gbit/s at 400 GHz and up to 100 Gbit/s in the 100 GHz band using digital signal processing and a complete solid-state receiver with active elements, such as heterojunction bipolar transistors.

The majority of the reviewed MMW application technologies are implemented using different receiver and transmitter systems. Recent progress in MMW technologies stimulates the development of components, such as MIMO antenna arrays, detectors, mixers, and other elements that greatly enhance system performance and can be packaged into MIMICs to fit small-size envelopes. The fast development of such technologies requires novel concepts of electromagnetic radiation sensors. Some MMW sensors require bulky cryogenic cooling equipment (a high-T_c Josephson junction detector (Du et al., 2008) or an yttrium barium copper oxide microbolometer (Xu, Essa, Zhou & Bao 2000)). Some of them are quite complex, such as a Golay cell, which, on the other hand, demonstrates its advantage of high voltage sensitivity at room temperature and the ability to sense electromagnetic radiation in a wide spectral range, from ultraviolet light up to K_a-band frequencies ("Tydex, Golay Cell GC-1D with Diamond Window"). The backward tunnel diodes (Takahashi et al., 2009), the Si CMOS FET (Čibiraitė-Lukenskienė et al., 2020), and a wide variety of MW diodes based on the Schottky junction (Liu et al., 2009) are also known as room temperature sensors of the MMW. The most popular of them are zero-biased LBS diodes which are useful in the application of wireless electromagnetic communication. The main drawback of Schottky diodes is vulnerability to environmental conditions and frailness to high-power radiation (Tohme et al., 2014).

It was already discussed that planar bow-tie design diodes are promising for use in wideband MW detectors, and several options of them were tested for heterodyne (Minkevičius et al., 2011) and spectroscopic (Kašalynas et al., 2011) imaging as well as imaging of concealed low-absorbing objects (Jokubauskis, Minkevičius, Seliuta, Kašalynas & Valušis, 2019). Thus, new concepts of electromagnetic radiation sensors, having detection processes located in the bulk of a device, can be implemented for potential MMW applications.

1.4. Probing Techniques for Studies of High-Frequency Properties of Microwave Diodes

The electrical performance of semiconductor devices was usually measured by means of conventional techniques, e.g., using test fixtures for waveguide sections. As device operation frequencies began shifting to MMW and subterahertz bands, more convenient measurement approaches using probing systems have been developed for on-wafer or so-called wafer-level semiconductor device characterization and production testing. Such techniques were first suggested for use at MW frequencies by Strid and Gleason in 1980 (Strid, Gleason & Jones, 1988), demonstrated experimentally in 1982 for GaAs FET measurements, and introduced commercially by Cascade Microtech (now FormFactor) in 1983 (Collier & Skinner, 2007). Since then, the probing technique has evolved into high-performance tools for on-wafer measurements, which is widely used for the characterization of active and passive components and transmission lines at frequencies as high as 1.1 THz ("FormFactor: Unparalleled Probing Solutions"). The components may be segments of a monolithic circuit or separate discrete devices (Breed, 2011). Precise measurements of transistors, such as HBTs ("Cascade Microtech: Calibration Tools Consistent Parameter Extraction for Advanced RF Devices"), FETs and MIMICs, diodes, and other devices or circuits across the semiconductor wafer ("40 GHz On-Wafer Measurements with the HP 8510 Network Analyzer and Cascade Microtech Wafer Probes"), as well as ceramic substrate or MW laminate material (Breed, 2011), have been reported.

Probes are usually used for measurements of scattering parameters (S-parameters) that can be converted to the characterization parameters, such as impedance (Collier & Skinner, 2007; "Cascade Microtech: Calibration Tools Consistent Parameter Extraction for Advanced RF Devices;" Sia, 2019; Fregonese et al., 2018; Savin, Guba, & Bykova, 2016).

A typical probing system consists of (Fisher, "A guide to Successful on Wafer RF characterization"):

1. Probe head with probe tips that contact the DUT;
2. Probe station (allows precise positioning of the probe tips in XYZ directions);
3. Vector Network Analyzer;
4. Coaxial cables or waveguides;
5. Bias supply (usually bias tees);
6. Contact substrate;
7. Calibration substrate (the characterized impedance standard GaAs or Si substrates containing various precision elements, including 0.3 % resistors, transmission lines, shorts, and troughs ("Cascade Microtech: High Speed Microprobing Principles and Applications"));
8. Calibration software.

Other known probing applications include ultrafast *CV* and *IV* measurements (Stauffer, 2011) of FETS or *p-n* and Schottky junctions, electron density measurements in plasma with probe tips (Knappmiller, Robertson & Sternovsky, 2006), permittivity measurements using MW irradiation probes (Mitani et al., 2019), planar antenna characterization (Fakharzadeh, 2014), near-field imaging systems using diode detector and open-ended coaxial probes (Baudry, Louis & Mazari, 2006) or rectangular waveguide probes for subsurface sensing (Ramzi, Abou-Khousa & Prayudi, 2017), field analysis in electronic devices using electro-optic probes and noise measurements on semiconductor devices (Chaar & Rheenen, 1994) as well as in scanning probe microscopes (Soshnikov, Gogolinsky, Blank & Reshetov, 2007). Typically, probing systems are designed to produce a DC signal proportional to the phase and/or magnitude of the electric field associated with the scattered/reflected wave (Ramzi et al., 2017).

Wafer probing is an optimal and useful tool in semiconductor devices and IC research and development. It allows the comparison of the performance of different batches and the gathering of statistical data of MW parameters, such as distribution of HF GaAs FET drain-source resistances ("40 GHz On-Wafer Measurements with the HP 8510 Network Analyzer and Cascade Microtech Wafer Probes"). The advantages of probe system measurements in comparison with test fixtures are associated with the following:

1. Commercially available single sweep systems from DC to MW and MMW frequencies with a single coaxial input (Collier & Skinner, 2007);
2. Measurements are much more accurate and repeatable since when guiding HF waves onto the DUT using probes, they introduce smaller systemic errors as well as a more precise way to hold and place the DUT (Collier & Skinner, 2007; Breed, 2011; "Cascade Microtech: High Speed Microprobing Principles and Applications"; Fakharzadeh, 2014);
3. Exclude procedures that can cause damage to the samples and thus, provide non-destructive testing (Breed, 2011; Fakharzadeh, 2014; Lee et al., 2014);
4. Multiple advanced and simple calibration methods, which can be automated and allow the calibration of the measurement systems up to the probe tips, i.e., the measurement system will measure only what is beyond the probe tips ("Cascade Microtech: Calibration Tools Consistent Parameter Extraction for Advanced RF Devices;" Fisher, "A guide to Successful on Wafer RF characterization;" "Cascade Microtech: High Speed Microprobing Principles and Applications;" "FormFactor: Cascade Autonomous RF Measurement Assistant");
5. Both CW and pulsed signals can be detected using the same system (Lee et al., 2014);
6. Probes assure low contact resistance and superior impedance control (Fisher, "A guide to Successful on Wafer RF characterization;" "Cascade Microtech: Z PROBE High-Frequency Wafer Probe").

In general, DC probes are needle-shaped, and HF probes have coaxial or coplanar structures (Collier & Skinner, 2007; Breed, 2011). Most of the applications are performed by using macroscopic or microelectromechanical probes for the on-wafer MW characterization of RF microelectronics (Marzouk et al., 2015).

The DC probes can typically handle a maximum of 40 V DC bias voltage and 500 mA (Collier & Skinner, 2007). However, high-power DC probes are commercially available for measurements of power semiconductors up to 60 A and 3000 V ("FormFactor: Unparalleled Probing Solutions"). At frequencies greater than a few hundred MHz, DC probe needles suffer from parasitic reactance components due to the excessive series inductance of long thin needles and shunt fringing capacitances (Collier & Skinner, 2007). For MW range applications, DC probes were primarily replaced by ordinary coaxial probes that were sufficiently grounded, allowing measurements up to a few gigahertz due to limitations by the poor coaxial-to-device transition (Collier & Skinner, 2007). The introduction of HF probes with a planar transmission line allowed for overcoming these limitations.

The basic HF probe configuration (Fig. 1.9) is a transmission line, which consists of a coaxial connector, a short piece of low-loss coaxial cable, an electromagnetic absorber, ACPW (Fig. 1.9 – a) or a thin-film microstrip line (Fig. 1.9 – b), and probe tips which are shaped to fit the signal width of the planar structure (ACPW/microstrip) (Phung et al., 2019). The probes are designed and calibrated in a way that the connection with the probe tips matches the measured fields from the DUT through the coaxial connector and all the way to the measuring device (network analyzer usually) and ensures a low contact resistance between the probe and the pads of the DUT ("Cascade Microtech: High Speed Microprobing Principles and Applications;" Marzouk et al., 2015).

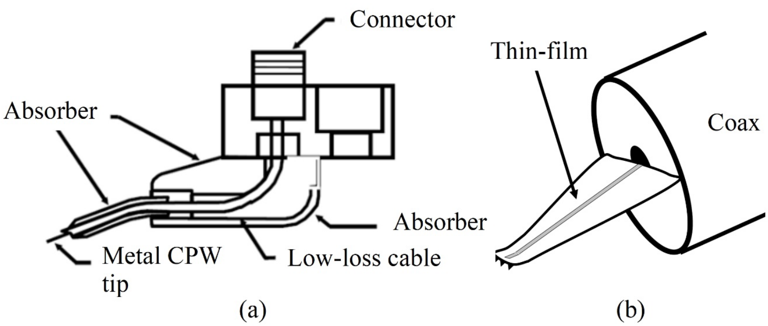

Fig. 1.9. Probe configuration: (a) a cross-sectional view of the probe with an ACPW tip; (b) the probe with a thin-film microstrip (Fisher, "A guide to Successful on Wafer RF characterization")

The transition from coaxial, with a radial electrical field pattern, to a planar transmission line with a much different (flatter) electrical field pattern is made within the probe. Fig. 1.10 illustrates the distribution of the electric field when applying the probe to DUT ("FormFactor: Infinity Probe Mechanical Layout Rules").

The typical probe contacts are SG, GSG, or SGS, where (S) is a signal and (G) is ground contacts, respectively. The signal contacts are electrically connected to a coaxial connector center pin, and the ground contacts are electrically connected to the coaxial-connector body ("FormFactor: Infinity Probe Mechanical Layout Rules"). At high frequencies, the ground is not an equipotential reference, as in low-frequency circuits, but is part of a transmission line that contains time-varying electric fields ("FormFactor: Infinity Probe Mechanical Layout Rules").

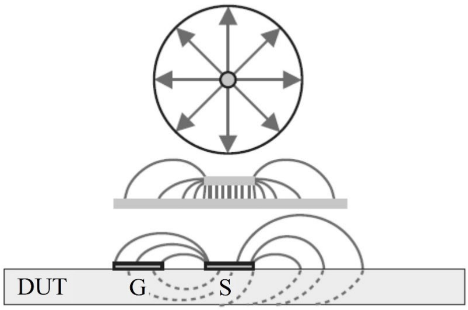

Fig. 1.10. Electric field distribution when applying the ACPW probe (in coaxial and planar transmission lines) to the DUT. Signal (S) and ground (G) contacts ("FormFactor: Infinity Probe Mechanical Layout Rules")

To minimize the extrinsic parasitic effect, the separation distance of the probe tips relative to one another is determined by the highest test wavelength (no further than 0.02 of the wavelength in the case of SG and 0.05 in the case of GSG (SGS)) ("FormFactor: Infinity Probe Mechanical Layout Rules"). Distances can range from 50 to 1250 μm depending on frequency. 200 μm is typical for MW applications, 100 μm for 40–120 GHz frequencies, and 75 μm for frequencies above 120 GHz (Collier & Skinner, 2007).

The probe tips are usually made using BeCu metal planting for devices based on GaAs with Au pads or W for devices based on Si and SiGe with Al pads (Collier & Skinner, 2007). The probe tip contact widths are typically 50–40 μm for frequencies up to 65 GHz and 25–12 μm for frequencies up to 220 GHz (Collier & Skinner, 2007; "FormFactor: Unparalleled Probing Solutions;"

"FormFactor: Infinity Probe Mechanical Layout Rules"). Although widths of several micrometers have been reported using a microelectromechanical technique for probe fabrication (Marzouk et al., 2015; Haddadi et al., 2015).

Both the coaxial components and planar transmission lines are characterized by very low losses allowing to have less than 1 dB insertion loss up to 110 GHz (Collier & Skinner, 2007; "FormFactor: Unparalleled Probing Solutions"). Moreover, it was reported (Goodshalk, Burr & Williams1994) that HF probes have high mechanical compliance and repeatable measurements for non-planar DUT surfaces (e.g., surface irregularities up to 25 μm high, or 10° of surface non-planarity cause less than –30 dB error in measured data up to 40 GHz).

The leading provider of probe systems for different measurement applications is Form Factor. Manufacturers provide a variety of probes, as well as other necessary equipment ("FormFactor: Unparalleled Probing Solutions"):

1. MW probes:
   - Infinity probes (with a coaxial to thin-film microstrip transition line) for probing up to 500 GHz. Key features: low contact resistance, small contact pads, and a minimum of unwanted couplings to nearby devices and transmission modes;
   - Air coplanar probes for probing from DC to 140 GHz. Key features: lowest losses and compliant tips;
   - Z probes for cryogenic measurements up to 67 GHz. Key features: wide operating temperature from 4 to 573 K and best impedance control;
   - T-wave probes for probing up to 1.1 THz;
2. DC probes for device characterization and reliability testing;
3. Probes for engineering tests on IC packages and circuit boards.

It should be noted that the main disadvantage of probes is their limited lifetime cycle (approx. 500000 cycles ("FormFactor: Unparalleled Probing Solutions")). Probe contacts can wear down, causing overtravel that must be applied to them, which can lead to wafer cracking or crumbling of the probe tips (Collier & Skinner, 2007).

To date, there are only several traceable studies of HF detection properties of MW semiconductor diodes.

Sužiedėlis et al. (Sužiedėlis et al., 2016a, 2016b) used DC and MW probes for on-wafer measurements of the *IV* and voltage sensitivity dependence on the frequency of the MW diodes based on the GaAs/AlGaAs heterojunction. The DC measurements were in good agreement with the theory. The room temperature VP measurements in the K_a-frequency region were held using the TWT generator, broad and coaxial cables, an MW probe, a bias tee, and a digital voltmeter. For comparison, the measurements by mounting the diodes into the waveguide were also performed. It was reported that the obtained voltage sensitivity values using MW probes were three times lower than those obtained using the waveguide text fixture. However, the dynamic range was wider when measured using MW probes and in better agreement with the theory at higher frequencies. It was suggested that the MW probing technique for the investigation of heterojunction MW diodes could give reliable experimental results.

1.5. Conclusions of the First Chapter and Formulation of the Dissertation Tasks

1. Planar MW diodes based on GaAs/AlGaAs structure were proposed as competitors for widely known sensitive Schottky diode detectors of MW radiation. These diodes experience non-linear *IV* characteristics and, due to rectifying action, can be used for electromagnetic sensing in the MW and MMW range.
2. Planar bow-tie MW diodes based on a 2DEG layer based on the GaAs/AlGaAs heterostructure can be used as detecting diodes in MW and MMW ranges due to non-uniform carrier heating phenomena arising from the asymmetrical structure of the diode. Metallic gating over a 2DEG gas channel can increase the voltage sensitivity of the microwave diodes.
3. The majority of MMW range applications require electromagnetic radiation sensors, which can be implemented using MW-detecting diodes with proper voltage sensitivity values.
4. The probing technique can be used for the determination of electrical and HF properties of MW diodes, allowing for on-wafer measurements.

Based on the literature survey performed, the following basic issues must be raised:

1. Creation of new planar MW diodes based on semiconductor structures for electromagnetic signal detection applications in the MMW range.
2. Investigation of *IV* characteristics using the DC probing measurement method and the determination of electrical parameters of the created MW diodes.
3. Investigation of detection properties of the created microwave diodes in the MMW range and the determination of their voltage sensitivity using HF probing techniques and by mounting the diodes in a waveguide transmission line.

2

Design and Fabrication of Microwave Diodes, Research Methodology

This chapter covers the development stages of AlGaAs/GaAs MW diodes investigated in this work: gated MW diodes with 2DEG layer and PD MW diodes based on SI or low-resistivity GaAs substrate. Next, the methodology is presented for investigation of the fabricated MW diodes: the *IV* measurements using a probe station and measurements of detected voltage and voltage sensitivity in the MMW range using a probe station and waveguide detector mount. In addition, methods are presented for evaluating the influence of temperature and illumination on the electrical parameters and detection properties of the investigated MW diodes. The research results presented in this chapter were published in the author's publications Sužiedėlis et al., 2017a, 2017b; Ašmontas et al., 2020; Anbinderis et al., 2020; Anbinderis et al., 2021 and in patent Sužiedėlis et al., 2019.

2.1. Design and Fabrication Technology of the Investigated Samples

Several semiconductors are most common in MW electronics: Ge, Si, SiC, GaAs, InGaAs, and InP. Si is widely known and the most used semiconductor material.

The dominance of silicon is conditioned by well-developed manufacturing technology and a rather low price. However, Si applications are limited by its low electron mobility. Modern emerging electronic technologies operate in HF bands and require semiconductors with better physical and electrical parameters. An III-V (also called "A_3B_5") compound semiconductor group, containing elements from the III and V groups in the periodic table, is widely used in MW and MMW devices because their parameters significantly outrun silicon-based devices with respect to electron mobility. In GaAs compounds, the electron mobility is six times higher than that of Si; thus, GaAs has found wide applications in HF and fast response-based semiconductor devices.

Furthermore, the main development aspects of the investigated GaAs, AlGaAs, and GaAs/AlGaAs semiconductor MW diodes are discussed.

2.1.1. Structure Simulation and Layer Growing in Semiconductor Compounds

The semiconductor compounds for fabrication of the MW semiconductor diodes (samples) based on GaAs, AlGaAs, and GaAs/AlGaAs were obtained using either the LPE or MBE technique. The growing protocols of the layered semiconductor structures for the MBE technique were prepared using Schrödinger-Poisson simulation software.

The main purpose of the semiconductor structure simulation is to provide validation tools for the new compounds. It delivers an analysis of the layered structure that allows for the calculation of an energy band diagram of the structure and electron distribution inside the compound. A band diagram includes the Fermi level, conduction band, and valence band. The alignment of these energy levels directly affects the electrical parameters of the semiconductor structure. Hence, the simulation allows for optimizing the performance of the devices fabricated based on appropriate semiconductor structure while avoiding the use of technological pre-testing compounds, which require significant and costly resources of both hardware and time. When the simulation is performed, the layers are introduced, starting from the upper surface of the structure and down to the substrate. For the software to execute the calculations, parameters of each layer have to be provided, such as AlAs mole fraction x in $Al_xGa_{1-x}As$, conductivity type (n, electrons in case of investigated structures), doping charge carrier density (cm^{-3}) and thickness of each layer (nm).

MBE is a technology used for the deposition of single-crystal monatomic semiconductor layers in ultra-high vacuum ($< 10^{-8}$ Torr). Ultra-high pure Ga, As, and Al are heated separately in the effusion cells until sublimation. Then, the gaseous elements condense on the heated substrate through molecular beam evaporators. The elements interact with each other, and, as a result, single-crystal

GaAs or AlGaAs layers are formed. The layers epitaxially grow onto the wafer by precise control of the deposition rate (depending on the heating temperature), composition, dopant density, and layer thickness (opening/closing effusion cell shutters) down to a single-atom layer. MBE technique lets to achieve the highest purity of the grown layers.

LPE is a technology for growing semiconductor crystal layers from high-temperature melts. Generally, a monocrystal layer crystallizes out of the grow material melt, i.e., the semiconductor substrate is dissolved into the melt, and the layer crystallizes on the surface of the substrate. GaAs and AlGaAs layers can be grown by means of the LPE technique using a quartz tube furnace. This technique allows for growing rather thick layers of the grow material. Although, LPE is only possible at temperatures well below the melting point of the semiconductor. The main advantage of the LPE is a relatively fast deposition rate, although the MBE technology lets achieve thinner and purer layers.

An optical microscope can be used to measure the thickness of the grown layers by taking a cross-sectional view of the epitaxial semiconductor structure. Electrical characteristics of the layers, i.e., electron density and mobility, are measured using the Van der Pauw technique at room or cryogenic temperatures.

2.1.2. Design of the Investigated Microwave Diode Patterns

For the fabrication of the investigated MW diodes based on GaAs, AlGaAs, and GaAs/AlGaAs semiconductor structures, photolithography masks with diode patterns were designed and fabricated. An example of photomask pattern designs for asymmetrically necked bow-tie-type MW diodes is presented in Fig. 2.1.

Separate patterns were designed for diode mesa formation, contact metallization, gating, and transfer of the active layer of the diode onto polyimide films. In Fig. 2.1, pattern (a) shows the photomask design for the first step of photolithography used to form the mesa of the bow-tie diodes. The length of one single diode is 500 μm, while the width is 100 μm. The so-called neck of the diode (the narrowest part of the mesa) is 1 and 2 μm. Pattern (b) was used for the second step of photolithography – creating the design for diode Ohmic contacts, which are further formed during thermal evaporation. Pattern (c) is used for the third step of photolithography to create the gates pattern for the diodes.

Different sizes of narrow and wide gates design are illustrated in Fig. 2.1 (c). Using patterns (d) and (e) allowed for the transfer of a layer of the diode array from the wafer onto a polyimide film. This procedure was necessary to avoid diode shunting when using a low-resistivity GaAs substrate or when measuring the HF parameters of the MW diode using a waveguide detector mount. Polyimide allows for mechanically dividing an array of diodes into single diodes of hundreds of micrometers in size and separately mounting them into a waveguide using a microstrip finline adapter and a detector mount. Each photomask pattern must be aligned to the previous one when performing photolithography steps; thus, the alignment marks are depicted in pattern (e). These alignment marks were used to precisely impose the patterns in pairs, e.g., (a) and (b), (b) and (c), (b) and (d), (d) and (e). Typically, two alignment marks are used to align a photomask and a wafer. One alignment mark is used to align the photomask and the wafer in the X and Y directions, whereas the second alignment mark (preferably spaced far apart from the first one) is used to make corrections for fine offset in rotation.

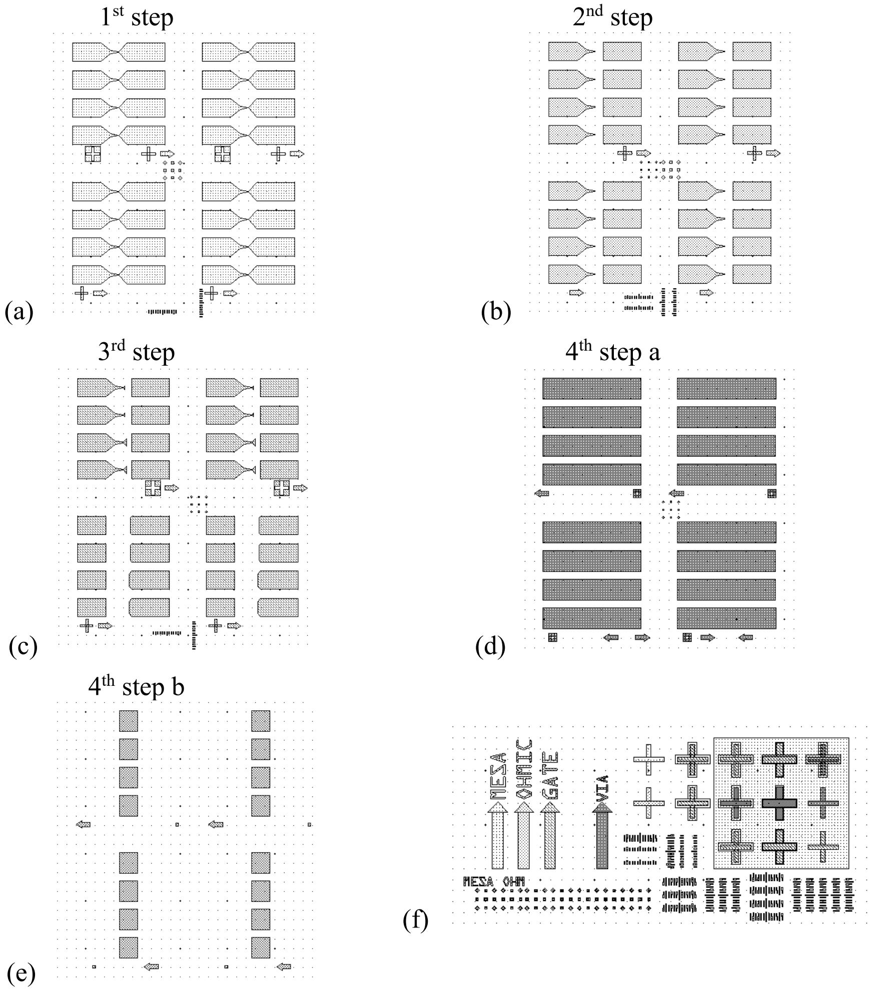

Fig. 2.1. Examples of photomask patterns of asymmetrically necked bow-tie-type diodes for photolithography steps: (a) mesa design, (b) contact metallization, (c) gating, (d) and (e) polyimide transfer, and (f) alignment marks

The photomask patterns were designed using the Layout Editor or Origin software and transferred onto quartz glass covered with a thin film of photoresist from one side using the Heidelberg Instruments DWL66+ laser lithography system.

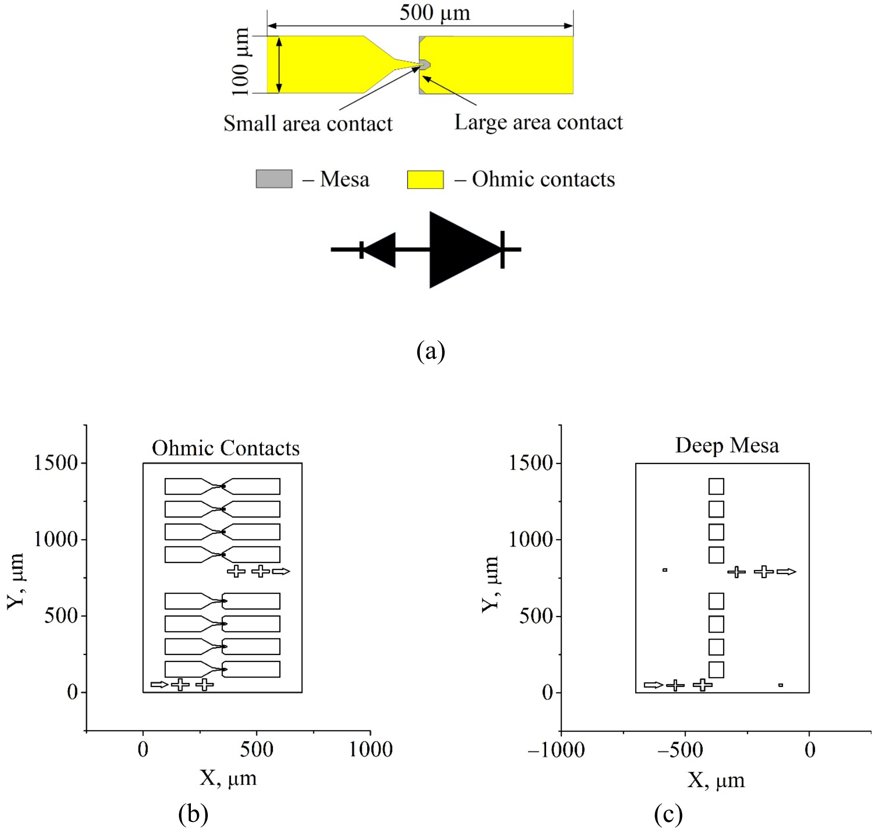

Fig. 2.2. Typical design of a planar MW diode with a small-area contact (a), Ohmic contacts photomask pattern (b), and deep mesa photomask pattern (c)

A typical design with geometrical parameters for a PD MW diode with small-area contact is illustrated in Fig. 2.2 (a). In the investigated PD MW diodes, the mesa pattern is a rectangular shape. As illustrated in Fig. 2.2 (a), there is a small-area Ohmic contact and a large-area Ohmic contact; thus, different areas of the contacts make the PD diode design asymmetric in the sense of an active region. Moreover, such an MW diode can be treated as a couple of different diodes connected in series with a common base, as it is schematically depicted in Fig. 2.2 (a). The tip of the left contact (Fig. 2.2) varied in the range of 1–4 μm.

The photomasks for the PD MW diodes were made in the same manner as for the bow-tie type MW diodes. Fig. 2.2 (b) shows the photomask pattern for Ohmic contacts, and pattern (c) is used for mesa formation. The polyimide transfer procedure had the same pattern as depicted in Fig. 2.1 (d).

2.1.3. Fabrication of Microwave Semiconductor Diodes

Generally, semiconductor device fabrication technology involves surface cleaning, photolithography, etching, thermal evaporation, and annealing procedures.

First, the grown semiconductor structures are prepared for the photolithography technique. The wafer surface must be cleaned and deoxidized for better photoresist adhesion. Usually, acetone, isopropyl alcohol, methanol, and nitrogen gas are used for cleaning wafers from dust, abrasive particles, lint, bacteria, film residues, and other contaminants. Wafer deoxidization should also be performed prior to fabrication processes. It is necessary to remove excess native oxide that forms on the surface of the wafer; otherwise, the etching reaction can be unpredictable due to the uneven thickness of the native oxides on the surface. The thickness of the native oxide depends on how long the wafer was exposed to the atmosphere. A solution of hydrochloric acid and DI water ($HCl: H_2O = 1:10$) was used for the deoxidization of the grown wafers. After the oxide and all surface impurities are removed, a layer of a photoresist (a polymer sensitive to UV light) can be deposited on the surface of a wafer (Fig. 2.3).

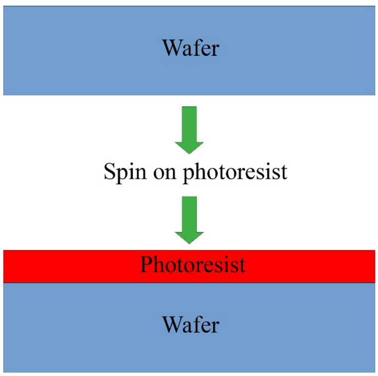

Fig. 2.3. Photoresist application on a wafer

The wafer was placed in a centrifuge spinner (800 RPM for 40 s), and the photoresist was applied using a special injector and uniformly coated by centrifugal force, forming a thin film. For the first step of photolithography, a positive photoresist, "PMGI SFII or Shipley S1805," was used. After the photoresist deposition, the wafer was placed onto a hot plate (100 °C, 1 min) for post-bake to harden the photoresist film by removing all the solvents and to improve the adhesion between the wafer and photoresist. Once the photoresist is deposited, the wafer can be exposed to intensive UV light through the photomask pattern, i.e., photolithography can be performed. Photolithography is performed using a mask aligner.

The principle of photolithography is illustrated in Fig. 2.4. This procedure was performed to define the shape of the MW diode on the wafer. As mentioned in Section 2.1.2, the first photolithography was used to create the mesas of the MW diodes (Fig. 2.1 (a) for bow-tie type MW diodes).

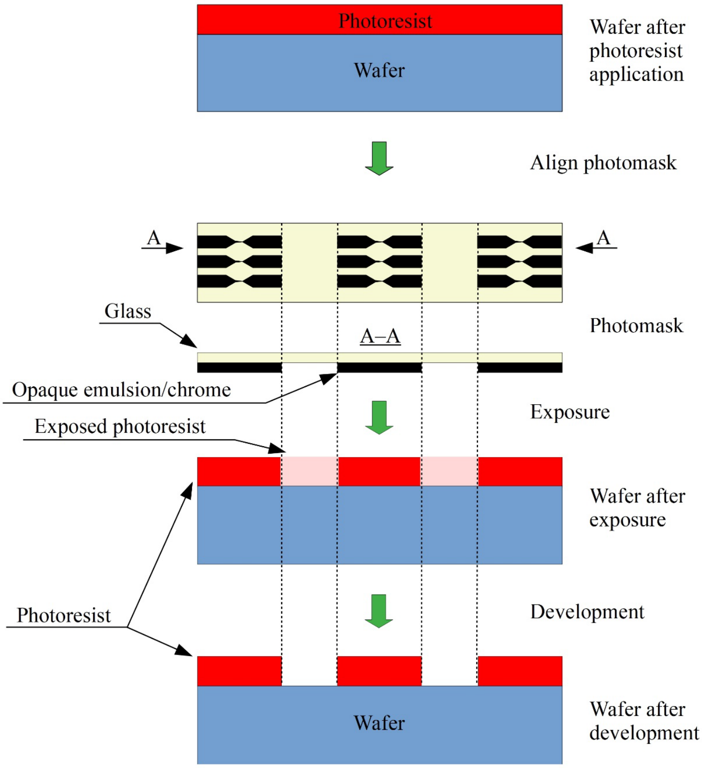

Fig. 2.4. Wafer photolithography procedure using positive photoresist

The designed photomask pattern and the wafer were placed into the photomask aligner, where the wafer was exposed to UV light (9–11 s for positive photoresist). When using a positive photoresist, only the part of the resist that is exposed becomes soluble to the photoresist developer. After exposure, the wafer was placed on a hot plate for post-bake (120 °C, 1 min) to polymerize the photoresist improving etch resistance. Next, the wafer was immersed in a developer "MF-319" for 20 s. The developer dissolves only the exposed part of the photoresist to achieve the desired pattern with the deposited photoresist on top of the upper layer. Subsequently, the wafer was rinsed in DI water and dried in nitrogen gas.

The next fabrication step was wet chemical etching. To form a functional semiconductor structure on a substrate, it is necessary to etch thin layers previously deposited during an epitaxial growth procedure and/or the substrate itself. In essence, the underlying layers are removed by etching through the openings in the photoresist pattern (Fig. 2.5). The semiconductor wafer was etched to reach the undoped AlGaAs spacer layer in the case of a selectively doped structure. The main advantages of the wet chemical etching method are its low cost and simplicity, high etching rate, and selectivity. However, wet etching is an isotropic process, and thus, the etching can also remove substrate material under the masking layer, which leads to undercut bias when etching epitaxial structures and requires very precise control. In addition, this method has poor repeatability (influenced by the temperature and concentration of chemical reagents) and produces chemical contamination, which requires the disposal and consistent replacement of large amounts of etching chemicals that result in toxic waste.

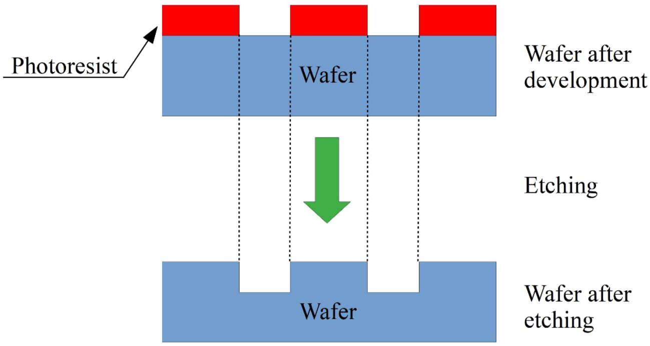

Fig. 2.5. Wafer wet chemical etching procedure

As mentioned previously, the wet chemical etching technique is isotropic but can also be anisotropic depending on the plane of the crystalline to which it is exposed. For comparison, anisotropic etching, in contrast to isotropic etching, means different etch rates in different directions in the material. Single-crystal materials, such as Si wafers, show high anisotropy; that is, etching is performed mainly in one direction. In the case of GaAs MW diodes fabrication, anisotropy is crucially important because it is necessary to remove layers only in the vertical direction. The result should be a pyramid-shaped hole instead of a hole with rounded sidewalls when using an isotropic etchant (Fig. 2.6); thus, during anisotropic etching, the undercut is much smaller, and during isotropic etching, the undercut is close to the etching depth. The etchant was obtained by preparing a solution that consisted of hydrogen peroxide (30 %), DI water, and phosphoric acid (85 %) H_2O_2:H_2O:H_3PO_4 = 1:50:1, respectively, and mixing the solvents with a strimmer. Also, phosphorus-based etchant of special composition, H_3O_4:H_2O_2:H_2O = 1:4:45 (Baca & Ashby, 2005), can be used purposefully, creating a mesa with flat slopes, as this is important to protect the metal terminal from cracking on the mesa slope. To predict the etching rate, a test wafer was used. The test wafer was immersed in the etchant for a certain amount of time (e.g., 30 s), and the etching depth of the test wafer was measured using a stylus profilometer "Dektak 6M, Veeco Metrology LLC." When the etching depth and time of exposure to the chemicals are determined, the desired etching rate can be calculated.

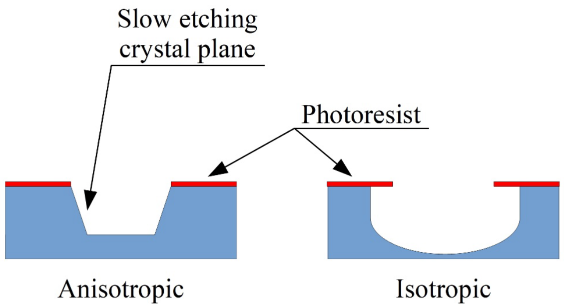

Fig. 2.6. Shapes of anisotropic and isotropic wet chemical etching

Finally, the sample wafer was etched in the described solution for a certain amount of time (depending on the desired depth – from 40 to 120 nm in the investigated MW diodes), i.e., the mesas of the semiconductor MW diodes were formed. To stop the etching process, the wafer was rinsed in DI water and dried in nitrogen gas. The dimensions of the neck of the diode mesas were measured using SEM.

After the formation of the mesas, the second step of photolithography was performed. This step was used for opening the windows for metallization of Ohmic contacts (Fig. 2.1 (b) for bow-tie type MW diodes). An image-reversal photoresist, "MicroChemicals AZ 5214E," is usually used for this step of photolithography to form the slopes for the lift-off procedure (Fig. 2.7). When using an image-reversal photoresist, unlike a positive photoresist, the unexposed area becomes soluble to the developer. The first two steps of photolithography were similar to those described previously, i.e., the exposure with a mask pattern and post-bake (2.6 s exposure time for image-reversal photoresist). However, when using an image-reversal photoresist, flood exposure is also performed after the post-bake procedure to increase the development rate. The wafer is exposed to UV light without a photomask to affect all the areas that were not initially exposed. After flood exposure, the wafer was immersed in the developer "AZ-726," dissolving the unexposed part of the photoresist, and the Ohmic contact metallization pattern was formed on the wafer's surface.

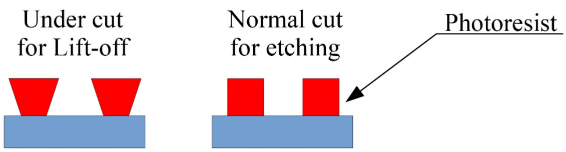

Fig. 2.7. Wafer slopes for lift-off and etching procedures

Plasma cleaning in the ozone gas atmosphere and adhesion improvement can be performed after the photolithography steps using plasma treatment equipment "March PX500." The samples are placed into a chamber, where organic contamination is swept away from the surface by an air plasma flow, i.e., organic contaminants are removed when they react with oxygen species in the plasma, creating low-weight (molecular) compounds.

To create Ohmic contacts for MW diodes, thermal evaporation was performed using "VAKSIS PVD Vapor-5S_Th." The principle of thermal evaporation is illustrated in Fig. 2.8. During the thermal evaporation procedure, the wafer is placed into a sealed and vented camera, where a vacuum of 6×10^{-6} Torr is achieved. The metal pellets in a boat are heated by an electric current source and evaporated onto the wafer surface coated with a photoresist pattern. It is essential to control the evaporation rate and thickness of the metallic film by controlling the current. The properties of the contacts are influenced by their composition, layer thickness, evaporation procedure conditions, and the quality of the prepared wafer surface. The most common recipe to ensure good Ohmic contacts to *n*-GaAs (Williams, 1990) is Ni (5 nm), Au (200 nm), Ge (100 nm), Ni (75 nm), and Au (100 nm). The Ohmic contacts of the investigated MW diodes were formed using the described recipe by evaporating metals in the exact sequence and thickness as listed above. During the evaporation, one of the metals (Ge) is used as a semiconductor doping layer, and thus, a specific number of dopants is put onto the wafer surface through openings in the photoresist layer.

After the metals are evaporated onto the wafer, the lift-off procedure is performed for pattering (Fig. 2.8). The wafer is placed into an organic solvent, and the part of photoresist that has been exposed to the organic solvent is removed together with the unnecessary metal by lifting it off. For the lift-off procedure, the wafer was placed in acetone.

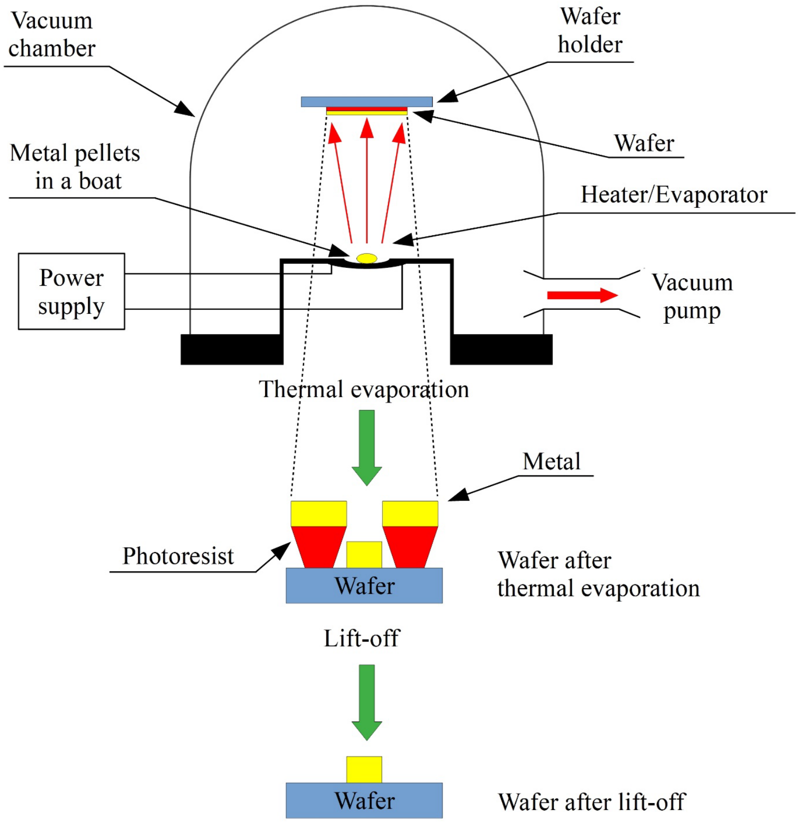

Fig. 2.8. Wafer thermal evaporation and lift-off procedures

The Ohmic contacts are, therefore, fully formed when the wafer is annealed in a forming hydrogen gas N_2-H_2 atmosphere while rapidly heated and cooled in the tube furnace. The annealing temperature usually varies from 380 to 450 °C. The heating regime is as follows: 10 s rapid rise to 200 °C/holding 200 °C for 60 s/10 s rise to 380–450 °C /holding 380–450 °C for 60 s/cooling stage for 150 s. To determine the most appropriate annealing temperature, the TLM was used. This method allows for determining the sheet resistance and specific contact resistance. Several test samples with metal contacts (same recipe as described for Ohmic contacts) were made according to the pattern illustrated in Fig. 2.9 and annealed at different temperatures. Contacts are separated by 2, 5, 10, 20, 50, and 100 μm gaps.

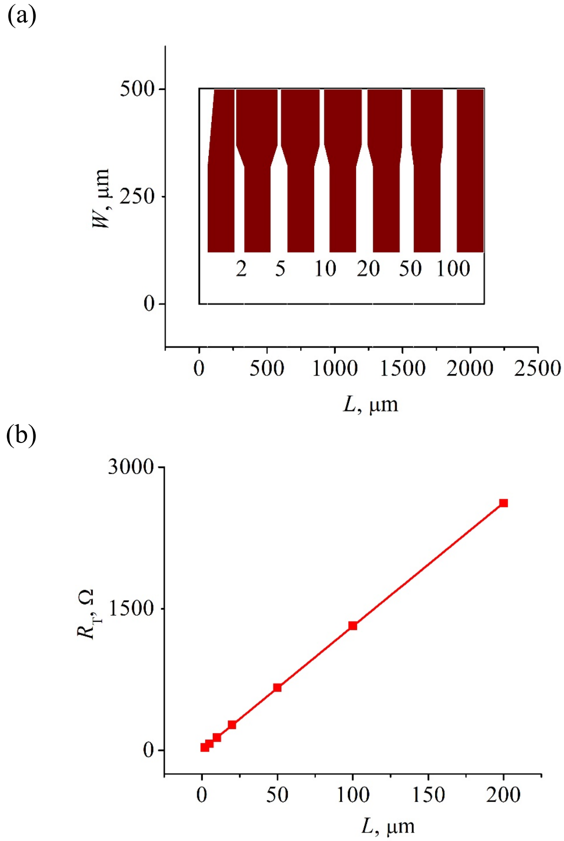

Fig. 2.9. Schematic view of TLM contacts (a) and a plot example of measured total resistance on the spacing gap (b)

DC probes are applied to pairs of contacts, and the total resistance between them is measured by applying a voltage across the contacts and measuring the resulting current using an ammeter (precision semiconductor parameter analyzer). The total measured resistance R_T is a sum of the contact resistance R_C of the first contact, the contact resistance of the second contact, and the bulk resistance R_B of the semiconductor gap in between the contacts. The contact spacing gap can then be expressed in terms of the ratio L/W, where L and W are the length and width of the area (gap) between two contacts. Test samples were measured, and the relation between measured total resistance and contacts spacing gap size was plotted at different contact annealing temperatures. The plot should be linear with a certain slope (Fig. 2.9), as the total resistance should increase with an increasing spacing gap due to an increase in bulk resistance. The slope of the line lets to extract the sheet resistance (R_{sh} = slope/W), while the intercept of the line with the Y-axis is the double of specific contact resistance R_C. Thus, the sheet resistance, as well as the specific contact resistance, can be determined from the plot. The lowest specific contact resistance corresponds to the best annealing temperature, and the sample wafer should be annealed at the most appropriate temperature. After the annealing step, the fabricated semiconductor MW diodes were ready for investigation and measurements using the probe station.

The third step of photolithography is necessary in the case of gating the active area of the semiconductor MW diode (Fig. 2.1 (c) for bow-tie type MW diodes). A transistor-like design of the bow-tie diode realized as a partial metal cover of either narrow or wide part of the asymmetrically shaped semiconductor structure was implemented with the aim of increasing the voltage sensitivity of the MW diode as additional current rectification occurs. A negative photoresist was used for gate patterning, and the photolithography procedure was the same as that for Ohmic contact formation. After the photolithography and development steps, the wafer was placed into the thermal evaporation chamber, where the metal gates were formed on the fabricated MW diodes. The recipe for the gates was Ti (15 nm) and Au (185 nm). Ti was used for better adhesion. Gates were finalized by the lift-off technique. It is worth mentioning that annealing is not performed during the gating procedure.

The fourth step of photolithography is used when semiconductor diodes are transferred onto an elastic dielectric polyimide film to avoid shunting the diode contacts through the GaAs substrate. The wafer surface is covered with photoresist according to the appropriate pattern, then chemically etched and mechanically thinned from the substrate side, leaving the fabricated semiconductor structures on the polyimide film. As mentioned in Section 2.1.2, this method is preferable for HF measurements when the dimensions of an MW transmission line drop to the submillimeter. The polyimide transfer procedure involves two steps of photolithography: photolithography using the pattern (d) (Fig. 2.1) for deep mesa etching and photolithography using the pattern (e) (Fig. 2.1) to unveil metal contacts. Several micrometer-deep trenches were chemically etched around each individual diode. Subsequently, these notches were used to control the substrate thinning process down to micrometric thickness. The notches also served as alignment marks during the last step of diode fabrication when the metallic contacts had to be stripped off. The face side of the substrate was then covered with polyimide using the spin-on technique and cured at a temperature of 250 °C in ambient air for one hour. The obtained elastic few-micrometers-thick film served later as a mechanical support for the finished diode. Finally, two steps of wet chemical etching were used, first, to thin the substrate from its back side down to several micrometers until the deep notches appeared, and, secondly, to remove the residual semiconductor material from the ends of the metallic contacts.

2.2. Investigated Samples

This work covers the investigations of a couple of PD MW diode types fabricated based on a SI GaAs substrate and a low-resistivity GaAs substrate. In addition, bow-tie diodes with gates over the 2DEG channel are presented. The design and parameters of the diodes and the main fabrication aspects are discussed in this section.

2.2.1. Planar Dual Microwave Diodes Based on Low-Resistivity GaAs Substrate

Three types of heavily doped polished GaAs substrates (350 µm AGChP-M-21a (1.0.0) 0° 30′, Ø 26 mm, Plant of Pure Metals, Svitlovodsk, Ukraine), n^{++}-GaAs with donor density 4×10^{18} cm^{-3}, n^{+}-GaAs, doped to 4×10^{17} cm^{-3}, and p^{++}-GaAs with acceptor density of 4×10^{18} cm^{-3}, were taken as a basic material for the fabrication of PD MW diodes instead of complex MBE structures used as a rule for Schottky and PDB diode fabrication. These MW diodes were chosen for the simplicity of design (Fig. 2.10) since only the heavily doped n^{+}-GaAs and p^{+}-GaAs semiconductor substrates with smoothly polished surfaces were chosen as basic materials for the diode fabrication. The number of fabrication steps is minimized if compared to the production of a heterojunction planar diode (Gradauskas et al., 2010).

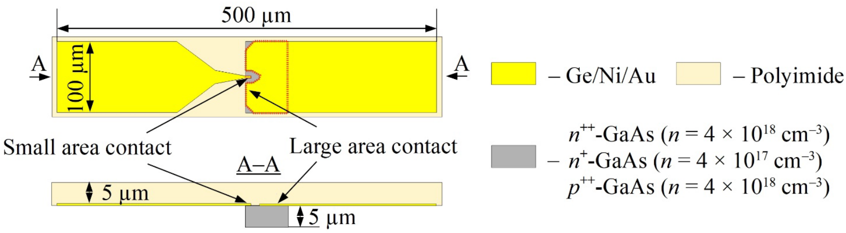

Fig. 2.10. Schematic view of a PD semiconductor MW diode based on three types of low-resistivity GaAs substrates

Firstly, photolithography was used to form patterns for metallic contacts of the diodes. Both contacts (Fig. 2.10 – small area on the left and large area on the right) were made in one step of thermal evaporation of Ge/Ni/Au metals followed by lift-off and rapid annealing at 430 °C temperature in the hydrogen atmosphere. Then, a polyimide film was created on the face side of the substrate. Afterward, thinning of the substrate was performed using wet chemical etching up to the thickness of several micrometers, and rectangular mesas of the MW diode were created using photolithography and wet chemical etching from the GaAs substrate side. The microphotograph of the active region of the PD MW diode is presented in Fig. 2.11.

(a)

(b)

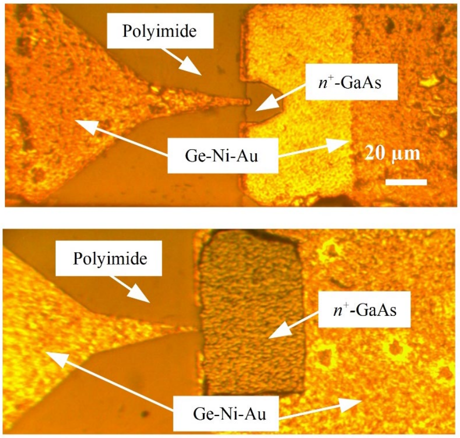

Fig. 2.11. Microphotograph of the planar MW diode: (a) a view from the side of the polyimide film and (b) a view from the side of the semiconductor mesa and metallic contacts

The small-area contact of the diode can be seen from the side of the polyimide film as a tip of the Ge-Ni-Au "finger" lying on n^+-GaAs. The area of a small-area contact varied from several up to tens of micrometers. The area of the large contact of the PD diode amounts to about 4000 µm^2. The electrical resistance and voltage sensitivity of the diodes were controlled by means of varying the small contact area on the diode's mesa (Fig. 2.12).

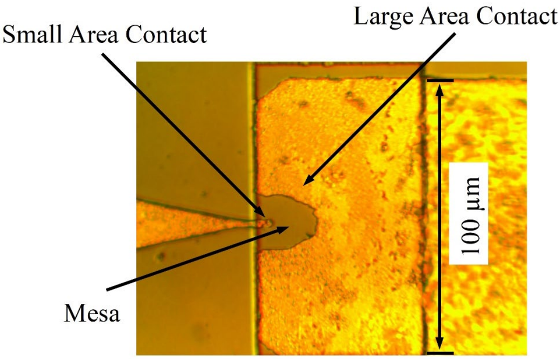

Fig. 2.12. Microphotograph of the mesa area of the planar MW diode

This novel design of PD MW diodes can be cost-effective since the simplified technological process, and use of simplex semiconductor material reduce time and fabrication costs. This design was also used for the fabrication of PD MW diodes with ternary n-type $Al_xGa_{1-x}As$ layer based on a SI GaAs substrate.

2.2.2. Planar Dual Microwave Diodes Based on Semi-Insulating GaAs Substrate

The active region of the MW diode was an epitaxial n-type $Al_xGa_{1-x}As$ layer of submicrometric thickness grown on a SI GaAs substrate (350 μm AGChP-I-26a (1.0.0) 0° 30′, Ø 26 mm, Plant of Pure Metals, Svitlovodsk, Ukraine) by means of LPE technique in the quartz tube furnace. Epitaxial layers were grown using the supercooled growth method in a "wipingless" horizontal graphite sliding boat. Initial supercooling was performed at 6 °C below the melting point of the Ga-GaAs mixture. The growth temperature interval was (803–802) °C with a cooling speed of 0.5 °C/min. The epitaxial layers were not intentionally doped. AlAs mole fraction x in the $Al_xGa_{1-x}As$ semiconductor was chosen as $x = 0$, 0.15, and 0.3. The cross-sectional view of the used structures is presented in Fig. 2.13. The i-$Al_{0.8}Ga_{0.2}As$ acts as a technological stop layer for the GaAs etchant. In the case of transferring these MW diodes onto a polyimide film, when etching is performed from the substrate side, the etching rate slows down drastically when the i-$Al_{0.8}Ga_{0.2}As$ layer is reached.

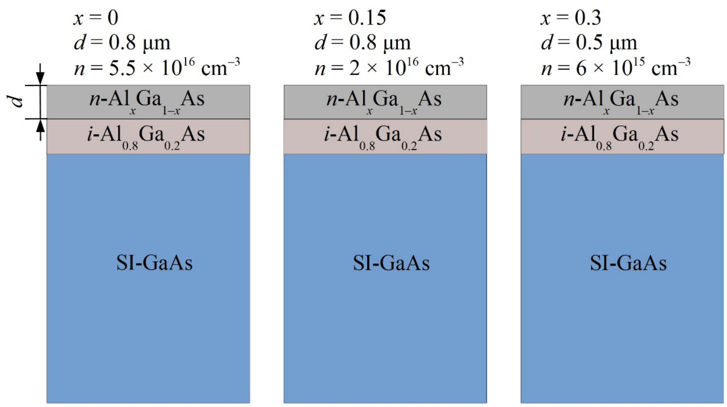

Fig.2.13. Cross-sectional view of the submicrometer-thick n-type $Al_xGa_{1-x}As$ layers grown based on a SI GaAs substrate for PD MW diodes with different aluminum arsenide mole fractions ($x = 0$; 0.15; 0.3)

Parameters of the epitaxial layers are presented in Table 2.1. An optical microscope was used to measure the thickness of the grown layers by taking a cross-sectional view of the structure fraction. The electrical characteristics of the layers were measured using the Van der Pauw technique at room temperature.

Table 2.1. Parameters of the epitaxially grown $Al_xGa_{1-x}As$ layers

AlAs Mole Fraction x	Layer Thickness t, µm	Electron Density n, cm^{-3}	Electron Mobility μ, $cm^2/(V \cdot s)$	Electrical Resistivity ρ, $\Omega \cdot cm$	Sheet Resistance R_{sh}, $\Omega/\square$
0	0.8	5.5×10^{16}	1820	6	780
0.15	0.8	2.0×10^{16}	1680	19	2330
0.3	0.5	6.0×10^{15}	1500	70	13880

The schematic view of the PD MW diode is presented in Fig. 2.14 (a), and its cross-sectional view is shown in Fig. 2.14 (b).

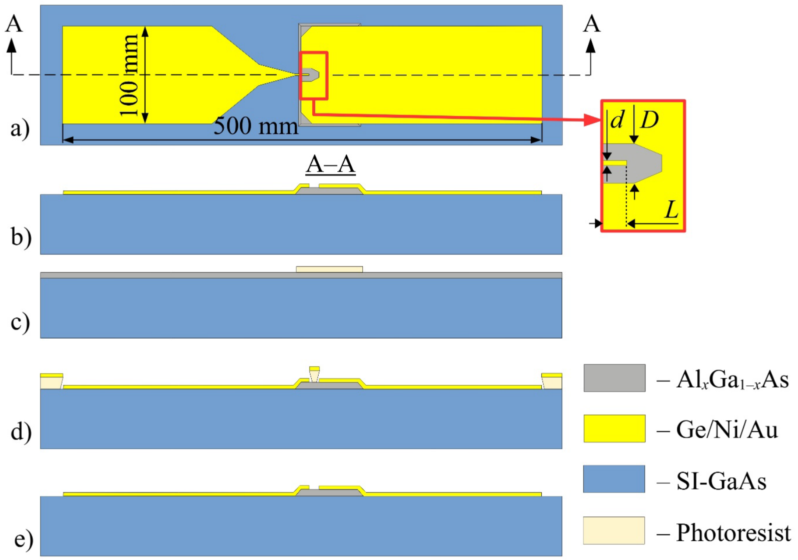

Fig. 2.14. Schematic top (a) and cross-sectional (b) views of the planar MW diode on a SI substrate GaAs. Successive fabrication steps of the diode are shown in parts (c–e)

The simple fabrication procedure of the diode is sketched in Fig. 2.14 (c), (e). First, photolithography was performed using a positive Shipley S1805 photoresist to form rectangular 105×60 µm^2 AlGaAs mesas (Fig. 2.14 – c). The phosphorus-based etchant with a special composition was chosen on purpose, creating a mesa with flat slopes measured using a profilometer. The slope angle ranged between 21° and 24°, independent of the orientation of the mesas, with respect to the crystallographic directions of the semiconductor substrate. Second, photolithography was carried out using an image-reversal photoresist to open the windows for the deposition of metallic contacts. The width *d* of the tip of the left contact (Fig. 2.14 – a) varied in the range of 1–4 μm in different MW diodes. The metallic contacts of the diodes were fabricated by means of successive thermal evaporation of Ge/Ni/Au metals (Fig. 2.14 – d) using the recipe discussed in Section 2.1.3. Contact patterns were formed using the lift-off technique with consequent annealing of the semiconductor structures at 430 °C in the hydrogen atmosphere in the tube furnace (Fig. 2.14 – e). At this stage, it is worth noting that the fabrication procedure of the PD MW diodes situated on the SI substrate was completed, and such samples were handy for measurements on the probe station. In contrast, the dual MW diodes that were based on a low-resistivity GaAs substrate additionally needed to be transferred onto a dielectric polyimide film to avoid electrical shunting through the low-resistivity GaAs substrate.

2.2.3. Bow-Tie Diodes with Gates over a Two-Dimensional Electron Gas Channel

Selectively doped GaAs/AlGaAs heterostructure epitaxially grown onto SI GaAs substrate (100 ± 0.3°, Ø 50 mm) served as the active layer of the diodes. The semiconductor structure was grown at the Braun Center for Submicron Research, Weizmann Institute of Science, Israel. The cross-sectional view, electron distribution, and energy band diagram of the epitaxially grown selectively doped GaAs/AlGaAs heterostructure on a SI GaAs substrate are presented in Fig. 2.15. The simulation was performed assuming that the semiconductor structure is at room temperature, all dopants are ionized, and the surface potential is equal to 0.6 eV. Solid lines represent the energy band diagram, and dotted lines represent the electron density. Fermi energy equals zero (eV). This structure was used for the fabrication of bow-tie type MW diodes with narrow and wide gates above the 2DEG layer.

The sheet of 2DEG is formed in the *i*-GaAs buffer layer beside the GaAs/AlGaAs interface. The widths of the layers of the heterostructure: *i*-GaAs cap layer (10 nm), spacers *i*-$Al_{0.3}Ga_{0.7}As$ (10 and 7 nm), doped barrier n^+-$Al_{0.3}Ga_{0.7}As$ (10 nm), and donor density in the doped barrier (3.7×10^{18} cm^{-3}) were chosen to diminish the parasitic parallel electron channel in the AlGaAs barrier and to make the selectively doped heterostructure more sensitive to an electrical bias voltage applied to the metal gate that partly covers the surface of the active area of the MW diode fabricated on the basis of this structure. The lower layer of *i*-GaAs in Fig. 2.15 acts as a buffer layer, stopping the diffusion of the dopants from the substrate into the epitaxially grown layers, lowering the density of the crystallographic defects, and allowing to grow layers with smooth surfaces.

The *i*-AlGaAs layer acts as an undoped spacer on which the doped n^+-AlGaAs layer is grown. The next layer is the intrinsic conductivity layer *i*-AlGaAs, also used as a spacer. The upper *i*-GaAs layer secures the *i*-AlGaAs layer from oxidation.

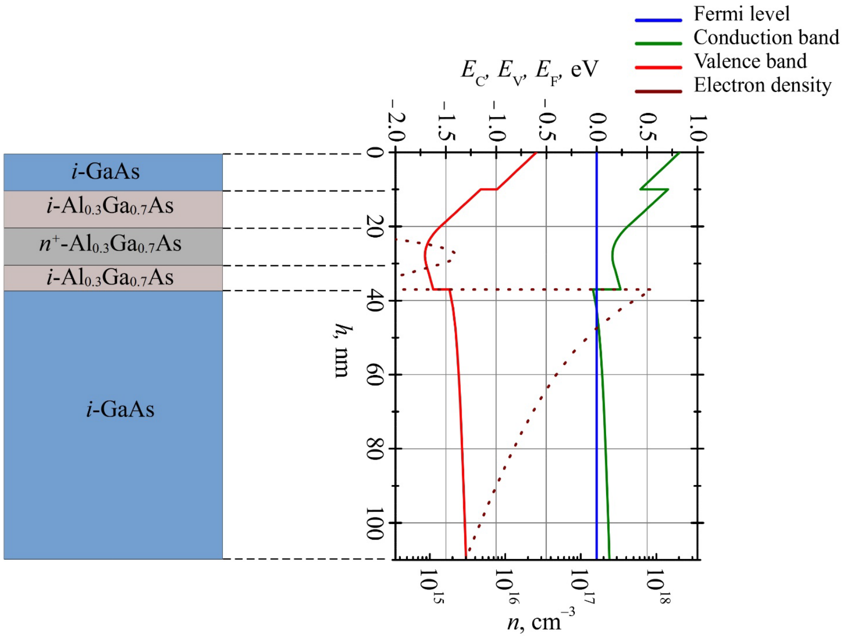

Fig. 2.15. Cross-sectional view, energy band diagram, and electron distribution of the selectively doped GaAs/AlGaAs heterostructure epitaxially grown on a semi-insulating GaAs substrate

The fabricated asymmetrically necked bow-tie diodes with narrow and wide gates above the 2DEG channel are schematically depicted in Fig. 2.16. The fabrication steps were the same as discussed in Section 2.1.3. Mesas of the asymmetrically shaped structure were formed by means of the wet chemical etching technique using a phosphorus acid solution. The etching depth was 35 nm, which ensured surefire confinement of the 2DEG channel. The width of the neck in the narrowest part of the diode was 1.5 μm. Ohmic contacts for the diodes were fabricated by thermal evaporation of Ge/Ni/Au metals and the lift-off technique. The Ohmic contacts were then finalized by means of rapid annealing in forming a gas ambient atmosphere. The temperature was raised up to 420 °C. The gates of the diodes were fabricated by applying the lift-off technique for the thermally evaporated Ti/Au metals layer. Both the wide and the narrow gates spanned the active layer for 8 μm, which covers up about 20 % of its length.

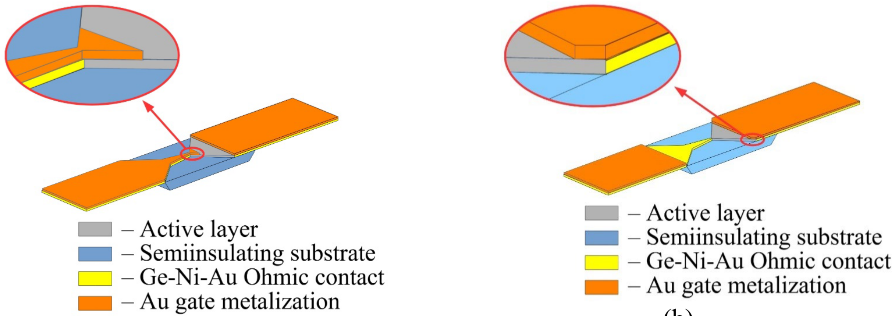

(a) (b)

Fig. 2.16. Schematic view of a bow-tie diode with (a) a narrow and (b) a wide gate placed over the active layer of the diode. The polyimide film is not depicted in the figure

Microphotographs of the fabricated bow-tie diodes with narrow and wide gates are presented in Fig. 2.17.

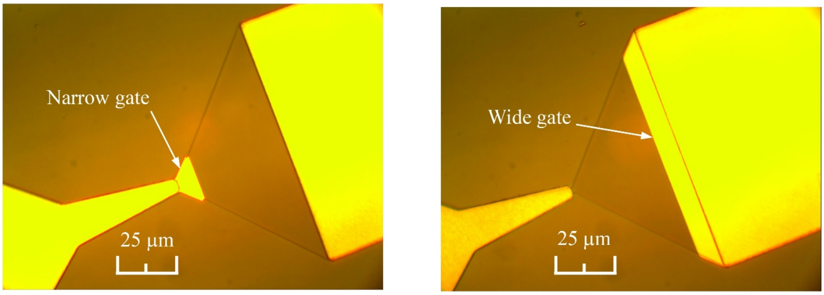

(a) (b)

Fig. 2.17. Microphotographs of the bow-tie diodes with a narrow gate near the neck of the diode (a) and with the gate near the wide metallic contact (b)

Subsequently, technological operations were performed to transfer the bow-tie diodes onto an elastic dielectric polyimide film.

2.3. Research of Electrical Properties of Samples in the Direct Current Mode

Measurements of the semiconductor MW diodes in the DC current mode were performed using a probe station. When this measurement approach is performed, probes are applied to the Ohmic contacts of the diode (Fig. 2.18).

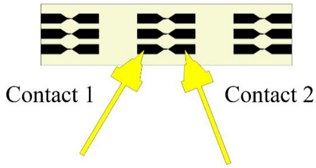

Fig. 2.18. Schematic view of the measurement of the MW diode electrical properties using probes

The current flows from the first probe (contact 1) into the metal contact across the metal-semiconductor junction, through the active area of the MW diode, across the other metal-semiconductor junction into the second contact, and from there, into the other probe (contact 2) and the external measuring circuit. This measurement technique allows for determining the main electrical properties of the MW semiconductor diode, such as the *IV* characteristics or electrical resistance. Using a probe station allows for performing measurements directly on-wafer, i.e., on separate diodes uncut out of the whole semiconductor diode array to determine light influence during the measurements and have more convenient possibilities for gathering informative statistical data of the diode properties.

The *IV* characteristic is usually used as one of the main tools to determine the basic electrical parameters of semiconductor MW diodes. It illustrates the relationship between the electric current flowing through the diode and the corresponding voltage that is applied to it. The *IV* characteristics were measured using the DC probe station "SUSS Microtec EP6" with "SUSS Microtec PH110" probes and precision measurement equipment – the *IV* analyzer "Agilent E5270B" with "Agilent E5287A" slots. The schematic block view of the measurement setup is illustrated in Fig. 2.19.

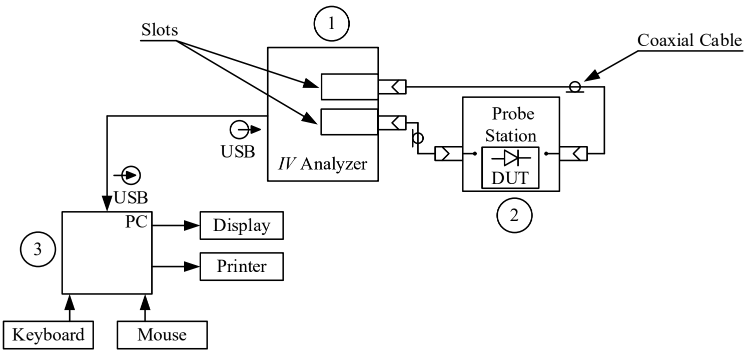

Fig. 2.19. Structure block diagram of the *IV* characteristics measurement setup using the probe station

Each of the two probes is connected to the *IV* analyzer (Fig. 2.19 – 1) slots using BNC coaxial cables. Both probes are placed onto the Ohmic contacts of the diode using the probe station (2), and the current flows from one probe to another through the metal-semiconductor contacts of the MW diode and the active region, as mentioned previously.

The measurements were performed using the PC software "Agilent EasyExpert," which allows for determining the voltage range and step size, as well as the polarity of the probes. The controlling PC (3) is connected to the *IV* analyzer via USB. The virtual control panel is presented in Fig. 2.20.

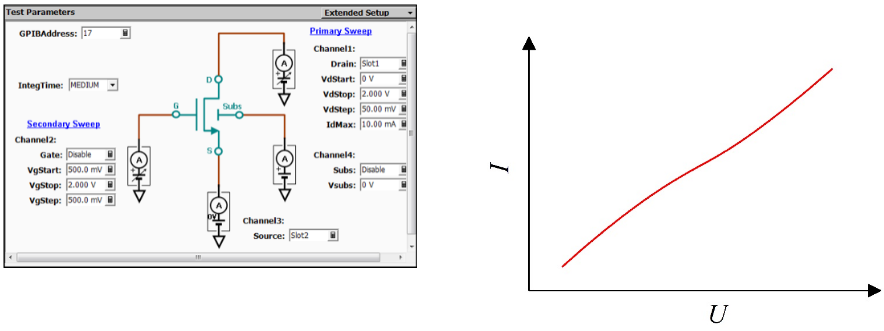

(a) (b)

Fig. 2.20. Virtual control panel of "Agilent EasyExpert" PC Software (a) for the *IV* measurements (b) using the probe station

During the measurement, the *IV* characteristics are obtained, which can be used for further analysis of the electrical properties of the samples under test, such as asymmetry and electrical resistance.

The current was measured as a function of voltage. Hence, the electrical resistance at zero bias voltage was calculated using the first derivative of the *IV* curve according to the classical differential expression of electrical resistance using Equation 2.1 (Pavasaris, 2009):

$$R = \frac{\mathrm{d}U}{\mathrm{d}I}. \tag{2.1}$$

According to Ašmontas and Sužiedėlis (Ašmontas & Sužiedėlis, 1994), asymmetry of the *IV* characteristics of the diodes can be related to their prospective voltage sensitivity to MW radiation. The voltage sensitivity *S* of an MW diode formed at the basis of the small-area n-n^+ junction depends on the asymmetry of the *IV* characteristic calculated according to Equation 2.2 (Ašmontas & Sužiedėlis, 1994):

$$Asymmetry = S = \frac{R_{\mathrm{r}} - R_{\mathrm{f}}}{2U}, \tag{2.2}$$

where R_{r} and R_{f} denote the electrical resistance of the diode under reverse and forward direction voltage U, respectively. It is worth mentioning that the MW power is assumed to be fully absorbed by the diode when the voltage sensitivity S is evaluated.

2.4. Investigation of High-Frequency Properties of Microwave Diodes

The MMW range requires certain specifications for MW detectors: the voltage sensitivity (thus, the detected voltage as well) should not depend on frequency, and the detectors must be both reliable and sensitive to the impact of electromagnetic radiation. It was discussed in Chapter 1 that the main element of an MW detector is a semiconductor MW diode. HF parameters of the MW diodes, such as detected voltage, are usually investigated by mounting a single diode into an MW waveguide transmission line. However, this process is rather complicated and time-consuming. These measurements can be achieved using an HF probe station, which allows for performing detected voltage and voltage sensitivity measurements. This measurement approach can both save time and exclude the possibility of diode damage during the diode mounting process, as the measurements are made right onto the semiconductor substrate without dividing it into single diodes. This measurement approach allows additional options in the investigation of the diodes and to have greater statistical data.

Detection properties of the MW diodes were investigated in frequency ranges 26–37.5 GHz, 75–110 GHz, 110–170 GHz, and 220–340 GHz.

At frequencies 26–37.5 GHz (K_a-band), detection properties were investigated using a probe station. During the experiment, the detected voltage of the semiconductor MW diodes was measured as a function of signal frequency and power.

At frequencies 75–110 GHz (W band) and 110–170 GHz (D band), the MW diodes were mounted into the waveguide transmission line using a detector mount, and the detected voltage was measured as a function of signal frequency.

At frequencies 220–340 GHz, the detected voltage of the semiconductor MW diodes was measured as a function of frequency in a waveguide detector mount using a frequency multiplier.

During the measurements, the VP characteristics were obtained by measuring the detected voltage as a function of the incident MW signal power at certain frequencies. The detected voltage dependencies on frequency were obtained by applying a certain level of incident power of the MW signal to the diode in the linear VP characteristics range.

The expression of voltage sensitivity S of the semiconductor MW diode with respect to the incident microwave power P_{i} was derived using Equation 2.3 (Ašmontas et al., 2000):

$$S = \frac{U_{\mathrm{d}}}{P_{\mathrm{i}}}, \quad (2.3)$$

where U_{d} is the detected voltage over the ends of the MW diode.

The hardness of the diodes to withstand the maximum power of the MW radiation was evaluated using the value of the highest applied voltage, at which the IV characteristic did not yet begin to change. The upper limit of the dynamic range of the diode was set by microwave power value that ends the linear dependence of the detected voltage on power. The minimum limit of the dynamic range was set as power level P_{min} within the noise floor, which was derived from NEP according to Equations 2.4 and 2.5:

$$NEP = \frac{U_{\mathrm{N}}}{S\sqrt{\Delta f}} = \frac{\sqrt{4kTR}}{S\sqrt{\Delta f}}, \quad (2.4)$$

where U_{N} is noise voltage spectral density, Δf – frequency bandwidth of the measuring device, k is the Boltzmann constant, R is electrical resistance (at zero bias, i.e., R_0), and T is temperature.

$$P_{\mathrm{min}} = NEP\sqrt{\Delta f}. \quad (2.5)$$

2.4.1. Measurements of Detected Voltage Dependencies on Frequency and Power Using a Probe Station

MW diodes were investigated directly on the semiconductor array either on the SI substrate or on the polyimide film using an HF probe station in the K_a-frequency range. The designed measurement setup involves TWT frequency generator "Elmika G4408E" working in the CW mode, coaxial-waveguide adapters "Elmika CWA-08/K(f)," WR28 waveguide transmission line, "Elmika" directional coupler, thermistor mount "M5-45," thermistor power meter "M3-22A," a flap waveguide attenuator, a direct reading attenuator, a broadband bias tee "SHF BT 45 B," a "Cascade Microtech EP6" probe station with air coplanar probes "ACP 40 A GS 250," a digital voltmeter "Agilent 34401A" and connecting cables. The structure block diagram is illustrated in Fig. 2.21.

The MW power in the K_a-frequency range is supplied from the generator (Fig. 2.21 – 1) to the diodes. The generator is connected to the waveguide transmission line. The power of the signal provided by the generator is measured using a thermistor power meter (4) connected to the thermistor mount (3) through a 3-wire shielded connecting cable. The thermistor mount is connected to the waveguide transmission line through a directional coupler (2) with 9 dB coupling. The transmission line also has a flap attenuator (5) that allows to shut down the signal from the generator and a variable direct reading attenuator (6) that allows for precise control of the power of the signal supplied to the MW diode to choose the range where detected voltage depends linearly on the power.

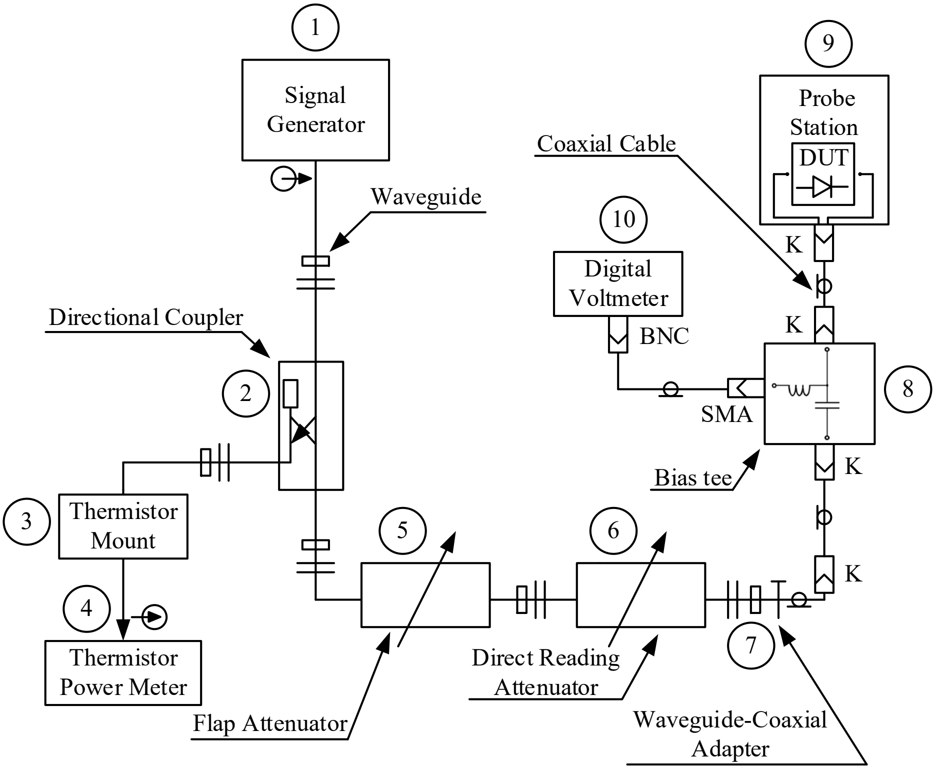

Fig. 2.21. Structure block diagram of designed measurement setup for the detected voltage investigation on power and detected voltage on frequency dependencies in the K_a-frequency band using a probe station

After the variable attenuator, the signal travels to the coaxial-waveguide adapter (7) through the bias tee (8) and then is supplied to the MW diode by means of the probe station (9). Both the bias tee and the probe station are connected using HF microcoaxial cables with K connectors. The air coplanar probes are connected to the Ohmic contacts of the MW diode. The signal goes from one probe to another through the MW diode and travels back to the bias tee, also using the same microcoaxial cable. The bias tee is used for the separation of the MW signal and identification of the detected voltage component. The detected voltage of the MW diodes is measured using a digital voltmeter (10) that connects to the bias tee through BNC to SMA connector. The voltage sensitivity is obtained from the relationship between the measured, detected voltage and the incident power supplied to the MW diode (Eq. 2.3).

Subsequently, an automated measurement setup was developed, allowing measurements to be quicker and more convenient.

The measurement setup involves the MMW range sweep generator "Elmika G4408E" based on the TWT working in either CW or a single pulse-modulated mode, a scalar network analyzer "Elmika R2400," a *p-i-n* attenuator, an "Elmika" directional coupler, a waveguide detector mount "Elmika DM03E," "Elmika" logarithmic amplifiers, a direct reading attenuator, a coaxial-waveguide adapter "Elmika CWA-08/K(f)," a WR28 waveguide transmission line, a broadband bias tee "SHF BT 45 B," a "Cascade Microtech EP6" probe station with air coplanar probes "ACP 40 A GS 250," a PC and connecting cables.

The structure block diagram of the automated HF probe station measurement setup developed to obtain the VP and voltage-frequency characteristics of the MW diodes is presented in Fig. 2.22.

The setup was developed for automated measurements of semiconductor MW diodes detection properties in the K_a-frequency range. The MMW sweep generator (Fig. 2.22 – 1) produces an internal square-pulsed amplitude 100 kHz modulated signal with the duty cycle 2 ± 0.4. The generator is connected to the scalar network analyzer (2) using the DB25 to XLR3 connector (for fast frequency sweep and retrace synchronization between the generator and controlling software), and both are connected via USB to the PC (13). The signal travels from the generator to the *p-i-n* attenuator (4), which is connected to the generator's output using a waveguide. From the *p-i-n* attenuator, the signal goes to a directional coupler (5) with 14.4–15 dB coupling. The designed lattice inside the directional coupler directs part of the signal to a waveguide branch. The waveguide branch is connected to the detector mount "R" (6), and together with the logarithmic amplifier "R" (7), they form a reference power sensor (connected using a microcoaxial cable with SMA connectors). The logarithmic amplifier "R" is connected to the input "R" (using an XLR5 connector) of the scalar network analyzer; thus, this circuit acts like a power meter of the pass-through type for power calibration in the main transmission line. The measured power level value is forwarded to the generator from the scalar network analyzer output "B" via a cable with XLR5 connectors. The generator has an ALC board inside, which stores the power level calibration coefficient codes for each frequency and controls the *p-i-n* attenuator by means of a *p-i-n* driver (3). The *p-i-n* attenuator is connected to the generator using a coaxial cable with a BNC connector. While setting the correspondent frequency, the power level coefficient code is forwarded to the *p-i-n* attenuator from the generator's *p-i-n* driver setting the 3 mW power on the output of the transmission line (Fig. 2.22 – point of calibrated power) for all measurement frequencies, i.e., ALC. Through the directional coupler, the signal goes to the direct reading attenuator (9), which can be used to add a proper attenuation in the transmission line while choosing the dynamic VP range of the MW diode. The direct reading attenuator is connected to the waveguide-coaxial adapter (10), and the signal travels through the bias tee (11) to the HF probe station (12) using HF microcoaxial cables with K connectors.

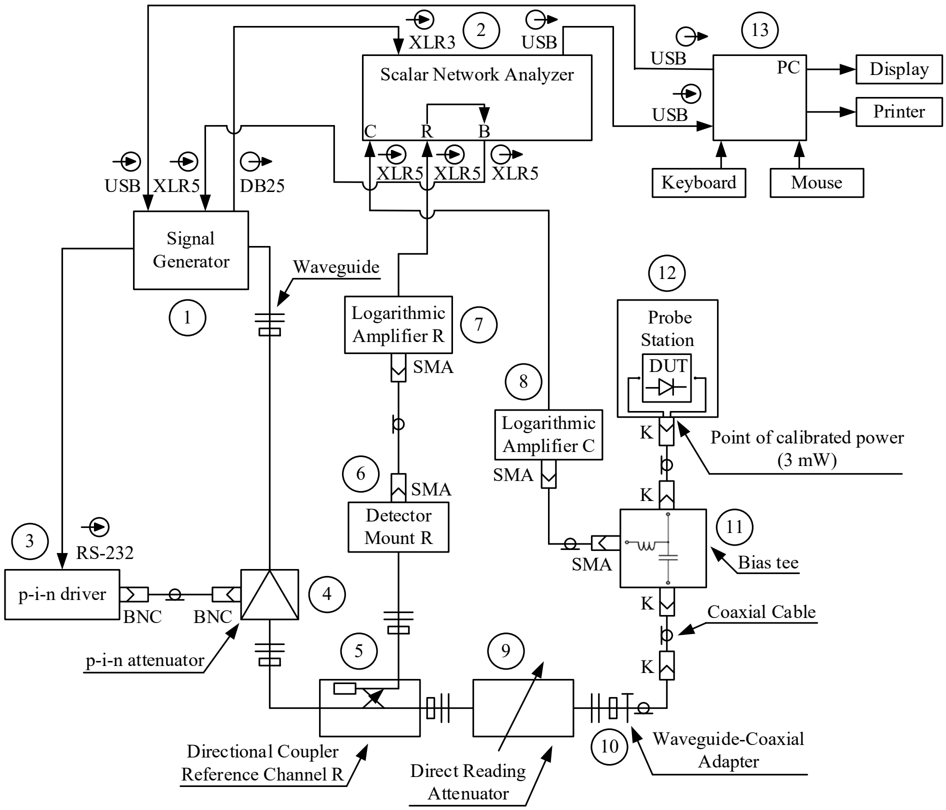

Fig. 2.22. Structure block diagram of the developed automated measurement setup for investigations of detected voltage on power and detected voltage on frequency in K_a-band using a probe station

The measurements are carried out by applying the MW signal to a diode located directly on a semiconductor array on a SI substrate or a polyimide film using air coplanar probes. The output signal from the MW diode travels back to the bias tee through the same HF microcoaxial cable. The broadband bias tee acts like an LC filter and is used for the separation of the MW component and DC component of the signal. Fig. 2.23 shows the equivalent circuit of the bias tee.

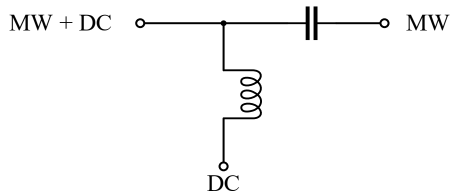

Fig. 2.23. Bias tee equivalent circuit

The filtered DC signal, i.e., the detected voltage, is supplied to the scalar network analyzer by passing a logarithmic amplifier "C" (8). The logarithmic amplifier is connected to the bias tee using a microcoaxial cable with SMA connectors. The logarithmic amplifier "C," together with the scalar network analyzer (connected using a cable with an XLR5 connector), amplifies and transforms the analog input 100 kHz signal into digital, sending the output information to the PC via USB. Voltage sensitivity on the frequency of the MW diode is obtained using PC software where a virtual voltmeter is realized.

PC software for measurement of this setup was designed using "LabVIEW" virtual instruments. The virtual control panel provides the readout of the voltage sensitivity measurement results on a real-time scale with the ability to compare and save (store) the data of the measurement results in the PC memory. It also allows the experimenter to control the signal generator. The output voltage of the MW diodes is measured at a certain incident power (3 mW by default at 0 dB attenuation) in the operating frequency range, and the voltage sensitivity is represented as a function of frequency at the desirable power levels of MMW radiation. Fig. 2.24 shows the virtual control panel of the PC software.

One of the main features of the developed setup is that the calibrated power from the generator is always set to 3 mW (at 0 dB attenuation) at the output–input of the probes (Fig. 2.22 – point of calibrated power) considering the losses in each section of the transmission line (directional coupler – 15 dB; direct reading attenuator – 0.3 dB; HF microcoaxial cables – 3 dB; air coplanar probes – 2 dB); thus, the precision of the diode voltage sensitivity measurements increases. Moreover, the setup allows the experimenter to smoothly regulate the power (supplied to an MW diode) in the range from 3 nW to 3 mW.

To test the measurement setup and determine the quality of the results, the detection properties of GaAs/AlGaAs heterostructure diodes (1 and 2 μm in the narrowest part – neck), capable of detecting the electromagnetic radiation in the measured frequency range, were measured by two methods (Fig. 2.25).

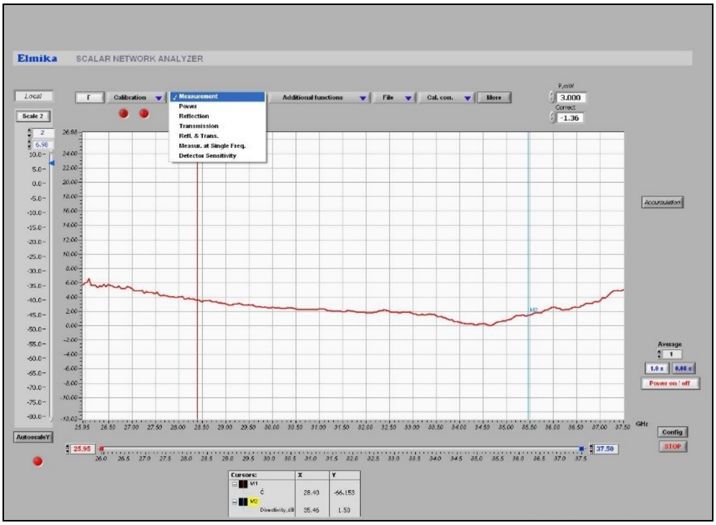

Fig. 2.24. Virtual control panel for automated measurements of the dependences of detected voltage on frequency in K_a-band using a probe station

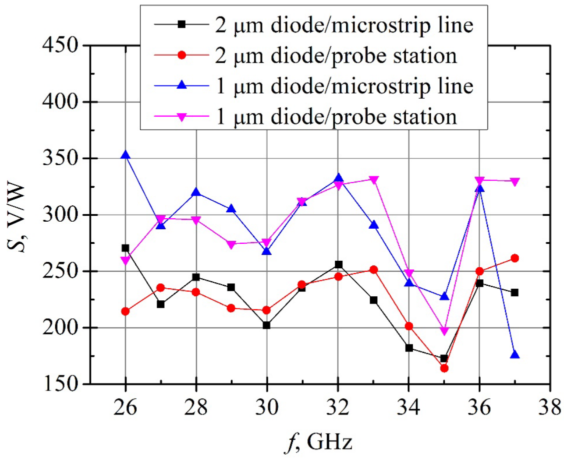

Fig. 2.25. Voltage sensitivity of the GaAs/AlGaAs heterostructure diodes in the K_a-band obtained by using the designed measurement setup with the HF probe station and a waveguide detector mount with a microstrip line. Lines are guides for eyes

The same diodes were investigated using the designed measurement setup and using a classical measurement approach, i.e., by mounting the diodes into a waveguide detector mount with a microstrip line where the quasi-TEM wave propagates (the finline adapter connects the microstrip line to a waveguide transmission line). A comparison of the experimental results showed that the results obtained using the designed setup with the HF probe station sufficiently matched the ones obtained using the classical measurement approach. The test measurements concluded that the presented measurement setup gives reliable results when measuring the voltage sensitivity of an MW diode in the K_a-frequency range.

The matching of the MW component in the measurement system, including the probe station with an MD diode, was evaluated using the VSWR dependency on the frequency in the K_a-range (Fig. 2.26).

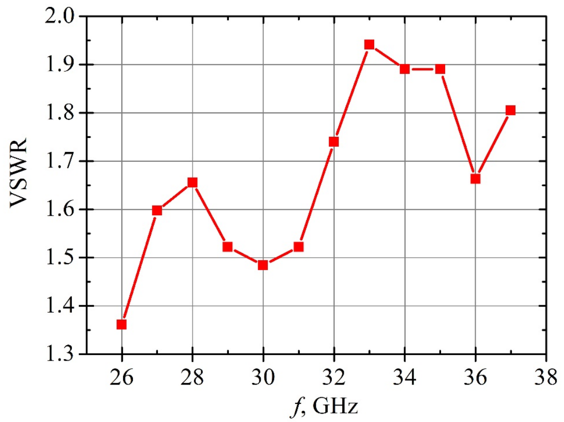

Fig. 2.26. VSWR dependency on the frequency of the developed measurement setup for the investigation of detected voltage on power and detected voltage on frequency in the K_a-band using a probe station

The VSWR of the measurement system changes non-monotonically from 1.36 to 1.94, i.e., power return losses are in the range of 9.9–16.3 dB.

Using the VSWR values, the reflection coefficient Γ was calculated using Equation 2.6:

$$\Gamma = \frac{\text{VSWR}-1}{\text{VSWR}+1}. \tag{2.6}$$

It can be assumed that:

$$P_\text{i} = P_\text{w} - P_\text{ref}, \tag{2.7}$$

where P_i is the incident power supplied to the diode, P_w is the power in a waveguide, and P_{ref} is the reflected power.

The relation between the reflection coefficient and the power of the signal is defined by Equation 2.8:

$$\Gamma = \sqrt{\frac{P_{\mathrm{ref}}}{P_{\mathrm{w}}}}. \quad (2.8)$$

In this case, the influence of the reflection coefficient on the measured voltage sensitivity of the MW diode can be evaluated using Equations 2.3, 2.7, and 2.8. The comparison of the measured voltage sensitivity S of the MW diode and the recalculated voltage sensitivity considering the reflection coefficient of the measurement system ($\frac{S}{1-\Gamma^2}$) is presented in Fig. 2.27.

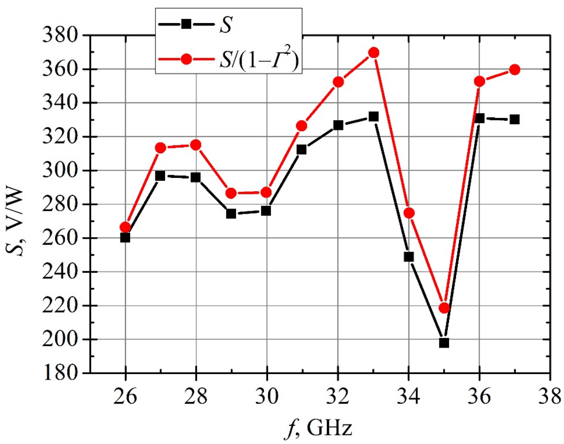

Fig. 2.27. Voltage sensitivity on the frequency of the GaAs/AlGaAs heterostructure MW diode with the evaluation of power losses due to the reflectance in the measurement system $S/(1–\Gamma^2)$ and without it, S

According to the obtained results, the recalculated voltage sensitivity $\frac{S}{1-\Gamma^2}$ is, on average, higher by 6.9 % than the measured voltage sensitivity S.

2.4.2. Measurements of Detected Voltage Dependencies on Frequency and Power Using Waveguide Detector Mount

The HF detection properties of the semiconductor MW diodes in the W- and D-frequency bands were investigated by embedding separate MW diodes on a microstrip line inside a waveguide detector mount, where the quasi-TEM wave propagates. During the experiment, the modulated MW signal travels through the waveguide transmission line with DUT, and the voltage sensitivity is measured using the scalar network analyzer and PC software.

The measurement setup involves the MMW range sweep generator "Elmika G4402E for the W-band/Elmika G4403E for the D-band" based on TWT working in panoramic measurement mode, a scalar network analyzer "Elmika R2400," a *p*-*i*-*n* attenuator, a Faraday ferrite isolator "Elva-1 IF," "Elmika" directional couplers, waveguide detector mounts "Elmika DM03E," "Elmika" logarithmic amplifiers, a "DA 03E/02E Elmika" direct reading attenuator, a waveguide transmission line, a PC, and connecting cables.

The structure block diagram (Fig. 2.28) presents the system operation for measuring the voltage sensitivity of the waveguide detector mount (MW diode inside). For both frequency ranges, the structure diagram and measurement principle are the same, only using different size waveguides (WR10 and WR6, respectively, for W- and D-bands) and appropriate components.

The output signal of the MMW sweep generator (Fig. 2.28 – 1) is modulated using 100 kHz (duty cycle 2 ± 0.4) internal square pulse AM. The generator is connected to the scalar network analyzer (2) using the DB25 to XLR3 connector (for fast frequency sweep and retrace synchronization between the generator and controlling software), and both are connected via USB to the PC (15). The signal travels from the generator to the *p*-*i*-*n* attenuator (5) through an appropriate waveguide. The ferrite isolator (3) between the generator and the *p*-*i*-*n* attenuator is used to protect the generator from reflected MW signals. The ALC in this measurement setup is implemented according to the same principle as described in Section 2.4.1. From the *p*-*i*-*n* attenuator, the signal goes to a directional coupler (6) with 15 dB coupling. The waveguide branch of the directional coupler is connected to the detector mount "R" (7) and, together with the logarithmic amplifier "R" (8), forms a reference power sensor (connected using a microcoaxial cable with SMA connectors). The logarithmic amplifier "R" is connected to the input "R" (using an XLR5 connector) of the scalar network analyzer; thus, this circuit acts like a power meter of the pass-through type for power calibration in the main transmission line. The measured power level value is forwarded to the generator from the scalar network analyzer using a coaxial cable with BNC connectors. The generator has an ALC board inside that controls the *p*-*i*-*n* attenuator using saved power level calibration coefficient codes for each frequency. The *p*-*i*-*n* attenuator is controlled using the *p*-*i*-*n* driver (4) inside the generator and a coaxial cable with a BNC connector. While setting the correspondent frequency, the power level coefficient code is forwarded to the *p*-*i*-*n* attenuator from the generator setting 1 mW output power on the waveguide transmission line (Fig. 2.28 – the point of calibrated power) for all measurement frequencies. Passing directional couplers (6) and (9), the signal goes to the direct reading attenuator (12), which can be used to add a proper power attenuation of the supplied signal. Waveguide detector mount "A" (10) with logarithmic amplifier "A" (11) is used for reflection signal measurements during the calibration procedure. After attenuation, the signal travels to the waveguide detector mount (13), where the semiconductor MW diode is placed. For this experiment, the diode array was transferred onto an elastic dielectric polyimide film, allowing for the mechanical separation of the MW diodes.

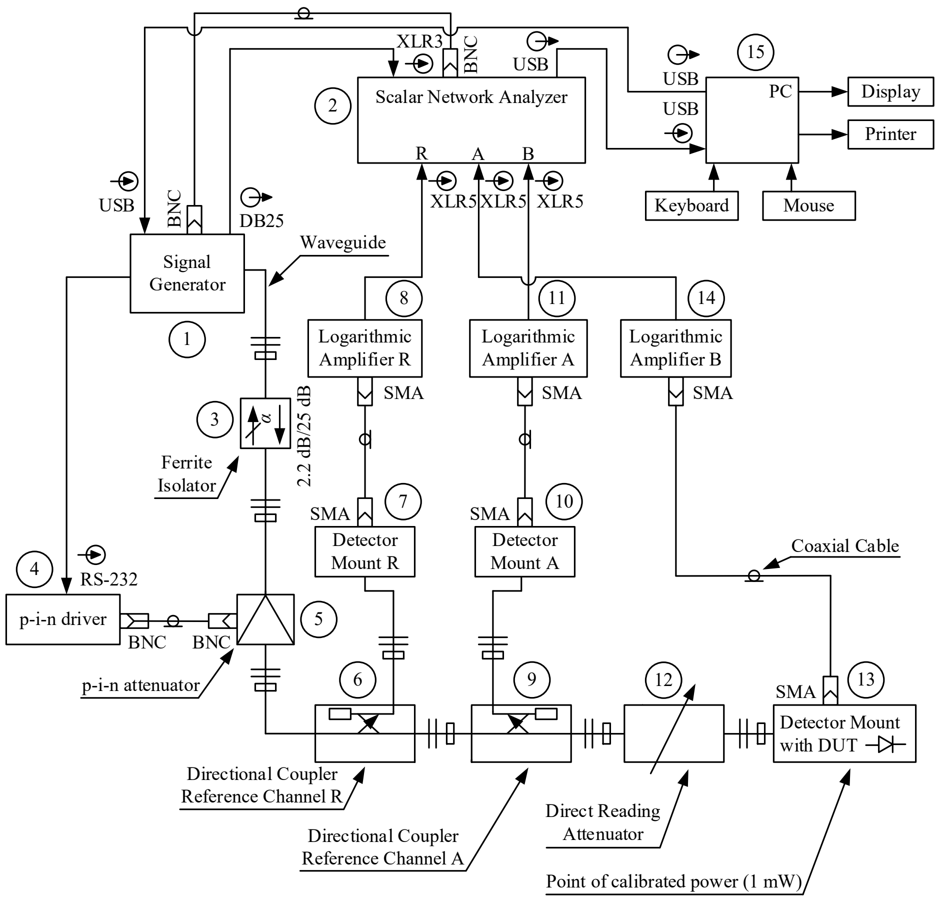

Fig. 2.28. Structure block diagram of the detected voltage on the frequency and the detected voltage on power measurement setups for W- and D-bands using a waveguide detector mount

A single MW diode on a polyimide film is placed into the waveguide detector mount using a microstrip line, thus together forming a detector system. The diode is mounted on a finline adapter using a GaAs/Au eutectic alloy. The finline adapter is specifically designed to match the diode to the transmission line and to minimize reflection. It connects the microstrip line (Fig. 2.29) with the embedded diode to a rectangular waveguide where the H_{10} TEM mode propagates.

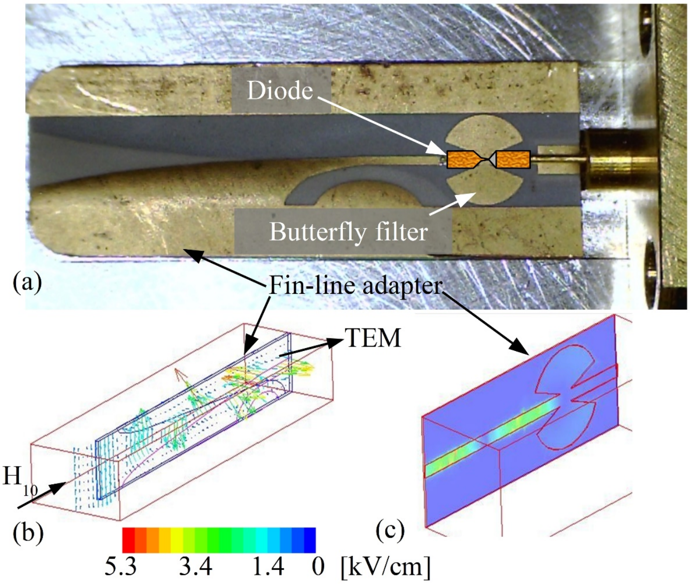

Fig. 2.29. Waveguide detector mount with finline adapter (a) converting the H_{10} wave propagating in a rectangular waveguide into the quasi-TEM wave propagating in the microstrip line (b) containing the butterfly-shaped low-pass filter (c)

The waveguide detector mount has a low-pass filter and separates the low-frequency 100 kHz signal from the MW signal. The low-frequency signal from the detector mount is supplied to the scalar network analyzer through the logarithmic amplifier “B” (14) using a microcoaxial cable with SMA connectors (from the detector mount to the logarithmic amplifier) and an XLR5 connector (from the logarithmic amplifier to the scalar network analyzer). The scalar network analyzer transforms the analog detected signal into digital. Then, the digital signal is transferred to the PC via USB, where a virtual voltmeter is realized. The voltage sensitivity of the MW diode is presented using PC software. The output voltage of the waveguide detector mount with DUT is measured as a function of incident power in the operating frequency range, and the voltage sensitivity of the detector mount is measured as a function of frequency at various levels of MMW power.

The PC virtual control panel ("LabVIEW") provides the readout of the waveguide detector mount output voltage measurement results on a real-time scale with the ability to compare and save (store) the data results of the measurement in PC memory and controls the generator (Fig. 2.30).

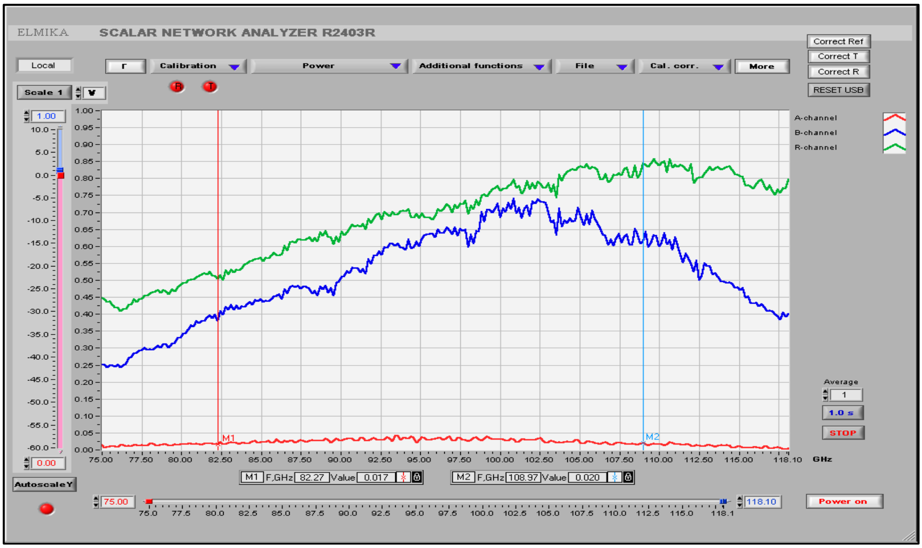

Fig. 2.30. Virtual control panel for the detected voltage on the frequency and on power measurement setups in W- and D-bands using a waveguide detector mount

The influence of the MW component matching issues with the MW diode was evaluated in K_a-, W-, and D-ranges using measurement setups with waveguide detector mounts for appropriate bands. The VSWR dependencies on frequency (Figs. 2.31–2.33) allow for evaluating power losses in the measurement system with DUT (MW diodes having zero bias voltage electrical resistance $R_0 = 200\ \Omega$; 2 kΩ and 5.1 kΩ). The value of the VSWR changes non-monotonically from 4.5 to 1.1 in the 26–170 GHz frequency range, which is typical for a waveguide measurement system with a detector mount due to heterogeneity. The electrical resistance of the MW diode does not significantly influence the VSWR value in the measured frequency range. Voltage sensitivity dependence on the frequency of the same MW diodes considering the power losses due to reflectance, i.e., reflectance coefficient (recalculated using the measured VSWR values according to Equations 2.3, 2.6, 2.7, 2.8) and without it is presented in Figs. 2.34–2.36.

According to the obtained results presented in Figs. 2.34–2.36, the evaluation of power losses due to reflectance in the measurement system with a waveguide detector mount gives voltage sensitivity values higher by 8 % (on average) in the

K_a-range, higher by 6 % (on average) in the W-range, and higher by 12.8 % (on average) in the D-range than the measured voltage sensitivity *S*.

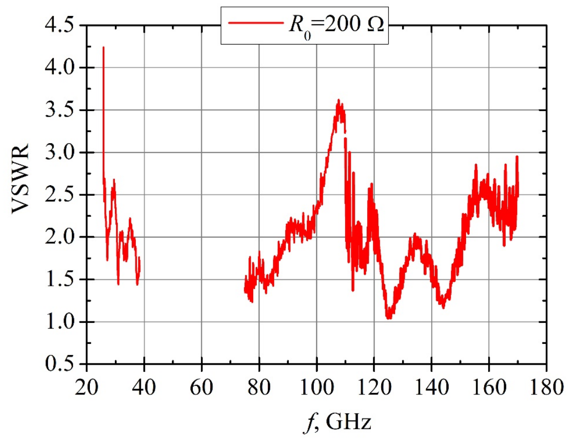

Fig. 2.31. VSWR measurements in K_a-, W-, and D-frequency ranges of the detector mount-based measurement system with the MW diode having the zero-bias voltage electrical resistance R_0 = 200 Ω

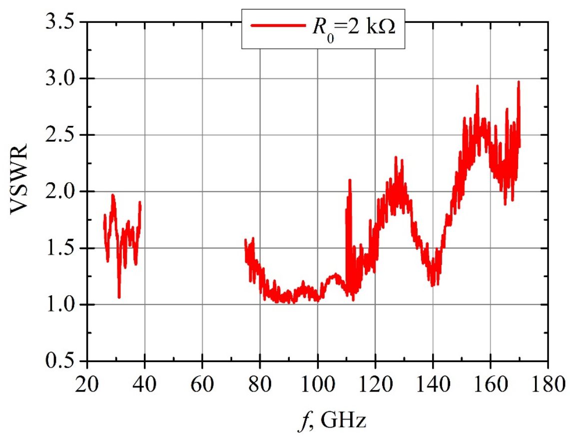

Fig. 2.32. VSWR measurements in K_a-, W-, and D-frequency ranges of the detector mount-based measurement system with the MW diode having the zero-bias voltage electrical resistance R_0 = 2 kΩ

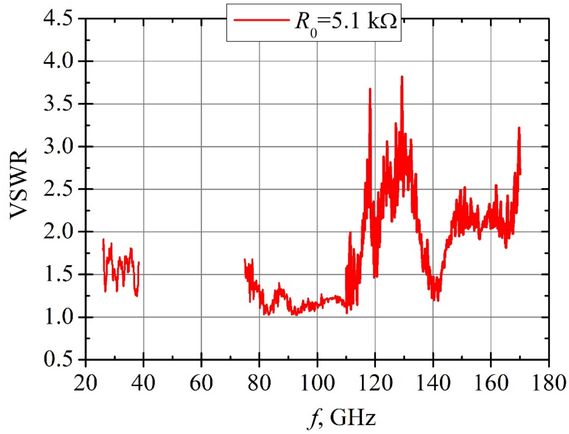

Fig. 2.33. VSWR measurements in K_a-, W-, and D-frequency ranges of the detector mount-based measurement system with the MW diode having the zero-bias voltage electrical resistance R_0 = 5.1 kΩ

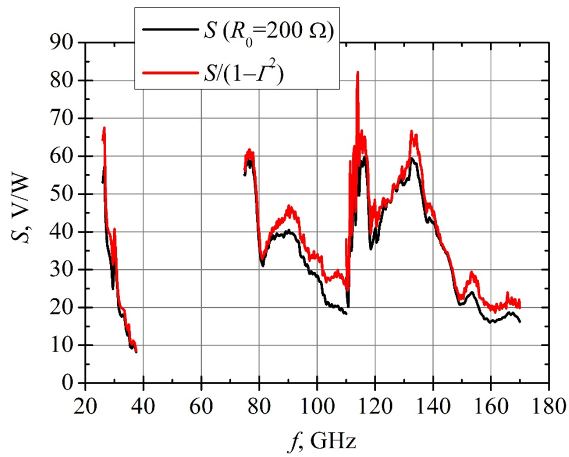

Fig. 2.34. Voltage sensitivity on the frequency of the MW diode having the zero-bias voltage electrical resistance R_0 = 200 Ω with the evaluation of power losses due to reflectance in the measurement system $S/(1-\Gamma^2)$ and without it, S

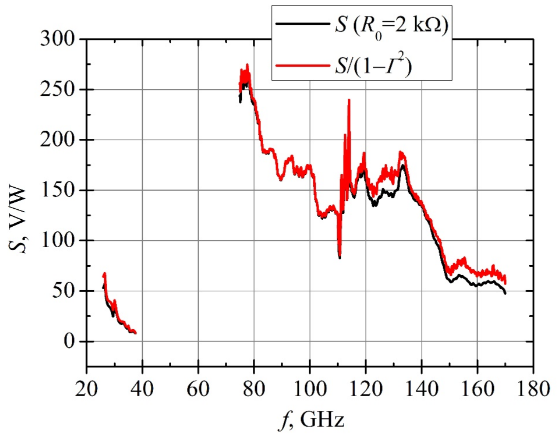

Fig. 2.35. Voltage sensitivity on the frequency of the MW diode having the zero-bias voltage electrical resistance R_0 = 2 kΩ with the evaluation of power losses due to reflectance in the measurement system $S/(1–Γ^2)$ and without it, S

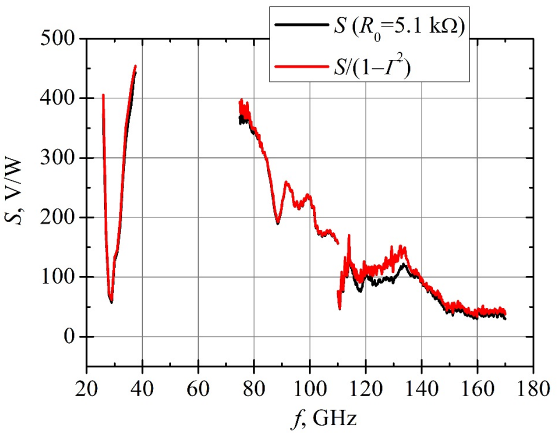

Fig. 2.36. Voltage sensitivity on the frequency of the MW diode having the zero-bias voltage electrical resistance R_0 = 5.1 kΩ with the evaluation of power losses due to reflectance in the measurement system $S/(1–Γ^2)$ and without it, S

Measurements of the HF detection properties of the MW diodes in the 220–340 GHz frequency range were made by taking the second harmonic of the D-frequency band MW signal. However, the real working range was 270–330 GHz due to measurement setup limitations.

"Virginia Diodes Inc. wideband frequency multiplier-doubler WR3" was used for this purpose. The measurement setup (Fig. 2.37) involves the MMW range sweep generator "Elmika G4-161M" based on the backward wave oscillator working in the CW mode, a ferrite isolator "FVVN1," a waveguide detector mount "Elmika DM03E," a "WR6-WR3 Elmika" waveguide transition adapter, a "DA 02E Elmika" direct reading attenuator, a waveguide transmission line, a digital voltmeter "Agilent 34401A," a calorimetric sensor "Elmika CA-02R," a power meter "Elmika M1-25M," and connecting cables.

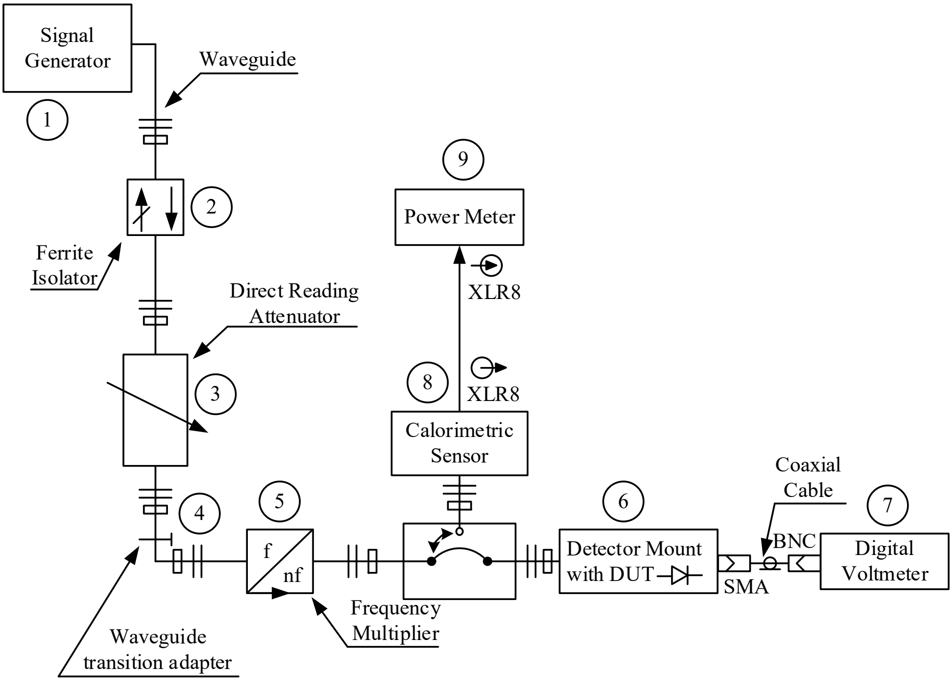

Fig. 2.37. Structure block diagram of the detected voltage on the frequency and the detected voltage on the power measurement setup in the 270–340 GHz range using a waveguide detector mount and a frequency multiplier

The output signal of the MMW sweep generator (Fig. 2.37 – 1) travels into the WR6 waveguide transmission line. The direct reading attenuator (3) allows for controlling the power level supplied to the diode from the generator. The ferrite isolator (2) between the generator and the direct reading attenuator secures the generator from the reflected signal. After the direct reading attenuator, the signal goes into the waveguide transition adapter (4), which is used for changing the WR6 waveguide flange size to WR3 to connect the frequency multiplier (5).

When measuring the power of the signal, the output of the frequency multiplier is connected (using the waveguide) to a broadband calorimetric sensor (8) that is working on the principle of substitution of MW power by DC power, using an auto-compensating transistor transducer. The calorimetric sensor is connected using an XLR8 connector to the power meter (9), where the absolute power is measured. To measure the detected voltage of the diode, the frequency multiplier is connected through a waveguide to the detector mount (6) with the diode inside (the working principle being the same as in the D- and W-frequency bands). The detector mount is connected to the digital voltmeter using an SMA-BNC coaxial cable. The voltage sensitivity is obtained from the relationship between the measured, detected voltage and the power supplied to the MW diode (Eq. 2.3).

2.4.3. Measurements of Light and Temperature Influence on Microwave Diode's Electrical and High-Frequency Properties

As mentioned in Section 2.3, using a probe station for the DC and HF measurements allows more possibilities for the investigation, i.e., to perform investigations by illuminating the semiconductor structures with the light of different wavelengths and different intensities (e.g., white-lamp illumination of 14400 lux) and in darkness, thus allowing for determining the light influence on the diodes electrical parameters and detection properties.

Most of the measurements were performed at room temperature. However, measurements at different temperatures were performed by heating the samples using a Peltier module, a thermocouple, and a current source. The working principle of the Peltier element (Fig. 2.38) is based on a heat flux at the junction of two *n*- and *p*-type semiconductors.

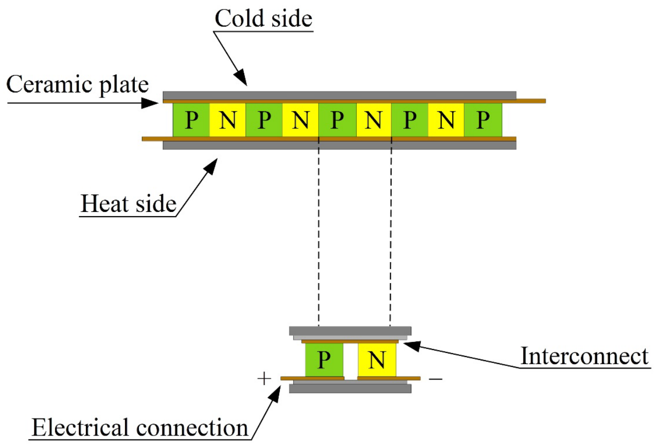

Fig. 2.38. Schematic view of the Peltier element

The element consists of *p* and *n*-type semiconductor pairs placed in series between two thermally conductive ceramic plates. The accumulation of this heat flux is called the Peltier effect, and it occurs because of different electron densities in semiconductors. Basically, a Peltier element works as a cooler/heater. It is a thermoelectric solid-state active heat pump that transfers heat, causing a temperature difference between the surfaces of the element. In other words, when the voltage is applied to the element, a DC electric current flows across the junction of the semiconductors. It brings heat from one side to another so that one side gets cooler while the other gets hotter depending on the direction of the current.

The samples were placed onto the Peltier module "Hebei TES1-12704," and a thermocouple was connected to it. The element was connected to a DC power supply, "Agilent 6613C," that allowed the control of the temperature by changing the voltage. The temperature was measured using a multimeter connected to the thermocouple. Experiments at different temperatures up to 80 °C were obtained using the methodologies described for DC and HF measurements with appropriate probe stations.

2.5. Conclusions of the Second Chapter

1. PD asymmetric MW diodes with a simple design and minimum fabrication steps were fabricated based on three types of polished GaAs substrates heavily doped, n^{++}-GaAs having the donor density 4×10^{18} cm^{-3}, n^{+}-GaAs, doped to 4×10^{17} cm^{-3}, and p^{++}-GaAs having the acceptor density of 4×10^{18} cm^{-3}, grown using the LPE method.
2. PD MW diodes were fabricated using a simple design based on the ternary *n*-type $Al_xGa_{1-x}As$ layer of submicrometric thickness grown onto the SI GaAs substrate by means of the LPE method. Submicrometer thickness layers (0.5–0.8 μm) have different mole fractions of AlAs ($x = 0$; 0.15; 0.3).
3. Bow-tie MW diodes of a transistor-like design realized with narrow and wide metallic gates above the 2DEG channel were fabricated based on the selectively doped GaAs/AlGaAs heterostructure epitaxially grown onto the SI GaAs substrate by means of the MBE method. The energy band diagram and electron distribution of the structure used for the fabrication of the bow-tie MW diodes were evaluated using the Schrödinger-Poisson simulation.
4. The *IV* characteristic measurements were carried out using a DC probe station and a precise *IV* analyzer that allowed for performing the

measurements directly on-wafer, and during a further analysis of the *IV* characteristics, the asymmetry and electrical resistance of the MW diodes were evaluated.

5. The measurements of detected voltage on the frequency and the detected voltage on power in K_a-frequency bands were carried out by using the developed HF probe station setup that allowed for performing the measurements directly on-wafer, and during a further analysis, the voltage sensitivity of the MW diodes was evaluated.
6. The measurements of the detected voltage dependence on the frequency in the 75–340 GHz range were carried out, and the voltage sensitivity of the diodes was evaluated by embedding separate MW diodes into a waveguide detector mount with a microstrip line, where the quasi-TEM wave propagated.
7. The DC and HF characteristics of MW diodes were investigated at different temperatures by heating the samples with a Peltier element and using an appropriate probe station setup.
8. The influence of illumination on the electrical parameters and HF properties of the MW diodes was evaluated using an appropriate probe station setup.

3

Investigation of Planar Dual Microwave Diodes

This chapter covers investigations of the electrical and HF properties of PD MW diodes based on a SI or low-resistivity GaAs substrate. It presents experimental results, including measurements of the *IV* characteristics using a probe station, measurements of detected voltage, and voltage sensitivity in the MMW range using both a probe station and a waveguide detector mount.
The research results presented in this chapter were published in the author's publications Sužiedėlis et al., 2017a, 2017b; Anbinderis et al., 2021.

3.1. Direct Current and High-Frequency Detection Properties of Planar Dual Microwave Diodes Based on a Low-Resistivity GaAs Substrate

The investigation focused on the electrical and detection properties of PD MW diodes based on three types of heavily doped polished GaAs substrates, n^{++}-GaAs having the donor density of 4×10^{18} cm^{-3}, n^{+}-GaAs, doped to 4×10^{17} cm^{-3}, and p^{++}-GaAs having the 4×10^{18} cm^{-3} acceptor density. The operation is based on hot carrier phenomena and rectification of MW currents flowing through the structure composed of two diodes connected in series and having different active region areas, as discussed in Section 2.1.2.

Contact resistivity was in the range of $(1 \div 50) \times 10^{-6}$ Ω cm^2 for the diodes fabricated based on the n^{++}-GaAs substrate and about $(3 \div 10) \times 10^{-5}$ Ω cm^2 for those fabricated from the n^{+}-GaAs substrate. Contact resistivity of the p^{++}-GaAs-based diodes was much higher, indicating typical Schottky contact behavior of large- and small-area diodes. Scattering of the contact resistivity values can be explained by the non-homogeneous recrystallization process during Ge/Ni/Au metal contacts alloying into GaAs. The surface morphology of the semiconductor structure after alloying becomes non-uniform, revealing Ge- and Ni-rich clusters having dimensions from half to several micrometers (Heiblum, Nathan & Chang, 1982). These sizes are comparable to the contact sizes; therefore, the electrical resistance of the PD MW diodes gains different values on the same GaAs substrate.

In the case of n^{++}- and n^{+}-GaAs substrates, the electrical resistance of the fabricated PD MW diodes was relatively low, between tens and hundreds of Ohms. However, the asymmetry of the *IV* characteristic of the MW diodes was either typical to Ohmic contact or Schottky, one having the quasilinear *IV* characteristic when the *IV* characteristic is slightly non-linear, which is inherent to a metal-semiconductor contact (Fig. 3.1). These diodes are labeled further as LS and LO (Low Schottky and Low Ohmic, bearing in mind low electrical resistance) diodes. Accordingly, high-resistance diodes made on the p^{++}-GaAs substrate were named HS (High Schottky, bearing in mind high electrical resistance) diodes.

Using appropriate probe stations, the measurements of DC *IV* and HF VP characteristics were performed directly on separate MW diodes uncut out of the whole semiconductor diode array held by the polyimide film. Measurements of the dependence of the output signal on frequency, as well as investigation of the diode's response time under pulsed MW excitation, were performed by embedding separate MW diodes into a waveguide detector mount. As discussed in Section 2.4.2, separate MW diodes were mounted into a microstrip line where the quasi-TEM wave propagates.

The *IV* characteristics of the investigated PD MW diodes are presented in Fig. 3.1. The Ohmic nature of the dependences was inherent to most PD MW diodes fabricated based on the n^{++}-GaAs substrate: 80 % of them were LO, and 20 % were LS. As for the ones on the n^{+}-GaAs substrate, 70 % of the MW diodes had Ohmic characteristics (LO), and the rest, 30 %, were LS. The forward direction of the Ohmic *IV* characteristic was assumed with a positive potential applied to the large-area contact (Fig. 2.2 – a). In the case of Schottky-like characteristics, the forward current flowed when a positive potential was applied to the small-area contact. Thus, the *IV* characteristics of the Schottky-like diodes are reversed in with respect to voltage polarity. As Fig. 3.1 shows, the HS diodes revealed distinct *IV* characteristics, extremely non-linear and asymmetric.

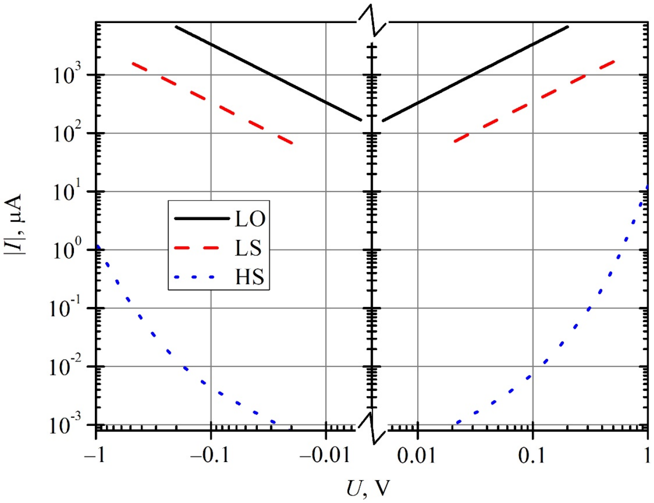

Fig. 3.1. *IV* characteristics of the LO, LS, and HS MW diodes (in a log/log scale)

As discussed in Section 2.1.2, the PD MW diode can be treated as a couple of two different diodes connected in series with a common base (Fig. 2.2 – a), resulting in the formation of the *IV* characteristic by reverse currents of two contacts. Also, a big difference in zero-bias voltage electrical resistance of the PD MW diodes has been identified due to non-uniform contact resistivity of the metallic contacts and scattered values of the small-area contact: tens of ohms, hundreds of ohms, and tens of megaohms for the LO, LS, and HS diodes, respectively.

Fig. 3.2 demonstrates the Ohmic nature of the LO diodes, while the decrease of the electrical resistance of the LS diode with applied voltage evidences the metal-semiconductor junction nature of the diode. The electrical resistance values of the LO diodes were distributed between 30 and 200 Ω. Higher electrical resistance was inherent to the LS diodes: their values varied from 50 up to 600 Ω.

The asymmetry of the *IV* characteristics of the diodes can be related to their prospective voltage sensitivity to the MW radiation. The voltage sensitivity of an MW diode formed based on the small-area n-n^+ junction (point contact diode) depends on the asymmetry of the *IV* characteristic calculated according to Equation 2.2 (Section 2.1.3).

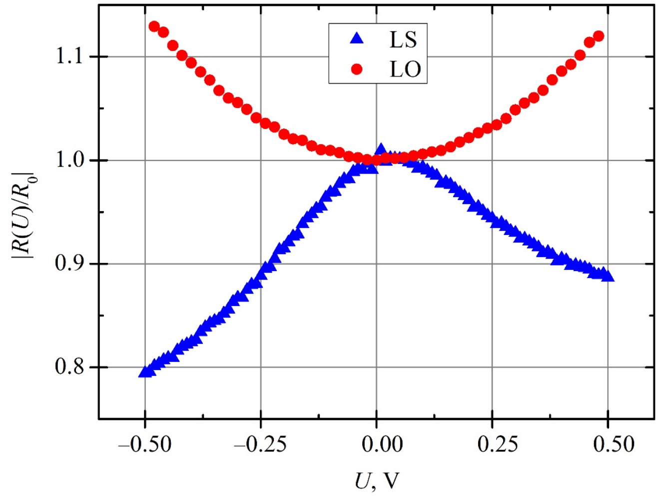

Fig. 3.2. Dependences of the relative electrical resistance $R(U)/R_0$ on voltage. Here, R_0 denotes the electrical resistance of the diode at zero voltage

The asymmetry sign of the *IV* characteristics particular to the Schottky-like and Ohmic-like diodes was different: it was positive for the LO diode and negative for the LS and HS diodes. Absolute values of the *IV* characteristics asymmetry versus applied voltage are presented in Fig. 3.3.

As the asymmetry of the *IV* characteristics forecasts the voltage sensitivity of the PD MW diodes, then the unit of the asymmetry is presented as V/W in Fig. 3.3. Naturally, Schottky-like characteristics demonstrate higher asymmetry values. A stronger asymmetry presumes the expectation of higher detection properties of the PD MW diodes. Practically, VP characteristics of the PD MW diodes measured at 28 GHz frequency support this consideration (Fig. 3.4).

A relatively huge discrepancy by several orders of magnitude between the prospective and experimental voltage sensitivity of the HS diode can be explained by a small portion of MW power that absorbs the diode due to the high electrical resistance of the HS diode, unlike in the case of the prospective evaluation when the incident power is considered to be fully absorbed. It should be noted that Equation 2.2 is reliable for the evaluation of voltage sensitivity of the Ohmic-like MW diode, where only conductivity current occurs, whereas in Schottky-like diodes, displacement current flows at high frequencies. Thus, Equation 2.2 can be used only for an accurate evaluation of voltage sensitivity for Ohmic-like diodes and Schottky-like diodes at low frequencies when displacement current is not present. At high frequencies, Equation 2.2 can be used for only harsh evaluation of voltage sensitivity in the case of Schottky diodes.

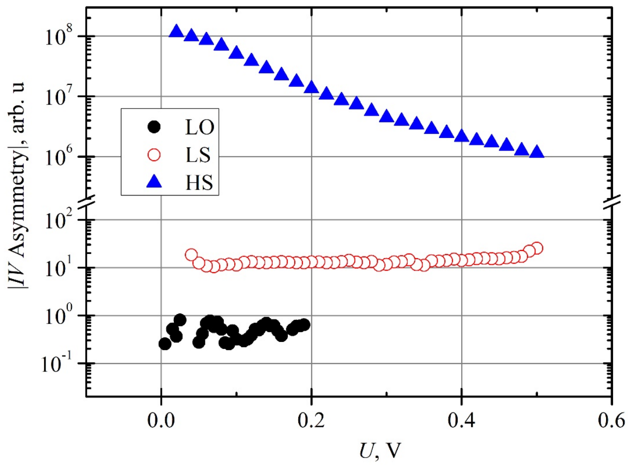

Fig. 3.3. Dependences of the *IV* characteristics asymmetry of LO (solid dots), LS (open dots), and HS (triangles) diodes on voltage calculated using Equation 2.2

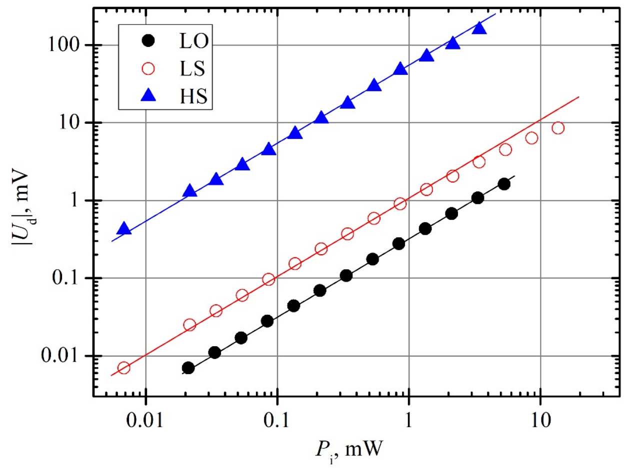

Fig. 3.4. Detected voltage versus the incident MW power of 28 GHz frequency. The lines are guides representing linear dependence

In the low-power range, all three types of PD MW diodes show linear dependences, whereas, at higher power levels, the VP characteristics of the LS and HS diodes start to be sublinear. The sublinear deviation of the VP characteristic is more pronounced for the HS diode having a higher non-linearity of the *IV* characteristic. This deviation from linearity can be explained by MW electric field-induced heating of the semiconductor crystal lattice occurring under the conditions of CW radiation. This presumption is also sustained by the change of the detected voltage magnitude with time at high-level pulsed MW radiation (Fig. 3.8). Still, the VP characteristic of LO keeps linearity in a wider range of MW power since the applied MW electric field is not strong enough to cause the decrease of electron mobility (Dargys & Kundrotas, 1994). The operational speed of the hot carrier EMF-based detector is limited by electron relaxation time, which is ~0.5 ps for GaAs at room temperature (Dargys & Kundrotas, 1994). Thus, in the case of electron heating by a strong electric field in the *n*-GaAs structure with different area Ohmic contacts, an increase in the detected voltage was observed, which can be explained by the rise of the electron energy relaxation time (Heiblum et al., 1982; Ašmontas & Sužiedėlis, 1993; Ashida, Inoue, Shirafuji & Inuishi, 1974) and the electron diffusion coefficient values (Vaitkus, Starikov, Subačius & Jarašiūnas, 1990) with the increase in the electric field strength.

The NEP (calculated according to Eq. 2.4) value is the highest (1.2×10^{-10} W/$\sqrt{\text{Hz}}$) for the HS diode and the lowest (3×10^{-11} W/$\sqrt{\text{Hz}}$) for the LO diode. The NEP of the LS diode is 2.6×10^{-10} W/$\sqrt{\text{Hz}}$. As for the calculated (Eq. 2.5) minimum power level (the minimum limit of the dynamic range), at which the detected voltage of the diodes can be registered using appropriate measurement equipment, it was 8.8, 1.8, and 2.1 nW for HS, LS and LO diodes, respectively.

The polarity of the voltage U_d detected across the PD MW diodes corresponds to the *IV* asymmetry sign. For example, a positive potential is induced on the small-area contact of the LO diode. In this case, U_d results from the hot electron EMF arising across the semiconductor planar MW diode structure having Ohmic contacts of different areas. On the other hand, LS diodes demonstrate the opposite polarity of the U_d. Although, the polarity of the voltage signal induced across diodes HS is the same as that across LO diodes since the former PD MW diodes are fabricated based on a *p*-type substrate.

The frequency dependences of the voltage sensitivity of the PD MW diodes measured using the HF probe station under conditions of CW radiation are presented in Fig. 3.5.

The absolute value of the voltage sensitivity increases with increasing resistivity of the semiconductor substrate (see graphs of the LO and LS diodes) due to stronger charge carrier heating in a less conductive semiconductor structure. Particularly high-voltage sensitivity is noted for HS diodes because the sensitivity of Schottky diodes, as a rule, exceeds that of diodes operating based on hot electron phenomena. Flat frequency dependence was inherent to all the investigated PD MW diodes in up to 34 GHz frequency. Such a weak dependence is typical of non-inertial carrier heating phenomena under the MW electric field and was observed in the case of LO diodes. On the other hand, for the Schottky-like diodes, LS and, especially, HS, their voltage sensitivity versus frequency dependences should be expressed stronger.

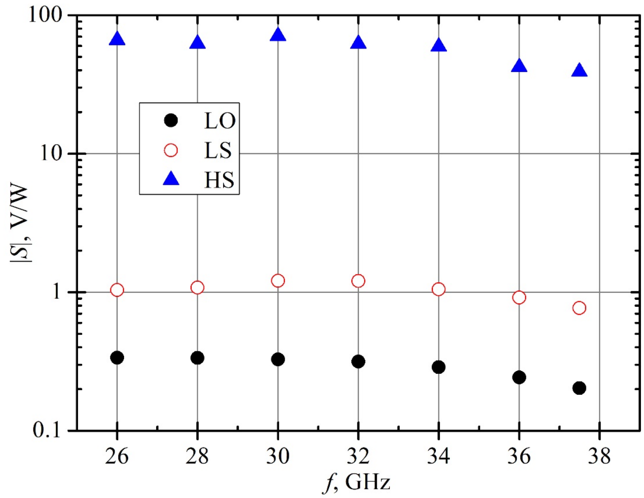

Fig. 3.5. Spectral distribution of the voltage sensitivity's absolute value of the MW diodes measured using an HF probe station

The LO and LS diodes were also mounted onto a waveguide detector mount to compare the frequency dependences of the PD MW diodes when measured using the HF probe station. The measured frequency dependences of voltage sensitivity are presented in Fig. 3.6. Voltage sensitivity values are more than two times higher as compared to the probe station measurements. As Fig. 3.6 shows, the waveguide-mounted diodes do not demonstrate any obvious decrease in the voltage sensitivity at frequencies above 34 GHz.

However, the frequency dependences of the MW diodes in the waveguide are more non-monotonic in comparison with probe station measurements due to the dependence of reflectance of the MW signal in the waveguide on frequency. This statement is supported by VSWR measurements in the K_a-frequency range illustrated in Fig. 3.7.

The value of the VSWR changed non-monotonically from 2.23 to 1.78 in this frequency range. The minimums of the VSWR at 28 GHz and 37 GHz frequencies corresponded to the maximums of voltage sensitivity of the LO and LS diodes at these frequencies.

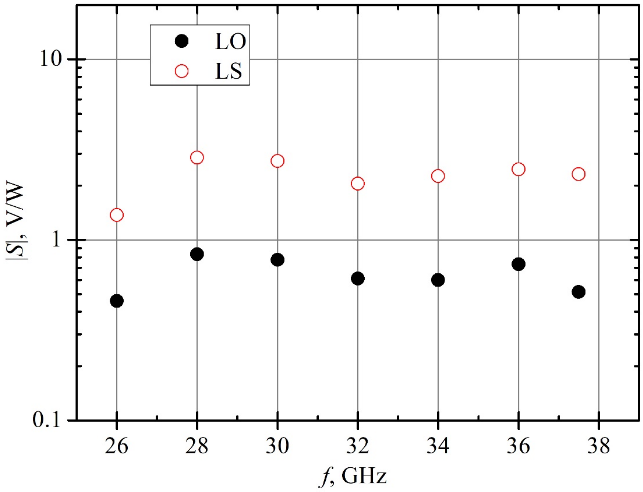

Fig. 3.6. Spectral distribution of the voltage sensitivity's absolute value of the MW diodes embedded in a waveguide

Low values of electrical resistance of diodes LO and LS, along with low values of their capacitance, open the possibility of using these diodes as fast detectors of short-duration pulsed MW radiation. Measurements of electrical capacitance were performed at 1 MHz frequency, and the values of the capacitance were as low as tens and hundreds of femtofarad range. The diodes operated in a zero-biased direct detection mode, making their use simple in MW power measurement devices. Fig. 3.8 depicts the response of the LO diode to a rectangular MW pulse. MW radiation was modulated into rectangular pulses of 1.5 μs duration with steep 10 ns-long fronts at a 100 Hz repetition rate. In Fig. 3.8, the generator pulse (not to voltage scale) and the detected voltage pulse are separated in the vertical direction for better visibility as the small contact of both diodes was grounded; thus, positive pulses were detected on the LS diodes, while the negative pulses were detected on LO diodes. The voltage detected across the LO diode grew exponentially with two characteristic time constants: one of the order of tens of ns and another in a microsecond time scale. The fast rise is attributed to electron heating phenomena in an MW electric field, whereas the longer time constant is determined by the crystal lattice heating. A similar two-process relaxation was observed after the end of the MW pulse. In the case of LS, a slow fall of the voltage magnitude under the action of the MW pulse, as well as slow relaxation after the pulse is gone, can be attributed to a decrease in the influence of MW current rectification due to the crystal lattice heating (and later cooling) and surface charge relaxation phenomena in the Schottky junction. The fast peaks at the start and end of the detected voltage pulse can be related to the hot carrier photocapacitive effect in the Schottky junction of the LS diode (Ašmontas et al., 2006).

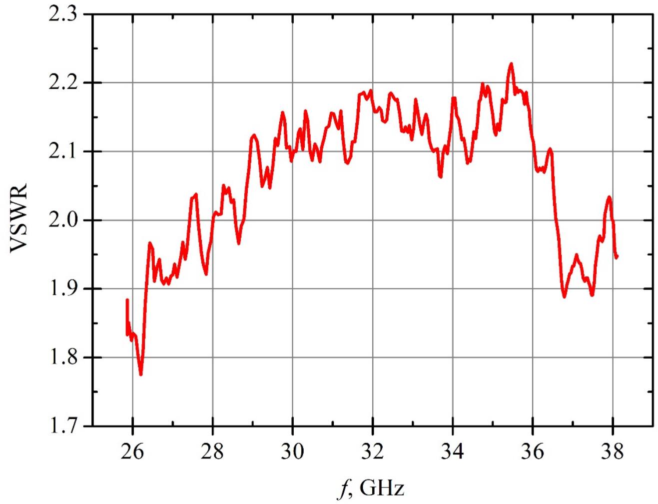

Fig. 3.7. Waveguide detector mount VSWR measurements in the K_a-frequency range

The voltage sensitivity of the PD MW LS diodes is approximately three times higher than that of LO. Nevertheless, the latter reveals better noise properties as compared to those of the diodes containing the Schottky junction.

The shortest MW pulses that the LO diodes were able to detect were approximately 50 ns in duration, as can be seen in Fig. 3.9. The improvement in the operational speed of the LO diode could be achieved by increasing its voltage sensitivity. The use of a more sensitive LS MW diode succeeded in the detection and power measurement of MW pulses of ns duration.

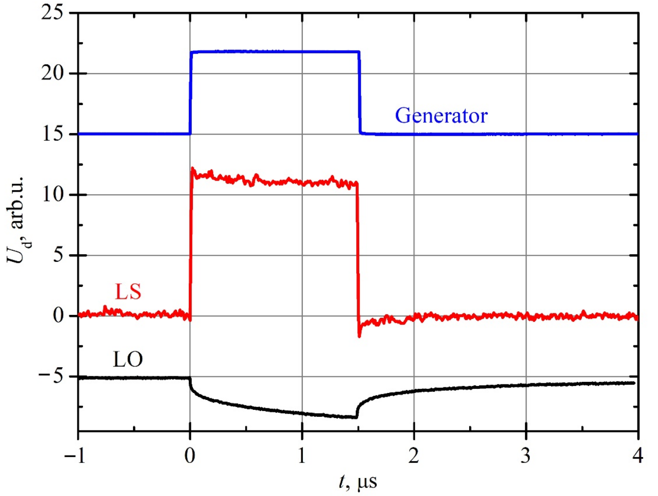

Fig. 3.8. Time dependences of voltage pulses across the diodes placed in a waveguide

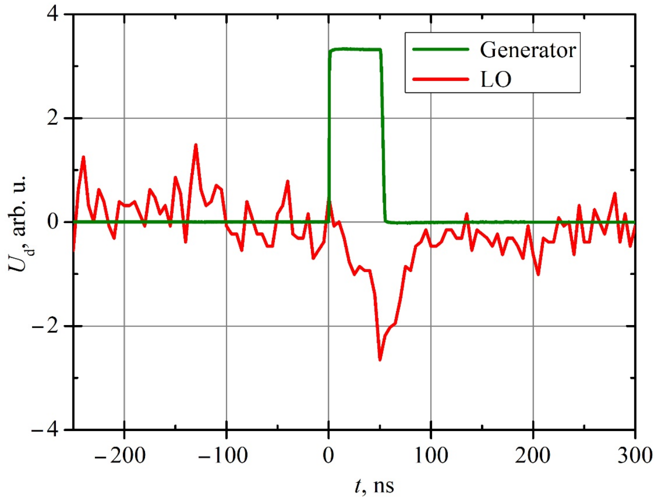

Fig. 3.9. Time dependence of voltage pulses across the Ohmic-like diodes placed in a waveguide

Fig. 3.10 depicts the 10 ns-long MW pulse detected using an LS diode.

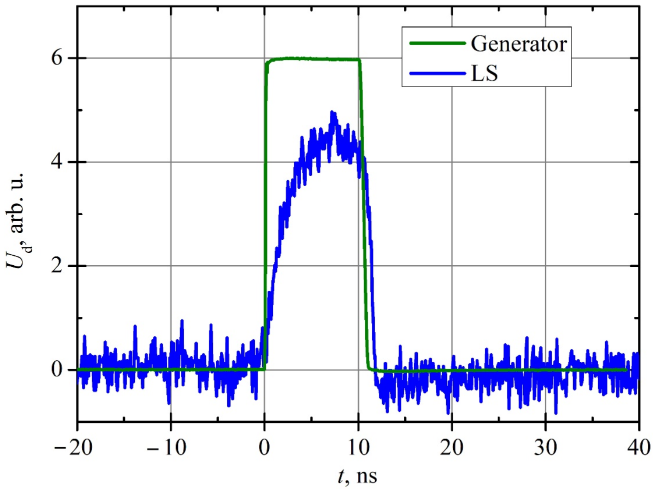

Fig. 3.10. Time dependence of voltage pulses across the LS diode placed in a waveguide

It is worth noting that shorter MW pulses allow for avoiding semiconductor crystal lattice heating by the MW radiation. Therefore, more powerful MW radiation can be detected.

3.2. Direct Current and High-Frequency Detection Properties of Planar Dual Microwave Diodes Based on $Al_xGa_{1-x}As$

The sequence of study of the fabricated PD MW diodes was as follows. First, separate MW diodes were tested in their array on the semiconductor substrate. Electrical resistance at zero applied voltage was evaluated from the measured *IV* characteristics. Then, the voltage sensitivity of the diodes was measured at the 30 GHz frequency. The level of MW power was chosen to be in the range where the detected voltage depended linearly on the power. The median values of the voltage sensitivity and electrical resistance of the diodes were calculated after statistical processing of the measured data. For a more detailed investigation, the diodes having electrical parameters close to the median values were selected from all three groups of different AlAs mole fraction-containing samples (having $x = 0$, 0.15, and 0.3).

To find out the influence of illumination on the electrical parameters of the MW diodes, the characteristics of *IV* and VP (at $f = 30$ GHz) were measured in the dark and under an Eiko EKE21V150W photolamp (color temperature 3240 K) light illumination. Frequency dependence of the voltage sensitivity was measured within the K_a-frequency range. The voltage sensitivity of the diodes in a wider frequency range was performed by fitting the experimental sensitivity data and using the phenomenological equation of the voltage sensitivity's dependence on non-linearity parameters of the *IV* characteristics of the diodes. The hardiness of the diodes to withstand the maximum power of the MW radiation was evaluated using the value of the highest measured applied voltage at which the *IV* characteristic did not yet begin to change.

Three batches of different kinds of diodes, DD0, DD15, and DD30, were named according to the percentage of the AlAs mole fraction in the $Al_xGa_{1-x}As$ semiconductor compound. The fabricated diodes also had different widths d of the small-area contact, as follows: 1.0, 1.5, 2.0, 2.5, 3.0, and 4.0 µm. Each batch contained 480 diodes. The output of the operative diodes in the batches DD0, DD15, and DD30 was 83 %, 78 %, and 46 %, respectively. The two-fold decrease in the number of the operative diodes in the case of DD30 can be explained by a significant increase in the diode's resistance when the molar fraction of AlAs exceeds 20 % and when the deep recombination centers (DX centers) in the AlGaAs compound begin to appear (Mooney, 1998). The negative potential of the detected voltage was predominantly measured on the small-area contact (Fig. 2.2, left contact, Section 2.1.2). This polarity of the detected voltage is labeled as a Schottky voltage. However, the voltage of the opposite polarity was detected across some operative DD0 and DD15 diodes and amounted to 7 % and 4 %, respectively. This detected voltage is labeled as TEMF voltage because its polarity is inherent to the thermoelectromotive force of the hot carriers measured across the MW diodes having perfect Ohmic contacts (Harrison & Zucker, 1963). The box charts of the statistical results are presented in Fig. 3.11. The median value of the voltage sensitivity of the diodes can be approximated by its linear dependence on the width of the contact, as follows:

$$S = S(0) - b \cdot d, \tag{3.1}$$

where $S(0)$ stands for the extrapolated value of the voltage sensitivity at $d = 0$, and b is the slope of the approximation line.

The voltage sensitivity of the DD0 diodes is almost independent of the contact width, while the linear dependence of the voltage sensitivity of the PD diodes base on AlGaAs is stronger, and the slope b increases with the increase in the AlAs mole fraction x in the semiconductor compound. It should be noted that the measurements of the detected voltage were performed using high-impedance loading. If a 50 Ω load is used, then the voltage sensitivity should decrease. In the case of the DD15 diode, the voltage sensitivity decreases from 100 V/W down to 3 V/W. However, in the case of the 50 Ω load, the DD15 diode can be used to detect pulsed nanosecond-long MW signals. The electrical resistance R_0 at zero voltage is scattered around its median value in the case of the DD0 and DD15 diodes and follows a linear dependence close to Equation 3.1, with coefficient b_R. Table 3.1 summarizes the values of the voltage sensitivity and electrical resistance of the PD MW diodes in respect of the width of their narrow contact.

Table 3.1. Parameters of the linear dependence of voltage sensitivity and electrical resistance on the diode's contact width

Diode	Voltage Sensitivity at $d = 0$ $S(0)$, V/W	Slope b, V/(W·μm)	Electrical Resistance at $d = 0$ $R_0(0)$, kΩ	Slope b_R, kΩ/μm
DD0	0.9 ± 0.16	0.02 ± 0.06	1.0 ± 0.1	0.03 ± 0.04
DD15	98 ± 10	20.5 ± 3.9	2.16 ± 0.33	0.2 ± 0.12
DD30	207 ± 19	40 ± 7	15.6 ± 3.1	2.6 ± 1.2

The statistical data of the experiments was approximated using the following various distribution functions: normal, lognormal, and Weibull. The last function was the best to fit the experimental results of the voltage sensitivity and electrical resistance, according to Equation 3.2 ("Characteristics of the Weibull Distribution"):

$$f(x) = \frac{\beta}{\eta}\left(\frac{x}{\eta}\right)^{\beta-1} \exp\left[-\left(\frac{x}{\eta}\right)^{\beta}\right], \tag{3.2}$$

where x stands for either voltage sensitivity or electrical resistance of the PD MW diode, β and η mark the shape and the scale parameters of the Weibull distribution, respectively.

Fig. 3.12 depicts histograms of the experimental data of the voltage sensitivity and electrical resistance of all three batches of the PD MW diodes, DD0, DD15, and DD30. The solid lines in Fig. 3.12 denote the Weibull distribution function. Its parameters, the shape β, and the scale η are presented in the legends of Fig. 3.12 and are summarized in Table 3.2.

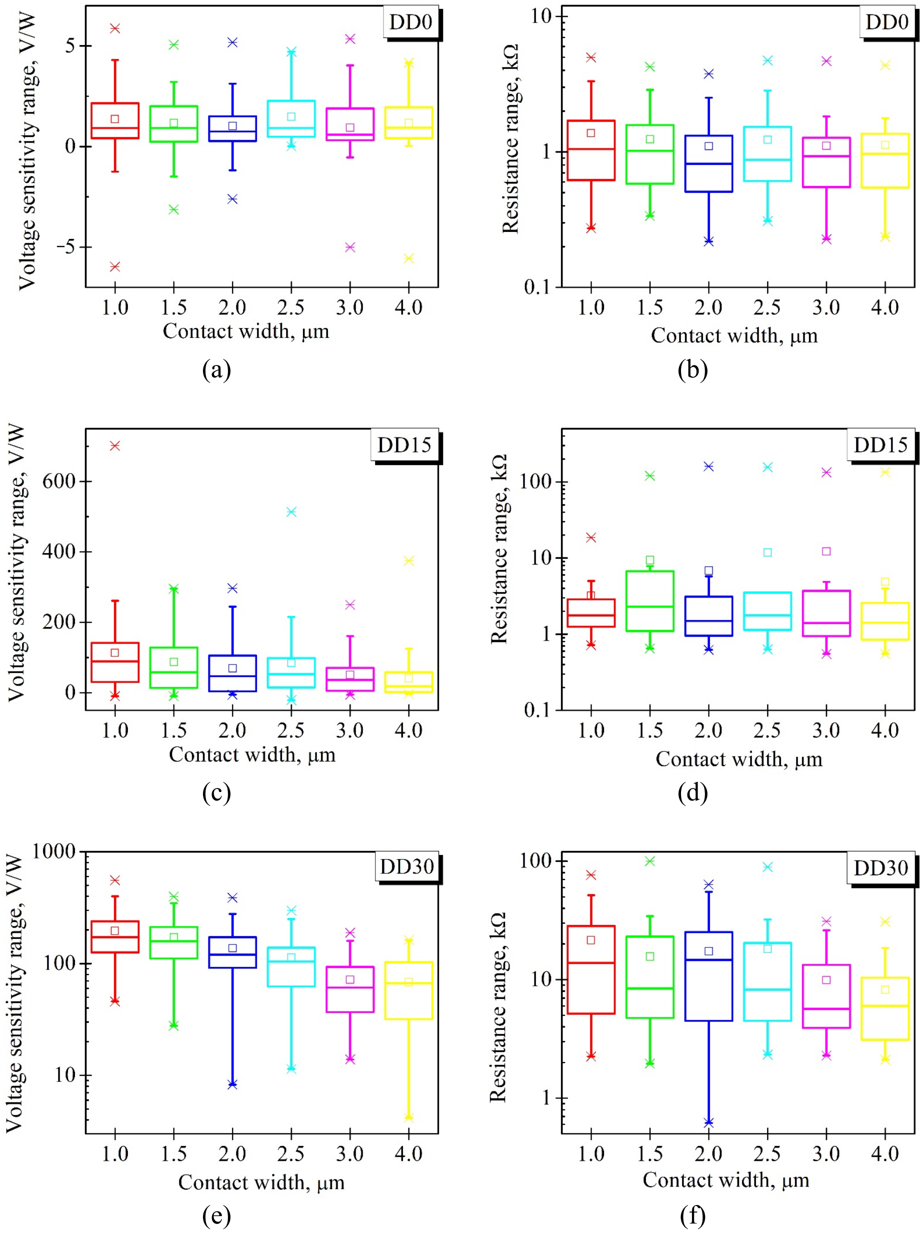

Fig. 3.11. Box-charts of the voltage sensitivity (a, c, and e) and electrical resistance (b, d, and f) of the PD MW diodes DD0 (a and b); DD15 (c and d); DD30 (e and f) with different widths of the small contact

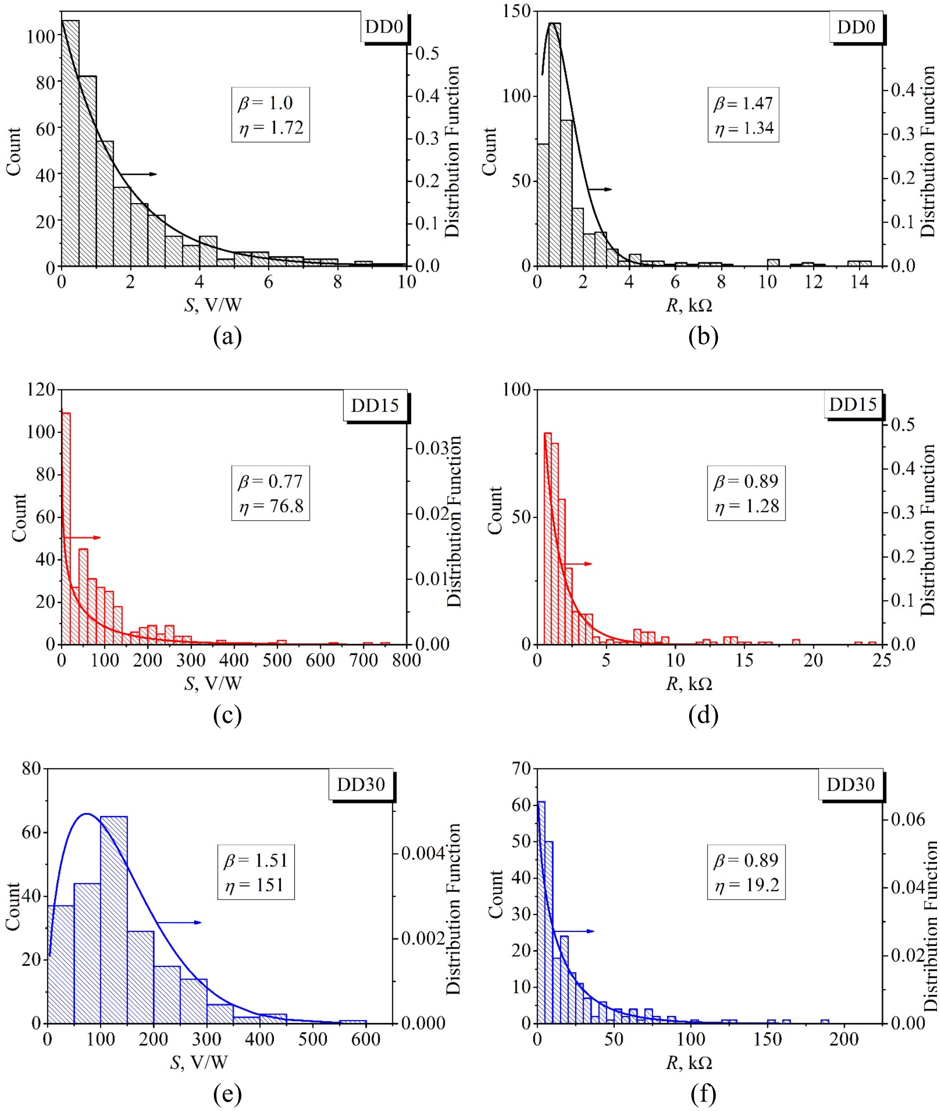

Fig. 3.12. Histograms of experimental data of voltage sensitivity (a, c, and e) and electrical resistance (b, d, and f) experimental data of diodes DD0 (a and b); DD15 (c and d); DD30 (e and f) approximated with the Weibull distribution function

A comparison of the data presented in Tables 3.1 and 3.2 shows a qualitative correlation between voltage sensitivity and the median data of electrical resistance and the scale parameter η, which is derived from the approximation of the data using the Weibull distribution function (Eq. 3.2).

Table 3.2. Shape and scale parameters of the Weibull distribution function for experimental voltage sensitivity S and electrical resistance R_0 data

Diode	Shape β		Scale η	
	for S	for R_0	for S	for R_0
DD0	1.0	1.47	1.72	1.34
DD15	0.77	0.89	76.8	1.28
DD30	1.51	0.89	151	19.2

For a more detailed investigation, representative diodes having median values of voltage sensitivity S and electrical resistance R_0 were selected from all three batches. Electrical parameters of the selected PD MW diodes measured under white-light illumination (Eiko EKE21V150W halogen lamp, 14400 lux intensity) and in the dark (0 lux) are presented in Table 3.3.

Table 3.3. Voltage sensitivity S and electrical resistance R_0 of the representative illuminated and darkened PD MW diodes

Diode	Illuminated		Dark	
	S, V/W	R_0, kΩ	S, V/W	R_0, kΩ
DD0	1.2	1.1	1.7	1.8
DD15	100	1.70	105	1.8
DD30	160	14.3	150	14.9

The *IV* characteristics of the white-light-illuminated diodes are presented in Fig. 3.13. The forward current flows through the diodes when a positive potential of the voltage is applied to the small-area contact, as shown in Fig. 3.13.

The *IV* characteristic of the DD0 diodes is quasilinear, while it becomes non-linear in the case of the DD15 and DD30 diodes based on AlGaAs. The non-linearity is more strongly pronounced for the DD30 diode, which is fabricated base on the higher resistivity $Al_{0.3}Ga_{0.7}As$ semiconductor material. The asymmetry of the *IV* characteristics also increases with the mole fraction x. The correlation of the asymmetry of the *IV* characteristics with the voltage sensitivity of the diodes allows expecting an appropriate increase in sensitivity when the diode demonstrates a more asymmetric *IV* characteristic. A reliable relation exists between the *IV* characteristic's asymmetry and the diode's voltage sensitivity. When the relaxation of the average energy of hot electrons in a semiconductor structure can be neglected, and the conductivity current exceeds the displacement current, then the voltage sensitivity of the MW diode with n-n^+ junction can be expressed using Equation 2.2 (Section 2.3.1).

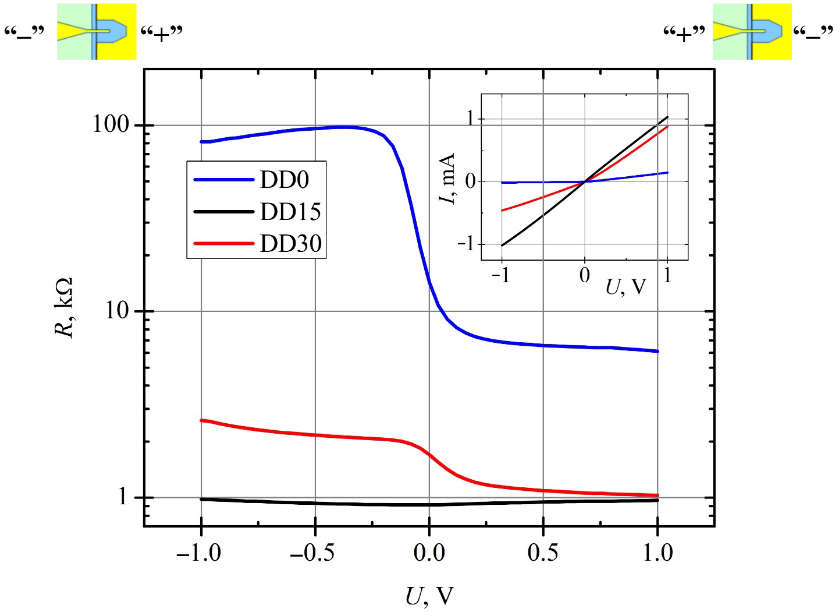

Fig. 3.13. Dependence of electrical resistance of the illuminated PD MW diodes on the applied voltage. The *IV* characteristics of the diodes are presented in the inset

The dependence of the detected voltage on the MW power, i.e., the VP characteristics of the PD MW diodes, was measured using an HF probe station at the 30 GHz frequency. The characteristics are presented in Fig. 3.14.

The MW power on the graph is the incident power (not the absorbed one), i.e., the power supplied to the HF probe. At low MW power, the detected voltage of all the PD MW diodes follows the linear law. However, the VP characteristics become different at higher power values; they turn sublinear in the case of the DD15 and DD30 diodes, while the characteristic of the DD0 diode remains linear within the dynamic range of measured MW power. The calculated NEP values of the diodes and the minimal power level within the noise floor (the minimum limit of the dynamic range), at which the detected voltage can be registered, are presented in Table 3.4. The DD0 diode has the highest NEP value and the minimum power level. DD15 diode has a slightly lower NEP value, and the minimum power is also lower than that of the DD30 diode. The difference in the VP characteristics can be partly explained by the difference in the asymmetry of the *IV* characteristics. Fig. 3.15 depicts the asymmetry versus applied voltage calculated using Equation 2.2.

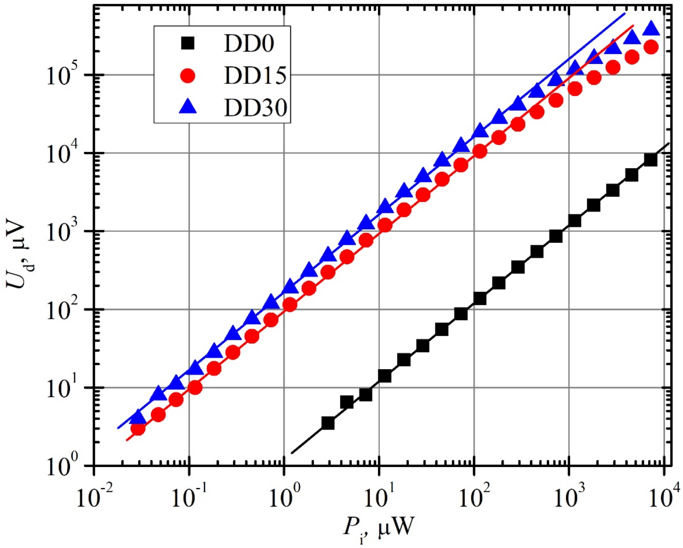

Fig. 3.14. VP characteristics of PD MW diodes measured under a white light illumination at the f = 30 GHz frequency. Lines are guides for the eye of linear dependence

Table 3.4. NEP of the PD MW diodes and minimum power for signal detection calculated using Equations 2.4 and 2.5

Diode	NEP, W/$\sqrt{\text{Hz}}$	P_{min}, nW
DD0	8.4×10^{-11}	6.1
DD15	5×10^{-12}	0.4
DD30	7.3×10^{-12}	0.5

The asymmetry of the DD0 diode's *IV* characteristic is the lowest, and that of the DD15 diode is higher by almost two orders of magnitude. This correlates well with the VP experimental results (Fig. 3.14), which found that the voltage sensitivity of the DD15 diode was higher by two orders of magnitude as compared to that of the DD0 diode. On the other hand, the *IV* asymmetry of the DD30 diode was higher by two orders of magnitude than that of the DD15 diode, while the voltage sensitivity was higher by only two times. The poor coincidence between the *IV* asymmetry and voltage sensitivity data of the DD15 and DD30 diodes can be explained by a weaker absorption of incident MW radiation by the DD30 diode due to the higher value of its electrical resistance (Table 3.3), whereas when using Equation 2.2 it is presumed, that the incident power is fully absorbed by the diode. As previously mentioned, Equation 2.2 is only valid for harsh qualitative evaluation of the voltage sensitivity of Schottky-like diodes at high frequencies. The deviation from the linear law (VP characteristics of diodes DD15 and DD30) most probably results from the decrease in the diode's *IV* asymmetry at a lower applied voltage than in the case of the DD0 diode.

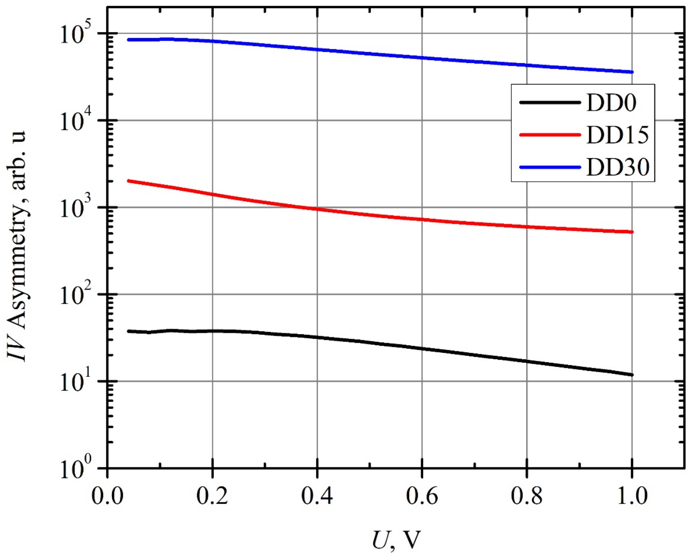

Fig. 3.15. Dependence of the *IV* asymmetry of the PD MW diodes on the applied voltage

As the data presented in Table 3.3 shows, white-light illumination has a different impact on the electrical parameters of the PD MW diodes. The DD0 diodes are more sensitive to illumination. Both their voltage sensitivity and electrical resistance decrease by about 30 % when the light is put on. The change in the parameters of the DD15 and DD30 diodes is lower by about one order of magnitude as compared to the DD0 diode. A weaker dependence of R_0 on illumination is associated with the formation of different densities of activation energy levels at the metal-semiconductor interface with an increase in the AlAs mole fraction *x* (Best, 1979) and also, with different nature of deep traps in the bulk of the $Al_xGa_{1-x}As$ ternary semiconductor structure depending on *x* (Lang, Logan & Jaros, 1979). It is worth noting that the voltage sensitivity of the diode DD30 increases with illumination. The *IV* asymmetry of the PD MW diodes also correlates with the voltage sensitivity, considering the impact of illumination: the light-induced change in the asymmetry decreases with the rise in x in the $Al_xGa_{1-x}As$ compound. This correlation also supports the assumption that the detected voltage arises due to the rectification of MW currents across the quasi-Ohmic metal-semiconductor junctions of the diodes.

As a matter of fact, the developed PD MW diodes are a composition of two quasi-Ohmic metal-semiconductor junctions. Therefore, a natural expectation is to describe the performance of the diodes using equations that are inherent to a metal-semiconductor junction. The experimental data of the *IV* characteristics of the diodes were fitted using the formula of a Schottky junction, i.e., Eq. 1.1 (Section 1.1). The saturation current I_s and the non-ideality factor n were chosen as the fitting parameters. The fitting was performed using *IV* data not exceeding 0.15 V of the applied voltage. The fitting parameters of the diodes are presented in Table 3.5.

Table 3.5. Fitting parameters of the *IV* characteristics approximated with Equation 1.1

Diode	Saturation Current I_s, A	Non-Ideality Factor n
DD0	$(3.5 \pm 2.1) \times 10^{-2}$	1520 ± 15
DD15	$(2.9 \pm 0.12) \times 10^{-4}$	20 ± 0.7
DD30	$(2.3 \pm 0.24) \times 10^{-5}$	11.2 ± 0.9

The experimental *IV* characteristics of the diodes DD15 and DD30 can only be satisfactorily fitted using Equation 1.1. The best fitting results are achieved for the DD15 diodes when the fitting parameters are scattered by ~4 %, while the parameters of the DD30 diodes are scattered by ~10 %. No satisfactory agreement was obtained between the *IV* experimental data and the approximation by Equation 1.1 for the DD0 diodes. An unusually high value of the non-ideality factor can be explained by the metal-semiconductor junction being far from the ideal Schottky junction. The Ge/Ni/Au metals annealed at high temperatures make the quasi-Ohmic metal-semiconductor junction have such a high value for the non-ideality factor.

If the *IV* characteristic of an MW diode is described by Equation 1.1, then its voltage sensitivity can be expressed as (Bahl & Bhartia, 2003):

$$S = \frac{\gamma R_{\mathrm{j}} k_{\mathrm{abs}}}{2\left(1+\frac{R_{\mathrm{S}}}{R_{\mathrm{j}}}\right)\left[1+\frac{R_{\mathrm{S}}}{R_{\mathrm{j}}}+(\omega C_{\mathrm{j}})^2 R_{\mathrm{S}} R_{\mathrm{j}}\right]}, \qquad (3.3)$$

where $\gamma = \frac{\mathrm{d}^2 I}{\mathrm{d}U^2} / \frac{\mathrm{d}I}{\mathrm{d}U}$ denotes the non-linearity of the *IV* characteristic, R_j and C_j stand for the barrier resistance and capacitance of a metal-semiconductor junction, respectively, R_s is the series resistance of the diode, ω is the angular frequency of an MW signal, and k_abs notes the part of MW radiation absorbed by the diode. Certain parameters in the formula can be derived from the *IV* characteristic of the diode, namely, the non-linearity parameter γ and the electrical resistances of the diode. The barrier resistance R_j can be calculated by subtracting the series resistance R_s from the experimentally measured resistance R_0 at zero bias applied voltage. However, in the case when the *IV* characteristic of the diode is far from the characteristic of an ideal Schottky junction (as one of the DD0 diode), the experimental estimation of R_s becomes complicated. Therefore, the geometrical series resistance of the diode was calculated using the experimental value of the sheet resistance R_sh of the epitaxial layer (Table 2.1, Section 2.2.2), with the following Equation 3.4:

$$R_\mathrm{s} = R_\mathrm{sh} \frac{(D-d)\ln\frac{D}{d}}{4L\ln\frac{D}{d} + \pi(D-d)}. \tag{3.4}$$

Here, the used geometrical parameters of the diode d, D, and L are according to the inset of Fig. 2.14 (Section 2.2.2). The series resistance of diodes DD0, DD15, and DD30, calculated using Equation 3.4, was 190 Ω, 580 Ω, and 3460 Ω, respectively, taking the small-contact width $d = 1$ μm, contact length $L = 10$ μm, and gap width $D = 15$ μm. Such evaluation of the series resistance of the diodes succeeded only in the case of the DD30 diode. In the case of DD15 and DD0 diodes, the calculated value was, respectively, 1.5 Ω, which is 5 times lower than the experimental one. The mismatch between the calculated and experimental values can be associated with a stronger influence of the surface states, as the AlAs mole fraction in the semiconductor compound is reduced. The absorbed MW power (absorption coefficient k_abs), as well as the barrier capacitance C_j of the diode, can be found using Equation 3.3 and can be used to approximate the experimental dependence of the voltage sensitivity of the PD MW diodes on frequency, as shown in Fig. 3.16.

The parameters used to fit the calculated *S* data to the experimental points are presented in Table 3.6.

Such an approximation technique opens the possibility of evaluating the HF capacitance of the PD MW diodes (as small as in the femtofarad range) and finding the MW power absorbed in the diode. Moreover, the performance of the PD MW diodes in the THz frequency range can also be forecasted. As Table 3.6 shows, the values of the voltage sensitivity of the DD15 and DD30 diodes allows expecting their application, even in the THz frequency range. The investigated PD MW diodes are weak competitors with the Schottky diodes in the sense of voltage sensitivity. However, diodes having voltage sensitivity of the order of 0.1–1.0 V/W can be used to detect electromagnetic radiation in the terahertz frequency range (Sužiedėlis et al., 2003; Kašalynas et al., 2013).

Table 3.6. Experimental and approximation parameters of PD MW diodes

Diode	γ, V^{-1}	R_j, kΩ	R_s, kΩ	C_j, fF	k_{abs}, %	S(1 GHz), V/W	S(1 THz), V/W
	Experimental Parameters			Approximation Parameters		Approximated Parameters	
DD0	0.07	0.9	0.19	12	10	1.8	0.003
DD15	2.2	1.23	0.54	10	44	290	0.16
DD30	8.5	10.9	3.6	1	1.4	370	0.35

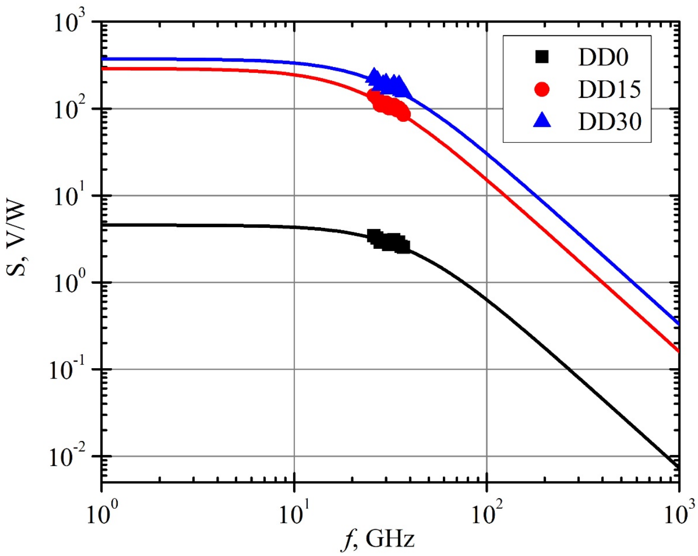

Fig. 3.16. Experimental frequency dependence of the voltage sensitivity of PD MW diodes (dots) in the K_a-frequency range. Solid lines mark the dependences in a wider frequency range calculated using Equation 3.3

The presumption of the detection nature of the PD MW diodes anticipates temperature dependence of the voltage sensitivity. As previously mentioned, the detection due to current rectification implies a non-linear *IV* characteristic, which depends on temperature, i.e., changes in temperature lead to changes in the non-linearity of the *IV* characteristic. The relative change in voltage sensitivity with temperatures of all three types of diodes is depicted in Fig. 3.17.

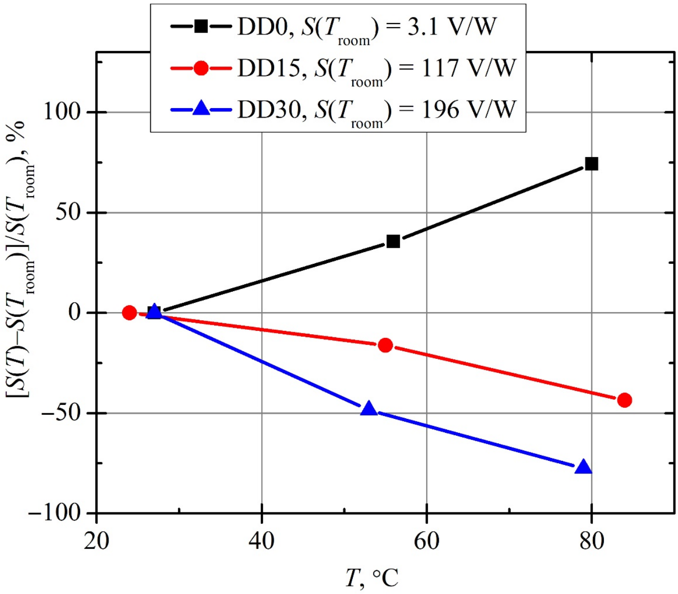

Fig. 3.17. Temperature dependence of the change in relative voltage sensitivity in the PD MW diodes

Since the PD MW diode is composed of two metal-semiconductor junctions, connected in series in opposite directions (Fig. 2.2, Section 2.1.2), the resulting *IV* characteristic of such a planar diode should be made of backward branches of both junctions, which depends on temperature. Therefore, by following Equation 3.5 of the saturation current of a Schottky junction (Rhoderick & Willimas, 1988):

$$I_s = A_R T^2 e^{-\frac{e\psi_{ms}}{kT}}, \tag{3.5}$$

(here, A_R is the Richardson constant, ψ_{ms} marks the barrier height of a Schottky junction), a decrease in electrical resistance of the PD MW diode at higher temperatures should be expected. The temperature dependence of the electrical resistance of the diodes at zero applied voltage is presented in Fig. 3.18, in solid points, and the values of the non-linearity coefficient γ of the *IV* characteristics are also depicted by open dots for comparison.

The electrical resistance of diodes DD15 and DD30 drops down as their temperature increases. This characteristic agrees with the saturation current dependence on temperature, as described in Equation 3.5. However, the dependence of the DD0 diode's resistance on temperature is more stipulated by the bulk resistance of GaAs, and therefore, the DD0 diode's resistance increases with temperature. Moreover, the sign of the non-linearity coefficient of its *IV* characteristic is also opposite to that of the diodes DD15 and DD30 (Table 3.6). As Figs. 3.17 and 3.18 show, there is a good correlation between all three parameters, i.e., voltage sensitivity, resistance, and the non-linearity coefficient for all presented temperature dependencies. The detection properties of the diodes based on the $Al_xGa_{1-x}As$ ternary semiconductor structure (diodes DD15 and DD30) are determined by the rectification of MW currents in the integrated PD MW diode, which is composed of two metal-semiconductor quasi-Ohmic junctions that are connected in series in opposite directions.

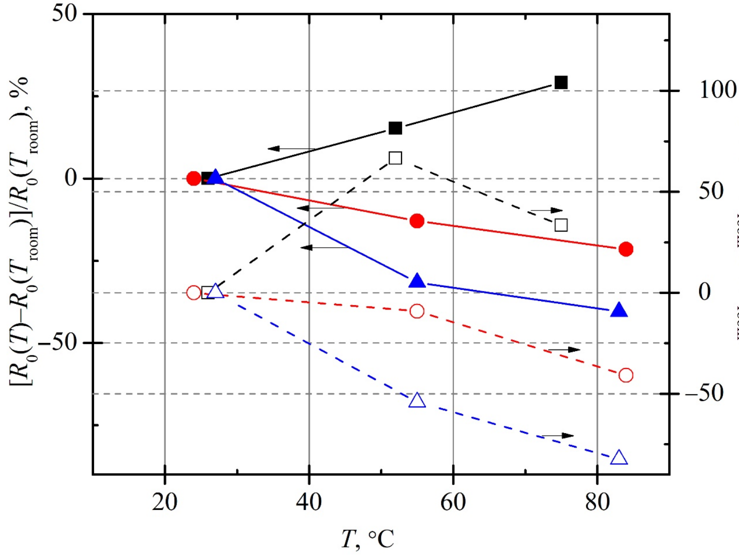

Fig. 3.18. Temperature dependence of the electrical resistance of the PD MW diodes at zero applied voltage (solid dots) and temperature dependence of the non-linearity coefficient γ of the *IV* characteristics of the diodes at zero voltage (open dots). The colors correspond to the same type of diodes as in Fig. 3.17

Finally, an evaluation of another important characteristic of an MW detector was carried out. It is the ability of the MW diode to withstand the impact of high-power MW radiation. Firstly, the maximum forward direction voltage (a positive potential is applied to the small-area contact) was measured, at which the non-reversible changes in the *IV* characteristic still do not take place. Then, the maximum electrical power absorbed by the diode was calculated, and the maximum incident MW power was found by taking the value of the absorption coefficient k_{abs} from Table 3.6. The most robust PD MW diode is DD30, which can withstand incident MW radiation of ~1 W without any changes in its electrical parameters. The diodes DD0 and DD15 were ten-fold weaker; their characteristics remain unchanged if the incident MW power value does not exceed 100 mW.

A comparison of the electrical parameters of several MMW zero voltage-biased room-temperature diodes is presented in Tables 4.2, 4.3, and 4.4 (Chapter 4).

3.3. Conclusions of the Third Chapter

1. PD asymmetric MW diodes based on three types of heavily doped polished GaAs substrates, n^{++}-GaAs, having the donor density 4×10^{18} cm^{-3}, n^{+}-GaAs, doped to 4×10^{17} cm^{-3}, and p^{++}-GaAs, having the 4×10^{18} cm^{-3} acceptor density demonstrated Ohmic-like and Schottky junction-like electrical and MW detection characteristics. Diodes of lower voltage sensitivity demonstrated good linearity of the VP characteristic in a wide MW power range; this feature makes these diodes suitable for MW power measurements. Higher voltage sensitivity was achieved by means of choosing the appropriate substrate material depending on the conductivity type and doping level, although the more sensitive diodes demonstrated higher electrical resistance.
2. PD asymmetric MW diodes based on three types of heavily doped polished GaAs substrates were able to detect MMW pulsed signal in the nanosecond time scale. MW pulses as short as 10 ns long can be sensed, and their power can be measured using Schottky-like diodes
3. Electromagnetic sensing properties of the PD MW n-$Al_xGa_{1-x}As$ diodes epitaxially grown on a SI substrate can be tailored by a proper choice of AlAs mole fraction x in the active semiconductor layer and by choice of size of the area of the smaller contact. Diodes based on n-GaAs are independent of the contact area of smaller diode contacts in terms of voltage sensitivity, while sensitivity increases with the decrease in the contact width of the smaller contact in n-$Al_xGa_{1-x}As$ diodes. The voltage sensitivity of the aluminum-containing PD MW diodes ($x = 0.15$ and 0.3) is two orders of magnitude higher than that of the n-GaAs-based diodes ($x = 0$). The higher voltage sensitivity of the PD MW diodes based on

n-$Al_xGa_{1-x}As$ is related to the effective rectification of the MW currents on the quasi-Ohmic contacts of the diodes. The voltage sensitivity of the investigated PD MW diodes is sensitive to white-light illumination. The lower the AlAs mole fraction in the n-$Al_xGa_{1-x}As$ diode, the stronger its sensitivity to the light.

4. The characteristics of voltage sensitivity versus temperature depend on the x content in PD MW n-$Al_xGa_{1-x}As$ diodes based on the SI substrate. As temperature increases, the voltage sensitivity of the n-GaAs-based diodes ($x = 0$) increases, while it decreases in the case of Al-containing diodes ($x = 0.15$ and 0.3). The diode with a higher x value ($x = 0.3$) is more sensitive to temperature. The different behavior of the diodes with temperature is related to the different quality of the quasi-Ohmic metal-semiconductor contacts of the diodes. A higher AlAs mole fraction in the compound semiconductor stipulates a higher asymmetry of the diode's *IV* characteristic. As a result, diodes with a higher x value behave more like metal-semiconductor Schottky junction diodes.
5. The PD MW diodes base on the n-$Al_{0.3}Ga_{0.7}As$ compound can withstand incident MW radiation power up to 1 W.

4

Investigation of Bow-Tie Microwave Diodes with a Gate over the Two-Dimensional Electron Gas Layer

This chapter covers the analytical approach and investigations of the electrical and HF detection properties of bow-tie type MW diodes with narrow and wide gates above the 2DEG channel based on a selectively doped GaAs/AlGaAs heterostructure. The operation principle of the bow-tie diode is based on non-uniform electron heating effects arising due to a specific shape and doping profile of the diode. Digital and analytical simulations are presented, including simulation of the electric field in bow-tie type MW diode as well as theoretical estimations for the HF properties of an MW diode with a gate over the 2DEG channel. The experimental results include measurements of the *IV* characteristics using a probe station and measurements of detected voltage and voltage sensitivity in the MMW range using both a probe station and a waveguide detector mount.
The research results presented in this chapter were published in the author's publications Ašmontas et al., 2020; Anbinderis et al., 2020 and in patent Sužiedėlis et al., 2019.

4.1. Simulation of an Electric Field Distribution in a Bow-Tie Microwave Diode

HFSS (by ANSYS Electromagnetics) software was used to simulate the distribution of MW electric field in the active area region of a bow-tie type semiconductor MW diode with the n-n^+ junction. HFSS uses the finite element method for solving electromagnetic calculations of different models. This is a procedure where a structure (model) is subdivided into a mesh of many smaller subsections called finite elements. A solution is found for the fields within the finite elements, and these fields are interrelated so that Maxwell's equations are satisfied across the inter-element boundaries. This yields a field solution for the entire original structure. Once the field solution has been found, the generalized S-matrix solution is determined ("An Introduction to HFSS: Fundamental Principles, Concepts, and Use").

The design of the simulated asymmetrically necked bow-tie MW diode is illustrated in Fig. 4.1, where a, d_{1-2}, L_{1-5}, and α refer to the geometrical parameters of the MW diode.

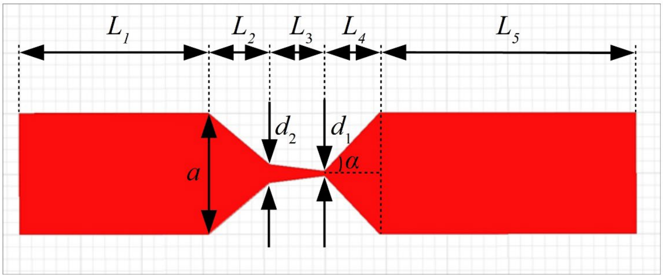

Fig. 4.1. Design of a simulated, asymmetrically necked bow-tie MW diode

In the simulated MW diodes, the neck width d_1 of the small metal-semiconductor contact is 1 µm.

According to the design, the length of the active area L_4 is 45 µm while the length of the Ohmic contact on the left (Fig. 4.1 and Fig. 4.2) L_5 is 200 µm and the Ohmic contact on the right is $L_1 + L_2 + L_3$ (155 + 50 + 45 = 250 µm). The width a at the ends of the Ohmic contacts is 100 µm. The width of the narrow metal-semiconductor contact d_2 is 3 µm, the width of the neck of the active area d_1 is 1 µm, and the angle α is equal to 45°.

The model of the bow-tie type MW diode with an n-n^+ junction is presented in Fig. 4.2. The yellow color represents Ohmic contacts, and the red color represents the GaAs mesa, i.e., the active area of the diode.

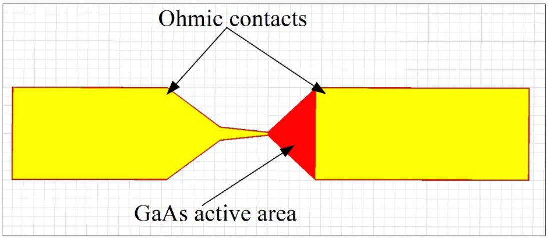

Fig. 4.2. Model of the bow-tie MW diode with an n-n^+ junction. The yellow color represents Ohmic contacts, and the red color represents the GaAs mesa

To excite the electric field in the simulated MW diode, the Ohmic contacts of the bow-tie diode were connected to a simplified two-terminal copper microstrip line with air between them serving as dielectric (Fig. 4.3).

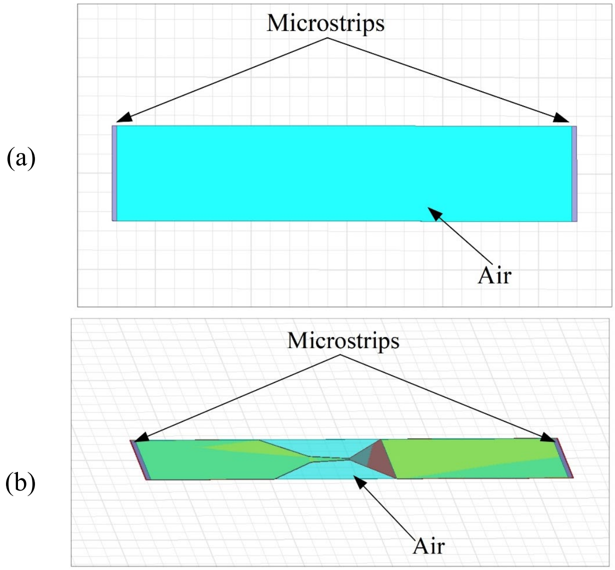

Fig. 4.3. Model of a simplified microstrip line (a) with a bow-tie MW diode inside (b)

As a source of the electric field, a lumped planar excitation port was used. The excitation port plane is illustrated in Fig. 4.4, through which a signal enters the simulated model. The field is parallel to the red arrow. The simulation was performed at 30 GHz frequency and 10 mW power.

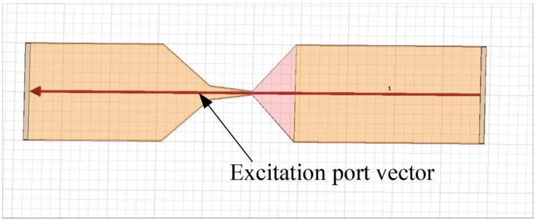

Fig. 4.4. View of the excitation port for the electric field in the model

The distribution of the simulated electric field in the asymmetrically necked bow-tie MW diode is presented in Fig. 4.5.

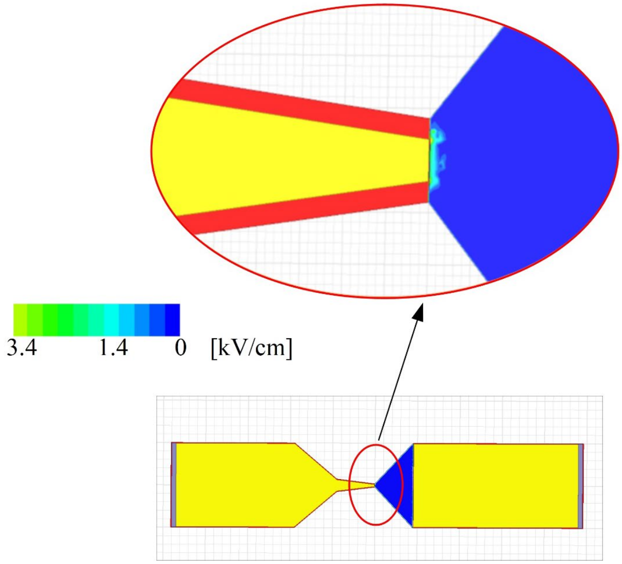

Fig. 4.5. Distribution of the electric field in an asymmetrically necked bow-tie MW diode

As demonstrated in the illustrations (Fig. 4.5), the strength peak of the electric field in the active area is located at the center of the neck of the metal-semiconductor contact reaching up to 20000 V/cm. It was shown by Kancleris (Kancleris, Šlekas & Čiegis, 2013) that the voltage sensitivity of a planar MW diode could be evaluated using Equation 4.1:

$$S = \frac{\mu_0((\frac{a}{d_1})^2-1)}{12\ln\left(\frac{a}{d_1}+1\right)}\frac{\langle E^2\rangle}{P_{\mathrm{i}}}(\tau_{\mathrm{M}} + (1+s)\tau_E), \quad (4.1)$$

where μ_0 is low-field electron mobility, a and d_1 refer to the dimensions of the active area of the diode (Fig. 4.1), $\langle E^2 \rangle$ is the square of the electric field averaged within the active area of the diode, P_i – is the power of the incident wave, τ_E denotes the phenomenological electron energy relaxation time, and τ_M stands for the Maxwell relaxation time and s is the exponent in the dependence of the electron momentum relaxation time on energy. It was used by authors for numerical diode response investigation of a similar model for a thin asymmetrically shaped planar diode in the MMW range. Thus, by knowing $\langle E^2 \rangle$ in the active area, which can be determined from the distribution of the electric field as well as the dimensions of the active area, the voltage sensitivity of the asymmetrically necked bow-tie MW diode can be predicted.

4.2. Analytical Simulation of a Microwave Diode with a Gate over the Two-Dimensional Electron Gas Channel

The phenomenological approach of carrier heating by the MW electric field in the asymmetrically shaped non-homogeneous semiconductor structure in the so-called bow-tie diode (Fig. 4.6) was used to solve current density, heat balance, heat flow density, and Poisson's equations within the warm electron approximation (Ašmontas & Sužiedėlis, 1994).

The expression of the voltage sensitivity S, classically defined as the ratio of the voltage signal U_d detected across the ends of the MW diode and microwave power in a waveguide P_i was taken from (Ašmontas & Sužiedėlis, 1994; Sužiedėlis et al., 2003) and readjusted for the asymmetrically shaped selectively doped semiconductor structure possessing 2DEG and containing the Ohmic metal-semiconductor junction (the n-n^+ junction) in the narrowest part of the structure (Fig. 4.6) as:

$$S = \frac{U_\mathrm{d}}{P_\mathrm{i}} = \frac{2R_\mathrm{sh}\mu_0 \tan\alpha}{3d^2 \ln\frac{a}{d}} \frac{P}{P_\mathrm{i}} N, \tag{4.2}$$

where U_d is the detected voltage over the ends of the MW diode; P_i notes the incident MW power in a waveguide; R_sh marks the sheet resistance of the active layer of the diode; μ_0 is the low field electron mobility; a and d indicate the width of the semiconductor structure in the widest and narrowest parts, respectively; α is the widening angle of the active layer, i.e., geometrical parameters of the active layer of the MW diode that can be found in Fig. 4.6. The frequency-dependent factor N in case of weakly and moderately doped semiconductor (in this case electron energy relaxation time τ_E is independent on electron density) can be expressed as (Sužiedėlis et al., 2003):

$$N = \left[\frac{1+(\omega\tau_{\mathrm{M}})^2}{(\omega\tau_{\mathrm{M}})^2}\right]\left\{\tau_E\left[1+\frac{s^2}{1+(\omega\tau_{\mathrm{M}})^2}\right]\ln[1+(\omega\tau_{\mathrm{M}})^2]+\tau_{\mathrm{M}}\left[\frac{3}{2}-\frac{s(1-s)(\omega\tau_E)^2}{1+(\omega\tau_E)^2}\right]\left[\frac{1}{\omega\tau_{\mathrm{M}}}\arctan(\omega\tau_{\mathrm{M}})-\frac{1}{1+(\omega\tau_{\mathrm{M}})^2}\right]\right\}+\frac{s(1-s)\tau_E}{1+(\omega\tau_E)^2}\bigg]\frac{1}{1+(\omega\tau_{\mathrm{i}})^2}. \quad (4.3)$$

Here, s is the exponent in the dependence of the electron momentum relaxation time τ_{i} on the electron energy E, τ_E denotes the phenomenological energy relaxation time of an electron, and τ_{M} stands for the Maxwell relaxation time in the lightly doped region n of the n-n^+ junction (Fig. 4.6). The Maxwell relaxation time was calculated using the expression:

$$\tau_{\mathrm{M}} = \varepsilon\varepsilon_0\rho = \varepsilon\varepsilon_0 R_{\mathrm{sh}}h, \quad (4.4)$$

where ε and ε_0 denote the relative permittivity of GaAs and permittivity of vacuum, respectively, ρ stands for the specific resistivity of the material, and $h = 5$ nm is the average thickness of the electron channel. Electron pulse relaxation time was calculated using the formula:

$$\tau_{\mathrm{i}} = \frac{m_{\mathrm{eff}}\mu_0}{e}, \quad (4.5)$$

where $m_{\mathrm{eff}} = 0.0636m_0$ is the effective mass of an electron in GaAs (m_0 and e note the free electron mass and charge, respectively).

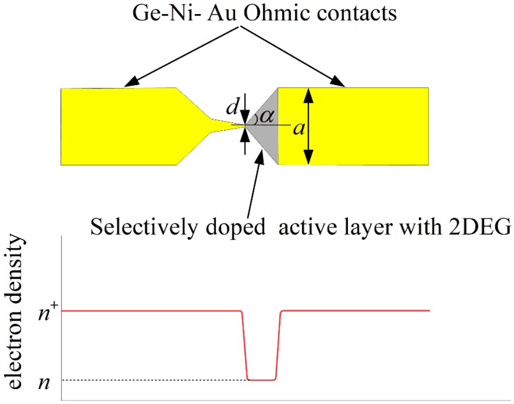

Fig. 4.6. Schematic view of the bow-tie diode and electron density distribution in the diode

A fast look into Equation 4.2 of the voltage sensitivity offers a way of increasing the sensitivity of the MW diode based on a gated asymmetrically necked selectively doped structure with the n-n^+ junction. The gate placed over the 2DEG channel can handle electron density, here depending on the polarity of the MW voltage applied to the MW diode with the gate and on the location of the gate. Therefore, additional detected voltage arises over the ends of the diode due to MW currents rectification on the gate.

Introduction of the Au gate on the surface of the active layer of the MW diode near its wide contact (Fig. 4.7 (c), the right contact) creates additional non-homogeneity in the structure of the diode: when a positive potential of the MW signal is applied to the wide gate, the current through the diode increases, and, contrarily, when a negative potential of the MW signal is applied to the gate, the current decreases. This way, additional rectification of the MW current on the wide gate of the MW diode should increase the voltage sensitivity of the diode.

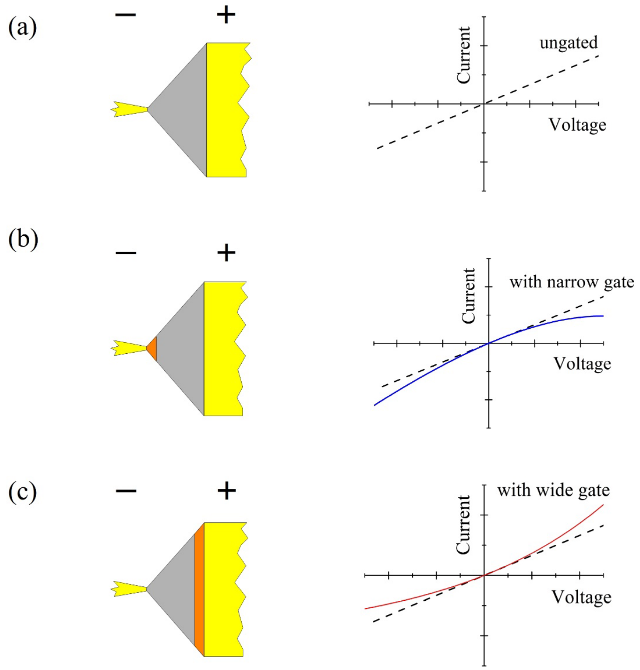

Fig. 4.7. MW currents in the bow-tie diode that delivers the detected voltage having polarity of TEMF: in the ungated diode (a), in the diodes with narrow (b) and wide (c) gates. The polarity sign + and – indicates the potentials applied to the junction when current flows in the forward direction

When the narrow gate is placed near the narrow contact of the diode, the applied negative potential of the MW signal diminishes the electrical current due to a decrease in the electron density under the narrow gate in the active region of the diode and current in the forward direction is decreased, while for the positive potential of the MW signal applied to the narrow gate, the electrical current increases. Therefore, the detected voltage due to the rectification of MW currents on the narrow gate is of opposite polarity compared to the polarity of the electromotive force of hot carriers in this diode. Thus, a decrease in the voltage sensitivity should be expected compared to that of an ungated MW diode in the case of the narrow gate.

Now, consider the case when the polarity of the detected voltage corresponds to the MW currents rectification in the metal-semiconductor junction (the Schottky junction) situated in the narrowest part of the bow-tie diode. This situation can take place when the Schottky junction manifests itself due to the perceptible contact resistivity in the metal-semiconductor junction. Applying the MW signal to the ungated bow-tie diode with a metal-semiconductor junction, one can measure the negative potential on the more necked part of the diode (Fig. 4.8 (a), left contact of the diode).

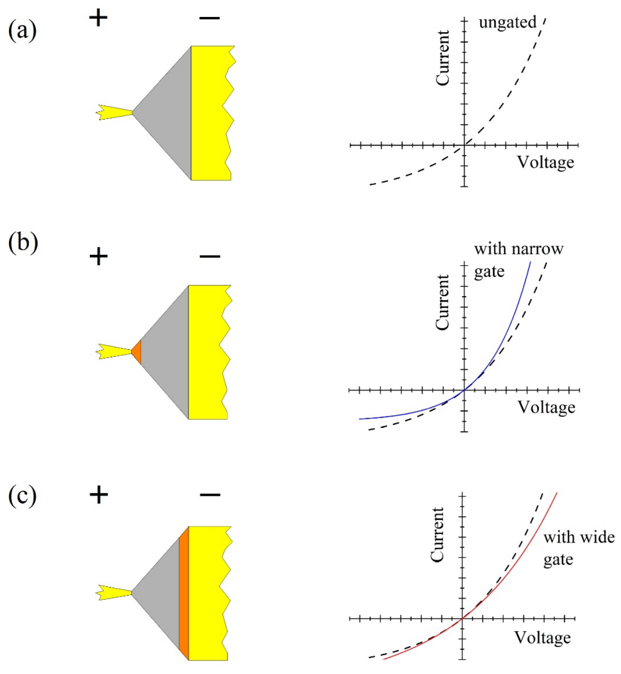

Fig. 4.8. Microwave currents in the bow-tie diode, which delivers the detected voltage having a polarity of the Schottky junction: in the ungated diode (a), in the diodes with narrow (b) and wide (c) gates. The polarity sign + and – indicates the potentials applied to the junction when current flows in the forward direction

The forward direction of the ungated diode is when a positive potential of the MW voltage is applied to the narrower part of the diode, as can be seen in

Fig. 4.8 (a). Placing a narrow gate on the surface of the active layer of the diode, the additional Schottky junction is created between the gate contact and the active layer of the diode. Therefore, the voltage sensitivity of the gated MW diode should be increased due to the increase in the asymmetry of the *IV* characteristic of the diode, as can be seen in Fig. 4.8 (b).

The wide gate placed near the wide right contact of the diode makes this contact less Ohmic because, during the first half-period of the MW signal, the active layer under the gate is depleted. This circumstance diminishes the asymmetry of the *IV* characteristic of the MW diode with a wide gate, as can be seen in Fig. 4.8 (c). That is why a lower value of the voltage sensitivity should be expected in the case when the detected voltage has the polarity of the Schottky voltage arising over the ends of the ungated bow-tie diode.

4.3. Direct Current and High-Frequency Detection Properties of Bow-Tie Diodes with and without a Gate over the Two-Dimensional Electron Gas Channel

The investigation of the bow-tie MW diodes was carried out in the following sequence. First, the VP characteristics of all the ungated bow-tie MW diodes situated on a semiconductor substrate were measured at the K_a-frequency band using an HF probe station. Further, the gates were formed on the MW diodes, and spectral measurements were performed on particular diodes. Finally, after the gated bow-tie MW diode batches were transferred onto the polyimide film, the diodes were separated and mounted into the waveguide detector mount. The frequency dependence of the detected voltage was investigated again. Depending on the value of contact resistivity of a particular bow-tie MW diode, the detected voltage had either the polarity of TEMF of hot electrons in the bow-tie-shaped semiconductor structure or the polarity of the voltage detected on the metal-semiconductor Schottky-like junction. In the case of the TEMF, voltage the positive potential of the detected voltage arises on the narrower contact of the bow-tie MW diode (the left side contact of the MW diode in Fig. 2.16). When the Schottky voltage arises over the ends of the bow-tie MW diodes, and vice versa, the negative potential is measured on the left contact. The statistics for the voltage sensitivity of the ungated bow-tie MW diodes are presented in Table 4.1.

Almost the same number of bow-tie MW diodes have detected the voltage of TEMF and of the Schottky voltage polarity. These diodes were named TEMF and SCHV, respectively. Median values of voltage sensitivity of the bow-tie SCHV diodes, having a width of the neck of 1 μm and 2 μm, were 0.55 V/W and 0.45 V/W, respectively. The TEMF diodes have practically the same median voltage sensitivity of –0.3 V/W for diodes having a width of the neck of 1 μm and

2 μm. The positive sign of the voltage sensitivity in Table 4.1 is attributed to SCHV diodes, and the negative one to TEMF diodes.

Table 4.1. Statistics on the voltage sensitivity of the ungated and gated bow-tie MW diodes with the 2DEG channel based on a selectively doped GaAs/AlGaAs heterostructure. The voltage sensitivity was measured at 30 GHz frequency using an HF probe station. Abbreviations BtDWG and BtDNG mark the bow-tie diode with wide and narrow gates, respectively. Numbers next to the abbreviations indicate the width of the neck of diodes in micrometers. Abbreviations TEMF and SCHV denote the polarity of the detected voltage assigned to thermoelectric electromotive force and Schottky voltage, respectively

Diodes	Width of the neck of the diodes d, μm	Polarity of the detected voltage	Number of diodes	Median value of voltage sensitivity $S_{without}$, V/W	Polarity of the detected voltage	Number of diodes	Median value of voltage sensitivity S_{with}, V/W	$S_{with}/S_{without}$
		Ungated diodes			Diodes with a gate			
Bow-tie diodes with wide gate (BtDWG)								
BtDWG1	1	TEMF	34	–0.31	TEMF	42	–5.9	19
BtDWG1	1	SCHV	20	0.63	SCHV	–	–	–
BtDWG2	2	TEMF	28	–0.27	TEMF	46	–5.4	20
BtDWG2	2	SCHV	26	0.45	SCHV	–	–	–
Bow-tie diodes with narrow gate (BtDNG)								
BtDNG1	1	TEMF	15	–0.29	TEMF	–	–	–
BtDNG1	1	SCHV	6	0.48	SCHV	22	44.4	93
BtDNG2	2	TEMF	12	–0.30	TEMF	–	–	–
BtDNG2	2	SCHV	13	0.36	SCHV	22	35.2	98

The measurement results for gated bow-tie MW diodes are presented in Table 4.1 as well. As it was prefigured in Section 4.2, the influence of the gates situated at narrow and wide contacts (Fig. 2.16) was different. The wide gate for the BtDWG diodes increases the voltage sensitivity of the ungated bow-tie MW diodes detecting the voltage of the TEMF polarity. The influence of the wide gate on the voltage of the Schottky polarity detected by the BtDWG diodes is more conspicuous: the detected voltage changes its polarity from Schottky to TEMF. The voltage sensitivity of the bow-tie MW diode is increased twenty times compared to the voltage sensitivity of the ungated bow-tie MW diode, which detects the voltage of the TEMF polarity. The narrow gate of the bow-tie MW diode situated at the narrow contact of the diode increases the detected voltage of the ungated bow-tie MW diode of the Schottky polarity. The gate changes the polarity of the detected voltage from TEMF to Schottky when the detected voltage of the ungated bow-tie MW diode has the polarity of TEMF, as can be seen from the data presented in Table 4.1. The overall increase of voltage sensitivity reaches two orders when comparing the ungated bow-tie MW diode with the diode having a narrow gate on its active layer near the narrow metallic contact.

The impact of gates in bow-tie MW diodes is clearly seen from their *IV* characteristics (Fig. 4.9).

The *IV* characteristic of the ungated bow-tie MW diode, which detects the voltage of the TEMF polarity, is presented in Fig. 4.9 (a) by the red dashed curve. The introduction of a wide gate makes the *IV* characteristic more asymmetric (Fig. 4.9 (a), solid red curve), which results in more effective MW current rectification and an increase of asymmetry of the *IV* characteristic, as well as voltage sensitivity of the TEMF polarity.

The *IV* characteristic of the ungated bow-tie MW diode that detects the voltage of Schottky polarity is depicted in Fig. 4.9 (b) by the blue dashed curve. The introduction of a narrow gate onto an active layer of this diode near its neck makes the asymmetry of the *IV* characteristic of the bow-tie MW diode more pronounced, as can be seen in Fig. 4.9 (b), where the *IV* characteristic of the bow-tie MW diode with the narrow gate is shown by the solid blue curve.

Quantitative estimation of the asymmetry of *IV* characteristics of bow-tie MW diodes (Fig. 4.9 – c) allows for predicting their detective properties under the impact of MW radiation. One of those estimations was done for the MW diode with the n-n^+ junction (Ašmontas & Sužiedėlis, 1994): when the relaxation of energy of hot electrons can be neglected (what holds true at lower frequencies) and the conductivity current exceeds the displacement current, the voltage sensitivity of the MW diode can be expressed according to Equation 2.2 (Section 2.3.1). It is worth noting that this estimation, according to Equation 2.2, gives a ten-times increased *IV* asymmetry when the gate is created beside the contacts of the bow-tie MW diode. Therefore, a respective increase in the voltage sensitivity should be expected in the bow-tie MW diodes containing the gate.

(a)

(b)

(c)

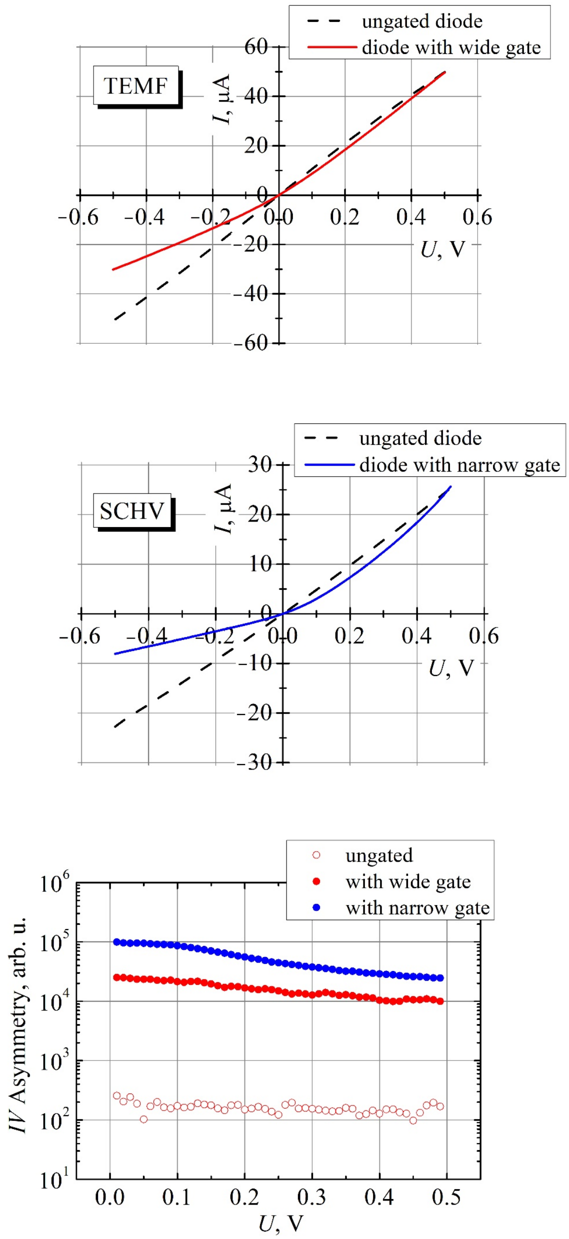

Fig. 4.9. *IV* characteristics of bow-tie MW diodes with the 2DEG channel based on a selectively doped GaAs/AlGaAs heterostructure: (a) diode detecting the voltage of the TEMF polarity; (b) diode detecting the voltage of the Schottky polarity; (c) the dependence of the *IV* asymmetry of the PD MW diodes on the applied voltage

Typical VP characteristics of the bow-tie MW diodes having the TEMF polarity are presented in Fig. 4.10 by open square dots.

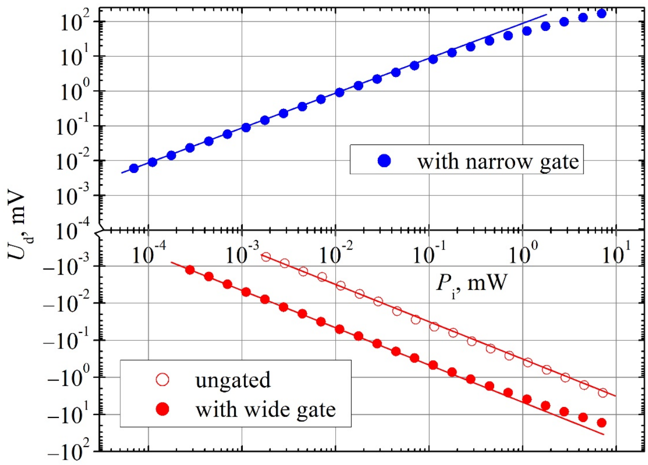

Fig. 4.10. Dependence of the detected voltage on the 30 GHz frequency MW power of the ungated (open red squares) and gated (circle dots) bow-tie MW diodes with the 2DEG channel based on a selectively doped GaAs/AlGaAs heterostructure. Open blue circles correspond to the diode with a narrow gate, and solid red circles belong to the bow-tie diode with a wide gate. The lines are guides for the eye of linear dependence

Wide dynamic range is one of the desirable features of an electromagnetic detector. As Fig. 4.10 shows, linear experimental dependence of the detected voltage is kept within at least four order-wide MW power range. The NEP values of the gated diodes were lower than those of the ungated (calculated according to Equation 2.4). It is 3.4×10^{-10} W/√Hz for the ungated diode, 1.9×10^{-12} W/√Hz for the diode with a wide gate, and 3.4×10^{-11} W/√Hz for the diode with a narrow gate. The minimum power level (the minimum limit of the dynamic range) at which the detected voltage of the diodes can be registered using appropriate measurement equipment (calculated using Eq. 2.5) was 23.9, 0.1, and 2.3 nW for the ungated diode, the diode with a wide gate and the diode with a narrow gate, respectively.

Usage of the probe station for the investigation of the detection properties of MW diodes enables the performance of the measurements of the detected voltage when the MW diode is illuminated by light. Therefore, the VP characteristics of the bow-tie MW diodes in Fig. 4.11 are presented when the diode is illuminated by a white halogen lamp (Eiko EKE21V150W, 14400 lux intensity) and when the diode is in darkness (0 lux).

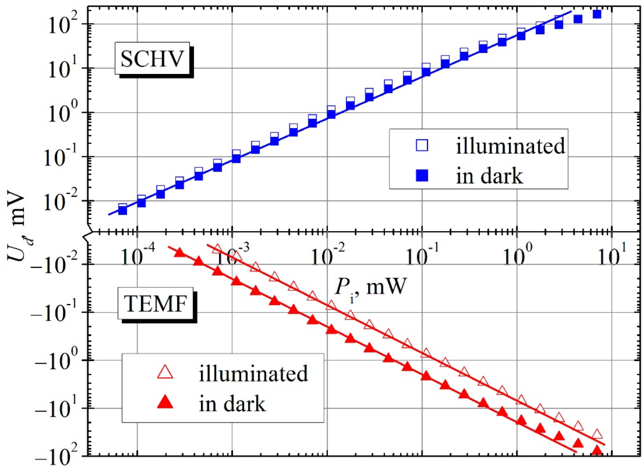

Fig. 4.11. Dependence of the detected voltage on the MW power of the gated bow-tie MW diodes with the 2DEG channel based on a selectively doped GaAs/AlGaAs heterostructure: in darkness (solid dots) and illuminated by a halogen lamp (open dots). Square dots mark the voltage power characteristics of the diodes exhibiting the detected voltage of the Schottky polarity, and the triangle dots belong to the diodes detecting TEMF. The lines are guides for the eye of the linear dependence of the detected voltage on MW power

The VP characteristics are linear at low MW power for both the bow-tie MW diodes detecting the voltage of the Schottky polarity and the diodes detecting TEMF.

In terms of voltage sensitivity, the value of the SCHV diode reached 80 V/W when the diode was in darkness, and the sensitivity increased up to 100 V/W when the diode was illuminated by light. The explanation of such dependence of the voltage sensitivity on illumination can be based on competing mechanisms of the MW radiation detection in the MW diode of the Schottky voltage and TEMF, which oppose each other. The illumination of such a diode by light diminishes the contribution of TEMF to the detected voltage of the SCHV diode due to an increase in electron density in the active region of the MW diode. Therefore, a slight increase in the detected voltage of the Schottky polarity is observed. The impact of the light illumination on the detected voltage of the TEMF polarity is more conspicuous: the voltage sensitivity increases three times when the diode is shielded from the light because the sheet resistance of the active region of the MW diode is increased. The measured power range of SCHV and TEMF diodes is 30 dB independent of illumination, as can be seen in Fig. 4.11.

The measured dependence of the voltage sensitivity of the ungated bow-tie MW diode that detects the TEMF polarity on the gigahertz-terahertz radiation frequency is presented in Fig. 4.12, and the dashed line depicts the calculated frequency dependence of the voltage sensitivity using the expression of the voltage sensitivity S for the asymmetrically shaped selectively doped semiconductor structure that possesses 2DEG and contains the Ohmic metal-semiconductor junction (the n^+-n junction) in the narrowest part of the semiconductor structure (Eq. 4.2).

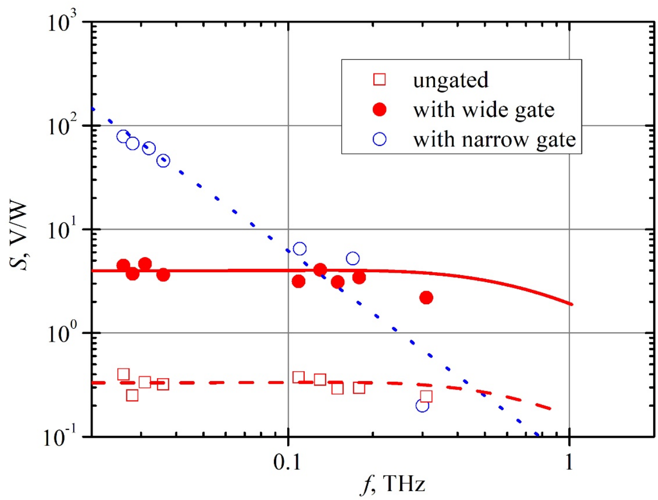

Fig. 4.12. Frequency dependence of the voltage sensitivity of the bow-tie MW diodes with the 2DEG channel based on a selectively doped GaAs/AlGaAs heterostructure: ungated (open red squares), with a wide gate (solid red circles), and with a narrow gate (open blue circles). The red dashed line shows the dependency of the ungated diode calculated according to Equation 4.2, and the solid red line calculated according to Equation 4.6 refers to the wide-gated diode. The blue dotted line is a guide for the eye of the $1/\omega^2$ dependence

Specified electrical parameters of the bow-tie MW diodes were measured experimentally: the sheet resistance $R_{sh} = 1850\ \Omega/\square$ was measured using the transmission line test structure, the electron mobility at low electric field strength

$\mu_0 = 5200\ \mathrm{cm^2/(V\cdot s)}$ was obtained using Hall measurements. Electron energy relaxation time $\tau_E = 0.45$ ps in *n*-GaAs at room temperature was taken from (Dienys et al., 1989; Ašmontas & Sužiedėlis, 1993). Considering the linear dependence of the electron pulse relaxation time on the electron energy in GaAs at room temperature, the value of the exponent $s = 1$ was taken (Dargys & Kundrotas, 1994).

The theoretical dependence of S on the frequency is in good agreement with the experimental data. The percentage of MW power absorbed by the diode $P/P_\mathrm{i} = 0.02$ was taken to fit the theoretical curve with the experimental points at lower frequencies. Noteworthy is the decrease in the voltage sensitivity at higher frequencies. Most probably, it is caused by the weakening of electron heating due to MW radiation because the frequency of the electric field becomes higher than the reciprocal momentum relaxation time of electrons.

After the wide gates were formed onto the same bow-tie MW diodes, the measurements of VP characteristic and voltage sensitivity of the gated diodes were carried out again at the same frequencies.

As Fig. 4.10 shows, the dependence of the detected voltage on the MW power of the wide-gated bow-tie MW diode is still linear over at least four orders of magnitude of the MW power at 30 GHz (solid red circles). The voltage sensitivity of bow-tie MW diodes with a wide gate is higher by one order of magnitude than S of the ungated bow-tie MW diode. Insertion of the wide gate did not change the character of S dependence on frequency (Fig. 4.12). Entering the terahertz frequency range is marked by a slight decrease in the voltage sensitivity for both wide-gated and ungated bow-tie MW diodes. Thus, using the same approach as Popov (2013), the dependence of the voltage sensitivity on frequency due to subterahertz current rectification by a periodic two-dimensional electron system can be readjusted according to Equation 4.6 (Popov, 2013):

$$S(\omega) = S(0)\frac{1}{1+(\omega\tau_\mathrm{i})^2}, \tag{4.6}$$

where $S(0)$ is the voltage sensitivity at low frequencies. Using empirical Equation 4.6, spectral dependence of the voltage sensitivity of the wide-gated bow-tie MW diode was calculated and fitted, also assuming $\tau_\mathrm{i} = 0.19$ ps. It is depicted in Fig. 4.12 by a solid red line. In the calculation, $S(0)$ was taken at 4 V/W to fit the theoretical curve with experimental points at low frequencies.

Insertion of the narrow gate essentially changes the electrical parameters of the bow-tie MW diode. The polarity of the detected voltage becomes opposite compared to that of the ungated case (Fig. 4.12). Measurements of voltage sensitivity's spectral dependency of the narrow-gated bow-tie MW diode reveal no presence of plateau, and $S(\omega)$ decreases according to the ω^{-2} law at high frequencies (Fig. 4.12). At low frequencies, its voltage sensitivity exceeds one of the ungated diodes by more than two orders of magnitude, whereas the sensitivity of both bow-tie MW diodes becomes practically equal at 0.3 THz.

A comparison of the electrical parameters of several MMW zero voltage-biased room temperature diodes is presented in Tables 4.2, 4.3, and 4.4.

Table 4.2. Technological parameters of several different MMW diodes operating at room temperature without bias voltage

Diode	Technology	Dimension of Active Part	Reference
Planar DD0	LPE	1 µm	This work
Planar DD15	LPE	1 µm	This work
Planar DD30	LPE	1 µm	This work
Planar LO	LPE	1 µm	This work
Planar LS	LPE	1 µm	This work
Planar HS	LPE	1 µm	This work
Gated bow-tie GaAs TEMF	MBE	2 µm	This work
Gated bow-tie GaAs Schottky	MBE	2 µm	This work
Bow-tie GaAs	VPE	10 µm	Sužiedėlis et al.,2003
Heterojunction	MBE	2 µm	Gradauskas et al., 2010
Bow-tie InGaAs	MBE	12 µm	Seliuta et al., 2006
Self-switching (SSD)	MOCVD	90 nm	Sangare et al., 2013
Graphene ballistic rectifier	Graphene/Boron nitride	500 nm	But et al., 2018
Schottky ZBD (W band)	–	–	Virginia Diodes, Inc., Zero Bias Detector
Schottky ZBD (G band)	–	–	Virginia Diodes, Inc., Zero Bias Detector

Table 4.3. Electrical and detection parameters of several different MMW diodes operating at room temperature without bias voltage (Part 1)

Diode	R_0, kΩ	C, fF	$S_{\text{at 30 GHz}}$, V/W	$S_{\text{at 1 THz}}$, V/W	NEP, W/√Hz	$P_{\min}$, nW	$P_{\max}$, mW	Reference
Planar DD0	1.1 (1.8)*	12	1.2 (1.7)*	0.003	8.4×10^{-11}	6.1	10	This work
Planar DD15	1.7 (1.8)*	10	100 (105)*	0.17	5×10^{-12}	0.4	0.3	This work
Planar DD30	14.3 (14.9)*	1	160 (150)*	0.33	7.3×10^{-12}	0.5	0.4	This work
Planar LO	0.03	–	0.33	–	3×10^{-11}	1.8	5	This work
Planar LS	0.3	–	1.2	–	2.6×10^{-10}	2.1	4	This work
Planar HS	23 000	–	70	–	1.2×10^{-10}	8.8	2	This work
Bow-tie GaAs	4.0	–	0.3	0.1	–	–	30	Sužiedėlis et al.,2003
Gated bow-tie GaAs TEMF	5.5	–	4.0	2.0	1.9×10^{-12}	0.1	2	This work
Gated bow-tie GaAs Schottky	5.5	–	70	0.06	3.4×10^{-11}	2.3	0.2	This work
Hetero-junction	1.0	–	300	0.4	–	–	2	Gradauskas et al., 2010
Bow-tie InGaAs	9.3	–	5.0	2.0	–	–	10	Seliuta et al., 2006

* – measurements in dark

Table 4.4. Electrical and detection parameters of several different MMW diodes operating at room temperature without bias voltage (Part 2)

Diode	R_0, kΩ	C, fF	$S_{\text{at 30 GHz}}$, V/W	$S_{\text{at 1 THz}}$, V/W	NEP, W/√Hz	P_{min}, nW	P_{max}, mW	Reference
Self-switching (SSD)	1.5	–	80	2.0	$280 \cdot 10^{-12}$	–	0.003	Sangare et al., 2013
Graphene ballistic rectifier	6.0	–	800	0.05	–	1000	1	But et al., 2018
Schottky ZBD (W band)	2.5–4.5	25	2800 (at W-band)		$9.5 \cdot 10^{-12}$	–	0.003	Virginia Diodes, Inc., Zero Bias Detector
Schottky ZBD (G band)	2–7	12	2400 (at G-band)		$11 \cdot 10^{-12}$	–	0.003	Virginia Diodes, Inc., Zero Bias Detector

* – measurements in dark

The developed and investigated planar MW diodes are not inferior to the other diodes in the sense of voltage sensitivity at low radiation frequency. The voltage sensitivity of the Schottky zero-bias diode detector, produced by the leading company "Virginia Diodes," is at least two orders higher. Moreover, though the voltage sensitivity of the investigated MW diodes decreases towards the higher frequencies, it remains sufficient to detect electromagnetic radiation in the subterahertz range, making them more broadband than in comparison with competing approaches. The NEP values of PD MW diodes DD15, DD30, and gated bow-tie GaAs diodes with TEMF polarity are of the same order as of the commercially available Schottky diode detectors, while the dynamic power range is wider for the developed MW diodes as the maximum power of linear VP range is by three orders higher.

It should be emphasized, once again, that the PD MW diodes are attractive in their simplicity and do not require complex manufacturing technologies, and gated bow-tie diodes suggest a technology for the improvement of voltage sensitivity. It should be noted that although higher voltage sensitivity is inherent to the investigated microwave diodes with higher electrical resistance, for the practical application, it is desirable to use microwave diodes with lower values of electrical resistance (thus lower impedance), as in this case, it is easier to match the impedance of the diode to the wave impedance of the transmission line. For example, the presented waveguide detector mount with investigated diode can be used as a detector of pulse-modulated signals in network analyzer measurement setup that is used for waveguide components characterization. The used finline adapter (Fig. 2.29) is designed to match the 2.5–4.5 kΩ impedance of the diode to 377 Ω. wave impedance (typical in waveguide transmission lines).

4.4. Conclusions of the Fourth Chapter

1. The simulation of the electric field distribution in the active area of an asymmetrically necked bow-tie MW diode acknowledged the peak of the electric field at the narrowest part of the metal-semiconductor junction.
2. The gate placed over the 2DEG channel can handle electron density here depending on the polarity of the MW voltage applied to the microwave diode with a gate as well as on the location of the gate. Therefore, the additional detected voltage should arise over the ends of the diode due to MW currents rectification on the gate.
3. The impact of the gate placed over an asymmetrically shaped 2D electron gas channel depends on the nature of the detected voltage in an ungated bow-tie MW diode based on a selectively doped GaAs/AlGaAs heterostructure and on the location of the gate in respect of the diode's terminals. Experimental results show that the gate does not influence the upper limit of the dynamic range of the bow-tie MW. As the gate is inserted at the wide contact, the voltage sensitivity of the diode increases ten times, and it depends on the frequency in the same manner as in the case of the ungated diode showing a plateau-like constancy up to 0.2 THz.
4. The voltage sensitivity of the bow-tie MW diode based on a selectively doped GaAs/AlGaAs heterostructure with the 2DEG channel can be increased by two orders of magnitude at 30 GHz if the gate is formed at the narrow contact. In this case, the polarity of the detected voltage signal changes into the opposite, and the frequency dependence of the voltage sensitivity changes its manner in a way that it decreases as ω^{-2}. As a result, at higher frequencies, the preference should be given to the wide-gated bow-tie MW diode since its voltage sensitivity is much higher, thus opening the possibility to use these diodes as broadband detectors of electromagnetic radiation operating without external voltage bias at room

temperature up to several hundreds of GHz. The asymmetry of the *IV* characteristics also increases in both cases of the gate design.

5. The impact of light illumination on the HF detection properties of the bow-tie MW diode based on a selectively doped GaAs/AlGaAs heterostructure with 2DEG channel electrical and HF detection properties is due to the change of carrier's density in heterostructures when they are illuminated by light.

General Conclusions

1. The developed measurement setup based on the probing technique allows for achieving certain advances in the characterization of the detection properties of planar microwave diodes as it gives efficient results of investigation of the detected voltage's dependence on power and frequency in the 26.5–40 GHz frequency range and on the influence of temperature and illumination on the physical properties of the wafer-based diodes.
2. Planar dual asymmetric microwave diodes based on heavily doped GaAs substrates can detect a millimeter-wavelength continuous wave and pulsed nanosecond time scale signals. The diodes operate at room temperature with no bias voltage.
3. Electromagnetic radiation sensing properties of the planar dual microwave n-$Al_xGa_{1-x}As$ diodes epitaxially grown on a semi-insulating substrate can be tailored by a proper choice of the AlAs mole fraction x in the active semiconductor layer and by a decrease in the smaller contact area. The voltage sensitivity of the n-GaAs diodes is independent of the contact area, while the sensitivity of the n-$Al_xGa_{1-x}As$ diodes increases with the decrease in a smaller contact area. The voltage sensitivity of the aluminum-containing planar dual microwave diodes ($x = 0.15$ and 0.3) is

two orders of magnitude higher than that of the *n*-GaAs-based diodes ($x = 0$).

4. The impact of the partial gate placed over an asymmetrically shaped two-dimensional electron gas channel depends: *a*) on the polarity (i.e., on its nature) of the voltage detected across the ungated bow-tie microwave diode based on selectively doped GaAs/AlGaAs heterostructure; *b*) on the location of the gate in respect of the diode's terminals. Experimental results show that the gate does not influence the upper limit of the dynamic range of the bow-tie microwave diode. As the gate is inserted at the wide contact, the voltage sensitivity of the diode increases ten times, and it depends on the frequency in the same manner as in the case of the ungated diode showing the plateau up to 0.2 THz.
5. At 30 GHz frequency, the voltage sensitivity of the bow-tie microwave diode based on a selectively doped GaAs/AlGaAs heterostructure with a two-dimensional electron gas channel can be increased by two orders of magnitude if the gate is formed at the narrow contact. In this case, the polarity of the detected voltage signal changes into the opposite, and the voltage sensitivity decreases with frequency as ω^{-2}. As a result, at subterahertz frequencies, the preference should be given to the wide-contact gated bow-tie microwave diode since its voltage sensitivity at these frequencies is much higher, which opens the possibility of using these diodes as broadband detectors of electromagnetic radiation operating without external voltage bias at room temperature.

References

Accardo, J., & Chaudhry, M. A. (2014). Radiation exposure and privacy concerns surrounding full-body scanners in airports. *Journal of Radiation Research and Applied Sciences*, *7*(2), 198–200. https://doi.org/10.1016/J.JRRAS.2014.02.005

Agilent Technologies. (2000). *Fundamentals of RF and Microwave Power Measurements*. Application Note 64-1B. Santa Clara: Agilent Technologies.

Al-Ogaili, F., & Shubair, R. M. (2016). Millimeter-wave mobile communications for 5G: Challenges and opportunities. *IEEE Antennas and Propagation Society International Symposium Proceedings*, 1003–1004. https://doi.org/10.1109/APS.2016.7696210

Anand, Y., & Hillson, J. (1991). Millimeter Wave Planar Doped Barrier Detector Diodes. *Second International Symposium on Space Terahertz Technology*, 340–352.

ANSYS. (2013). *An Introduction to HFSS: Fundamental Principles, Concepts, and Use*. Canonsburg: ANSYS.

Armbrecht, G., Denicke, E., Rolfes, I., Pohl, N., Musch, T., & Schiek, B. (2008). Compact mode-matched excitation structures for radar distance measurements in overmoded circular waveguides. *Advances in Radio Science*, *6*(A.1), 9–17. https://doi.org/10.5194/ARS-6-9-2008

Ashida, K., Inoue, M., Shirafuji, J., & Inuishi, Y. (1974). Energy Relaxation Effect of Hot Electrons in GaAs. *Journal of the Physical Society of Japan*, *37*(2), 408–414. https://doi.org/10.1143/JPSJ.37.408

Ašmontas, S. (1975). Study of electron heating by nonuniform electric fields in n-Si. *Physica Status Solidi A*, *31*(2), 409–414. https://doi.org/10.1002/PSSA.2210310208

Ašmontas, S., Gradauskas, J., Kozič, A., Shtrikmann, H., & Sužiedėlis, A. (2005). Submicrometric Heavily Doped n-GaAs Structures for Microwave Detection. *Acta Physica Polonica A*, *107*(1), 147. https://doi.org/10.12693/APHYSPOLA.107.147

Ašmontas, S., Gradauskas, J., Kundrotas, J., Sužiedėlis, A., Šilėnas, A., & Valušis, G. (1999). Influence of Composition in GaAs/AlGaAs Heterojunctions on Microwave Detection. *Materials Science Forum*, *297–298*, 319–322. https://doi.org/10.4028/WWW.SCIENTIFIC.NET/MSF.297-298.319

Ašmontas, S., Gradauskas, J., Seliuta, D., Sužiedėlis, A., Šilėnas, A., & Valušis, G. (1997). GaAs/AlGaAs heterojunction: a promising detector for infrared radiation. *Gallium Arsenide Applications Symposium*, 345–348. https://doi.org/10.6092/unibo/amsacta/1336

Ašmontas, S., Gradauskas, J., Sužiedėlis, A., Kozič, A., Paškevič, Č., Kazlauskaitė, V., & Širmulis, E. (2007, November). Microwave to terahertz radiation detection by semiconductor nanostructures. *Tenth Annual Directed Energy Symposium*.

Ašmontas, S., Gradauskas, J., Sužiedėlis, A., & Valušis, G. (2000). Submicron semiconductor structure for microwave detection. *Microelectronic Engineering*, *53*(1–4), 553–556. https://doi.org/10.1016/S0167-9317(00)00376-2

Ašmontas, S., Gradauskas, J., Seliuta, D., Sužiedėlis, A., Širmulis, E., & Valušis, G. (1998). Application of Hot-Carrier Thermo-Electromotive Force for Measurement of Pulsed Microwave and Infrared Radiati. *Journal of Thermoelectricity*, *4*, 15–28.

Ašmontas, S., Požela, J., & Repšas, K. (1971). Karštų srovės nešėjų sąlygota bigradientinė evj. *Lietuvos Fizikos Rinkinys*, *9*, 245–251.

Ašmontas, S., Požela, J., & Repšas, K. (1975). Kintamo skerspiūvio germanio ir silicio pavyzdėlių voltamperinių charakteristikų tyrimas. *Lietuvos Fizikos Rinkinys*, *15*(2), 257.

Ašmontas, S., & Sužiedėlis, A. (1993). Electric properties of small area GaAs nn+ junction. *Lietuvos Fizikos Rinkinys*, *33*(1), 45–51.

Ašmontas, S. (1984). *Electrogradient phenomena in semiconductors*. Vilnius: Mokslas.

Ašmontas, S. P., Gradauskas, J., Seliuta, D., & Širmulis, E. (2001). Photoelectrical properties of nonuniform semiconductor under infrared laser radiation. *Nonresonant Laser-Matter Interaction*, *4423*, 18–27. https://doi.org/10.1117/12.431223

Ašmontas, S., Gradauskas, J., Sužiedėlis, A., Širmulis, E., & Urbelis, A. (2006). Hot carrier photocapacitive effect. *Optical Materials and Applications*, *5946*, 353–358. https://doi.org/10.1117/12.639324

Ašmontas, S., Kazlauskaitė, V., Sužiedėlis, A., Gradauskas, J., Širmulis, E., & Derkach, V. (2009). Detectors of microwave and terahertz radiation on the basis of semiconductor nanostructures. *European Microwave Conference*, 1650–1653. https://doi.org/10.23919/EUMC.2009.5296374

Ašmontas, S., Kiprijanovič, O., Levitas, B., Matuzas, J., & Naidionova, I. (2015). Microwave radiation imaging using inverse synthetic aperture radar technique. *Elektronika Ir Elektrotechnika*, *21*(1), 33–36. https://doi.org/10.5755/J01.EEE.21.1.5389

Ašmontas, S., & Sužiedėlis, A. (1994). New microwave detector. *International Journal of Infrared and Millimeter Waves*, *15*(3), 525–538. https://doi.org/10.1007/BF02096235

Ašmontas, S., Sužiedėlis, A., Širmulis, E., Gradauskas, J., Kazlauskaitė, V., Lučun, A., & Anbinderis, T. (2010). New Planar Heterojunction Diode for Microwave and Infrared Applications. *AIP Conference Proceedings*, *213*, 10–12. https://doi.org/10.1063/1.3295374

Baca, A. G., & Ashby, C. I. H. (2005). *Fabrication of GaAs devices*. Institution of Engineering and Technology. https://doi.org/10.1049/PBEP006E

Bahl, I. J., & Bhartia, P. (2003). *Microwave Solid State Circuit Design* (2nd ed.). Hoboken: Wiley-Interscience.

Baudry, D., Louis, A., & Mazari, B. (2006). Characterization of the Open-Ended Coaxial Probe Used for Near-Field Measurements in EMC Applications. *Progress In Electromagnetics Research*, *60*, 311–333. https://doi.org/10.2528/PIER05112501

Belen, M. A., Mahouti, P., Güneş, F., & Partal, H. (2018). Design and Implementation of Doppler Microwave Motion Sensor for Indoor Application. *Sigma Journal of Engineering and Natural Sciences*, *36*(3), 849–859.

Best, J. S. (1979). The Schottky-barrier height of Au on n-Ga1−xAlxAs as a function of AlAs content. *Applied Physics Letters*, *34*(8), 522. https://doi.org/10.1063/1.90850

Boonton. (2011). *Principles of Power Measurement A Primer on RF & Microwave Power Measurement*. Parsipanny: Boonton.

Boppel, S., Lisauskas, A., Mundt, M., Seliuta, D., Minkevičius, L., Kašalynas, I., Valušis, G., Mittendorff, M., Winnerl, S., Krozer, V., & Roskos, H. G. (2012). CMOS integrated antenna-coupled field-effect transistors for the detection of radiation from 0.2 to 4.3 THz. *IEEE Transactions on Microwave Theory and Techniques*, *60*(12), 3834–3843. https://doi.org/10.1109/TMTT.2012.2221732

Breed, G. (2011). The Basics of Probe Measurements on Wafers and Other Substrates. *High Frequency Electronics*, *10*(5) 78–80. Retrieved November 29, 2022, from https://www.highfrequencyelectronics.com/May11/HFE0511_tutorial.pdf

Brooker, G. (2005). Millimetre Wave Radar for Tracking and Imaging applications. *1st International Conference on Sensing Technology*, 158–163.

Brooker, G., Bishop, M., & Scheding, S. (2001). Millimetre Waves for Robotics. *Australasian Conference on Robotics and Automation*, 91–97.

Burrus, C. A. (1963). Backward Diodes for Low-Level Millimeter-Wave Detection. *IEEE Transactions on Microwave Theory and Techniques*, *11*(5), 357–362. https://doi.org/10.1109/TMTT.1963.1125675

But, D. B., Consejo, C., Coquillat, D., Teppe, F., Knap, W., Varani, L., Torres, J., Auton, G., Zhang, J., Hill, E., & Song, A. (2018). Millimeter and submillimeter range detector based on graphene ballistic rectifiers. *22nd International Microwave and Radar Conference*, 585–588. https://doi.org/10.23919/MIKON.2018.8405293

Cascade Microtech. (n.d.). *Z PROBE High-Frequency Wafer Probe*. Retrieved December 8, 2021, from https://www.formfactor.com/product/probes/z-probe/z-probe-coaxial/

Cascade Microtech. (2017). *Calibration Tools Consistent Parameter Extraction for Advanced RF Devices*. Beaverton: Cascade Microtech.

Cascade Microtech. (n.d.). *High Speed Microprobing Principles and Applications*. Beaverton: Cascade Microtech.

Cenanovic, A., Köppel, T., Ringel, J., & Schmidt, L. P. (2013). Broadband orthomode transducer for the WR12-band. *International Conference on Infrared, Millimeter, and Terahertz Waves, IRMMW-THz*. https://doi.org/10.1109/IRMMW-THZ.2013.6665685

Chaar, L. R., & van Rheenen, A. D. (1994). Low-frequency noise measurements on semiconductor devices using a probe station. *IEEE Transactions on Instrumentation and Measurement* , *43*(4), 658–660. https://doi.org/10.1109/19.310184

Chahal, P., Morris, F., & Frazier, G. (2005). Zero bias resonant tunnel Schottky contact diode for wide-band direct detection. *IEEE Electron Device Letters*, *26*(12), 894–896. https://doi.org/10.1109/LED.2005.859622

Chan, K. T., Lightner, M. J., Patterson, G. A., & Yu, K. M. (1990). Growth studies of pseudomorphic GaAs/InGaAs/AlGaAs modulation-doped field-effect transistor structures. *Applied Physics Letters*, *56*(20), 2022. https://doi.org/10.1063/1.103005

Čibiraitė-Lukenskienė, D., Ikamas, K., Lisauskas, T., Krozer, V., Roskos, H. G., & Lisauskas, A. (2020). Passive Detection and Imaging of Human Body Radiation Using an Uncooled Field-Effect Transistor-Based THz Detector. *MDPI Sensors*, *20*(15), 4087. https://doi.org/10.3390/S20154087

Collier, R., & Skinner, D. (2007). *Microwave Measurements (Materials, Circuits and Devices)* (3rd ed.). IET Digital Library. https://doi.org/10.1049/PBEL012E

Collins, M. J., Ross Warren, F. G., & Paul, J. L. (1996). Airborne imaging microwave radiometer – Part I: radiometric analysis. *IEEE Transactions on Geoscience and Remote Sensing*, *34*(3), 643–655. https://doi.org/10.1109/36.499744

Cortes-Medellin, G., Vishwas, A., Parshley, S. C., Campbell, D. B., Perilatt, P., Black, R., Brady, J., Warnick, K. F., & Jeffs, B. D. (2015). A fully cryogenic phased array camera for radio astronomy. *IEEE Transactions on Antennas and Propagation*, *63*(6), 2471–2481. https://doi.org/10.1109/TAP.2015.2415527

Couch, N. R., & Kearney, M. J. (1998). Hot-electron properties of GaAs planar-doped barrier diodes. *Journal of Applied Physics*, *66*(10), 5083. https://doi.org/10.1063/1.343734

Dale, I., Neylon, S., Condie, A., Hobden, M., & Kearney, M. J. (1990). 1/F noise performance of GaAs planar doped barrier mixer diodes. *Conference Proceedings –*

European Microwave Conference, *1*(20), 605–610. https://doi.org/10.1109/euma.1990.336109

Dale, I., Neylon, S., Condie, A., & Kearney, M. J. (1989a). Planar doped barrier diodes offering improved microwave burnout performance over Si and GaAs Schottky diodes. *European Microwave Conference*, *19*, 237–243. https://doi.org/10.1109/EUMA.1989.333972

Dale, I., Neylon, S., Condie, A., & Kearney, M. J. (1989b, February). The application of coplanar GaAs planar doped barrier diode technology for use in microwave and millimetre wave mixers and detectors. *Microwave and Optronics Conference, 4th Exhibition and Conference for Ultra High Frequency Technology*.

Dalmay, C., Cheray, M., Pothier, A., Lalloué, F., Jauberteau, M. O., & Blondy, P. (2010). Ultra sensitive biosensor based on impedance spectroscopy at microwave frequencies for cell scale analysis. *Sensors and Actuators A: Physical*, *162*(2), 189–197. https://doi.org/10.1016/J.SNA.2010.04.023

Dargys, A., & Kundrotas, J. (1994). *Handbook on physical properties of Ge, Si, GaAs and InP*. Science and Encyclopedia Publishers.

Dienys, V., Dedulevič, S., Kancleris, Ž., Martūnas, Z., & Šetkus, A. (1989). Warm electron conductivity of GaAs in dc and ac electric fields. *Lietuvos Fizikos Rinkinys*, *29*(1), 46–52.

Du, J., Hellicar, A. D., Li, L., Hanham, S. M., Nikolic, N., MacFarlane, J. C., & Leslie, K. E. (2008). Terahertz imaging using a high-Tc superconducting Josephson junction detector. *Superconductor Science and Technology*, *21*(12), 125025. https://doi.org/10.1088/0953-2048/21/12/125025

Dyakonov, M., & Shur, M. (1996). Detection, mixing, and frequency multiplication of terahertz radiation by two-dimensional electronic fluid. *IEEE Transactions on Electron Devices*, *43*(3), 380–387. https://doi.org/10.1109/16.485650

Elbamby, M. S., Perfecto, C., Bennis, M., & Doppler, K. (2018). Edge computing meets millimeter-wave enabled VR: Paving the way to cutting the cord. *ArXiv*. https://doi.org/10.1109/WCNC.2018.8377419

European Radiocommunications Committee (ERC) within the European Conference of Postal and Telecommunications Administrations (CEPT). (1994). *The Use of Radio Frequencies Above 20 GHz by Fixed Services and ENG/OB*.

Fakharzadeh, M. (2014). Antenna measurement in probe station. *IEEE Antennas and Propagation Society, AP-S International Symposium (Digest)*, 293–294. https://doi.org/10.1109/APS.2014.6904478

Fisher, G. (n.d.). *A guide to Successful on Wafer Rf characterisation*. Oxford: Cascade Microtech Europe.

FormFactor. (n.d.). *Unparalleled Probing Solutions*. Retrieved December 8, 2021, from https://www.formfactor.com/products/probes/

FormFactor. (2017, June 27). *Infinity Probe Mechanical Layout Rules*. https://www.formfactor.com/download/infinity-probe-mechanical-layout-rules/

FormFactor. (n.d.). *Cascade Autonomous RF Measurement Assistant*. Retrieved December 8, 2021, from https://www.formfactor.com/product/probe-systems/autonomous-assistants/autonomous-rf/

Fregonese, S., De Matos, M., Deng, M., Potéreau, M., Ayela, C., Aufinger, K., & Zimmer, T. (2018). On-Wafer Characterization of Silicon Transistors Up To 500 GHz and Analysis of Measurement Discontinuities Between the Frequency Bands. *IEEE Transactions on Microwave Theory and Techniques*, *66*(7), 3332–3341. https://doi.org/10.1109/TMTT.2018.2832067ï

Gennarelli, G., Romeo, S., Scarfi, M. R., & Soldovieri, F. (2013). A microwave resonant sensor for concentration measurements of liquid solutions. *IEEE Sensors Journal*, *13*(5), 1857–1864. https://doi.org/10.1109/JSEN.2013.2244035

Godshalk, E. M., Burr, J., & Williams, J. (1994). An Air Coplanar Wafer Probe. *ARFTG Conference*, *2*, 1380–1385. https://doi.org/10.1109/EUMA.1994.337408

Goldsmith, P. F., Hsieh, C. T., Huguenin, G. R., Kapitzky, J., & Moore, E. L. (1993). Focal Plane Imaging Systems for Millimeter Wavelengths. *IEEE Transactions on Microwave Theory and Techniques*, *41*(10), 1664–1675. https://doi.org/10.1109/22.247910

Gradauskas, J., Sužiedėlis, A., Ašmontas, S., Širmulis, E., Kazlauskaitė, V., Lučun, A., & Vingelis, M. (2010). Sensitive planar semiconductor detector from microwave to IR applications. *IEEE Sensors Journal*, *10*(3), 662–667. https://doi.org/10.1109/JSEN.2009.2038654

Guerboukha, H., Nallappan, K., & Skorobogatiy, M. (2018). Toward real-time terahertz imaging. *Advances in Optics and Photonics*, *10*(4), 843–938. https://doi.org/10.1364/AOP.10.000843

Haddadi, K., El Fellahi, A., Marzouk, J., Arscott, S., Boyaval, C., Lasri, T., & Dambrine, G. (2015, July 24). Robotic on-wafer probe station for microwave characterization in a scanning electron microscope. *IEEE MTT-S International Microwave Symposium*. https://doi.org/10.1109/MWSYM.2015.7166970

Häfner, S., Dürr, A., Waldschmidt, C., & Thomä, R. (2020). Mitigation of RF Impairments of a 160-GHz MMIC FMCW Radar Using Model-Based Estimation. *IEEE Transactions on Microwave Theory and Techniques*, *68*(3), 1065–1073. https://doi.org/10.1109/TMTT.2019.2950204

Harrison, R. I., & Zucker, J. (1963). Microwave Detection and Mixing Using the Thermoelectric Effect of Hot Carriers in Semiconductors. *Applied Physics Letters*, *3*(9), 153. https://doi.org/10.1063/1.1753909

Harrison, R. I., & Zucker, J. (1966). Hot-Carrier Microwave Detector. *Proceedings of the IEEE*, *54*(4), 588–595. https://doi.org/10.1109/PROC.1966.4778

HBM Prenscia. (n.d.). *Characteristics of the Weibull Distribution*. Retrieved December 4, 2021, from https://www.weibull.com/hotwire/issue14/relbasics14.htm

Heiblum, M., Nathan, M. I., & Chang, C. A. (1982). Characteristics of AuGeNi ohmic contacts to GaAs. *Solid-State Electronics*, *25*(3), 185–195. https://doi.org/10.1016/0038-1101(82)90106-X

Hesler, J., & Crowe, T. (2008). Responsivity and Noise Measurements of Zero-Bias Schottky Diode Detectors. *18th International Symposium on Space Terahertz Technology*, 89–92.

Hesler, J., & Crowe, T. (2007). NEP and responsivity of THz zero-bias Schottky diode detectors. *Conference Digest of the Joint 32nd International Conference on Infrared and Millimetre Waves, and 15th International Conference on Terahertz Electronics*, 844–845. https://doi.org/10.1109/ICIMW.2007.4516758

Hill, G., & Robson, P. N. (1982). Electron drift velocity in GaAs using a variable frequency microwave time-of-flight technique. *Solid-State Electronics*, *25*(7), 589–597. https://doi.org/10.1016/0038-1101(82)90061-2

Hiyamizu, S., Saito, J., Nanbu, K., & Ishikawa, T. (1983). Improved Electron Mobility Higher than 106 cm2/Vs in Selectively Doped GaAs/N-AlGaAs Heterostructures Grown by MBE. *Japanese Journal of Applied Physics, Part 2: Letters*, *22*(10), 609–611. https://doi.org/10.1143/JJAP.22.L609/XML

Hoefle, M., Haehnsen, K., Oprea, I., Cojocari, O., Penirschke, A., Jakoby, R., Hoefle, M., Haehnsen, K., Oprea, I., Cojocari, O., Penirschke, A., & Jakoby, R. (2014). Compact and Sensitive Millimetre Wave Detectors Based on Low Barrier Schottky Diodes on Impedance Matched Planar Antennas. *Journal of Infrared, Millimeter, and Terahertz Waves*, *35*(11), 891–908. https://doi.org/10.1007/S10762-014-0090-Z

HP. (1977). *Fundamentals of RF and Microwave Power Measurements*. Palo Alto: Hewlett Packard.

HP. (1994). *The Zero Bias Schottky Detector*. Palo Alto: Hewlett Packard.

Hu, Z., Van Tuyen, V., & Rezazadeh, A. A. (2005). High tangential signal sensitivity GaAs planar doped barrier diodes for microwave/millimeter-wave power detector applications. *IEEE Microwave and Wireless Components Letters*, *15*(3), 150–152. https://doi.org/10.1109/LMWC.2005.844204

Huo, Y., Dong, X., & Xu, W. (2017). 5G cellular user equipment: From theory to practical hardware design. *IEEE Access*, *5*, 13992–14010. https://doi.org/10.1109/ACCESS.2017.2727550

Iovescu, C., & Rao, S. (2020). *Texas Instruments. The fundamentals of millimeter wave radar sensors*. https://www.ti.com/lit/wp/spyy005a/spyy005a.pdf?ts=1638892332620&ref_url=https%253A%252F%252Fwww.google.com%252F

Ito, H., & Ishibashi, T. (2017). InP/InGaAs Fermi-level managed barrier diode for broadband and low-noise terahertz-wave detection. *Japanese Journal of Applied Physics*, *56*(1), 014101. https://doi.org/10.7567/JJAP.56.014101/XML

Jepsen, P. U., Cooke, D. G., & Koch, M. (2011). Terahertz spectroscopy and imaging – Modern techniques and applications. *Laser & Photonics Reviews*, *5*(1), 124–166. https://doi.org/10.1002/LPOR.201000011

Jin, N., Yu, R., Chung, S. Y., Berger, P. R., Thompson, P. E., & Fay, P. (2005). High sensitivity Si-based backward diodes for zero-biased square-law detection and the effect of post-growth annealing on performance. *IEEE Electron Device Letters*, *26*(8), 575–578. https://doi.org/10.1109/LED.2005.852738

Jokubauskis, D., Minkevičius, L., Seliuta, D., Kašalynas, I., & Valušis, G. (2019). Terahertz homodyne spectroscopic imaging of concealed low-absorbing objects. *Optical Engennering*, *58*(2). https://doi.org/10.1117/1.OE.58.2.023104

Juozapavičius, A., Ardaravičius, L., Sužiedėlis, A., Kozič, A., Gradauskas, J., Kundrotas, J., Seliuta, D., Širmulis, E., Ašmontas, S., Valušis, G., Roskos, H. G., & Köhler, K. (2004). Microwave sensor based on modulation-doped GaAs/AlGaAs structure. *Semiconductor Science and Technology*, *19*(4), S436. https://doi.org/10.1088/0268-1242/19/4/143

Kancleris, Ž., Laurinavičius, A., & Anbinderis, T. (2004). Sensitivity of Homogeneity Mapping of Dielectric Wafer Using Millimeter Waves. *International Journal of Infrared and Millimeter Waves*, *25*(7), 1099–1108. https://doi.org/10.1023/B:IJIM.0000037658.48407.23

Kancleris, Ž., Šlekas, G., & Čiegis, R. (2013). Sensitivity of Asymmetrically Necked Planar Millimeter-Wave Detectors. *IEEE Sensors Journal, 13*(4), 1143–1147. https://doi.org/10.1109/JSEN.2012.2228187

Kärcher, D. (2016). Transport in two-dimensional electron systems in ZnO under the influence of microwave radiation [University of Stuttgart]. In *OPUS – Publication Server of the University of Stuttgart*. https://doi.org/10.18419/OPUS-6896

Kašalynas, I., Venckevičius, R., Seliuta, D., Grigelionis, I., & Valušis, G. (2011). InGaAs-based bow-tie diode for spectroscopic terahertz imaging. *Journal of Applied Physics*, *110*(11), 114505. https://doi.org/10.1063/1.3658017

Kašalynas, I., Venckevičius, R., Minkevičius, L., Sešek, A., Wahaia, F., Tamošiūnas, V., Voisiat, B., Seliuta, D., Valušis, G., Švigelj, A., & Trontelj, J. (2016). Spectroscopic Terahertz Imaging at Room Temperature Employing Microbolometer Terahertz Sensors and Its Application to the Study of Carcinoma Tissues. *MDPI Sensors*, *16*(4), 432. https://doi.org/10.3390/S16040432

Kašalynas, I., Venckevičius, R., & Valušis, G. (2013). Continuous Wave Spectroscopic Terahertz Imaging With InGaAs Bow-Tie Diodes at Room Temperature. *IEEE Sensors Journal*, *13*(1), 50–54. https://doi.org/10.1109/JSEN.2012.2223459

Kawaguchi, Y., Hirakawa, K., & Komiyama, S. (2002). High-sensitivity quantum Hall far-infrared photodetector integrated with log-periodic antenna. *Applied Physics Letters*, *80*(18), 3418. https://doi.org/10.1063/1.1476061

Kearney, M. J. (1992). Planar doped barrier diodes for high frequency mixer and detector applications. *17th Conference of the Automated RF and Microwave Measurement Society*, *1*, 19–23.

Kearney, M. J., Condie, A., & Dale, I. (1991). GaAs planar doped barrier diodes for milli metre-wave detector applications. *Electronics Letters*, *27*(9), 721–722. https://doi.org/10.1049/EL:19910448

Kearney, M. J., & Dale, I. (1990). GaAs planar doped barrier diodes for mixer and detector applications. *GEC Journal of Research*, *8*(1), 1–12.

Kearney, M. J., Kelly, M. J., Davies, R. A., Kerr, T. M., Rees, P. K., Condie, A., & Dale, I. (1989a). Asymmetric Planar Doped Barrier Diodes for Mixer and Detector Applications. *Electronics Letters*, *25*(21), 1454–1456. https://doi.org/10.1049/EL:19890971

Kearney, M. J., Kerr, T. M., Kelly, M. J., Condie, A., & Dale, I. (1989b). Testing models of I/V characteristics of planar-doped barrier diodes. *Electronics Letters*, *25*(17), 1145–1147. https://doi.org/10.1049/EL:19890769

Kelly M. J. (1996). *Low-dimensional Semiconductors: Materials, Physics, Technology, Devices* (1st ed.). Clarendon Press.

Kikuchi, K., & Oshimoto, A. (1981). Broad-Band High-Speed Microwave Power Sensor Using Hot Carriers in Semiconductor. *IEEE Transactions on Instrumentation and Measurement*, *IM–30*(4), 238–242. https://doi.org/10.1109/TIM.1981.6312398

Knap, W., But, D., Diakonova, N., Coquillat, D., Vitiello, M. S., Blin, S., Fatimy, A. El, Teppe, F., Tredicucci, A., Nagatsuma, T., & Ganichev, S. (2013). Nanotransistor based THz plasma detectors: low tempeatures, graphene, linearity, and circular polarization studies. *Terahertz Emitters, Receivers, and Applications IV*, *8846*, 102–114. https://doi.org/10.1117/12.2024206

Knap, W., Deng, Y., Rumyantsev, S., & Shur, M. S. (2002a). Resonant detection of subterahertz and terahertz radiation by plasma waves in submicron field-effect transistors. *Applied Physics Letters*, *81*(24), 4637. https://doi.org/10.1063/1.1525851

Knap, W., Kachorovskii, V., Deng, Y., Rumyantsev, S., Lü, J. Q., Gaska, R., Shur, M. S., Simin, G., Hu, X., Khan, M. A., Saylor, C. A., & Brunel, L. C. (2002b). Nonresonant detection of terahertz radiation in field effect transistors. *Journal of Applied Physics*, *91*(11), 9346. https://doi.org/10.1063/1.1468257

Knap, W., Teppe, F., Meziani, Y., Dyakonova, N., Lusakowski, J., Boeuf, F., Skotnicki, T., Maude, D., Rumyantsev, S., & Shur, M. S. (2004). Plasma wave detection of sub-terahertz and terahertz radiation by silicon field-effect transistors. *Applied Physics Letters*, *85*(4), 675. https://doi.org/10.1063/1.1775034

Knappmiller, S., Robertson, S., & Sternovsky, Z. (2006). Comparison of two microwave and two probe methods for measuring plasma density. *IEEE Transactions on Plasma Science*, *34*(3 PART 2), 786–791. https://doi.org/10.1109/TPS.2006.874849

Kozič, A., Paškevič, Č., Sužiedėlis, A., Gradauskas, J., Ašmontas, S., Szerling, A., Wrzesińska, H., Kozič, A., Paškevič, Č., Sužiedėlis, A., Gradauskas, J., Ašmontas, S., Szerling, A., & Wrzesińska, H. (2006). Asymmetrically Shaped Pseudomorphic Modulation Doped Structure for Microwave Detection. *Acta Physica Polonica A*, *110*(6), 845. https://doi.org/10.12693/APHYSPOLA.110.845

Kozič, A., Suziedėlis, A., Petkun, V., Čerškus, A., Shtrikmann, H., Gradauskas, J., Kundrotas, J., & Ašmontas, S. (2005). Properties of constricted 2DEG/metal structures in microwave electric fields. *Optica Applicata*, *35*(3), 465–470.

Lang, D. V., Logan, R. A., & Jaros, M. (1979). Trapping characteristics and a donor-complex (<span class. *Physical Review B*, *19*(2), 1015. https://doi.org/10.1103/PhysRevB.19.1015

Lechner A., Kneidinger M., Thim H. W., & Kuch R. (1979). Microwave detection with n-GaAsN-GaAlAs heterojunctions. *Electronic Letters*, *15*(9), 254–255. https://doi.org/0013-5194/79/090254-02$1.50/0

Lechner, A., Kneidinger, M., Kuch, R., Lechner, A., Kneidinger, M., & Kuch, R. (1980). Planar n-GaAs/N-GaAlAs microwave diodes. *Electronics Letters*, *16*(1), 1–2. https://doi.org/10.1049/EL:19800001

Lee, D.-J., Kwon, J.-Y., Kang, N.-W., Yang, K., David, G., Robertson, S., Whitaker, J. F., B Katehi, L. P., Lee, D. J., Kang, N. W., Choi, J. H., & Kim, J. Y. (2014). Field analysis of electro-optic probes for minimally invasive microwave sampling. *Optics Express*, *22*(3), 2897–2909. https://doi.org/10.1364/OE.22.002897

Lee, M., Pfeiffer, L. N., & West, K. W. (2002). Ballistic cooling in a wideband two-dimensional electron gas bolometric mixer. *Applied Physics Letters*, *81*(7), 1243. https://doi.org/10.1063/1.1500429

Lindsay, R. (2016). *Anritsu. How to Select a Power Sensor*. Atsugi: Anritsu.

Lisauskas, A., Pfeiffer, U., Öjefors, E., Bolvar, P. H., Glaab, D., & Roskos, H. G. (2009). Rational design of high-responsivity detectors of terahertz radiation based on distributed self-mixing in silicon field-effect transistors. *Journal of Applied Physics*, *105*(11), 114511. https://doi.org/10.1063/1.3140611

Liu, L., Xu, H., Duan, Y., Lichtenberger, A., Hesler, J., & Weikle, R. (2009). A 200 GHz Schottky Diode Quasi-Optical Detector Based on Folded Dipole Antenna. *20th International Symposium on Space Terahertz Technology*, 145–149.

Ma, J., Shrestha, R., Moeller, L., & Mittleman, D. M. (2018). Invited Article: Channel performance for indoor and outdoor terahertz wireless links. *APL Photonics*, *3*(5), 051601. https://doi.org/10.1063/1.5014037

Malik, R. J., Aucoin, T. R., Ross, R. L., Board, K., Wood, C. E. C., & Eastman, L. F. (1980). Planar-doped barriers in GaAs by molecular beam epitaxy. *Electronics Letters*, *16*(22), 836–838. https://doi.org/10.1049/EL:19800594

Marzouk, J., Arscott, S., El Fellahi, A., Haddadi, K., Lasri, T., Boyaval, C., & Dambrine, G. (2015). MEMS probes for on-wafer RF microwave characterization of future microelectronics: design, fabrication and characterization. *Journal of Micromechanics and Microengineering*, *25*(7), 075024. https://doi.org/10.1088/0960-1317/25/7/075024

Meng, Y., Qing, A., Lin, C., Zang, J., Zhao, Y., & Zhang, C. (2018). Passive Millimeter Wave Imaging System Based on Helical Scanning. *Nature: Scientific Reports*, *8*(1), 1–12. https://doi.org/10.1038/s41598-018-25637-9

Minkevičius, L., Tamošiunas, V., Kašalynas, I., Seliuta, D., Valušis, G., Lisauskas, A., Boppel, S., Roskos, H. G., & Köhler, K. (2011). Terahertz heterodyne imaging with InGaAs-based bow-tie diodes. *Applied Physics Letters*, *99*(13), 131101. https://doi.org/10.1063/1.3641907

Misiewicz, J. (1996). Photoreflectance spectroscopy for semiconductor structure investigations. *Metal/Nonmetal Microsystems: Physics, Technology, and Application*, *2780*, 141–148. https://doi.org/10.1117/12.238143

Mitani, T., Nakajima, R., Shinohara, N., Nozaki, Y., Chikata, T., & Watanabe, T. (2019). Development of a Microwave Irradiation Probe for a Cylindrical Applicator. *MDPI Processes*, *7*(3), 143. https://doi.org/10.3390/PR7030143

Mittleman, D. M. (2017). Perspective: Terahertz science and technology. *Journal of Applied Physics*, *122*(23), 230901. https://doi.org/10.1063/1.5007683

Mooney, P. M. (1998). Deep donor levels (DX centers) in III-V semiconductors. *Journal of Applied Physics*, *67*(3), R1. https://doi.org/10.1063/1.345628

Nadar, S., Zaknoune, M., Wallart, X., Coinon, C., Peytavit, E., Ducournau, G., Gamand, F., Thirault, M., Werquin, M., Jonniau, S., Thouvenin, N., Gaquiere, C., Vellas, N., & Lampin, J. F. (2017). High performance heterostructure low barrier diodes for sub-THz detection. *IEEE Transactions on Terahertz Science and Technology*, *7*(6), 780–788. https://doi.org/10.1109/TTHZ.2017.2755503

Nagatsuma, T., Ducournau, G., & Renaud, C. C. (2016). Advances in terahertz communications accelerated by photonics. *Nature Photonics*, *10*(6), 371–379. https://doi.org/10.1038/nphoton.2016.65

NASA. (1986). *60 GHz intersatellite communication link definition study, Baseline document*. Palo Alto: Ford Aerospace & Communications Corporation.

Novac, B. M., Senior, P., Farage, M., Smith, I. R., & Xiao, R. (2018). Unconventional Microwave Source. *IEEE Transactions on Microwave Theory and Techniques*, *66*(7), 3245–3252. https://doi.org/10.1109/TMTT.2018.2831685

Oka, S., Togo, H., Kukutsu, N., & Nagatsuma, T. (2008). Latest Trends in Millimeter-Wave Imaging Technology. *Progress In Electromagnetics Research Letters*, *1*, 197–204. https://doi.org/10.2528/PIERL07120604

Oshimoto, A., & Kikuchi, K. (1973). Microwave Power Meter using Hot Electron. *3rd European Microwave Conference*. https://doi.org/10.1109/EUMA.1973.331792

Palenskis, V., Minkevičius, L., Matukas, J., Jokubauskis, D., Pralgauskaitė, S., Seliuta, D., Čechavičius, B., Butkutė, R., & Valušis, G. (2018). InGaAs Diodes for Terahertz Sensing-Effect of Molecular Beam Epitaxy Growth Conditions. *MDPI Sensors*, *18*(11), 3760. https://doi.org/10.3390/S18113760

Park, S. Y., Yu, R., Chung, S. Y., Berger, P. R., Thompson, P. E., & Fay, P. (2007). Sensitivity of Si-based zero-bias backward diodes for microwave detection. *Electronics Letters*, *43*(5), 295–296. https://doi.org/10.1049/EL:20070299

Pastorino, M. (2015). Electromagnetic imaging: Methods and applications. *Mediterranean Microwave Symposium*, *2015-January*. https://doi.org/10.1109/MMS.2015.7375427

Patrashin, M., Sekine, N., Kasamatsu, A., Watanabe, I., Hosako, I., Takahashi, T., Sato, M., Nakasha, Y., & Hara, N. (2015a, November 11). Optimization of GaAsSb/InAlAs/InGaAs tunnel diodes for millimeter-wave detection. *40th International Conference on Infrared, Millimeter, and Terahertz Waves*. https://doi.org/10.1109/IRMMW-THZ.2015.7327614

Patrashin, M., Sekine, N., Kasamatsu, A., Watanabe, I., Hosako, I., Takahashi, T., Sato, M., Nakasha, Y., & Hara, N. (2015b). GaAsSb/InAlAs/InGaAs tunnel diodes for millimeter wave detection in 220–330-GHz band. *IEEE Transactions on Electron Devices*, *62*(3), 1068–1071. https://doi.org/10.1109/TED.2015.2393358

Pavasaris, Č. (2009). *Puslaidininkiniai Įtaisai*. Vilnius: Vilniaus Universitetas.

Peichl, M., Dill, S., Greiner, M., & Reutlingen, H. (2007). Microwave Radiometry – Imaging Technologies and Applications. *Proceedings of Wave Propagation in Communication, Microwave Systems and Navigation*, 75–83.

Peralta, X. G., Allen, S. J., Wanke, M. C., Harff, N. E., Simmons, J. A., Lilly, M. P., Reno, J. L., Burke, P. J., & Eisenstein, J. P. (2002). Terahertz photoconductivity and plasmon modes in double-quantum-well field-effect transistors. *Applied Physics Letters*, *81*(9), 1627. https://doi.org/10.1063/1.1497433

Phung, G. N., Schmuckle, F. J., Doerner, R., Kahne, B., Fritzsch, T., Arz, U., & Heinrich, W. (2019). Influence of microwave probes on calibrated on-wafer measurements. *IEEE Transactions on Microwave Theory and Techniques*, *67*(5), 1892–1900. https://doi.org/10.1109/TMTT.2019.2903400

Polivka, J. (2007). An Overview of Microwave Sensor Technology. *High Frequency Electronics*, 32–42.

Popov, V. V. (2013). Terahertz rectification by periodic two-dimensional electron plasma. *Applied Physics Letters*, *102*(25), 253504. https://doi.org/10.1063/1.4811706

Požela, J., & Repšas, K. (1968). Thermoelectric Force of hot Carriers. *Physica Status Solidi B*, *27*(2), 757–762. https://doi.org/10.1002/PSSB.19680270233

Ramzi, M. R., Abou-Khousa, M., & Prayudi, I. (2017). Near-Field Microwave Imaging Using Open-Ended Circular Waveguide Probes. *IEEE Sensors Journal*, *17*(8), 2359–2366. https://doi.org/10.1109/JSEN.2017.2669301

Rappaport, T. S., Sun, S., Mayzus, R., Zhao, H., Azar, Y., Wang, K., Wong, G. N., Schulz, J. K., Samimi, M., & Gutierrez, F. (2013). Millimeter wave mobile communications for 5G cellular: It will work! *IEEE Access*, *1*, 335–349. https://doi.org/10.1109/ACCESS.2013.2260813

Rhoderick, E. H., & Williams, R. H. (1988). *Metal-semiconductor contacts* (2nd ed.). Clarendon Press Oxford University Press.

Rogalski, A., & Sizov, F. (2011). Terahertz detectors and focal plane arrays. *Opto-Electronics Review*, *19*(3), 346–404. https://doi.org/10.2478/S11772-011-0033-3

Roy, R., Kush, A. K., & Dixit, R. P. (2011). Design and development of thermistor based power meter at 140 GHz frequency band. *Journal of Infrared, Millimeter, and Terahertz Waves*, *32*(12), 1407–1414. https://doi.org/10.1007/S10762-011-9837-Y/FIGURES/12

Ryzhii, V., Khmyrova, I., & Shur, M. (2000). Resonant detection and frequency multiplication of terahertz radiation utilizing plasma waves in resonant-tunneling transistors. *Journal of Applied Physics*, *88*(5), 2868. https://doi.org/10.1063/1.1287759

Sangaré, P., Ducournau, G., Grimbert, B., Brandli, V., Faucher, M., Gaquière, C., De-La-Torre, A. Í., De-La-Torre, I. Í., Millithaler, J. F., Mateos, J., & González, T. (2013). Experimental demonstration of direct terahertz detection at room-temperature in AlGaN/GaN asymmetric nanochannels. *Journal of Applied Physics*, *113*(3), 034305. https://doi.org/10.1063/1.4775406

Sankaran, S., & Kenneth, K. O. (2005). Schottky barrier diodes for millimeter wave detection in a foundry CMOS process. *IEEE Electron Device Letters*, *26*(7), 492–494. https://doi.org/10.1109/LED.2005.851127

Sato, M., & Mizuno, K. (2010). Millimeter-Wave Imaging Sensor. In Minin Igor (Ed.), *Microwave and Millimeter Wave Technologies from Photonic Bandgap Devices to Antenna and Applications* (pp. 331–350). IntechOpen. https://doi.org/10.5772/9059

Savin, A. A., Guba, V. G., & Bykova, O. N. (2016). Measurement of the Parameters of On-Wafer Semiconductor Devices. *Measurement Techniques*, *59*(7), 56–61. https://doi.org/10.1007/s11018-016-1044-8

Schubert, E. F., Pfeiffer, L., West, K. W., & Izabelle, A. (1989). Dopant distribution for maximum carrier mobility in selectively doped Al0.30Ga0.70As/GaAs heterostructures. *Applied Physics Letters*, *54*(14), 1350. https://doi.org/10.1063/1.100712

Schulman, J. N., & Chow, D. H. (2000). Sb-heterostructure interband backward diodes. *IEEE Electron Device Letters*, *21*(7), 353–355. https://doi.org/10.1109/55.847378

Schulman, J. N., Croke, E. T., Chow, D. H., Dunlap, H. L., Holabird, K. S., Morgan, M. A., & Weinreb, S. (2001). Quantum tunneling Sb-heterostructure millimeter-wave diodes.

Technical Digest-International Electron Devices Meeting, 765–767. https://doi.org/10.1109/IEDM.2001.979627

Schulman, J. N., Thomas, S., Chow, D. H., Croke, E. T., Dunlap, H. L., Holabird, K. S., Clark, W. M., Morgan, M. A., & Weinreb, S. (2002). High frequency performance of Sb-heterostructure millimeter-wave diodes. *Conference Proceedings-International Conference on Indium Phosphide and Related Materials*, 151–154. https://doi.org/10.1109/ICIPRM.2002.1014164

Seliuta, D., Juozapavičius, A., Gružinskis, V., Balakauskas, S., Ašmontas, S., Valušis, G., Chow, W.-H., Steenson, P., Harrison, P., Lisauskas, A., Roskos, H. G., & Koehler, K. (2007a). Electric field gradient induced effects in GaAs/AlGaAs modulation-doped structures and high frequency sensing. *ArXiv*.

Seliuta, D., Kašalynas, I., Tamošiunas, V., Balakauskas, S., Martunas, Z., Ašmontas, S., Valušis, G., Lisauskas, A., Roskos, H. G., & Köhler, K. (2006). Silicon lens-coupled bow-tie InGaAs-based broadband terahertz sensor operating at room temperature. *Electronics Letters*, *42*(14), 825–827. https://doi.org/10.1049/EL:20061224

Seliuta, D., Širmulis, E., Tamošiunas, V., Balakauskas, S., Ašmontas, S., Sužiedelis, A., Gradauskas, J., Valušis, G., Lisauskas, A., Roskos, H. G., & Köhler, K. (2004). Detection of terahertz/sub-terahertz radiation by asymmetrically-shaped 2DEG layers. *Electronics Letters*, *40*(10), 631–632. https://doi.org/10.1049/EL:20040412

Seliuta, D., Gružinskis, V., Tamošiunas, V., Juozapavičius, A., Kašalynas, I., Ašmontas, S., Valušis, G., Steenson, P., Chow, W. H., Harrison, P., Lisauskas, A., Roskos, H. G., & Köhler, K. (2007b). The Two-Dimensional Bigradient Effect and Its Application for GHz-THz Sensing. *AIP Conference Proceedings*, *893*(1), 1419. https://doi.org/10.1063/1.2730437

Seok, E., Shim, D., Mao, C., Han, R., Sankaran, S., Cao C., Knap, W., & Kenneth, K.O. (2010). Progress and Challenges Towards Terahertz CMOS Integrated Circuits. *IEEE Journal of Solid-State Circuits,* *45*(8), 1554-1564. https://doi.org/10.1109/JSSC.2010.2049793

Shannon, J. M. (1979). A majority-carrier camel diode. *Applied Physics Letters*, *35*(1), 63. https://doi.org/10.1063/1.90931

Shashkin, V. I., Drjagin, Y. A., Zakamov, V. R., Krivov, S. V., Kukin, L. M., Murel, A. V., & Chechenin, Y. I. (2007). Millimeter-wave detectors based on antenna-coupled low-barrier schottky diodes. *International Journal of Infrared and Millimeter Waves*, *28*(11), 945–952. https://doi.org/10.1007/S10762-007-9272-2/FIGURES/5

Shen, Z., Yang, L., Luhmann Jr., N. C., Domier, C. W., Ito, N., Kogi, Y., Liang, Y., Mase, A., Park, H., Sakata, E., Tsai, W., Xia, Z. G., & Zhang, P. (2007). Advanced Microwave/Millimeter-Wave Imaging Technology. *Plasma and Fusion Research*, *2*(S1019), 1–9. https://doi.org/10.1585/PFR.2.S1019

Shur, M., & Ryzhii, V. (2004). New Concepts for Submillimeter-Wave Detection and Generation. *11th GAAS Symposium*, 301–304. https://doi.org/10.6092/unibo/amsacta/558

Sia, C. B. (2019). *Improving Wafer-Level S-parameters Measurement Accuracy and Stability with Probe-Tip Power Calibration up to 110 GHz for 5G Applications*.

Siegel, P. H. (2002). Terahertz technology. *IEEE Transactions on Microwave Theory and Techniques*, *50*(3), 910–928. https://doi.org/10.1109/22.989974

Smith, B. T., Weatherall, J. C., & Barber, J. B. (2015). *Method for identifying materials using dielectric properties through active millimeter wave illumination* (Patent No. US8946641B2).

Smiths Detection. (n.d.). *eqo People screening with automatic detection*. Retrieved December 8, 2021, from https://www.smithsdetection.com/products/eqo/#:~:text=eqo people screening system uses,of the person being screened.

Soshnikov, A. I., Gogolinsky, K. V., Blank, V. D., & Reshetov, V. N. (2007). The measurement of electrical properties of nanostructures with use of conductive diamond tip. *Journal of Physics: Conference Series*, *61*(1), 730–734. https://doi.org/10.1088/1742-6596/61/1/146

Stauffer, L. (2011). *C-V Measurement Tips, Tricks, and Traps* (Keithley Whitepaper). Cleveland: Keithley Instruments.

Störmer, H. L., Dingle, R., Gossard, A. C., Wiegmann, W., & Sturge, M. D. (1979). Two-dimensional electron gas at a semiconductor-semiconductor interface. *Solid State Communications*, *29*(10), 705–709. https://doi.org/10.1016/0038-1098(79)91010-X

Strid, E., Gleason, R., & Jones, K. (1988). 40 GHz On-Wafer Measurements with the HP 8510 Network Analyzer and Cascade Microtech Wafer Probes. In *RF & Microwave Measurement Symposium and Exhibition*.

Sužiedėlis A., Kozic A., Paškevič Č., Petkun V., Kazlauskaitė V., Gradauskas J., Požela J., Ašmontas S., Shtrikrnann H., Kiseliov V., & T. Anbinderis. (2006). Gate-Influenced Increase of Voltage Sensitivity in Asymmetrically shaped 2DEG Microwave Diodes. *Proceedings: International Joint Conference of 4th ESA Workshop on Millimetre-Wave Technology and Applications*, 239–244.

Sužiedėlis, A., Ašmontas, S., Gradauskas, J., Lučun, A., Čerškus, A., Paškevič, Č., & Anbinderis, T. (2016a). Investigation of microwave properties of planar heterojunction diodes in Ka frequency range using probe station. *Progress In Electromagnetics Research Symposium Proceedings*, 3899–3903. https://doi.org/10.1109/PIERS.2016.7735466

Sužiedėlis, A., Ašmontas, S., Kazlauskaite, V., & Gradauskas, J. (2009). Sensitivity increase of point contact hot carrier microwave detector. *Electronics Letters*, *45*(25), 1328–1329. https://doi.org/10.1049/EL.2009.1345/CITE/REFWORKS

Sužiedėlis, A., Ašmontas, S., Kundrotas, A. J., Gradauskas, J., Lučun, A., Čerškus, A., Nargelienė, V., Anbinderis, T., & Anbinderis, P. (2013). Microwave diode on the base of symmetrically and asymmetrically doped semiconductor heterojunction. *Progress in Electromagnetics Research Symposium*, 1605–1609.

Sužiedėlis, A., Ašmontas, S., Kundrotas, J., Nargeliene, V., & Gradauskas, J. (2012a). Voltage sensitivity of a point-contact GaAs/AlGaAs heterojunction microwave detector. *Physica Scripta*, *85*(3), 035702. https://doi.org/10.1088/0031-8949/85/03/035702

Sužiedėlis, A., Ašrnontas, S., Požela, J., Gradauskas, J., Petkun, V., Kazlauskaitė, V., Anbinderis, T., Papsujeva, I., & Narkünas, A. (2007a). Millimeter wave detection on gated selectivelly doped semiconductor structure. *The 6th International Kharkov Symposium on Physics and Engineering of Microwaves, Millimeter and Submillimeter Waves and Workshop on Terahertz Technologies*, *2*, 596–598. https://doi.org/10.1109/MSMW.2007.4294747

Sužiedėlis, A., Gradauskas, J., Ašmontas, S., Valušis, G., & Roskos, H. G. (2003). Giga- and terahertz frequency band detector based on an asymmetrically necked n-n+-GaAs planar structure. *Journal of Applied Physics*, *93*(5), 3034. https://doi.org/10.1063/1.1536024

Sužiedėlis, A., Ašmontas, S., Kundrotas, J., Gradauskas, J., Čerškus, A., Nargelienė, V., & Anbinderis, T. (2012b). Planar Heterojunction Diode for Millimeter Waves Detection. *Progress in Electromagnetics Research Symposium*, 906–909.

Sužiedėlis, A., Ašmontas, S., Gradauskas, J., Gružinskis, V., Lučun, A., & Čerškus, A. (2016b). Novel microwave diode for millimeter waves on the base of asymmetrically doped semiconductor structure. *46th European Microwave Conference*, 1103–1106. https://doi.org/10.1109/EUMC.2016.7824540

Sužiedėlis, A., Ašmontas, S., Gradauskas, J., Nargelienė, V., Čerškus, A., Lučun, A., Anbinderis, T., Papsujeva, I., Narkunas, A., Kundrotas, B., & Rinkevičiene, R. (2014). Peculiarities of Temperature Dependence of Detected Voltage by GaAs/Al0.25Ga0.75As Heterojunction Microwave Diode Near Interwalley Crossover. *Materials Science*, *20*(2), 138–140. https://doi.org/10.5755/J01.MS.20.2.6319

Sužiedelis, A., Petkun, V., Kozič, A., Kazlauskaitė, V., Čerškus, A., Steikunas, G., Gradauskas, J., Kundrotas, J., Ašmontas, S., Papsujeva, I., Narkunas, A., Anbinderis, T., Umansky, V., & Shtrikmann, H. (2007b). GaAs/AlGaAs structures with δ-doped layer for microwave detection. *Advanced Optical Materials, Technologies, and Devices*, *6596*(65960N), 1–6. https://doi.org/10.1117/12.726409

Sze, S. M. (1981). *Physics of semiconductor devices* (2nd ed.). Hoboken: Wiley.

Takahashi, T., Sato, M., Hirose, T., & Hara, N. (2009). GaAsSb-based backward diodes for highly sensitive millimetre-wave detectors. *Electronics Letters*, *45*(24), 1269–1270. https://doi.org/10.1049/el.2009.2496

Takahashi, T., Sato, M., Nakasha, Y., & Hara, N. (2012). Lattice-matched p+-GaAsSb/i-InAlAs/n-InGaAs zero-bias backward diodes for millimeter-wave detectors and mixers. *International Conference on Indium Phosphide and Related Materials*, 95–98. https://doi.org/10.1109/ICIPRM.2012.6403328

Teppe, F., Knap, W., Veksler, D., Shur, M. S., Dmitriev, A. P., Kachorovskii, V. Y., & Rumyantsev, S. (2005). Room-temperature plasma waves resonant detection of subterahertz radiation by nanometer field-effect transistor. *Applied Physics Letters*, *87*(5), 052107. https://doi.org/10.1063/1.2005394

Teppone, M., & Avakyan, R. (2010). Extremely high-frequency therapy in oncology. *Journal of Alternative and Complementary Medicine*, *16*(11), 1211–1216. https://doi.org/10.1089/ACM.2009.0208

Texas Instruments. (n.d.). *Industrial mmWave radar sensors*. Retrieved December 8, 2021, from https://www.ti.com/sensors/mmwave-radar/industrial/overview.html

Texas Instruments. (n.d.). *Automotive mmWave Sensors*. Retrieved December 8, 2021, from https://www.ti.com/sensors/mmwave-radar/overview.html

Tohmé, L., Blin, S., Ducournau, G., Nouvel, P., Coquillat, D., Hisatake, S., Nagatsuma, T., Pénarier, A., Varani, L., Knap, W., & Lampin, J. F. (2014). Terahertz wireless communication using GaAs transistors as detectors. *Electronics Letters*, *50*(4), 323–325. https://doi.org/10.1049/EL.2013.3702

Tokoro, S., Kuroda, K., Kawakubo, A., Fujita, K., & Fujinami, H. (2003). Electronically scanned millimeter-wave radar for pre-crash safety and adaptive cruise control system. *IEEE Intelligent Vehicles Symposium, Proceedings*, 304–309. https://doi.org/10.1109/IVS.2003.1212927

Tydex. (n.d.). *Golay Cell GC-1D with Diamond Window*. Retrieved December 8, 2021, from http://www.tydexoptics.com/products/thz_devices/golay_cell/

Vaitkus J., Starikov E., Subačius L., & Jarašiūnas K. (1990). Field dependences of light selfdiffraction efficiency and hot carrier diffusion coefficient in gallium arsenide and silicon. Lietuvos Fizikos Rinkinys, 30(3), 336–351.

Valušis, G., Sachs, R., Roskos, H. G., Sužiedelis, A., Gradauskas, J., Ašmontas, S., Širmulis, E., & Köhler, K. (2002). GHz-THz detection by asymmetrically-shaped GaAs: Bulk material versus nanostructures. *Materials Science Forum*, *384–385*, 193–196. https://doi.org/10.4028/WWW.SCIENTIFIC.NET/MSF.384-385.193

Valušis, G., Seliuta, D., Tamošiunas, V., Širmulis, E., Balakauskas, S., Gradauskas, J., Sužiedėlis, A., Ašmontas, S., Anbinderis, T., Narkunas, A., Papsujeva, I., Lisauskas, A., Roskos, H. G., & Köhler, K. (2005). Broad Band THz Sensing by 2DEG Bow-Tie-Type Diodes. *Acta Physica Polonica A*, *107*(1), 184–187. https://doi.org/10.12693/APHYSPOLA.107.184

Van, N. T. P., Tang, L., Demir, V., Hasan, S. F., Minh, N. D., & Mukhopadhyay, S. (2019). Review-Microwave Radar Sensing Systems for Search and Rescue Purposes. *MDPI Sensors*, *19*(13), 2879. https://doi.org/10.3390/S19132879

Vega. (n.d.). *First radar level sensor for liquids with 80 GHz*. Retrieved December 8, 2021, from https://www.vega.com/en/products/product-catalog/level/radar/vegapuls-64/first-radar-level-sensor-for-liquids-with-80-ghz-vegapuls-64#:~:text=VEGA%2C for more than 20,a frequency of 80 GHz.

Veksler, D., Teppe, F., Dmitriev, A. P., Kachorovskii, V. Y., Knap, W., & Shur, M. S. (2006). Detection of terahertz radiation in gated two-dimensional structures governed by dc current. *Physical Review B - Condensed Matter and Materials Physics*, *73*(12), 125328. https://doi.org/10.1103/PHYSREVB.73.125328/FIGURES/4/MEDIUM

Virginia Diodes. (n.d.). *Zero Bias Detector*. Retrieved December 1, 2021, from https://www.vadiodes.com/en/products/detectors

Vo, V. T., & Hu, Z. (2006). Optimization and realization of planar isolated GaAs zero-biased planar doped barrier diodes for microwave/millimeter-wave power detectors/sensors. *IEEE Transactions on Microwave Theory and Techniques*, *54*(11), 3836–3842. https://doi.org/10.1109/TMTT.2006.884628

Vo, V. T., Koon, K. L., Hu, Z. R., Dharmasiri, C. N., Subramaniam, S. C., & Rezazadeh, A. A. (2004). High voltage sensitivity GaAs planar doped barrier diodes for microwave/millimeter-wave power detector applications. *IEEE MTT-S International Microwave Symposium Digest*, *2*, 995–998. https://doi.org/10.1109/MWSYM.2004.1339147

Vostokov, N. V., Revin, M. V., & Shashkin, V. I. (2020). Microwave detector diodes based on InGaAs/AlGaAs/GaAs heterostructures. *Journal of Applied Physics*, *127*(4), 044503. https://doi.org/10.1063/1.5131737

Wang, Z., Chang, T., & Cui, H. L. (2019). Review of active millimeter wave imaging techniques for personnel security screening. *IEEE Access*, *7*, 148336–148350. https://doi.org/10.1109/ACCESS.2019.2946736

Watanabe, T., Boubanga-Tombet, S. A., Tanimoto, Y., Fateev, D., Popov, V., Coquillat, D., Knap, W., Meziani, Y. M., Wang, Y., Minamide, H., Ito, H., & Otsuji, T. (2013). InP- and GaAs-based plasmonic high-electron-mobility transistors for room-temperature ultrahigh-sensitive terahertz sensing and imaging. *IEEE Sensors Journal*, *13*(1), 89–99. https://doi.org/10.1109/JSEN.2012.2225831

Williams, R. E. (1990). *Modern GaAs processing methods*. Artech House.

Winters, M., Thorsell, M., Strupiński, W., & Rorsman, N. (2015). High frequency electromagnetic detection by nonlinear conduction modulation in graphene nanowire diodes. *Applied Physics Letters*, *107*(14), 143508. https://doi.org/10.1063/1.4932970

Womac, J. F., & Rediker, R. H. (1972). The graded-gap Alx Ga1 − x As–GaAs heterojunction. *Journal of Applied Physics*, *43*(10), 4129. https://doi.org/10.1063/1.1660885

Woodward, R. M., Wallace, V. P., Arnone, D. D., Linfield, E. H., & Pepper, M. (2003). Terahertz pulsed imaging of skin cancer in the time and frequency domain. *Journal of Biological Physics*, *29*(2–3), 257–259. https://doi.org/10.1023/A:1024409329416

Xu, K. X., Essa, A. A., Zhou, S. P., & Bao, J. S. (2000). Microwave detection using Y–Ba–Cu–O granular film bridge device. *Physica C: Superconductivity*, *339*(1), 42–48. https://doi.org/10.1016/S0921-4534(00)00316-6

Yngvesson, K. S. (2000). Ultrafast two-dimensional electron gas detector and mixer for terahertz radiation. *Applied Physics Letters*, *76*(6), 777. https://doi.org/10.1063/1.125892

Young, A. C., Zimmerman, J. D., Brown, E. R., & Gossard, A. C. (2005). Semimetal-semiconductor rectifiers for sensitive room-temperature microwave detectors. *Applied Physics Letters*, *87*(16), 163506. https://doi.org/10.1063/1.2112201

Yu, C., Fan, S., Sun, Y., & Pickwell-Macpherson, E. (2012). The potential of terahertz imaging for cancer diagnosis: A review of investigations to date. *Quantitative Imaging in Medicine and Surgery*, *2*(1), 33–45. https://doi.org/10.3978/J.ISSN.2223-4292.2012.01.04

Zagrajek, P., Danilov, S. N., Marczewski, J., Zaborowski, M., Kolacinski, C., Obrebski, D., Kopyt, P., Salski, B., But, D., Knap, W., & Ganichev, S. D. (2019). Time Resolution and Dynamic Range of Field-Effect Transistor–Based Terahertz Detectors. *Journal of Infrared, Millimeter, and Terahertz Waves*, *40*(7), 703–719. https://doi.org/10.1007/S10762-019-00605-0/FIGURES/11

Zainul Ariffin, K. N., Wang, Y., Abdullah, M. R. R., Muttlak, S. G., Abdulwahid, O. S., Sexton, J., Ian, K. W., Kelly, M. J., & Missous, M. (2018). Investigations of asymmetric spacer tunnel layer diodes for high-frequency applications. *IEEE Transactions on Electron Devices*, *65*(1), 64–71. https://doi.org/10.1109/TED.2017.2777803

Zhang, X., Liang, J., Wang, N., Chang, T., Guo, Q., & Cui, H. L. (2020). Broadband Millimeter-Wave Imaging Radar-Based 3-D Holographic Reconstruction for Nondestructive Testing. *IEEE Transactions on Microwave Theory and Techniques*, *68*(3), 1074–1085. https://doi.org/10.1109/TMTT.2019.2948349

Zhang, Z., Rajavel, R., Deelman, P., & Fay, P. (2011). Sub-micron area heterojunction backward diode millimeter-wave detectors with 0.18 pW/Hz1/2 noise equivalent power. *IEEE Microwave and Wireless Components Letters*, *21*(5), 267–269. https://doi.org/10.1109/LMWC.2011.2123878

Zheng, S. Y., Su, Z. L., Pan, Y. M., Qamar, Z., & Ho, D. (2018). New Dual-/Tri-Band Bandpass Filters and Diplexer With Large Frequency Ratio. *IEEE Transactions on Microwave Theory and Techniques*, *66*(6), 2978–2992. https://doi.org/10.1109/TMTT.2018.2833862

Zucker, J. (1964). Thermoelectric power of hot carriers. *Journal of Applied Physics*, *35*(3), 618–621. https://doi.org/10.1063/1.1713425

List of Scientific Publications by the Author on the Topic of the Dissertation

Papers in Reviewed Scientific Journals

Sužiedėlis, A., Ašmontas, S., Gradauskas, J., Šilėnas, A., Čerškus, A., Lučun, A., Paškevič, Anbinderis, M., & Žalys, O. (2017a). Planar Asymmetric Dual Diode for Millimeter Wave Detection and Power Measurement. *Lithuanian Journal of Physics*, *57*(4), 225–231. https://doi.org/10.3952/PHYSICS.V57I4.3601

Ašmontas, S., Anbinderis, M., Čerškus, A., Gradauskas, J., Sužiedėlis, A., Šilėnas, A., Širmulis, E., & Umansky, V. (2020). Gated Bow-Tie Diode for Microwave to Sub-Terahertz Detection. *MDPI Sensors*, *20*(3), 829. https://doi.org/10.3390/S20030829

Anbinderis, M., Ašmontas, S., Čerškus, A., Gradauskas, J., Lučun, A., Šilėnas, A., & Sužiedėlis, A. (2021). Sensitive Planar Microwave Diode on the Base of Ternary $Al_xGa_{1-x}As$ Semiconductor Compound. *MDPI Sensors*, *21*(13), 4487. https://doi.org/10.3390/S21134487

Papers in Other Editions

Sužiedėlis, A., Ašmontas, S., Gradauskas, J., Šilėnas, A., Lučun, A., Čerškus, A., Paškevič, Žalys, O., & Anbinderis, M. (2017b). Pulsed Microwave Sensor on Heavily Doped Semiconductor Substrate. *Progress in Electromagnetics Research Symposium*, 1037–1042. https://doi.org/10.1109/PIERS-FALL.2017.8293286

Anbinderis, M., Ašmontas, S., Gradauskas, J., Derkach, V., Golovashchenko, R., & Sužiedėlis, A. (2020). Gated Bow-Tie Diode with Selectively Doped 2DEG Active Layer for Microwave Sensing. *IEEE Ukrainian Microwave Week, UkrMW 2020 Proceedings*, 907–911. https://doi.org/10.1109/UKRMW49653.2020.9252700

Patents

Sužiedėlis, A., Ašmontas, S., Gradauskas, J., Steikūnienė, A., Steikūnas, G., Anbinderis, M. (2019). *Sensor for Electromagnetic Radiation of Microwave and Terahertz Frequencies*. (European Patent No. 3582269). State Patent Bureau of the Republic of Lithuania.
https://worldwide.espacenet.com/patent/search/family/066379847/publication/EP3582269A1?q=3582269

Summary in Lithuanian

Įvadas

Problemos formulavimas

Mikrobangos apima labai platų elektromagnetinės spinduliuotės dažnių diapazoną nuo 300 MHz iki 300 GHz ir skirstomos į ruožus pagal taikymo galimybes. Vienas iš mikrobangų ruožų yra vadinamasis milimetrinių bangų (arba ekstremaliai aukštų dažnių) ruožas nuo 30 GHz iki 300 GHz (Zhang et al., 2020). Elektromagnetinė spinduliuotė milimetrinių bangų ruože pritraukia mokslininkų ir inžinierių dėmesį dėl plačių taikymo galimybių šiuolaikinių technologijų srityse, pavyzdžiui, tokių kaip vaizdavimas (Oka et al., 2008; Wang et al., 2019), biomedicina (Dalmay et al., 2010; Pastorino, 2015) medžiagotyra (Smith et al., 2012; Kancleris et al., 2004) ir plačiajuosčiai bevieliai komunikacijos tinklai (Rappaport et al., 2013; Huo et al., 2017). Kadangi mikrobangų ruožo elektromagnetinės spinduliuotės bangos ilgis yra mažas, tai lemia labai mažus elektronikos įrenginių matmenis, o tai atveria papildomas plataus taikymo galimybes.

Norint naudotis mikrobangų ruožu, reikalingi elektromagnetinės spinduliuotės detektoriai, gebantys aptikti silpnus aukštadažnius signalus. Milimetrinių bangų spinduliuotei detektuoti yra naudojami lauko tranzistoriai (Teppe et al., 2005), tuneliniai diodai (Takahashi et al., 2009) ir didelė įvairovė mikrobangų diodų, pagamintų Šotkio sandūros pagrindu (Siegel, 2002; Shashkin et al., 2007). Žemo barjero Šotki diodai, veikiantys be priešįtampio (Hesler & Crowe, 2007), yra komerciškai populiariausi dėl gero atkartojamumo ir patikimumo bei aukšto voltvatinio jautrio, plačios dažnių juostos ir galimybės veikti kambario temperatūros aplinkoje. Iš kitos pusės, Šotkio diodai yra sudėtingi įrenginiai, kurie blogai apsaugoti nuo aplinkos poveikio ir yra jautrūs gamybos sąlygoms, nes iš esmės Šotki diodai yra paviršiniai diodai, t. y. jų veikimo mechanizmai sukoncentruoti puslaidininkinio darinio paviršiuje. Šie faktoriai skatina mokslininkus ir inžinierius kurti naujas originalias mikrobangų diodų koncepcijas, kuriose detektavimo mechanizmai yra sukoncentruoti įtaiso darinio tūryje, o ne paviršiuje.

Buvo pasiūlyti įvairūs diodai su nevienalyte sandūra tūryje, kurių veikimas pagrįstas pagrindinių krūvininkų reiškiniu. Pavyzdžiui, karštųjų krūvininkų diodai (Harrison & Zucker, 1966) ir heterosandūriniai diodai (Lechner et al., 1980). Šių diodų savybių tobulinimas nulėmė planarinių asimetrinės formos ir peteliškės formos diodų konstrukcijos atsiradimą. Planariniai didelio krūvininkų judrio heterosandūriniai mikrobangų diodai pagaminti A_3B_5 junginių pagrindu (Gradauskas et al., 2010) ir diodai, pagaminti selektyviai legiruotų puslaidininkinių darinių pagrindu su dvimačiu elektronų dujų kanalais (Seliuta et al., 2004), yra perspektyvūs aukštadažnės elektromagnetinės spinduliuotės detektavimo taikymo srityje. Skirtingos tokių diodų versijos buvo tiriamos ieškant optimalių darinių konstrukcijos, leidžiančios pagerinti šių diodų detekcijos savybes (Sužiedėlis et al., 2012b, 2016a; Minkevičius et al., 2011; Kašalynas et al., 2011, 2013). Tačiau pagrindinė kliūtis šių diodų taikymo srityje yra žemos jų voltvatinio jautrio reikšmės ir didelė elektrinė varža.

Darbo aktualumas

Elektromagnetinės spinduliuotės detektoriai reikalingi didžioje dalyje perspektyviųjų mikrobangų taikymų, kurie apima pagrindines technologijų sritis, tokias kaip komunikacijos tinklai, vaizdavimas, mokslas ir medicina. Šie detektoriai turi atitikti specifinius reikalavimus norint juos pritaikyti įvairiose mikrobangų technologijų srityse. Įrenginiai, kurie gali aptikti ir matuoti mikrobangų spinduliuotės galią, turi būti tvirtos konstrukcijos, ekonomiški gamybos kainos atžvilgiu ir išsiskirti trumpu signalo atsako laiku, jiems veikiant kambario temperatūroje. Itin svarbu turėti ir sąlygiškai didelį voltvatinį jautrį plačiame dažnių diapazone ir mažą elektrinę varžą. Detekcijos savybės taip pat turi minimaliai priklausyti nuo temperatūros, slėgio, drėgmės ir kitų aplinkos faktorių. Patobulintos konstrukcijos puslaidininkiniai mikrobangų diodai su energetiniu barjeru puslaidininkio tūryje, tokie kaip planariniai asimetriniai mikrobangų diodai, veikiantys nevienalyčio krūvininkų kaitimo reiškinio pagrindu su dvimačių elektronų dujų sluoksniu arba su mažu darbinio kontakto plotu bei diodai su daline sklende virš dvimačio elektronų dujų sluoksnio, yra perspektyvūs ieškant naujos koncepcijos, skirtos aukštadažnei elektromagnetinei spinduliuotei detektuoti.

Taip pat svarbu turėti našias ir patogias sistemas, leidžiančias charakterizuoti minėtus detektorius. Planarinių mikrobangų diodų elektriniai parametrai ir detekcijos savybės gali būti įvertinamos taikant zondavimo metodus, tai leidžia atlikti patikimus ir laiką taupančius matavimus tiesiai ant puslaidininkinio padėklo.

Tyrimo objektas

Tyrimo objektas yra nauji planariniai mikrobangų diodai, pagaminti GaAs, AlGaAs ir AlGaAs/GaAs junginių pagrindu.

Darbo tikslas

Disertacijos tikslas – sukurti ir ištirti naujus originalius planarinius mikrobangų diodus, kurie pasižymėtų mažesniu elektrinių parametrų išbarstymu ir galėtų detektuoti elektromagnetinę spinduliuotę milimetrinių bangų ruože.

Darbo uždaviniai

Siekiant pasiekti iškeltą disertacijos tikslą turi būti įgyvendinti šie uždaviniai:

1. Įvaldyti puslaidininkinių darinių gamybos technologijas ir sukurti naujus planarinius mikrobangų diodus puslaidininkinio darinio pagrindu, kurie yra skirti elektromagnetinio signalo detekcijai milimetrinių bangų ruože.
2. Ištirti sukurtų mikrobangų diodų voltamperines charakteristikas taikant nuolatinės srovės zondavimo metodiką ir nustatyti tiriamų diodų elektrinius parametrus.
3. Ištirti sukurtų mikrobangų diodų detekcijos savybes milimetrinių bangų ruože ir nustatyti jų voltvatinį jautrį taikant aukštadažnes zondavimo metodikas bei montuojant diodus į bangolaidinę perdavimo liniją.

Tyrimų metodika

Darbe taikomi šie moksliniai metodai: Poisson simuliacija (puslaidininkinių darinių energijos juostų diagramos ir elektronų pasiskirstymas); fotolitografijos, cheminio ėsdinimo, kontaktų terminio garinimo ir atkaitinimo metodikos (mikrobangų diodų gamyba); baigtinių elementų modeliavimas (elektrinio lauko pasiskirstymas mikrobangų dioduose); nuolatinės srovės zondavimo metodika (mikrobangų diodų elektriniai parametrai); aukštadažnio zondavimo metodika ir bangolaidinės detektorinės galvutės su mikrojuosteline linija metodika (mikrobangų diodų detekcijos savybės); statistinio ir analitinio vertinimo metodikos (eksperimentinių rezultatų įvertinimas).

Darbo mokslinis naujumas

Disertacijoje pasiekti šie mokslui reikšmingi rezultatai:

1. AlGaAs/GaAs, AlGaAs ir GaAs junginių pagrindu sukurti naujos konstrukcijos planariniai dvigubi mikrobangų diodai ir peteliškės formos diodai su daline sklende virš dvimačio elektronų dujų sluoksnio. Nustatyti jų elektriniai parametrai bei ištirtos šių diodų detekcijos savybės plačiame dažnių ruože nuo 26 iki 330 GHz.
2. Parodyta, kad dalinė metalinė sklendė, dengianti asimetrinio puslaidininkinio darinio siaurąją arba plačiąją dalį, leidžia padidinti peteliškės formos diodo voltvatinį jautrį.
3. Pasiūlyta matavimo metodika, leidžianti aukštadažniu zondiniu manipuliatoriumi našiai tirti planarinių mikrobangų diodų detektuotos įtampos priklausomybę nuo galios ir dažnio 26,5–40 GHz dažnių ruože.

Darbo rezultatų praktinė reikšmė

Sukurti ir ištirti nauji originalūs planariniai dvigubi mikrobangų diodai ir peteliškės formos diodai su daline sklende virš dvimačio elektronų dujų sluoksnio, pagaminti AlGaAs/GaAs, AlGaAs ir GaAs junginių pagrindu, gali būti naudojami kaip detektavimo diodai mažų galių perdavimo linijose. Mikrobangų diodų elektriniai parametrai ir aukštadažnės savybės gali būti tiriamos naudojant pasiūlytus matavimo stendus su nuolatinės srovės ir aukštų dažnių zondiniais manipuliatoriais. Pateiktos matavimo metodikos leidžia atlikti greitus mikrobangų diodų tyrimus ir sumažinti tiriamų diodų pažeidimo riziką, nes matavimai yra atliekami tiesiai ant puslaidininkinio padėklo nedalinant diodų matricos į atskirus elementus. AlGaAs/GaAs junginio pagrindu pagamintų peteliškės formos diodų su daline sklende virš dvimačio elektronų dujų kanalo tyrimo rezultatai šioje disertacijoje buvo panaudoti rengiant Europinį patentą „Sensor for Electromagnetic Radiation of Microwave and Terahertz Frequencies/Mikrobangų ir terahercinių bangų ruožo elektromagnetinės spinduliuotės jutiklis“ (Nr. EP 3582269). Šioje disertacijoje pristatyti tyrimo rezultatai taip pat buvo panaudoti vykdant du mokslinius projektus:

1. Lietuvos mokslo tarybos inicijuotoje Nacionalinėje programoje „Link ateities technologijų“ projektas „Nauji plačiajuosčiai elektromagnetinės spinduliuotės jutikliai su dvimatėmis elektronų protakomis“ (Nr. LAT-03/2016).
2. Lietuvos mokslo tarybos vykdomoje Tarptautinio bendradarbiavimo programoje „Lietuva-Ukraina“, projekte „Nauji mikrobangų diodai kryptinei elektromagnetinei spinduliuotei aptikti“ (Nr. S-LU-20-7).

Ginamieji teiginiai

1. Planariniai dvigubi mikrobangų diodai ir peteliškės formos mikrobangų diodai su daline sklende virš dvimačio elektronų dujų sluoksnio, pagaminti GaAs, AlGaAs ir AlGaAs/GaAs junginių pagrindu, yra tinkami impulsinės ir nuolatinės generacijos milimetrinių bangų spinduliuotės detekcijai nuo pikovatų iki milivatų signalo galios ruože.
2. Dalinės sklendės formavimas uždengiant asimetrinio selektyviai legiruoto puslaidininkinio darinio siaurąją arba plačiąją dalį metaliniu sluoksniu leidžia padidinti peteliškės formos diodų su dvimačiu elektronų dujų sluoksniu voltvatinio jautrio dydį iki dviejų eilių.
3. Sukurtas matavimo stendas su aukštadažniu zondiniu manipuliatoriumi leidžia našiai tirti planarinių mikrobangų diodų, suformuotų ant puslaidininkinio padėklo, detektuotos įtampos priklausomybes nuo galios ir dažnio 26,5–40 GHz dažnių ruože esant skirtingai temperatūrai ir apšviestumui.

Darbo rezultatų aprobavimas

Pagrindiniai disertacijos rezultatai buvo paskelbti 5 mokslo straipsniuose: 3 – mokslo žurnaluose, įtrauktuose į *Clarivate Analytics Web of Science* duomenų bazės sąrašą su citavimo rodikliu, 2 – tarptautinių konferencijų medžiagoje, įtrauktoje į *Clarivate Analytics Web of Science* ir *Scopus* duomenų bazes.

Disertacijoje atliktų tyrimų rezultatai buvo paskelbti 12 mokslinių konferencijų Lietuvoje ir užsienyje, jos yra tokios:

- Tarptautinė studentų ir jaunųjų mokslinikų konferencija *Open Readings* (2017 ir 2019 m.), Vilnius, Lietuva.
- Jaunųjų mokslininkų konferencija *Mokslas – Lietuvos ateitis: Elektros ir elektronikos inžinierija* (2017 ir 2019 m.), Vilnius, Lietuva.
- *42-oji ir 43-ioji Lietuvos nacionalinė fizikos konferencija* (2017 ir 2019 m.), Vilnius ir Kaunas, Lietuva.
- Jaunųjų mokslininkų konferencija *FizTech* (2017 m.), Vilnius, Lietuva.
- Tarptautinė konferencija *Progress in Electromagnetics Symposium* (2017 m.), Singapūras.
- Tarptautinė konferencija *Energy Materials and Nanotechnology Vienna Meeting* (2018 m.), Viena, Austrija.
- Tarptautinė konferencija *The 8th International Conference on Electronics, Communications and Networks* (2018 m.), Bankokas, Tailandas.
- Tarptautinė konferencija *6th International Conference on Sensors and Electronic Instrumentation Advances* (2020 m.), Porto, Portugalija.
- Tarptautinė konferencija *Ukrainian Microwave Week* (2020 m.), Charkivas, Ukraina.

Disertacijos struktūra

Disertacija parengta anglų kalba ir sudaryta iš bendrosios charakteristikos, keturių pagrindinių skyrių, bendrųjų išvadų, literatūros sąrašo ir autoriaus publikacijų disertacijos tema sąrašo.

Disertacijos apimtis yra 175 puslapiai, tekste panaudoti: 85 paveikslai, 26 formulės ir 11 lentelių. Rašant disertaciją panaudoti 224 literatūros šaltiniai.

1. Mikrobangų detektorių elektrinės ir aukštadažnės savybės bei jų taikymas

Populiariausiuose mikrobangų detektoriuose naudojami žemo barjero Šotkio diodai, kurie veikia be priešįtampio. Jie yra tinkami kvadratiniam signalų detektavimui (Hesler & Crowe, 2007; Hoefle et al., 2014). Pagrindiniai Šotkio diodų privalumai, kurie lemia šių diodų panaudojimą detektoriuose, yra didelis voltvatinis jautris, geros žemadažnės charakteristikos, galimybė efektyviai veikti kambario temperatūroje, plati dažnių juosta ir geras parametrų atkartojamumas. Šotkio diodai pasiekė aukštą komercilizavimo lygį ir yra plačiai prienami rinkoje („Virginia Diodes, Inc. Zero Bias Detector“). Tačiau fundamentiniu požiūriu Šotkio sandūros konstrukcijos sudėtingumas reikalauja, kad ji būtų formuojama puslaidininkio paviršiuje, todėl Šotkio diodo savybės yra jautrios gamybos sąlygoms ir aplinkos poveikiui. Taip pat Šotkio diodai yra neatsparūs didelės galios spinduliuotei (Tohme et al., 2014). Daugiau nei prieš 50 metų buvo pasiūlyti perspektyvūs mikrobangų diodai, kurių veikimo principas pagrįstas karštųjų krūvininkų reiškiniu nevienalyčiame elektriniame lauke (Harrison & Zucker, 1963). Šiuose dioduose veikimo mechanizmas yra sukoncentruotas puslaidininkinės medžiagos tūryje (viduje), o ne paviršiuje. Harrison ir Zucker (Harrison & Zucker, 1963) pirmieji pasiūlė tokį originalų mikrobangų diodą. Šotkio diodų vystymas atvedė mokslininkus ir inžinierius prie „Camel“ diodų, kai 1979 m. Shannon pasiūlė pakeisti metalo-puslaidininkio barjerą n^{++}-p^{+}-n sandūra (Shannon, 1979). 1980 m. Malik et al. pasiūlė įterpti nuosavo laidumo puslaidininkinius sluoksnius tarp priešingo elektrinio laidumo legiruotų sluoksnių, todėl „Camel“ diodo struktūra buvo pakeista į n^{+}-i-p^{+}-i-n^{+} planarinį legiruoto barjero darinį (Malik et al., 1980). Šotkio sandūros diodai ir planariniai legiruoto barjero diodai buvo pritaikyti impulsinės mikrobangų spinduliuotės galios matavimams. Tolesnis šių taškinio kontakto diodų tobulinimas nulėmė planarinės peteliškės formos asimetriškai susiaurintos konstrukcijos atsiradimą su n^{+}-n Si homosandūra (Ašmontas & Sužiedėlis, 1994). Buvo parodyta, kad planariniai diodai sėkmingai gali detektuoti elektromagnetinę spinduliuotę nuo mikrobangų iki infraraudonosios spinduliuotės ruožo, įskaitant teraherecinių dažnių ruožą (Ašmontas & Sužiedėlis, 1994; Sužiedėlis et al., 2003; Minkevičius et al., 2011). Šie planariniai diodai buvo sėkmingai pritaikyti heterodininiam (Minkevičius et al., 2011) ir spektroskopiniam vaizdavimui terahercinių dažnių ruože (Kašalynas et al., 2011) bei signalui detektuoti ir matuoti (Seliuta et al., 2004, Palenskis et al., 2018). Kitas diodo tipas, kurio aktyvioji sritis yra puslaidininkinio darinio tūryje, yra heterosandūriniai diodai. 1980 m. Lechner et al. sukūrė diodą su heterosandūriniu GaAs/AlGaAs barjeru, kuris galėjo detektuoti mikrobangų spinduliuotę. Toliau jautrūs heterosandūriniai diodai buvo tiriami kaip elektromagnetinės spinduliuotės detektoriai plačiame dažnių ruože nuo mikrobangų iki infraraudonojo spektro dažnių (Gradaukas et al., 2010). Buvo parodyta, kad asimetriškai susiaurinti planariniai karštųjų krūvininkų mikrobangų diodai gali detektuoti plačiajuostę elektromagnetinę spinduliuotę nuo mikrobangų iki terahercinių dažnių ruožo (Sužiedėlis et al., 2003). Plačiajuostį veikimą riboja elektronų impulso relaksacijos trukmė, tačiau šitų diodų voltvatinis jautris buvo sąlygiškai mažas. Buvo pasiūlyta (Seliuta et al., 2004) panaudoti puslaidininkinius darinius su dvimatėmis elektronų dujomis sėkmingai vystant mikrobangų detektavimo diodus. Dvimatis elektronų dujų sluoksnis susiformuoja selektyviai legiruotame puslaidininkiniame darinyje, nes laisvi elektronai yra atskirti erdvėje nuo jonizuotų donorų ir susikoncentruoja kelių nanometrų potencinėje duobėje šalia heterosandūros (Seliuta et al., 2007a; Stormer et al., 1979; Hiyamizu et al., 1983). Selektyviai legiruotose heterosandūrose padidėja laisvųjų krūvininkų laidumas, tai nulemia voltvatinio jautrio padidėjimą. Tačiau, norint kad tokio tipo diodai būtų komerciškai sėkmingi, jie turi pasižymėti ne tik dideliu voltvatinių jautriu ir greitu atsaku, bet būti patikimi ir nebrangūs.

Milimetrinio ilgio bangų taikymo galimybės apima tokias šiuolaikines sritis kaip plačiajuosčiai didelės spartos belaidžio ryšio tinklai (Huo et al., 2017, Zheng et al., 2018, Rappaport et al., 2013), radarų technologijos (Polivka, 2007; Brooker et al., 2001, Iovescu & Rao, 2020), vaizdavimo sistemos (Oka et al., 2008; Zhang et al., 2020; Goldsmith et al., 1993; Polivka, 2007; Sato & Mizuno, 2010; Meng et al., 2018; Shen et al., 2007; Peichl et al., 2007; Smith et al., 2012; Cortes-Medellin et al., 2015) ir biomedicina (Dalmay et al., 2010, Yu et al., 2012, Pastorino, 2015). Daugumai taikymo sričių reikalingi detektoriai, kurie veikia nepriklausomai nuo aplinkos ir atmosferos sąlygų (Goldsmith et al., 1993). Kaip jau buvo minėta, planariniai peteliškės formos diodai yra perspektyvūs kaip plačiajuosčiai mikrobangų detektoriai ir keli iš jų buvo išbandyti heterodininės detekcijos taikymams (Minkevičius et al., 2011), spektroskopiniam vaizdavimui (Kašalynas et al., 2011) bei paslėptų mažai spinduliuotę sugeriančių objektų vaizdavimui (Jokubauskis et al., 2019). Taigi, naujos koncepcijos elektromagnetinės spinduliuotės detektavimo diodai, kurių aktyvioji sritis yra puslaidininkinio darinio tūryje, gali būti panaudoti įvairiems taikymams milimetrinių bangų ruože.

Puslaidininkinių įtaisų detekcijos charakteristikos dažniausiai buvo matuojamos taikant tradicines metodikas, pavyzdžiui, naudojant bangolaidines sekcijas. Didėjant veikimo dažniams iki milimetrinio ir subterahercinio ruožų, buvo sukurti labiau tinkami matavimo metodai, naudojant zondavimo sistemas, jie buvo skirti puslaidininkiniams įrenginiams charakterizuoti tiesiai ant padėklo ir gamybos išeigai testuoti. Pirmą kartą tokio metodo taikymą mikrobangų dažniais pasiūlė Strid ir Gleason 1980 m. Šiandien tokie metodai yra plačiai taikomi perdavimo linijų bei aktyvių ir pasyvių komponentų, kurių veikimo dažnis siekia net 1,1 THz, parametrų matavimams („FormFactor: Unparalleled Probing Solutions“). Zondai naudojami sklaidos parametrų (S parametrų) matavimams, kuriuos galima konvertuoti į elektrinių parametrų, pvz., impedanso, matavimą (Collier & Skinner, 2007; „Cascade Microtech: Calibration Tools Consistent Parameter Extraction for Advanced RF Devices“; Sia, 2019; Fregonese et al., 2018; Savin et al., 2016). Iki šiol yra pateikti tik keli atsekami mikrobangų puslaidininkinių diodų aukštadažnių detekcjos savybių tyrimų bandymai naudojant zondus (Sužiedėlis et al., 2016a, 2016b).

2. Mikrobangų diodų kūrimas ir gamyba, tyrimų metodologija

Planariniai mikrobangų diodai ant laidaus padėklo buvo pagaminti naudojant trijų tipų stipriai legiruotas GaAs plokšteles (350 μm AGChP-M-21a (1.0.0) 0° 30′, Ø 26 mm, Grynųjų metalų gamykla, Svitlovodsk, Ukraina): n^{++}-GaAs su donorų koncentracija 4×10^{18} cm^{-3}, n^{+}-GaAs, legiruota 4×10^{17} cm^{-3} ir p^{++}-GaAs su akceptorių koncentracija 4×10^{18} cm^{-3}.

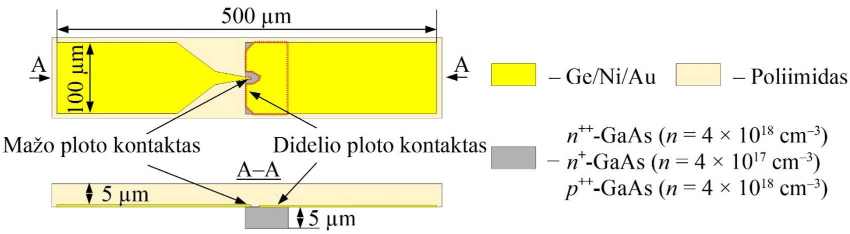

S2.1 pav. Schematinis planarinių dvigubų mikrobangų diodų, pagamintų ant trijų tipų laidžių GaAs padėklų, atvaizdavimas

Šie diodai buvo pasirinkti dėl savo konstrukcijos paprastumo lyginant su Šotkio ir planarinių legiruoto barjero diodų dariniais, kurie auginami molekulinio pluošto epitaksijos būdu. Schematinis šitų diodų vaizdas parodytas S2.1 paveikslėlyje.

Tokia diodų konstrukcija leidžia sumažinti diodų gamybos proceso etapus, naudojant paprastesnius puslaidininkinius darinius, todėl ji buvo pasirinkta gaminant planarinius mikrobangų diodus su *n*-tipo $Al_xGa_{1-x}As$ sluoksniu ant pusiau izoliuojančio padėklo (350 μm AGChP-I-26a (1.0.0) 0° 30′, Ø 26 mm, Grynųjų metalų gamykla, Svitlovodsk, Ukraina). Buvo pagaminti trijų tipų bandiniai su skirtinga AlAs koncentracija $Al_xGa_{1-x}As$ sluoksnyje (x = 0; 0,15 ir 0,3). Schematiniai šių diodų konstrukcijos ir darinio skerspjūvio vaizdai parodyti S2.2 paveikslėlyje.

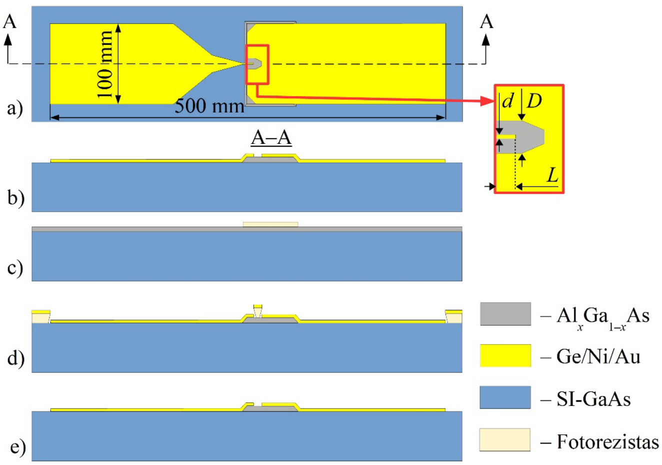

S2.2 pav. Planarinių mikrobangų diodų ant pusiau izoliuojančio GaAs padėklo schematinis vaizdas iš viršaus (a) ir skerspjūvio vaizdas (b). Diodų gamybos etapai pavaizduoti (c–e) paveikslėliuose

Lyginant su planariniais mikrobangų diodais ant laidaus padėklo, šių diodų nereikia perkėlinėti ant poliimido tam, kad būtų galima išvengti šuntavimo per puslaidininkinį padėklą.

Asimetriškai susiaurinti peteliškės formos mikrobangų diodai su daline sklende virš dvimačio elektronų dujų sluoksnio buvo pagaminti naudojant selektyviai legiruotą GaAs/AlGaAs heterodarinį, užaugintą ant pusiau izoliuojančio GaAs padėklo (100 ± 0,3°, Ø 50 mm, Weizmann institutas, Rehovot, Izraelis). Dalinė sklendė buvo formuojama virš diodo aktyviosios srities plačiosios dalies arba jos siaurosios dalies. Šių diodų schematinis vaizdavimas yra pateiktas S2.3 paveikslėlyje.

Mikrobangų diodų voltamperinės charakteristikos buvo matuojamos naudojant nuolatinės srovės zondinį manipuliatorių („SUSS Microtec EP6“ ir „SUSS Microtec PH110“ zondai) ir *IV* analizatorių („Agilent E5270B“ su „Agilent E5287A“ lizdais). Srovės stipris buvo matuojamas kaip įtampos funkcija, o diodų elektrinė varža (esant nuliniam priešįtampiui) buvo nustatoma iš voltamperinių charakteristikų pagal S2.1 išraišką (Pavasaris, 2009):

$$R = \frac{\mathrm{d}U}{\mathrm{d}I}. \tag{S2.1}$$

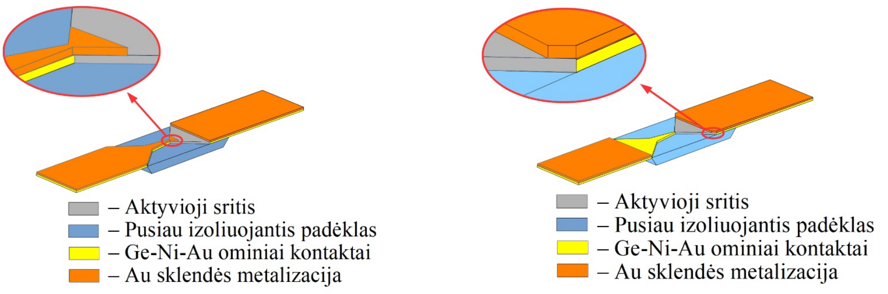

(a) (b)

S2.3 pav. Peteliškės formos mikrobangų diodų su siaurąja daline sklende (a) ir plačiąja daline sklende (b) virš aktyviosios srities schematinis vaizdavimas

Mikrobangų diodų detekcijos savybės, t. y. detektuotos įtampos priklausomybės nuo signalo galios ir dažnio, buvo matuojamos keliuose dažnių ruožuose: 26–37,5 GHz, 75–110 GHz, 110–170 GHz ir iki 340 GHz.

K_a (26–37,5 GHz) dažnių ruože diodai buvo tiriami naudojant sukurtą matavimo stendą su zondiniu manipuliatoriumi.

Signalas iš generatoriaus į mikrobangų diodą buvo siunčiamas naudojant bangolaidinę perdavimo liniją ir aukštadažnius bendraašius kabelius bei zondus, kurie yra uždedami ant abiejų diodo darbinių kontaktų. Detektuotas nuolatinės srovės signalas buvo atskiriamas nuo mikrobangų dedamosios naudojant postūmio trišakį, kuris veikia kaip LC filtras ir matuojamas naudojant skaitmeninį voltmetrą. Galia buvo nustatoma naudojant termistorinį galios matuoklį, įvertinant signalo praėjimo ir atspindžio nuostolius perdavimo trakte.

Mikrobangų diodų voltvatinės charakteristikos buvo tiriamos matuojant detektuotą įtampą kaip krentančio signalo galios funkciją skirtinguose dažniuose. Dažninės charakteristikos buvo tiriamos matuojant detektuotos įtampos priklausomybę nuo dažnio esant skirtingai krentančio signalo galiai tiesiniame voltvatinės charakteristikos ruože. Mikrobangų diodų voltvatinis jautris buvo nustatomas pagal S2.2 išraišką (Ašmontas et al., 2000):

$$S = \frac{U_\mathrm{d}}{P_\mathrm{k}}, \tag{S2.2}$$

čia U_d yra detektuota įtampa tarp mikrobangų diodo galų; P_k yra krentanti į diodą galia.

Taip pat buvo nustatomas mikrobangų diodų dinaminis galios ruožas bei triukšmą atitinkanti galia.

Galiausiai matavimo stendas buvo patobulintas, tai leido atlikti greitus automatizuotus matavimus. Naudojant automatinio lygio valdymo plokštę, *p-i-n* slopintuvą, detektorinę galvutę bei logaritminį stiprintuvą ir skaliarinį grandinės analizatorių buvo palaikoma 3 mW (esant nuliniam slopinimui) į diodą krintantį galia. Iš generatoriaus į diodą analogišku principu buvo siunčiamas impulsinis 100 kHz amplitudės moduliuotas mikrobangų signalas, o detektuotas signalas buvo matuojamas naudojant postūmio trišakį, logaritminį stiprintuvą ir skaliarinį grandinės analizatorių bei atvaizduojamas naudojant PK programinės įrangos virtualiuosius įrankius.

Reikia pabrėžti, kad taikant zondinę matavimo metodiką, diodai yra tiriami tiesiai ant puslaidininkinio padėklo, nedalinat diodų matricos į atskirus elementus, tai leidžia greitai tirti dideles diodų grupes bei statistiškai įvertinti jų charakteristikas ir parametrus. Taip pat zondų panaudojimas leido įvertinti temperatūros ir apšvietimo įtaką mikrobangų diodų detekcijos savybėms K_a dažnių ruože. Temperatūros matavimai vyko naudojant Peltier elementą, o apšvietimo įtakos įvertinimui diodai buvo apšviečiami skirtingo intensyvumo šviesa bei laikant juos tamsoje.

W ir D dažnių ruožuose (75–110 GHz ir 110–170 GHz) mikrobangų diodai buvo tiriami dedant juos į bangolaidinę detektorinę galvutę. Detektuota įtampa ir voltvatinis jautris buvo matuojami kaip signalo dažnio funkcija skirtinguose paduodamos galios lygiuose. Matavimai aukštesniuose dažniuose 270–330 GHz buvo vykdomi analogišku principu naudojant D dažnių ruožo signalo antrąją harmoniką.

3. Planarinių dvigubų mikrobangų diodų tyrimai

Buvo ištirti planariniai mikrobangų diodai ant laidaus padėklo, pagaminti naudojant trijų tipų stipriai legiruotus GaAs darinius: n^{++}-GaAs su donorų koncentracija 4×10^{18} cm^{-3}, n^{+}-GaAs, legiruota 4×10^{17} cm^{-3} ir p^{++}-GaAs su akceptorių koncentracija 4×10^{18} cm^{-3}. Jų veikimo principas pagrįstas karštųjų krūvininkų reiškiniu ir mikrobangų srovių lyginimu dviejų priešingomis kryptimis sujungtų diodų darinyje su skirtingo ploto darbiniais kontaktais.

Planarinių dvigubų mikrobangų diodų, pagamintų ant n^{++}- ir n^{+}-GaAs padėklų, elektrinė varža buvo sąlygiškai maža (dešimtys-šimtai omų). Tačiau diodų išmatuotos voltamperinės charakteristikos buvo arba kvazitiesinės, būdingos ominiams kontaktams, arba Šotkio tipo, t. y. netiesinės charakteristikos, būdingos metalo-puslaidininkio kontaktui. Atitinkamai diodai buvo pavadinti LS (mažos varžos Šotkio tipo) ir LO (mažos varžos ominio tipo). Diodai, pagaminti ant p^{++}-GaAs padėklo, turėjo didelę elektrinę varžą (dešimtys megaomų) ir buvo pavadinti HS (didelės varžos Šotkio tipo). LO diodų elektrinė varža buvo tarp 30–200 Ω, o LS – tarp 50–600 Ω.

Planarinių dvigubų mikrobangų diodų voltvatinės charakteristikos buvo išmatuotos 28 GHz dažnyje. Mažų galių srityje visų trijų tipų planarinių dvigubų mikrobangų diodų voltvatinės priklausomybės buvo tiesinės, o didėjant galiai LS ir HS diodų charakteristikos tapo subtiesinės. LO diodų charakteristikos išliko tiesinės platesniame mikrobangų galios ruože. Taip pat buvo įvertinta triukšmą atitinkanti galia: 8,8 nW HS diodo atveju, 1,8 nW LS diodo atveju ir 2,1 nW LO diodo atveju.

LO diodo atveju detektuotos įtampos teigiamas potencialas buvo matuojamas ant mažo ploto darbinio kontakto. Šiuo atveju detektuota įtampa lemia karštųjų elektronų evj., kuri atsiranda planariniuose mikrobangų dioduose su skirtingo ploto darbiniais kontaktais. LS dioduose detektuota įtampa yra priešingo poliškumo, HS diode – tokio pat poliškumo kaip ir LO, nes HS diodai pagaminti ant *p*-tipo padėklo.

Diodų voltvatinio jautrio dažninės charakteristikos K_a dažnių ruože yra pateiktos S3.1 paveikslėlyje.

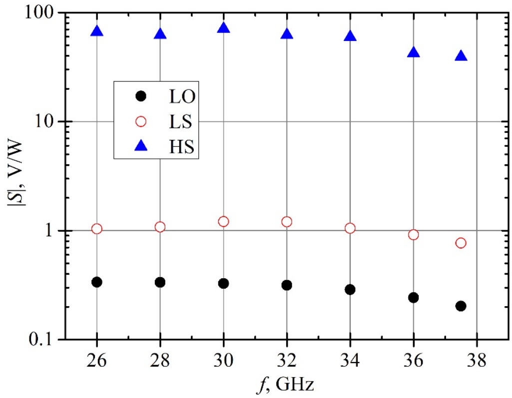

S3.1 pav. Planarinių dvigubų mikrobangų diodų ant laidaus padėklo voltvatinio jautrio dažninės priklausomybės K_a dažnių ruože

Voltvatinio jautrio dažninės priklausomybės yra beveik plokščios visų trijų tipų diodams iki 34 GHz. Šotkio tipo diodų voltvatinis jautris yra didesnis negu ominio tipo diodų, kurių veikimas pagrįstas karštųjų krūvininkų reiškiniu. HS diodo voltvatinis jautris yra didžiausias, nes jo elektrinė varža yra didžiausia.

Tačiau mažos LO ir LS diodų varžos leidžia naudoti šiuos diodus kaip greitus trumpų impulsų detektorius. Kadangi šie diodai veikia be priešįtampio, tai žymiai supaprastina jų taikymą mikrobangų įrangoje. Trumpiausi impulsai, kuriuos LO diodai detektavo, buvo apytiksliai 50 ns trukmės. Pagerinti LO diodo greitį galima padidinant jo voltvatinį jautrį. Jautresnis LS diodas galėjo detektuoti 10 ns trukmės mikrobangų impulsus. Trumpesni mikrobangų impulsai leidžia išvengti puslaidininkio kristalinės gardelės kaitimo dėl mikrobangų spinduliuotės poveikio, todėl gali būti detektuojamas didesnės galios mikrobangų signalas.

Taip pat buvo ištirti trijų tipų planariniai mikrobangų diodai su *n*-tipo $Al_xGa_{1-x}As$ sluoksniu (skirtingos AlAs koncentracijos $x = 0$; 0,15 ir 0,3) ant pusiau izoliuojančio padėklo. Atitinkamai diodai buvo pavadinti DD0 ($x = 0$), DD15 ($x = 0{,}15$) ir DD30 ($x = 0{,}3$). Šotkio tipo diodo poliškumas buvo tuo atveju, kai ant mažo ploto darbinio kontakto buvo matuojama neigiamo ženklo detektuota įtampa. Priešingo ženklo poliškumas yra termo-evj., tai yra būdinga karštiems krūvininkams ir atsiranda mikrobangų dioduose su ominiais kontaktais (Harrison & Zucker, 1963).

Diodų voltvatinės charakteristikos buvo tiriamos 30 GHz dažnyje. Mažos galios srityje visų trijų tipų diodų detektuotos įtampos priklausomybės buvo tiesinės. Tačiau, esant aukštesnėms galioms, DD15 ir DD30 diodų priklausomybės tapo subtiesinės, o DD0 diodo priklausomybė buvo tiesinė visame matuotos galios ruože. Apskaičiuotos triukšmui prilygstančios atitinkamos galios: DD0 diodo – 6,1 mW, DD15 diodo – 0,4 nW, o DD30 diodo – 0,5 nW. Skirtumas tarp voltvatinių charakteristikų yra dėl skirtingo voltamperinių charakteristikų asimetriškumo. Įvertinta didžiausia galia, kurią gali atlaikyti DD30 diodas nepakeičiant savo elektrinių parametrų – 1 W, o DD0 ir DD15 – apytiksliai 100 mW.

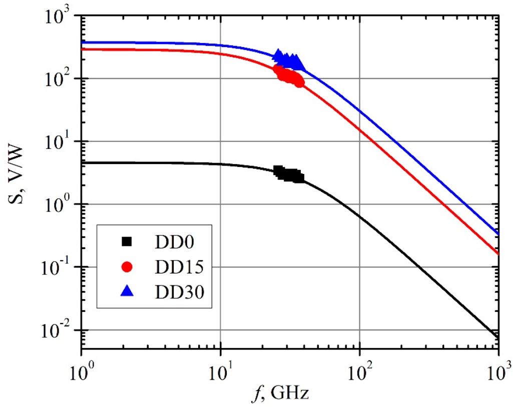

S3.2 pav. Planarinių mikrobangų diodų ant pusiau izoliuojančio padėklo voltvatinio jautrio dažninės priklausomybės. Eksperimentiniai taškai atvaizduoti taškais, o vientisos linijos yra analitiškai įvertintas jautris pagal S3.1 išraišką

DD15 ir DD30 diodų voltvatiniai jautriai yra dviem eilėmis didesni negu DD0 diodo. Diodų voltvatinio jautrio dažninės priklausomybės yra pateiktos S3.2 paveikslėlyje.

Voltvatinis jautris buvo aproksimuojamas pagal S3.1 išraišką (Bahl & Bhartia, 2003):

$$S = \frac{\gamma R_\mathrm{n} k_\mathrm{abs}}{2\left(1+\frac{R_\mathrm{n}}{R_\mathrm{b}}\right)\left[1+\frac{R_\mathrm{n}}{R_\mathrm{b}}+(\omega C_\mathrm{b})^2 R_\mathrm{n} R_\mathrm{b}\right]}, \quad \text{(S3.1)}$$

čia $\gamma = \frac{\mathrm{d}^2 I}{\mathrm{d}U^2} / \frac{\mathrm{d}I}{\mathrm{d}U}$ yra voltamperinės charakteristikos netiesiškumas, R_b ir C_b yra atitinkamai metalo-puslaidininkio sandūros barjerinė varža ir talpa, R_n yra diodo nuoseklioji varža, ω yra mikrobangų signalo kampinis dažninis, k_abs yra diode absorbuota mikrobangų spinduliuotės galios dalis.

Tirti diodai nėra konkurencingi Šotkio diodams voltvatinio jautrio atžvilgiu, tačiau diodai, kurių voltvatinis jautris yra 0,1–1 V/W (DD15 ir DD30), gali būti naudojami elektromagnetinei spinduliuotei detektuoti terahercinių dažnių ruože (Sužiedėlis et al., 2003; Kašalynas et al., 2013).

Verta pabrėžti, kad pagaminti diodai turėjo skirtingą mažo darbinio kontakto plotį (1,0; 1,5; 2,0; 2,5; 3,0 ir 4,0 μm). Didėjant pločiui, diodų voltvatinis jautris ir elektrinė varža mažėjo.

Tai pat buvo įvertintas temperatūros poveikis diodų voltvatiniam jautriui. Temperatūros poveikis priklauso nuo AlAs molinės dalies x n-$Al_xGa_{1-x}As$ planariniuose mikrobangų dioduose ant pusiau izoliuojančio padėklo. Temperatūrai didėjant n-GaAs ($x = 0$) voltvatinis jautris didėja, o dioduose, kuriuose yra Al ($x = 0,15$ ir 0,3), – mažėja. Labiausiai jautrus temperatūros poveikiui yra DD30 diodas.

4. Peteliškės formos mikrobangų diodų su daline sklende virš dvimačio elektronų dujų sluoksnio tyrimai

Taikant aprašytas zondavimo metodikas, iš pradžių peteliškės formos mikrobangų diodai su dvimačiu elektronų dujų sluoksniu GaAs/AlGaAs selektyviai legiruotame darinyje buvo ištirti K_a dažnių ruože be dalinės sklendės, o vėliau matavimai buvo pakartoti uždengiant diodo aktyviąją sritį su daline sklende. Diodų detektuota įtampa buvo karštųjų krūvininkų termo-evj. (TEMF) poliškumo, kai teigiamas potencialas buvo matuojamas ant siaurosios diodo dalies darbinio kontakto, arba metalo-puslaidininkio Šotkio tipo sandūros poliškumo (SCH), kai siaurosios dalies kontakte buvo matuojamas neigiamas potencialas. Atitinkamai, atsižvelgiant į poliškumą, diodai buvo pavadinti TEMF ir SCH.

Tiriant diodų voltamperines charakteristikas, buvo įvertintas voltamperinių charakteristikų asimetriškumas (tai leidžia prognozuoti diodų voltvatinį jautrį) bei elektrinė varža. Taip pat buvo išmatuotos diodų be dalinės sklendės ir diodų su skirtinga daline sklende (ant siaurosios aktyviosios srities dalies ir ant plačiosios dalies) voltvatinės charakteristikos 30 GHz dažnyje. Jos yra pateiktos S4.1 paveikslėlyje.

Detektuotos įtampos priklausomybės nuo mikrobangų galios išlieka beveik tiesinės mažiausia per 4 eiles iki kelių mW galios. Taip pat buvo įvertinta triukšmo lygį atitinkanti galia dioduose: diodas be sklendės – 23,9 nW, diodas su plačiąja sklende – 0,1 nW, diodas su siaurąja sklende – 2,3 nW. Dalinės sklendės panaudojimas nekeičia diodo dinaminio diapazono viršutinės ribos, bet padidina detektuotos įtampos vertes. Taip pat buvo nustatyta, kad siaurosios dalinės sklendės panaudojimas pakeičia detektuotos įtampos poliškumą iš TEMF į SCH.

Iš voltvatinių charakteristikų buvo įvertintas diodų jautris. Plačioji dalinė sklendė padidina peteliškės formos mikrobangų diodų voltvatinį jautrį 20 kartų, o siauroji sklendė padidina jautrį dviem eilėmis. Diodų voltvatinio jautrio dažninės priklausomybės pateiktos S4.2 paveikslėlyje.

Diodo be sklendės ir diodo su plačiąja daline sklende priklausomybės buvo aproksimuojamos pagal S4.1 išraišką:

$$S = \frac{U_{\mathrm{d}}}{P_{\mathrm{k}}} = \frac{2R_{\mathrm{p}}\mu_0 \tan\alpha}{3d^2 \ln\frac{a}{d}} \frac{P}{P_{\mathrm{k}}} N, \tag{S4.1}$$

čia U_{d} detektuota įtampa tarp mikrobangų diodo galų; P_{k} yra krintanti į diodą galia; R_{p} diodo aktyviosios srities paviršinė sluoksnio varža; μ_0 yra elektronų judris silpname lauke; a ir d yra plačiosios ir siaurosios diodo dalių pločiai, o α aktyviosios srities platėjimo kampas. Nuo dažnio priklausantis koeficientas N, kai puslaidininkinis darinys nėra stipriai legiruotas ir elektronų energijos relaksacijos trukmė τ_ε nepriklauso nuo elektronų tankio. Diodo su siaurąja daline sklende dažninė priklausomybė kinta pagal $1/\omega^2$ dėsnį.

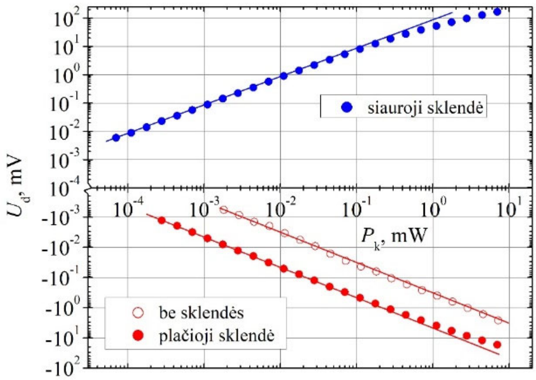

S4.1 pav. Peteliškės formos mikrobangų diodų su dvimačiu elektronų dujų sluoksniu selektyviai legiruotame GaAs/AlGaAs darinyje detektuotos įtampos priklausomybės nuo mikrobangų signalo galios 30 GHz dažnyje, kai diodas yra be dalinės sklendės ir kai diodo aktyvioji sritis yra uždengta su dalinėmis sklendėmis plačiojoje arba siaurojoje diodo aktyviosios srities vietoje

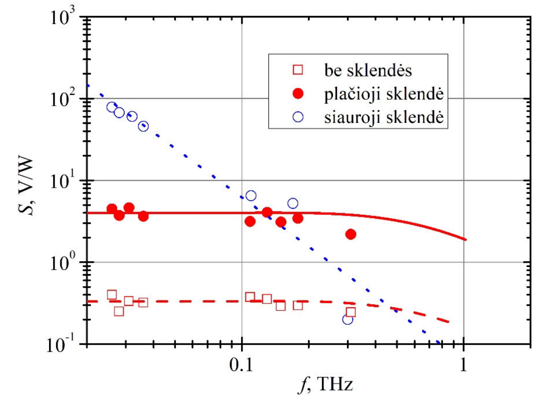

S4.2 pav. Peteliškės formos mikrobangų diodų su dvimačiu elektronų dujų sluoksniu selektyviai legiruotame GaAs/AlGaAs darinyje voltvatinio jautrio dažninės priklausomybės, kai diodas yra be dalinės sklendės ir kai diodo aktyvioji sritis yra uždengta daline sklende plačiojoje arba siaurojoje vietoje

Plačiosios sklendės panaudojimas nekeičia peteliškės formos mikrobangų diodo (TEMF poliškumo) dažninės priklausomybės pobūdžio. Siaurosios sklendės panaudojimas ne tik pakeičia diodo detektuotos įtampos poliškumą iš TEMF į SCH, bet ir pakeičia voltvatinio jautrio dažninę charakteristiką – jautris labiau priklauso nuo dažnio ir mažėja keliomis eilėmis dažniui artėjant prie terahercinių dažnių. Diodo be sklendės ir diodo su plačiąja sklende (abu TEMF poliškumo) voltvatinis jautris beveik nepriklauso nuo dažnio iki subterahercinės ribos ir nežymiai pradeda mažėti artėjat prie terahercinių dažnių. Pagal S3.1 išraišką buvo nustatytas į mikrobangų diodą krintančios ir absorbuojamos galios santykis $P/P_k = 0,02$.

Taip pat buvo įvertintas šviesos poveikis diodų voltvatiniam jautriui. Diodai buvo apšviečiami halogeninės lempos balta šviesa (14400 lx) bei laikomi tamsoje (0 lx). Apšvietus SCH mikrobangų diodą jo voltvatinis jautris padidėjo nuo 80 V/W iki 100 V/W, o TEMF poliškumo diodo voltvatinis jautris padidėjo trigubai, lyginant su jautriu, kai diodas buvo tiriamas tamsoje.

Bendrosios išvados

1. Sukurtas aukštadažnis matavimo stendas su zondiniu manipuliatoriumi, leidžiantis našiai charakterizuoti planarinių mikrobangų diodų, suformuotų ant puslaidininkinio padėklo, detekcijos savybes, matuojant detektuotos įtampos voltvatines ir dažnines priklausomybes 26,5–40 GHz dažnių ruože ir įvertinant temperatūros bei šviesos poveikį diodų fizikinėms savybėms.
2. Planariniai asimetriškai susiaurinti dvigubi mikrobangų diodai suformuoti ant stipriai legiruotų puslaidininkinių GaAs padėklų gali detektuoti milimetrinių bangų ruožo nanosekundžių trukmės impulsinį bei nuolatinės bangos signalą. Diodai veikia kambario temperatūroje be priešįtampio.
3. Planarinių dvigubų mikrobangų n-$Al_xGa_{1-x}As$ diodų epitaksijos būdu užaugintų ant pusiau izoliuojančio padėklo elektromagnetinės spinduliuotės detekcijos savybes galima valdyti tinkamai parenkat AlAs molinę dalį x aktyviojoje diodo srityje bei sumažinant mažojo darbinio kontakto matmenis. Planarinių dvigubų mikrobangų n-GaAs diodų voltvatinis jautris nepriklauso nuo mažojo darbinio kontakto matmenų, o n-$Al_xGa_{1-x}As$ diodų jautris didėja mažėjant mažojo darbinio kontakto plotui. Planarinių dvigubų mikrobangų diodų, turinčių dalį aliuminio ($x = 0,15$ ir $0,3$), voltvatinio jautrio vertės yra dviem eilėmis didesnės negu n-GaAs diodų ($x = 0$).
4. Dalinės sklendės virš asimetriškai susiaurintos formos dvimačio elektronų dujų kanalo poveikis priklauso: *a*) nuo įtampos, detektuotos peteliškės formos mikrobangų dioduose su selektyviai legiruotu heterodariniu, poliškumo (t. y. prigimties); *b*) nuo sklendės padėties diodų darbinių kontaktų atžvilgiu. Eksperimentiniai rezultatai parodė, kad dalinė sklendė neturi įtakos viršutinei peteliškės formos mikrobangų diodų dinaminio diapazono ribai. Kai dalinė sklendė yra šalia plačiojo darbinio kontakto, diodo voltvatinis jautris padidėja viena eile ir nekinta iki 0,2 THz dažnio kaip ir peteliškės formos mikrobangų diodo be sklendės atveju.

5. Peteliškės formos mikrobangų diodų su dvimačiu elektronų dujų sluoksniu selektyviai legiruotame heterodarinyje voltvatinio jautrio vertė 30 GHz dažnyje padidėja dviem eilėmis, jei dalinė sklendė yra formuojama šalia siaurojo diodo darbinio kontakto. Dalinė sklendė šalia siaurojo kontakto pakeičia detektuoto signalo įtampos poliškumą į priešingą, o voltvatinio jautrio dažninė priklausomybė atitinka ω^{-2} dėsnį. Peteliškės formos mikrobangų diodas su plačiąja daline sklende yra efektyvesnis subterahercų dažnių ruože, nes jo voltvatinis jautris yra žymiai didesnis šiuose dažniuose; tokie diodai gali būti naudojami kaip plačiajuosčiai elektromagnetinės spinduliuotės detektoriai, veikiantys kambario temperatūroje be priešįtampio.

Maksimas ANBINDERIS

INVESTIGATION OF DETECTION PROPERTIES OF PLANAR MICROWAVE DIODES BASED ON A3B5 SEMICONDUCTOR COMPOUNDS IN MILLIMETER–WAVELENGTH RANGE

Doctoral Dissertation

Technological Sciences,
Electrical and Electronic Engineering (T 001)

PLANARINIŲ MIKROBANGŲ DIODŲ A3B5 PUSLAIDININKINIŲ JUNGINIŲ PAGRINDU DETEKCINIŲ SAVYBIŲ TYRIMAI MILIMETRINIŲ BANGŲ RUOŽE

Daktaro disertacija

Technologijos mokslai,
elektros ir elektronikos inžinerija (T 001)

Lietuvių kalbos redaktorė Dalia Markevičiūtė

Anglų kalbos redaktorė Jūratė Griškėnaitė

2023 01 09. 16,0 sp. l. Tiražas 20 egz.
Leidinio el. versija *https://doi.org/10.20334/2023-001-M*
Vilniaus Gedimino technikos universitetas
Saulėtekio al. 11, 10223 Vilnius
Spausdino UAB „Ciklonas“
Žirmūnų g. 68, 09124 Vilnius